POROUS FRAMEWORKS FOR BIOCATALYSIS APPLICATIONS

A thesis presented to

The School of Physics, Chemistry, and Earth Sciences

at

The University of Adelaide

in fulfillment of the requirements for

The Degree of

Master of Philosophy in Chemical Science

by

Joe Richard Ian Milne

THE UNIVERSITY of ADELAIDE

Adelaide, Australia

April 2023

Contents

Abstract

Biocatalysis is a growing field, which involves the use of enzymes or other biological materials to speed up chemical reactions. Often, biocatalytic pathways are superior to traditional chemical synthesis, owing to the high selectivity, efficiency, and non-toxicity of enzymes. However, due to their structural complexity, biomolecules are unstable to the harsh conditions often used in industrial synthesis. To provide protection to enzymes, metal-organic frameworks (MOFs) and hydrogen-bonded organic frameworks (HOFs) have arisen as promising materials for enzyme immobilization.

The most widely utilized MOF for enzyme encapsulation is ZIF-8, which can protect enzymes from harsh conditions including organic solvents, heating, and proteolysis. However, certain enzymes, such as catalase, lose activity when immobilized in/on ZIF-8, due to unfolding upon contact with the hydrophobic framework surface. Single enzyme nanogels and polymer-enzyme conjugates were used as methods of tuning the enzyme-MOF interface, aiming to prevent this detrimental surface interaction. Neither method allowed catalase activity to be retained, suggesting that additional factors may contribute to enzyme unfolding. Re-evaluation of the system revealed gradual decomposition of ZIF-8 when stored as an aqueous suspension, leading to the release of free 2-methylimidazole. This was detrimental to catalase activity, either by direct interaction between the linker and catalase, or indirectly by pH effects on the enzyme structure. This indicated that physical barriers would be an ineffective method to protect catalase from denaturation upon encapsulation in ZIF-8.

To overcome the limitations of MOFs, HOFs may be used for enzyme encapsulation. However, there are few studies that investigate the spatial distribution of proteins in HOFs, which is critical to their eventual application as it can impact how effective the HOF is at protecting protein. Ferritin was determined to be a convenient model protein for studying the localization of proteins in HOFs, as its iron core can be visualized using transmission electron microscopy (TEM). Combined with a washing procedure of 10% SDS, it allowed individual protein macromolecules encapsulated within the framework to be identified. Various methods were trialed to increase the loading of protein in BioHOF-1, including slowed framework growth by use of a modulator, surface modification of protein, and incubation with a guanidinium-decorated polymer. All

methods showed either marginal impact on protein loading or were not broadly applicable to other proteins. To offer additional protection to surface-bound protein, layer-by-layer encapsulation of BioHOF-1 was performed. This was able to protect surface-bound catalase from proteolysis by a Trypsin enzyme. With further work, this system could be employed to create high-loading enzyme@HOF biocomposites with enhanced protective properties.

Declaration

I certify that this work contains no material which has been accepted for the award of any other degree or diploma in my name, in any university or other tertiary institution and, to the best of my knowledge and belief, contains no material previously published or written by another person, except where due reference has been made in the text. In addition, I certify that no part of this work will, in the future, be used in a submission in my name, for any other degree or diploma in any university or other tertiary institution without the prior approval of the University of Adelaide and where applicable, any partner institution responsible for the joint award of this degree.

I give permission for the digital version of my thesis to be made available on the web, via the University's digital research repository, the Library Search and also through web search engines, unless permission has been granted by the University to restrict access for a period of time.

I acknowledge the support I have received for my research through the provision of an Australian Government Research Training Program Scholarship.

Joe Milne

4 April 2023

Acknowledgements

There are several people that have provided their time, support, and guidance to me throughout my master's candidature.

Foremost, I would like to thank my supervisor, Prof. Christian Doonan, for the constant advice and feedback. You have always pushed for my writing and presenting to be the best it can be, and hopefully that is reflected in this thesis that sits before you.

Secondly, a big thank you to my legion of post-docs: Hamish Toop, Adrian Markwell-Heys, and Kate Flint. Each of you has played a significant part in the direction my master's has taken, and your varying fields of expertise have broadened my skillset and understanding of chemistry as a whole. I am yet to discover what it is about me that keeps scaring away post-docs. I also extend my thanks to Natasha Maddigan, who laid the groundwork for many of the enzyme immobilization projects that I have been involved in.

Further abroad, I'd like to extend my gratitude towards the entire Sumby-Doonan group. You have been an incredible group to work with, and I wish all of you the best for your future endeavors. In particular, Mei, your impeccable knowledge of food in the Adelaide area is second to none, and I hope to see a YouTube channel with your name on it sometime soon. Thank you also to the technical staff who keep everything running behind the scenes. Notably, Matt Bull, who maintains a countless array of instruments without which the chemistry department would collapse, and the staff at Adelaide microscopy, who have kept the microscopes running whilst providing invaluable advice to ensure my images looked more Da Vinci and less Picasso.

Finally, I would like to thank my friends and family. To Josie, who has been with me for the entire journey through my master's. It's been fun doing this alongside you, and I don't regret a moment of it. To my family, Tim, Tanya, Charlie, and Jesse, thank you for supplying me with a house, food, and above all, joy and company, for the last 23 years. Your support has not gone unnoticed.

Abbreviations

AAm	Acrylamide
APS	Ammonium persulfate
BCA	Bicinchoninic acid
BIS	N,N'-Methylenebisacrylamide
BSA	Bovine serum albumin
CAT	Catalase from Bovine liver
CLSM	Confocal laser scanning microscopy
Dia-	Diamondoid
DLS	Dynamic light scattering
DMSO	Dimethyl sulfoxide
EDA	Ethylenediamine
EDC	1-Ethyl-3-(3-dimethylaminopropyl)carbodiimide
EtOH	Ethanol
F-BSA	FITC-tagged BSA
FITC	Fluorescein isothiocyanate
FOX	Ferrous oxidation−xylenol orange
F-PAH	FITC-tagged poly(allylamine hydrochloride)
G-PEI	Guanylated polyethyleneimine
HICA	Imidazolate-2-carboxaldehyde
HmIM	2-methyl imidazole
Hmtz	3-methyl-1,2,4-triazolate
HOF	Hydrogen-bonded organic framework
ICP-MS	Inductively coupled plasma mass spectrometry
MAF	Metal azolate framework

MeOH	Methanol
MOF	Metal organic framework
PAA	Poly(acrylic acid)
PAH	Poly(allylamine hydrochloride)
PBS	Phosphate buffered saline
PEI	Polyethyleneimine
PSS	Poly(sodium 4-styrene sulfonate)
PXRD	Powder X-ray diffraction
SDS	Sodium dodecyl sulfate
SEM	Scanning electron microscopy
SEN	Single enzyme nanogel
Sod-	Sodalite
TEM	Transmission electron microscopy
TMEDA	Tetramethylethylenediamine
ZIF	Zeolitic imidazolate framework

CHAPTER 1

Introduction

1.1 Enzymes as a Platform for Biocatalysis

Enzymes are arguably the most important class of molecule for the existence of life. They are biological catalysts, which carry out specific, tailored reactions. Many metabolic processes require enzymatic catalysis to maintain the reaction rates needed to sustain life.[1] This is achievable due to the highly specific and tunable structure of proteins, which comprise the majority of enzymes. It is estimated that the human body expresses approximately 70,000 different proteins, not including post-translationally modified variants,[2] with infinitely many possible structures available due to the unique modular nature of protein structure. For these reasons, enzymes are of much interest in the growing field of biocatalysis.

Biocatalysis involves the use of biological substances to catalyze complex chemical reactions. Where traditional synthesis techniques face difficulties achieving high enantio- and/or regio-selectivity, enzymes provide an alternative route to access complex molecular structures.[3] Additionally, the high selectivity of enzymes results in reactions with minimal by-products, increasing reaction efficiency and commercial benefit. Some of the most common reactions catalyzed by enzymes include hydrolysis and isomerization reactions.[3] However, a variety of other reactions can also be catalyzed, some of which have no straightforward alternative route or require a toxic metal catalyst when conducted using conventional synthesis methods.[4] The applications of biocatalysis extend beyond stock chemical production, with enzymes also being used throughout the pharmaceutical and food industries (**Table** 1.1).[5-7] For example, the production of high-fructose corn syrup from starch requires several enzymatic reactions, most significantly the isomerization of glucose to fructose using glucose isomerase. This reaction can be undertaken non-enzymatically but yields undesirable by-products,[5] thus making the enzymatic route more industrially favorable. Developments in our understanding of protein structure-function relationships mean that new, currently unconceived applications of enzymes will arise in the future. In 2020, the industrial enzymes market was valued at USD $5.93 billion, with a forecasted revenue of USD $9.14 billion in 2027.[8] Biocatalysis is therefore poised to play a significant role in the future of industrial chemical synthesis.

Table 1.1: Examples of current applications of enzymes in industry.

Enzyme	Reaction	Application	Ref.
Glucose isomerase	Isomerization of glucose to fructose	Production of high-fructose corn syrup	9, 10
Chymosin	Cleavage of κ-casein	Cheese curd formation	11
Amylases	Hydrolysis of starch into sugars	Fuel alcohol production	12
Penicillin acylase	Conversion of penicillin G to 6-aminopenicillanic acid	Production of β-lactam antibiotics	13
Cellulases	Breakdown of cellulose into simple sugars	Biofuel production & pulping for paper production	14

1.2 Protein Structure-Function Relationship

Currently, biocatalysis is an imperfect alternative to conventional organic synthesis. Enzymes have limited functionality when removed from their native environment,[3] and unfortunately the conditions used in chemical synthesis often do not align with the relatively mild biological conditions enzymes have evolved to function in. The loss of functionality in non-native environments is due to the complex, hierarchical structure of proteins, which grants them their broad range of biological functions.

In general, proteins have four levels of structure (**Figure 1.1**). A protein is effectively a polypeptide, i.e., a chain of amino acids linked by amide bonds.[15] There are twenty naturally occurring amino acids, each possessing unique chemical properties. The extensive variety of amino acids leads to an unfathomable amount of potential protein structures, with even a simple tripeptide having 8000 possible amino acid sequences. It is the sequence of amino acids that defines the primary protein structure.[15] As the number of amino acids in a protein can be extremely large, with the largest known protein having a length of up to 35,000 amino acids,[16] the folding of the protein in 3D space must also be considered. The folding of the peptide chain can be categorized into secondary structure, whereby hydrogen bonding along the peptide backbone creates repeating, localized substructures, and tertiary structure, which involves the positioning of secondary structures relative to each other, dictated by a broad variety of intra- and intermolecular forces.[15, 17] The most significant of the forces contributing to tertiary structure is hydrophobic clustering, whereby hydrophobic amino acids place themselves towards the core of the protein, to minimize contact with the exterior, hydrophilic environment.[17] In addition to this, salt bridges may form between oppositely charged amino acids, and disulfide bonds may form between cysteine residues.[18] Finally, once the peptide chain is completely folded, it may associate with other polypeptide subunits, giving rise to quaternary protein structure.[15]

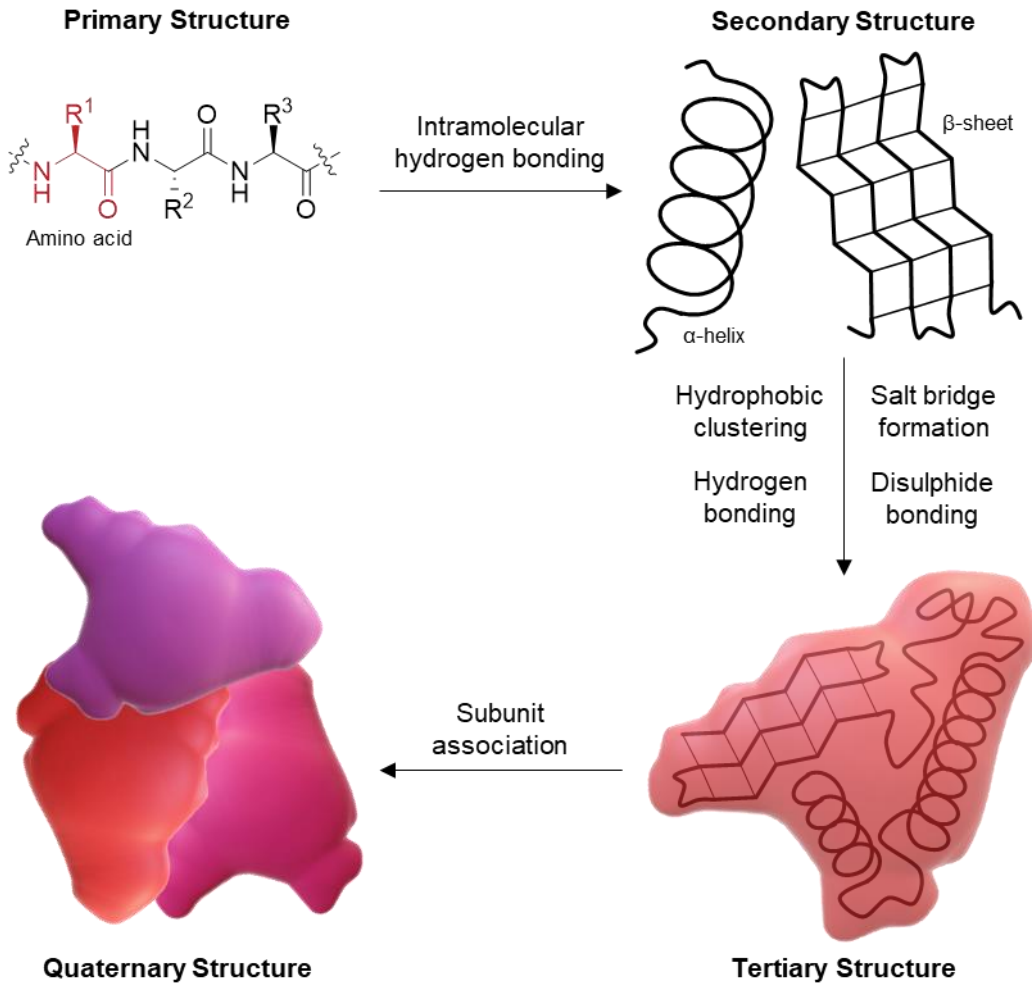

Figure 1.1: Schematic of the different levels of protein structure. Primary structure refers to the sequence of amino acids within the polypeptide chain. Secondary structure describes the formation of localized substructures, such as α-helices and β-sheets, due to hydrogen bonding along the peptide backbone. Tertiary structure involves the arrangement of these substructures with respect to each other, determined by a broad variety of intra- and intermolecular forces. Finally, multiple individual peptide chains may associate, which determines the quaternary structure of the protein.

The forces responsible for establishing and maintaining protein structure are easily influenced by the surrounding environment. In a biological system, significant environmental changes are not encountered as cells are able to regulate internal pH and temperature.[19, 20] However, when proteins are taken outside of their natural operating environment, protein stability becomes a significant issue. For an enzyme, unfolding can result in diminished activity, as structure is closely linked to enzyme function. Thus, manipulating enzymes to carry out reactions under traditional synthesis conditions is challenging. For example, many synthetic reactions require organic solvents to maintain

the solubility of reactants/products or prevent the participation of water molecules in the reaction. However, when an enzyme is submerged in an organic solvent, water molecules which are crucial to its structure may be displaced, leading to unfolding.[21] Similarly, exposure of a protein to acid and/or base can change the charge on certain residues and alter salt bridge formation, thus impacting the protein structure.[22] Furthermore, to maintain an appreciable reaction rate or drive a reaction towards a specific equilibrium state, temperature is often manipulated in chemical synthesis. High temperatures supply proteins with sufficient kinetic energy to overcome the secondary interactions holding the protein in its native conformation, causing unfolding. Thus, unless the targeted reactions can take place under mild, aqueous conditions, usage of unmodified enzymes in biocatalysis is unfeasible.

1.3 Enzyme Stabilization

Enzyme stabilization is a strategy which involves modifying an enzyme or its operating environment to boost its stability, resulting in a higher catalytic turnover under previously inoperable conditions. Reactions can be altered to maintain efficacy under many of the conditions mentioned previously, including pH changes, high temperature, and the use of an organic solvent. Broadly, enzyme protection can be divided into five categories: alteration of the chemical environment,[23-25] protein engineering,[10, 26, 27] chemical modification,[28] encapsulation within a single enzyme nanogel,[29-33] and enzyme immobilization (**Figure 1.2**).[22, 34-40] These protection methods are all independent, and thus an ideal biocatalytic system may use multiple approaches to achieve optimal reaction efficiency. In this work, we are primarily concerned with the immobilization strategy for enzyme stabilization. This approach is applicable to many different proteins, facile, and allows easy protein separation and reuse.

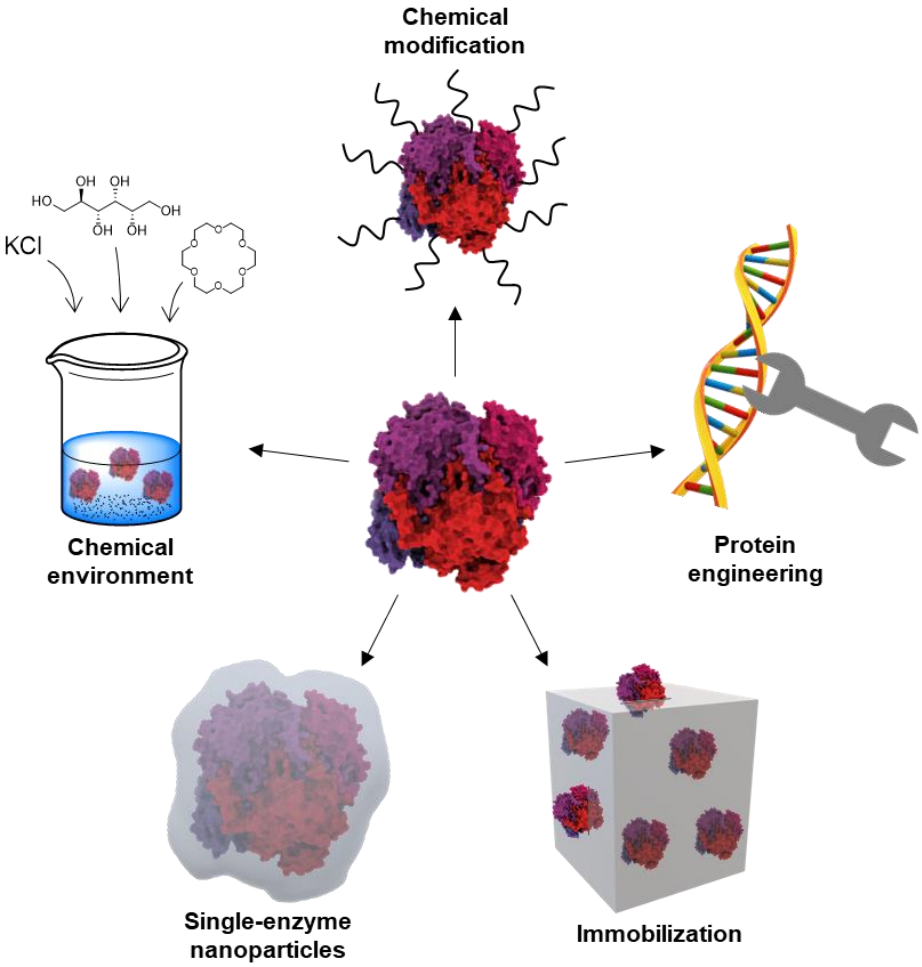

Figure 1.2: Strategies for the stabilization of enzymes to harsh conditions.[10, 23-35, 37-40]

Enzyme immobilization involves the adsorption or encapsulation of a protein in/on an insoluble support.[41] This imparts resistance to conditions including organic solvents, high temperatures, pH extremes, and proteolysis.[35, 37, 39, 40, 42-48] Further, separation of the enzyme and products is streamlined, as the enzyme remains bound to the insoluble support and so can be easily separated from the bulk mixture by filtration.[37, 49, 50] Protection is provided to the enzyme through several modes. Foremost, attachment of the enzyme to the support at multiple points limits the conformational freedom of the enzyme, ensuring it stays in its native, active conformation.[51, 52] In conjunction, it has been suggested that immobilization stabilizes enzymes by mimicking the natural structures within a cell that enzymes are normally attached to, such as cytoskeleton, membrane, or organelle structures.[53] Undesirable intermolecular processes, such as protein aggregation, are also unable to occur.[50] Finally, in cases where the enzyme is encapsulated inside the support, a physical barrier separates the enzyme from the outside environment,[54] preventing access by proteases and other detrimental macromolecules. Thus, enzyme immobilization is a proven method of allowing enzymes to retain activity in harsh conditions, with many supports under investigation for biocatalysis applications.

1.4 Metal Organic Frameworks for Enzyme Immobilization

Metal organic frameworks (MOFs) are promising candidates for enzyme immobilization. MOFs are composed of metal nodes coordinated to organic linkers to form a repeating, crystalline framework (**Figure 1.3**). Due to their high surface areas and porosity, MOFs have been explored as candidates for applications such as gas storage, catalysis, and molecular separations.[55-57] Selection of specific combinations of organic linkers and metal nodes allows materials to be designed based on the desired function. Further, MOFs can encapsulate other species, such as metal nanoparticles,[58, 59] which allows for further functionalization.

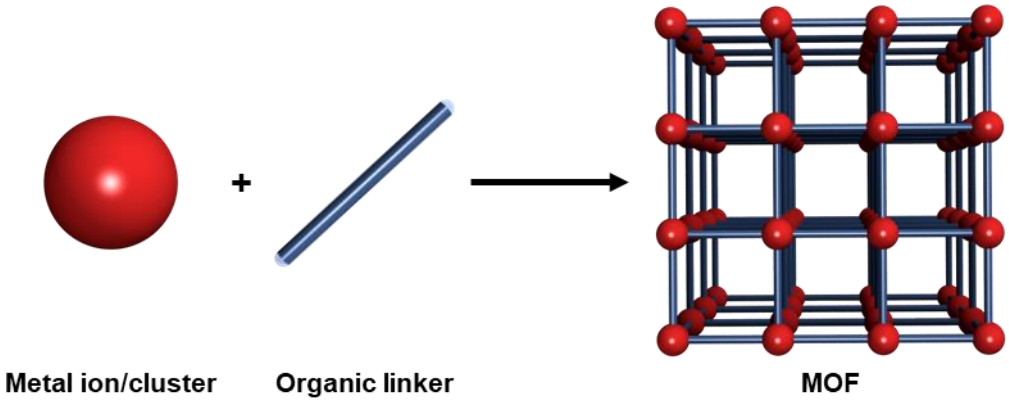

Figure 1.3: Simplified schematic of metal organic framework (MOF) synthesis.

MOFs have substantial potential for use as supports for enzyme immobilization, due to their porosity, thermal and chemical stability, capacity to encapsulate a broad variety of species, and ability to be synthesized under relatively mild conditions.[48] Porosity is critical, as it is needed for substrate/product diffusion from the surface of the framework to the enzyme and vice versa. For immobilization of enzymes on/in MOFs there are three approaches which may be used: encapsulation, surface binding, and pore infiltration (**Figure 1.4**).[41] Encapsulation involves growing the framework around the enzyme, creating its own cavity inside the framework which is larger than the pores normally found in the structure, preventing the enzyme from escaping the framework.[45, 48] Encapsulation requires the synthesis conditions of the MOF to be compatible with the biomolecule being immobilized. The framework must also possess pore apertures large enough to accommodate reaction substrates/products, placing further constraints on the MOFs that can be used for enzyme encapsulation. Such limitations are not encountered for the surface binding approach to enzyme immobilization, as framework porosity and biocompatible synthesis are not essential criteria. Rather, the enzyme is adsorbed on the exterior surface

of the framework and so can access substrate in the bulk solution, whilst the framework can be pre-formed and transferred into a biocompatible medium prior to immobilization. However, surface binding ultimately provides less protection to the enzyme as it is exposed to the bulk solution, and so can undergo partial unfolding and be digested by proteases.[41, 45] Additionally, leaching of the enzyme from the surface is more prevalent when compared to encapsulation, which can be promoted by certain species in solution such as surfactants.[41, 48] Finally, pore infiltration presents a middle-ground between surface binding and encapsulation, as it allows a preformed MOF to be used, which the enzyme is then incorporated into. This procedure places a significant constraint on the frameworks which can be utilized, since to achieve high loading they must possess pore apertures at least three times the size of the protein, assuming rapid and irreversible immobilization.[41] As such, pore infiltration has limited applicability to MOF-based enzyme biocomposites, as few MOFs have native pore windows able to accommodate proteins. There are, however, examples of proteins undergoing partial unfolding to enter a framework,[60, 61] allowing a MOF with smaller pore diameter than the size of the enzyme to be used. Nonetheless, such cases are rare, and so the widespread applicability of MOFs to pore infiltration of enzymes is minimal. With the above considered, the ideal approach for enzyme immobilization in/on a MOF is encapsulation, as it provides superior protection to a broader range of conditions, minimizes enzyme leaching, and does not place excessive constraints on the framework structure.

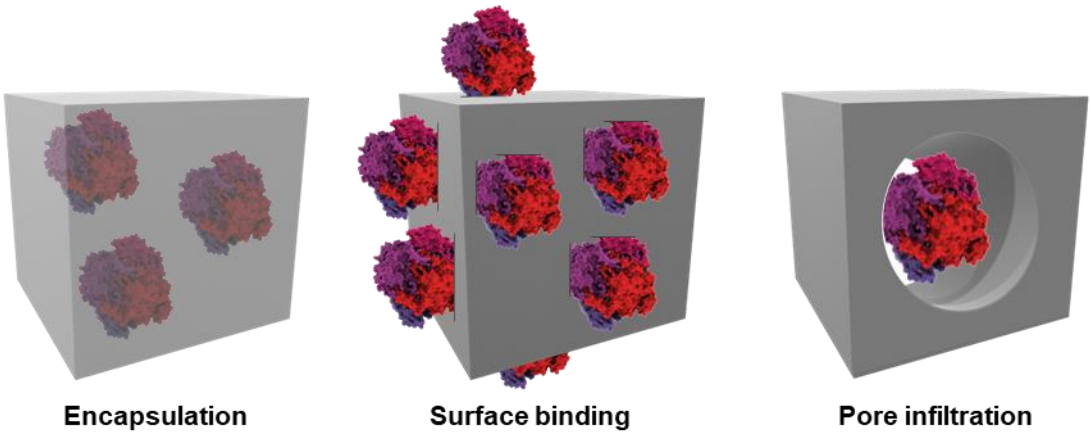

Figure 1.4: Modes of immobilization of proteins in/on MOFs. Encapsulation involves the formation of the framework around the enzyme, whilst surface binding and pore infiltration involve immobilizing the enzyme in/on a pre-formed material.

The most widely utilized MOF for enzyme encapsulation is Zeolitic Imidazolate Framework 8 (ZIF-8). ZIF-8 is composed of zinc (II) ions connected using 2-methylimidazole (HmIM) linkers, forming a framework with typically sodalite topology (**Figure 1.5**).[62-67] Other framework topologies can also be obtained by varying the synthesis conditions, including *dia*-ZIF-8,[63, 65-67] *kat*-ZIF-8,[63, 64, 67] ZIF-L,[68] and ZIF-C.[66] Morphological variation of ZIF-8 is also ubiquitous, with *sod*-ZIF-8 alone possessing morphologies including rhombic dodecahedral[69], cubic,[48, 69] nanoleaf,[48] nanoflower,[48] and nanostar.[48] Sodalite ZIF-8 has characteristics ideal for enzyme encapsulation. The framework has pores of size 11.6 Å with apertures of 3.4 Å,[70] sufficient to allow diffusion of small molecules through the framework, whilst preventing the leaching of encapsulated enzyme from the framework. Further, ZIF-8 forms spontaneously under biocompatible conditions. The addition of aqueous zinc acetate ($Zn(OAc)_2$) to 2-methylimidazole (HmIM) is sufficient to cause ZIF-8 precipitation. However, in order to obtain the desired sodalite topology, high concentrations of both precursors and a high HmIM:Zn ratio must be used.[67]

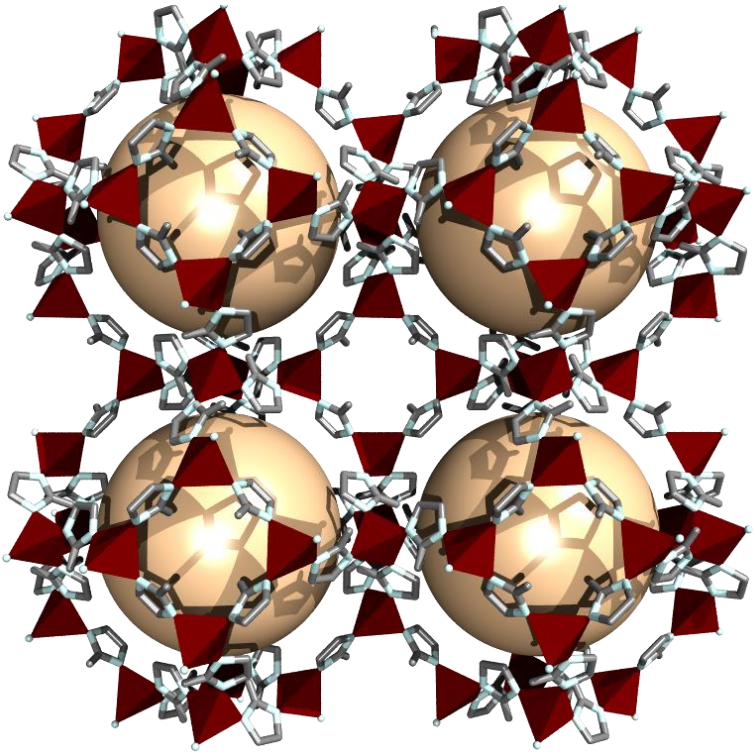

Figure 1.5: Structure of ZIF-8. Zinc acetate and 2-methylimidazole can be used to synthesize ZIF-8 under biocompatible conditions, allowing enzymes to be encapsulated in the MOF.

Intriguingly, certain HmIM:Zn molar ratios, such as 4:1, only result in formation of *sod*-ZIF-8 in the presence of protein.[48] Studies have shown that proteins promote the formation of the framework by accumulating zinc ions,[71] akin to how biological systems naturally promote the construction of materials such as shell and bone.[72] This naturally occurring process is known as biomineralization,[72] with the occurrence for artificial materials such as ZIF-8 referred to as biomimetic mineralization.[48] However, biomimetic mineralization does not form sodalite ZIF-8 in a single step as per forced precipitation using higher HmIM:Zn ratios. Instead, an ethanol wash and air-dry is required to convert the initial, amorphous product into a sodalite material.[67] Furthermore, the biomimetic mineralization process using a 4:1 HmIM:Zn ratio is not universally applicable to all proteins. Doonan and co-workers (2018) found that certain proteins including haemoglobin, myoglobin, trypsin, and lysozyme did not induce the formation of ZIF-8.[71] Further investigation revealed that proteins with a zeta potential lower (i.e. more negative) than -30.4 mV were able to nucleate ZIF-8 growth, whilst proteins with a zeta potential greater (i.e. less negative) than -21 mV were unable to form ZIF-8.[71] By surface functionalization, the zeta potential of certain proteins was shifted to either induce or inhibit biomimetic mineralization, further verifying the observed trend.[71] For situations in which surface functionalization is not practical, it is important to note that ZIF-8 formation can be forced by using a higher HmIM:Zn ratio.

ZIF-8 shows substantial ability to protect encapsulated enzymes from harsh conditions. For example, encapsulated horseradish peroxidase retains activity after being subjected to a variety of conditions, including exposure to a proteolytic agent, thermal treatment, and thermal treatment in an organic solvent (**Figure 1.6A**).[48] Likewise, urease demonstrates increased resistance to thermal treatment when encapsulated in ZIF-8 (**Figure 1.6B**).[48] Typically, under ambient conditions, encapsulated enzymes show reduced activity relative to the free enzyme, due to limited diffusion of reagents and products through the framework.[41] However, there are exceptional cases in which enzymes demonstrate enhanced activity in ZIF-8. For example, cytochrome C was shown to be over ten times more active when encapsulated in ZIF-8. This is due to increased substrate affinity for H_2O_2, potentially due to conformational changes after incubation in methanol that result in exposure of the heme group, in addition to subtle changes in the enzyme microenvironment caused by immobilization.[47] Other enzymes which have been encapsulated and protected in ZIF-8 include urease,[48, 73] pyroloquinoline quinonedependent glucose dehydrogenase,[48]

Candida antarctica lipase B,[74] laccase,[75] and thermophilic lipase QLM,[44] amongst many others. The diversity of enzymes which can be encapsulated in ZIF-8 allows for the construction of multi-enzyme biocomposites tailored for a specific catalytic pathway.[76] This further broadens the potential applications of ZIF-8 biocomposites.

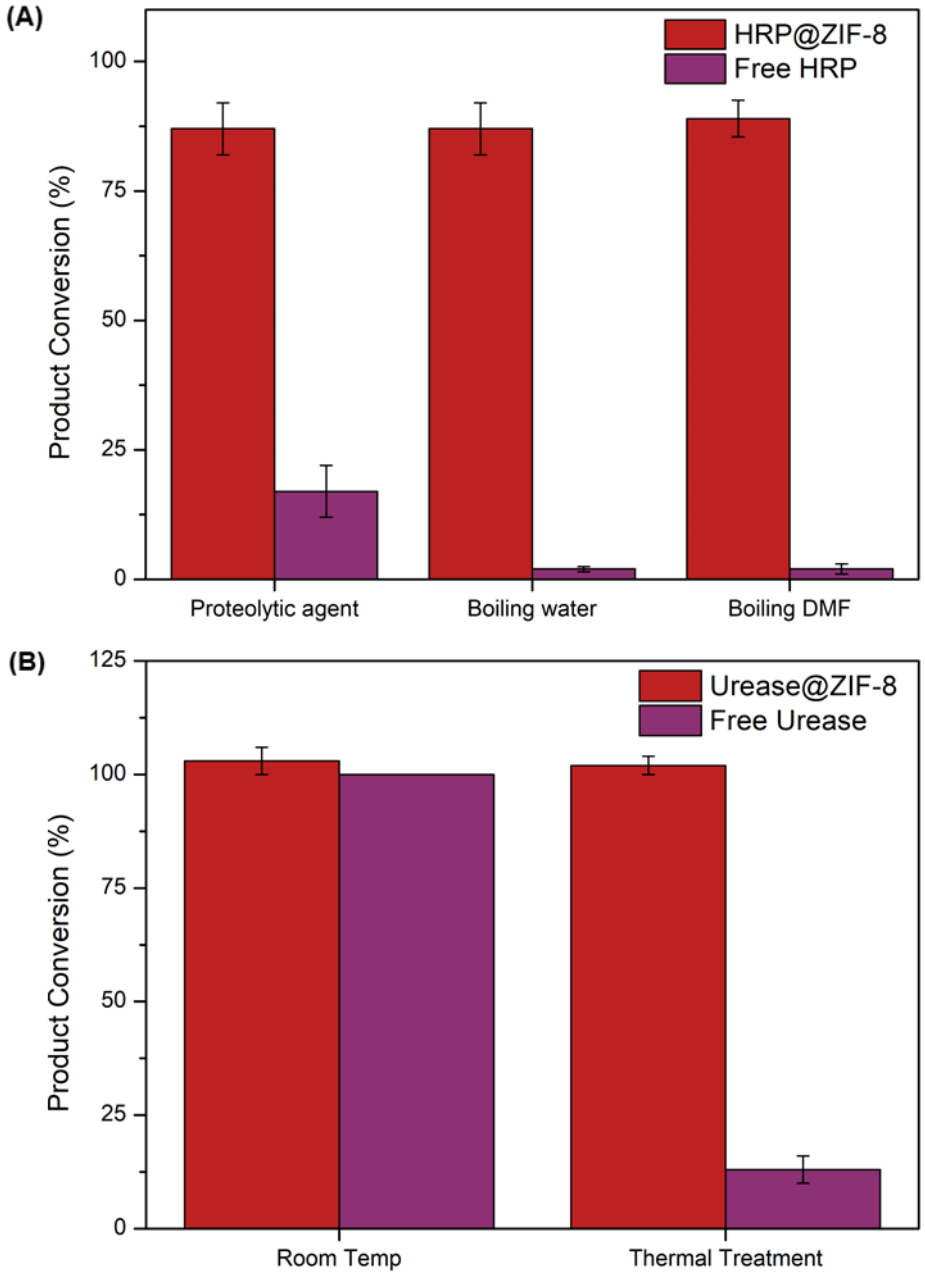

Figure 1.6: (**A**) Activity retention of horseradish peroxidase@ZIF-8 biocomposites after exposure to proteolysis, boiling water, and boiling DMF. (**B**) Activity retention of urease@ZIF-8 biocomposites after thermal treatment (figure adapted from ref. 48). Encapsulation in ZIF-8 provides protection of these enzymes from harsh conditions.

However, not all enzymes retain activity when encapsulated in ZIF-8. For example, catalase, which catalyzes the breakdown of hydrogen peroxide to oxygen and water,[77-81] shows negligible activity when immobilized in/on ZIF-8 (**Figure 1.7**).[45] Since immobilization on the surface of ZIF-8 yields an inactive composite, this is not due to limited diffusion of hydrogen peroxide or its degradation products through the framework.[45] Rather, catalase is thought to interact with the hydrophobic surface of ZIF-8, resulting in partial unfolding and rendering the enzyme inactive.[45] To avoid this, alternative, hydrophilic frameworks can be used. Two such frameworks are ZIF-90 and MAF-7. These MOFs are topologically identical to *sod*-ZIF-8, however instead utilize imidazolate-2-carboxaldehyde (HICA) and 3-methyl-1,2,4-triazolate (Hmtz) linkers, for ZIF-90 and MAF-7, respectively.[62, 82] These linkers are more polar than HmIM, making the frameworks more hydrophilic and thus allowing adsorbed or encapsulated catalase to maintain its native structure and function (**Figure 1.7**).[45] This further broadens the catalogue of enzymes which can be used to make active MOF biocomposites.

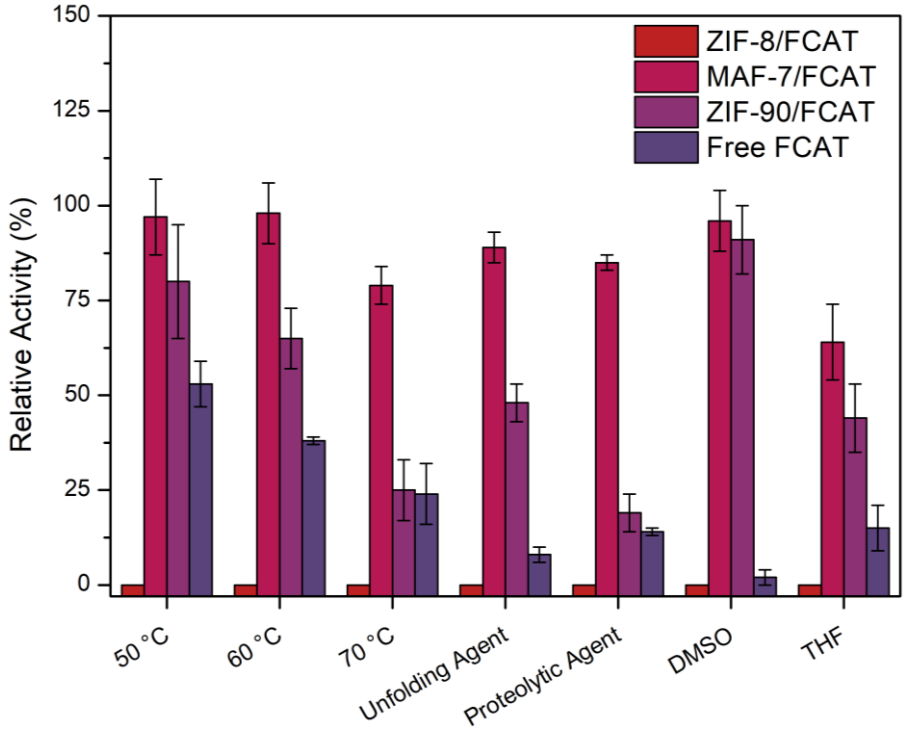

Figure 1.7: Activity of catalase encapsulated in ZIF-8, MAF-7, and ZIF-90, after thermal treatment, in the presence of an unfolding agent (urea), in the presence of a proteolytic agent (protease), and after exposure to organic solvents (figure adapted from ref. 45). Catalase shows no activity when encapsulated in ZIF-8, whilst MAF-7 and ZIF-90 biocomposites retain activity and demonstrate increased resistance to harsh conditions.

However, there remains some enzymes for which activity retention has not been observed in any MOFs. Alcohol oxidase from *pichia pastoris*, for instance, is unable to function in ZIF-8, ZIF-90, or MAF-7.[42] Thus, though MOFs have demonstrated significant potential as supports for enzyme immobilization, benefitted by their synthesis from cheap, readily available precursors, they are not the definitive method of protecting enzymes for biocatalysis. For a more broadly applicable enzyme immobilization system, alternative frameworks must be considered.

1.5 Hydrogen-bonded Organic Frameworks for Enzyme Immobilization

A relatively new class of supports for biomolecule encapsulation is hydrogen-bonded organic frameworks (HOFs), which hold promise for use in situations where MOFs are ineffective. HOFs have similar structural features to MOFs, however do not require metal nodes and instead rely on hydrogen bonding interactions between organic linkers to form a crystalline structure. The first HOF was reported in 1969, consisting of trimesic acid units linked by the $R_2^2(8)$ hydrogen bonding motif between carboxylic acid groups.[83] However, applications were limited in the following decades as permanent porosity had not been demonstrated.[84] It wasn't until the early 2010s that permanent porosity was achieved,[84-89] by which point numerous motifs had been utilized in the construction of HOFs (**Figure 1.8**). Like MOFs, the porosity of HOFs lends them to a broad variety of potential applications such as gas capture and storage,[85, 90] molecular separations,[86] and molecular recognition,[91], in addition to more novel applications such as antimicrobial membrane construction[92] and relative temperature sensing.[93]

HOFs have many unique features that make them well-suited for biocatalysis applications. The flexible and reversible nature of hydrogen bonds means that HOFs can be synthesized under relatively mild conditions,[94] with stable, porous HOFs able to be constructed in water at room temperature.[42, 95-97] This means a broad variety of framework topologies, with potentially enhanced porosity over biocompatible MOFs, may be attained. Compared to ZIF-8, the stability of HOFs in water/buffers is also enhanced,[42, 74, 89, 98-104] resulting in biocomposites that are more compatible with biological conditions. Finally, being metal-free, HOFs can have relatively low toxicity,[94, 105] and thus the encapsulation of biomolecules in HOFs may be extended to other biological applications, such as drug delivery, in the future. Meanwhile, MOFs such as ZIF-8 have shown mixed toxicity results,[105-108] and thus have limited potential for such applications. As such, HOFs are an ideal candidate for a broad variety of biological applications, with biocatalysis representing only a small portion of these potential uses.

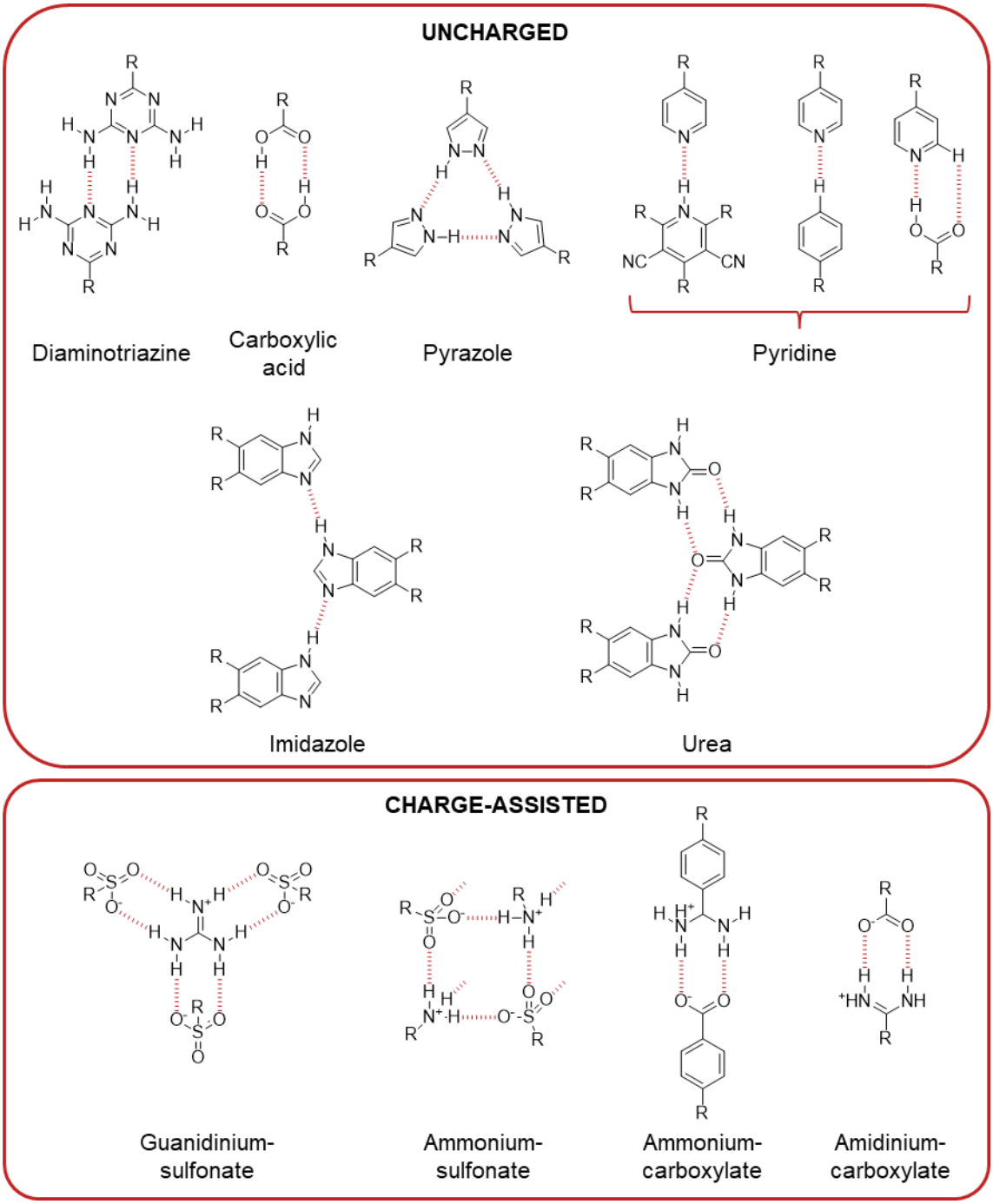

Figure 1.8: Examples of common hydrogen bonding motifs used in the construction of porous HOFs (figure adapted from refs. 89, 94, 109, 110). This work focusses primarily on the amidinium-carboxylate hydrogen bonding motif.

Biomolecule encapsulation in HOFs was first reported in 2019, utilizing a framework composed of tetrahedral amidinium and carboxylate linkers,[42, 110, 111] henceforth referred to as BioHOF-1. When sodium 4,4',4",4"'-methanetetrayltetrabenzoate (tetra-carboxylate) and 4,4',4",4"'-methanetetrayltetrabenzimidamide hydrochloride (tetra-amidinium) are combined in the presence of protein, it enables the formation of the HOF

around the protein (**Scheme 1.1**). As opposed to ZIF-8, the protein itself does not actively nucleate HOF growth, rather the protein is incorporated into the framework via particle aggregation. The framework has a limiting pore aperture of 6.4 Å, significantly greater than the 3.4 Å pore aperture of ZIF-8.[70] This enables faster diffusion of substrates and products to and from the encapsulated enzyme, leading to higher conversion rates, as well as broadening the size range of substrates that can be used. Certain enzymes retain activity inside BioHOF-1 that have no activity inside MOF-based biocomposites. For example, alcohol oxidase, which was previously stated to have no activity when encapsulated in ZIF-8, ZIF-90 and MAF-7, retains activity when encapsulated in BioHOF-1 (**Figure 1.9**).[42] Catalase also shows activity encapsulated within the HOF, not exhibiting the detrimental hydrophobic surface interaction which occurs for catalase@ZIF-8 samples.[42] As such, HOFs have significant potential for use in a broader range of biocatalysis applications than existing MOF systems.

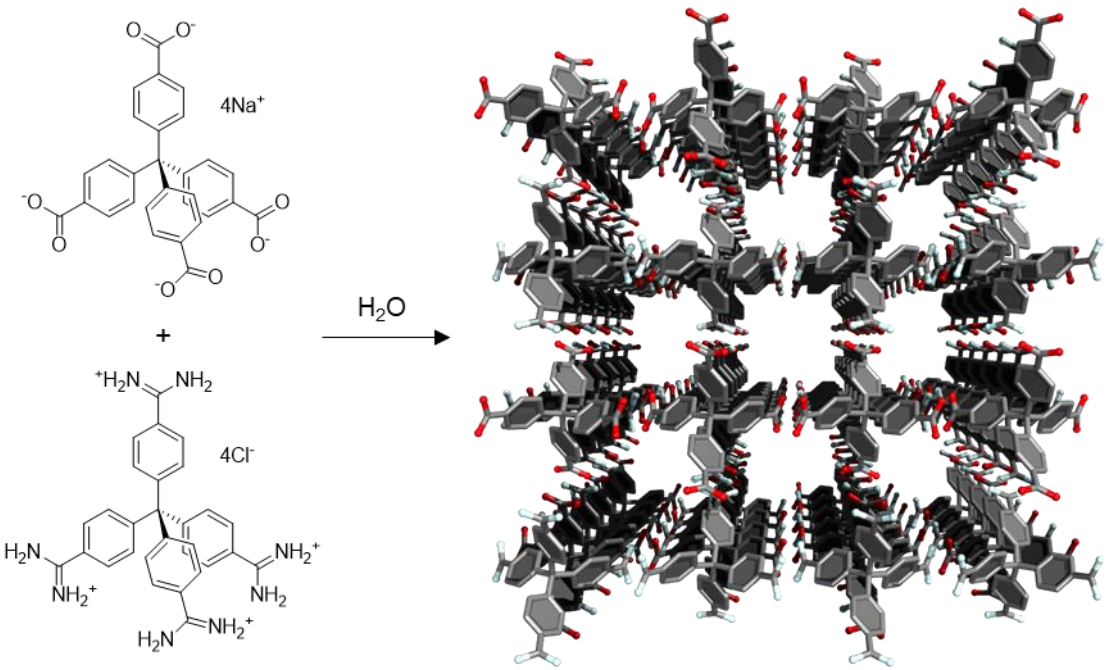

Scheme 1.1: BioHOF-1 formation from tetra-carboxylate and tetra-amidinium linkers. BioHOF-1 can be synthesized under biocompatible conditions, allowing enzymes to be encapsulated in the HOF.

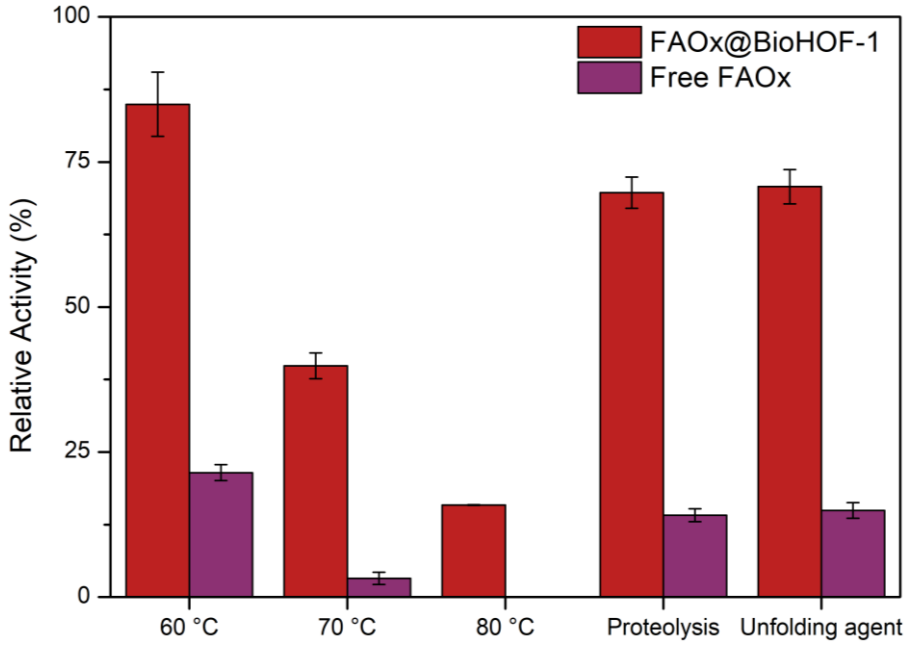

Figure 1.9: Activity of alcohol oxidase encapsulated in BioHOF-1 after thermal treatment, in the presence of a proteolytic agent (trypsin), and in the presence of an unfolding agent (urea) (figure adapted from ref. 42). When encapsulated, alcohol oxidase exhibits enhanced resistance to these harsh conditions.

Since the use of BioHOF-1 for enzyme immobilization, biomolecule encapsulation has been achieved using a variety of other HOFs. Ouyang and coworkers reported the synthesis of single-component HOF systems around a variety of proteins.[112] This process involved the addition of a planar tetra-carboxylic acid (focusing primarily on 1,3,6,8-tetrakis (p-benzoic acid) pyrene) in a small quantity of organic solvent to an aqueous solution of protein, forming frameworks with pore apertures of up to 24 Å. Intriguingly, framework formation occurred only when the samples contained protein, suggesting some form of protein-driven assembly process. The group postulated that the growth of the framework was initiated by strong hydrogen bonding interaction between the protein and the deprotonated carboxylates of the linker, resulting in a high local concentration of the linker, followed by face-to-face π-π stacking propagating crystal growth. Further research on these single-component HOFs has yielded a variety of interesting applications. For example, they can induce non-native enzymatic activity for encapsulated cytochrome c, enabling it to breakdown hydrogen peroxide similar to a catalase enzyme.[96] Encapsulation of multiple enzymes within the framework also provides an avenue for biocatalytic cascade reactions. For example, glucose oxidase and horseradish peroxidase have been co-encapsulated, enabling a cascade reaction that ultimately produces ox-TMB, a blue-colored

product, when glucose is present. This system has potential application in point-of-care diabetes testing.[95] Thus, it is clear that biocatalysis using enzyme-HOF biocomposites has significant potential to compete with existing immobilization supports.

However, limited studies have investigated the factors that impact the encapsulation of proteins in HOFs. Understanding how protein is incorporated into these frameworks is a crucial step towards their eventual use for industrial biocatalysis, as higher protein loading leads to materials that have higher activities per weight of framework and more efficiently utilize the framework precursors. Currently, the loading of proteins in BioHOF-1 remains relatively low, with the highest reported loading for unmodified protein being 6.0 ± 0.5 wt.%.[42] Studies indicate that protein surface charge can impact the loading, similar to how it can impact ZIF-8 nucleation. Falcaro and coworkers genetically engineered a protein, D-amino acid oxidase, to contain a large positively charged module attached to the N-terminus of the enzyme. This module increased the loading of protein in the framework to approximately 55 wt.%, with a 6.5-fold enhancement in specific activity. However, digestion with Trypsin, a protease, resulted in >90% loss of enzymatic activity.[113] This suggests that most of the protein immobilized is partially exposed to the surface, and thus is not as well-protected as fully encapsulated enzyme. Single-component HOFs have demonstrated higher loadings than those reported for BioHOF-1, up to 67.4 wt.%.[112] Increasing the proportion of surface amine residues increases the loading of protein in such HOFs, likely a result of the greater number of sites available for interaction between the tetra-carboxylic acid and the protein.[112] However, these studies do not thoroughly investigate if the protein is surface bound or encapsulated, and so a significant portion of the protein may be experiencing only partial protection. Thus, thorough investigation of the localization of proteins in HOFs is necessary, for both BioHOF-1 and single-component frameworks, to truly appreciate the loading of protein in these frameworks.

Overall, both MOFs and HOFs have significant potential as supports for enzyme immobilization. However, each class of framework has unique limitations, and thus neither is fully developed for use in industrial biocatalysis. For MOFs, one of the most significant issues is the limited range of enzymatic reactions that can be performed within them. This is due to the limited porosity that has been achieved for biocompatible MOFs (e.g., 3.4 Å pore aperture for ZIF-8), as well as the deactivation of certain enzymes by these MOFs upon encapsulation. Meanwhile, biocompatible HOFs can possess larger pores (e.g., 6.4 Å pore aperture for BioHOF-1) and have a less detrimental impact on the encapsulated

protein. However, the loading of protein in HOFs has not been thoroughly investigated, meaning that the cost efficiency and protective function of these composites sits below what could be theoretically achieved. If these issues were to be addressed, MOFs and HOFs would be more attractive candidates for biocatalysis applications.

1.6 Thesis Coverage

This thesis consists of four chapters, covering research into increasing the utility of porous frameworks for biocatalysis. In this first chapter, MOFs and HOFs as supports for enzyme immobilization have been introduced, alongside the current limitations of these frameworks.

Chapter 2 encompasses a variety of approaches to retain the activity of sensitive enzymes immobilized in/on ZIF-8. Focus was primarily directed towards methods of tuning the enzyme-MOF interface, to prevent detrimental interaction between the enzyme and the hydrophobic framework surface. This included incorporating the protein in a single enzyme nanogel or polymer conjugate, which was then encapsulated in ZIF-8. Limited success of these approaches led to a review of the mechanism behind the deactivation of catalase encapsulated in ZIF-8.

Chapter 3 focuses on developing approaches to increase the encapsulation of proteins in BioHOF-1, by utilizing ferritin as a model protein. Protein surface modification and use of modulators were both investigated as methods of increasing protein loading. Additionally, studies on the interaction between guanidinium-decorated polymers and protein were undertaken, with potential links to increased incorporation of protein in HOFs. With these methods resulting in a large portion of surface-bound protein, layer-by-layer encapsulation of protein@HOF biocomposites was investigated as an approach for imparting additional protection to enzymes exposed to the outside environment.

Chapter 4 provides a summary of the work, and the potential future directions for the research.

1.7 References

1. Berg, J. M.; Tymoczko, J. L.; Stryer, L. *Biochemistry, Fifth Edition*; W. H. Freeman, 2002.

2. Aebersold, R.; Agar, J. N.; Amster, I. J.; Baker, M. S.; Bertozzi, C. R.; Boja, E. S.; Costello, C. E.; Cravatt, B. F.; Fenselau, C.; Garcia, B. A.; et al. How many human proteoforms are there? *Nature Chemical Biology* **2018**, *14* (3), 206-214. DOI: 10.1038/nchembio.2576.

3. Schmid, A.; Dordick, J. S.; Hauer, B.; Kiener, A.; Wubbolts, M.; Witholt, B. Industrial biocatalysis today and tomorrow. *Nature* **2001**, *409* (6817), 258-268. DOI: 10.1038/35051736.

4. Greimel, K. J.; Perz, V.; Koren, K.; Feola, R.; Temel, A.; Sohar, C.; Herrero Acero, E.; Klimant, I.; Guebitz, G. M. Banning toxic heavy-metal catalysts from paints: enzymatic cross-linking of alkyd resins. *Green Chemistry* **2013**, *15* (2), 381-388. DOI: 10.1039/C2GC36666E.

5. Hobbs, L. Chapter 21 - sweeteners from starch: Production, properties and uses. In *Starch (Third Edition)*, BeMiller, J., Whistler, R. Eds.; Academic Press, 2009; pp 797-832.

6. White, J. S. Sucrose, HFCS, and fructose: History, manufacture, composition, applications, and production. In *Fructose, high fructose corn syrup, sucrose and health*, Rippe, J. M. Ed.; Springer New York, 2014; pp 13-33.

7. Wells, A. S.; Finch, G. L.; Michels, P. C.; Wong, J. W. Use of enzymes in the manufacture of active pharmaceutical ingredients - A science and safety-based approach to ensure patient safety and drug quality. *Organic Process Research & Development* **2012**, *16* (12), 1986-1993. DOI: 10.1021/op300153b.

8. Grand View Research. *Industrial Enzymes Market Size, Share & Trends Analysis Report By Product (Carbohydrases, Proteases, Lipases, Polymerases & Nucleases), By Source, By Application, By Region, And Segment Forecasts, 2020 - 2027*; San Francisco, 2020. https://www.grandviewresearch.com/industry-analysis/industrial-enzymes-market.

9. Jin, L. Q.; Xu, Q.; Liu, Z. Q.; Jia, D. X.; Liao, C. J.; Chen, D. S.; Zheng, Y. G. Immobilization of recombinant glucose isomerase for efficient production of high fructose corn syrup. *Applied Biochemistry and Biotechnology* **2017**, *183* (1), 293-306. DOI: 10.1007/s12010-017-2445-0.

10. Quax, W. J.; Mrabet, N. T.; Luiten, R. G. M.; Schuurhuizen, P. W.; Stanssens, P.; Lasters, I. Enhancing the thermostability of glucose isomerase by protein engineering. *Nature Biotechnology* **1991**, *9* (8), 738-742. DOI: 10.1038/nbt0891-738.

11. Gilliland, G. L.; Oliva, M. T.; Dill, J. Functional implications of the three-dimensional structure of Bovine chymosin. In *Structure and Function of the Aspartic Proteinases: Genetics, Structures, and Mechanisms*, Dunn, B. M. Ed.; Springer US, 1991; pp 23-37.

12. de Souza, P. M.; de Oliveira Magalhães, P. Application of microbial α-amylase in industry - A review. *Brazilian Journal of Microbiology* **2010**, *41* (4), 850-861. DOI: 10.1590/s1517-83822010000400004.

13. Bruggink, A.; Roos, E. C.; de Vroom, E. Penicillin Acylase in the Industrial Production of β-Lactam Antibiotics. *Organic Process Research & Development* **1998**, *2* (2), 128-133. DOI: 10.1021/op9700643.

14. Ejaz, U.; Sohail, M.; Ghanemi, A. Cellulases: From bioactivity to a variety of industrial applications. *Biomimetics* **2021**, *6* (3). DOI: 10.3390/biomimetics6030044.

15. Sun, P. D.; Foster, C. E.; Boyington, J. C. Overview of protein structural and functional folds. *Current Protocols in Protein Science* **2004**, *Chapter 17* (1), Unit 17.11. DOI: 10.1002/0471140864.ps1701s35.

16. Krüger, M.; Linke, W. A. The giant protein titin: a regulatory node that integrates myocyte signaling pathways. *Journal of Biological Chemistry* **2011**, *286* (12), 9905-9912. DOI: 10.1074/jbc.R110.173260.

17. Newberry, R. W.; Raines, R. T. Secondary forces in protein folding. *ACS Chemical Biology* **2019**, *14* (8), 1677-1686. DOI: 10.1021/acschembio.9b00339.

18. Karimi, M.; Ignasiak, M. T.; Chan, B.; Croft, A. K.; Radom, L.; Schiesser, C. H.; Pattison, D. I.; Davies, M. J. Reactivity of disulfide bonds is markedly affected by structure and environment: implications for protein modification and stability. *Scientific Reports* **2016**, *6* (1), 38572. DOI: 10.1038/srep38572.

19. Boron, W. F. Regulation of intracellular pH. *Advances in Physiology Education* **2004**, *28* (4), 160-179. DOI: 10.1152/advan.00045.2004.

20. Katschinski, D. M. On heat and cells and proteins. *Physiology* **2004**, *19* (1), 11-15. DOI: 10.1152/nips.01403.2002.

21. Serdakowski, A. L.; Dordick, J. S. Enzyme activation for organic solvents made easy. *Trends in Biotechnology* **2008**, *26* (1), 48-54. DOI: 10.1016/j.tibtech.2007.10.007.

22. Robinson, P. K. Enzymes: Principles and biotechnological applications. *Essays Biochem* **2015**, *59*, 1-41. DOI: 10.1042/bse0590001.

23. Stepankova, V.; Bidmanova, S.; Koudelakova, T.; Prokop, Z.; Chaloupkova, R.; Damborsky, J. Strategies for stabilization of enzymes in organic solvents. *ACS Catalysis* **2013**, *3* (12), 2823-2836. DOI: 10.1021/cs400684x.

24. Eppler, R. K.; Komor, R. S.; Huynh, J.; Dordick, J. S.; Reimer, J. A.; Clark, D. S. Water dynamics and salt-activation of enzymes in organic media: mechanistic implications revealed by NMR spectroscopy. *Proc Natl Acad Sci U S A* **2006**, *103* (15), 5706-5710. DOI: 10.1073/pnas.0601113103.

25. van Unen, D.-J.; Engbersen, J. F. J.; Reinhoudt, D. N. Why do crown ethers activate enzymes in organic solvents? *Biotechnology and Bioengineering* **2002**, *77* (3), 248-255. DOI: 10.1002/bit.10032.

26. Chen, K.; Arnold, F. H. Tuning the activity of an enzyme for unusual environments: sequential random mutagenesis of subtilisin E for catalysis in dimethylformamide. *Proc Natl Acad Sci U S A* **1993**, *90* (12), 5618-5622. DOI: 10.1073/pnas.90.12.5618.

27. Yu, H.; Yan, Y.; Zhang, C.; Dalby, P. A. Two strategies to engineer flexible loops for improved enzyme thermostability. *Scientific Reports* **2017**, *7* (1), 41212. DOI: 10.1038/srep41212.

28. DeSantis, G.; Jones, J. B. Chemical modification of enzymes for enhanced functionality. *Current Opinion in Biotechnology* **1999**, *10* (4), 324-330. DOI: 10.1016/S0958-1669(99)80059-7.

29. Rodriguez-Abetxuko, A.; Morant-Miñana, M. C.; López-Gallego, F.; Yate, L.; Seifert, A.; Knez, M.; Beloqui, A. Imidazole-grafted nanogels for the fabrication of organic–inorganic protein hybrids. *Advanced Functional Materials* **2018**, *28* (35), 1803115. DOI: 10.1002/adfm.201803115.

30. Beloqui, A.; Kobitski, A. Y.; Nienhaus, G. U.; Delaittre, G. A simple route to highly active single-enzyme nanogels. *Chemical Science* **2018**, *9* (4), 1006-1013. DOI: 10.1039/C7SC04438K.

31. Beloqui, A.; Baur, S.; Trouillet, V.; Welle, A.; Madsen, J.; Bastmeyer, M.; Delaittre, G. Single-molecule encapsulation: A straightforward route to highly stable and printable enzymes. *Small* **2016**, *12* (13), 1716-1722. DOI: 10.1002/smll.201503405.

32. Chapman, R.; Stenzel, M. H. All wrapped up: Stabilization of enzymes within single enzyme nanoparticles. *Journal of the American Chemical Society* **2019**, *141* (7), 2754-2769. DOI: 10.1021/jacs.8b10338.

33. Yan, M.; Ge, J.; Liu, Z.; Ouyang, P. Encapsulation of single enzyme in nanogel with enhanced biocatalytic activity and stability. *Journal of the American Chemical Society* **2006**, *128* (34), 11008-11009. DOI: 10.1021/ja064126t.

34. Rodriguez-Abetxuko, A.; Morant-Miñana, M. C.; Knez, M.; Beloqui, A. Carrierless immobilization route for highly robust metal–organic hybrid enzymes. *ACS Omega* **2019**, *4* (3), 5172-5179. DOI: 10.1021/acsomega.8b03559.

35. Hirsh, S. L.; Bilek, M. M. M.; Nosworthy, N. J.; Kondyurin, A.; dos Remedios, C. G.; McKenzie, D. R. A comparison of covalent immobilization and physical adsorption of a cellulase enzyme mixture. *Langmuir* **2010**, *26* (17), 14380-14388. DOI: 10.1021/la1019845.

36. Morhardt, C.; Ketterer, B.; Heißler, S.; Franzreb, M. Direct quantification of immobilized enzymes by means of FTIR ATR spectroscopy – A process analytics tool for biotransformations applying non-porous magnetic enzyme carriers. *Journal of Molecular Catalysis B: Enzymatic* **2014**, *107*, 55-63. DOI: 10.1016/j.molcatb.2014.05.018.

37. Sheldon, R. A.; van Pelt, S. Enzyme immobilisation in biocatalysis: why, what and how. *Chemical Society Reviews* **2013**, *42* (15), 6223-6235, 10.1039/C3CS60075K. DOI: 10.1039/C3CS60075K.

38. Maddigan, N. K. Enzyme immobilisation using porous frameworks. University of Adelaide, Adelaide, 2020. https://hdl.handle.net/2440/126087.

39. Datta, S.; Christena, L. R.; Rajaram, Y. R. S. Enzyme immobilization: an overview on techniques and support materials. *3 Biotech* **2013**, *3* (1), 1-9. DOI: 10.1007/s13205-012-0071-7 PubMed.

40. Wang, X.; Lan, P. C.; Ma, S. Metal–organic frameworks for enzyme immobilization: beyond host matrix materials. *ACS Central Science* **2020**, *6* (9), 1497-1506. DOI: 10.1021/acscentsci.0c00687.

41. Liang, W.; Wied, P.; Carraro, F.; Sumby, C. J.; Nidetzky, B.; Tsung, C.-K.; Falcaro, P.; Doonan, C. J. Metal–organic framework-based enzyme biocomposites. *Chemical Reviews* **2021**, *121* (3), 1077-1129. DOI: 10.1021/acs.chemrev.0c01029.

42. Liang, W.; Carraro, F.; Solomon, M. B.; Bell, S. G.; Amenitsch, H.; Sumby, C. J.; White, N. G.; Falcaro, P.; Doonan, C. J. Enzyme encapsulation in a porous hydrogen-bonded organic framework. *Journal of the American Chemical Society* **2019**, *141* (36), 14298-14305. DOI: 10.1021/jacs.9b06589.

43. Sheldon, R. A. Cross-linked enzyme aggregates as industrial biocatalysts. *Organic Process Research & Development* **2011**, *15* (1), 213-223. DOI: 10.1021/op100289f.

44. He, H.; Han, H.; Shi, H.; Tian, Y.; Sun, F.; Song, Y.; Li, Q.; Zhu, G. Construction of thermophilic lipase-embedded metal-organic frameworks via biomimetic mineralization: A biocatalyst for ester hydrolysis and kinetic resolution. *ACS Applied Materials & Interfaces* **2016**, *8* (37), 24517-24524. DOI: 10.1021/acsami.6b05538.

45. Liang, W.; Xu, H.; Carraro, F.; Maddigan, N. K.; Li, Q.; Bell, S. G.; Huang, D. M.; Tarzia, A.; Solomon, M. B.; Amenitsch, H.; et al. Enhanced activity of enzymes encapsulated in hydrophilic metal–organic frameworks. *Journal of the American Chemical Society* **2019**, *141* (6), 2348-2355. DOI: 10.1021/jacs.8b10302.

46. Shieh, F.-K.; Wang, S.-C.; Yen, C.-I.; Wu, C.-C.; Dutta, S.; Chou, L.-Y.; Morabito, J. V.; Hu, P.; Hsu, M.-H.; Wu, K. C. W.; et al. Imparting functionality to biocatalysts via embedding enzymes into nanoporous materials by a de novo approach: Size-selective sheltering of catalase in metal-organic framework microcrystals. *Journal of the American Chemical Society* **2015**, *137* (13), 4276-4279. DOI: 10.1021/ja513058h.

47. Lyu, F.; Zhang, Y.; Zare, R. N.; Ge, J.; Liu, Z. One-pot synthesis of protein-embedded metal–organic frameworks with enhanced biological activities. *Nano Letters* **2014**, *14* (10), 5761-5765. DOI: 10.1021/nl5026419.

48. Liang, K.; Ricco, R.; Doherty, C. M.; Styles, M. J.; Bell, S.; Kirby, N.; Mudie, S.; Haylock, D.; Hill, A. J.; Doonan, C. J.; et al. Biomimetic mineralization of metal-organic frameworks as protective coatings for biomacromolecules. *Nature Communications* **2015**, *6* (1), 7240. DOI: 10.1038/ncomms8240.

49. Cao, L.; Langen, L. v.; Sheldon, R. A. Immobilised enzymes: carrier-bound or carrier-free? *Current Opinion in Biotechnology* **2003**, *14* (4), 387-394. DOI: 10.1016/S0958-1669(03)00096-X.

50. Brena, B.; González-Pombo, P.; Batista-Viera, F. Immobilization of enzymes: A literature survey. In *Immobilization of enzymes and cells: third edition*, Guisan, J. M. Ed.; Humana Press, 2013; pp 15-31.

51. Guisán, J. Aldehyde-agarose gels as activated supports for immobilization-stabilization of enzymes. *Enzyme and Microbial Technology* **1988**, *10* (6), 375-382. DOI: 10.1016/0141-0229(88)90018-X.

52. Guisán, J. M.; Bastida, A.; Cuesta, C.; Fernandez-Lufuente, R.; Rosell, C. M. Immobilization-stabilization of alpha-chymotrypsin by covalent attachment to aldehyde-agarose gels. *Biotechnology and Bioengineering* **1991**, *38* (10), 1144-1152. DOI: 10.1002/bit.260381005.

53. Homaei, A. A.; Sariri, R.; Vianello, F.; Stevanato, R. Enzyme immobilization: an update. *Journal of Chemical Biology* **2013**, *6* (4), 185-205. DOI: 10.1007/s12154-013-0102-9.

54. Garcia-Galan, C.; Berenguer-Murcia, Á.; Fernandez-Lafuente, R.; Rodrigues, R. C. Potential of different enzyme immobilization strategies to improve enzyme performance. *Advanced Synthesis & Catalysis* **2011**, *353* (16), 2885-2904. DOI: 10.1002/adsc.201100534.

55. Alezi, D.; Belmabkhout, Y.; Suyetin, M.; Bhatt, P. M.; Weseliński, Ł. J.; Solovyeva, V.; Adil, K.; Spanopoulos, I.; Trikalitis, P. N.; Emwas, A.-H.; et al. MOF crystal chemistry paving the way to gas storage needs: Aluminum-based soc-MOF for CH4, O2, and CO2 storage. *Journal of the American Chemical Society* **2015**, *137* (41), 13308-13318. DOI: 10.1021/jacs.5b07053.

56. Zhang, M.; Dai, Q.; Zheng, H.; Chen, M.; Dai, L. Novel MOF-derived Co@N-C bifunctional catalysts for highly efficient Zn–air batteries and water splitting. *Advanced Materials* **2018**, *30* (10), 1705431. DOI: 10.1002/adma.201705431.

57. Zhang, Y.; Feng, X.; Yuan, S.; Zhou, J.; Wang, B. Challenges and recent advances in MOF–polymer composite membranes for gas separation. *Inorganic Chemistry Frontiers* **2016**, *3* (7), 896-909, 10.1039/C6QI00042H. DOI: 10.1039/C6QI00042H.

58. Lu, G.; Li, S.; Guo, Z.; Farha, O. K.; Hauser, B. G.; Qi, X.; Wang, Y.; Wang, X.; Han, S.; Liu, X.; et al. Imparting functionality to a metal–organic framework material by controlled nanoparticle encapsulation. *Nature Chemistry* **2012**, *4* (4), 310-316. DOI: 10.1038/nchem.1272.

59. Pan, Y.; Sun, K.; Liu, S.; Cao, X.; Wu, K.; Cheong, W.-C.; Chen, Z.; Wang, Y.; Li, Y.; Liu, Y.; et al. Core-shell ZIF-8@ZIF-67-derived CoP nanoparticle-embedded N-doped carbon nanotube hollow polyhedron for efficient overall water splitting. *Journal of the American Chemical Society* **2018**, *140* (7), 2610-2618. DOI: 10.1021/jacs.7b12420.

60. Chen, Y.; Lykourinou, V.; Vetromile, C.; Hoang, T.; Ming, L.-J.; Larsen, R. W.; Ma, S. How can proteins enter the interior of a MOF? Investigation of cytochrome c translocation into a MOF consisting of mesoporous cages with microporous windows. *Journal of the American Chemical Society* **2012**, *134* (32), 13188-13191. DOI: 10.1021/ja305144x.

61. Navarro-Sánchez, J.; Almora-Barrios, N.; Lerma-Berlanga, B.; Ruiz-Pernía, J. J.; Lorenz-Fonfria, V. A.; Tuñón, I.; Martí-Gastaldo, C. Translocation of enzymes into a

mesoporous MOF for enhanced catalytic activity under extreme conditions. *Chemical Science* **2019**, *10* (14), 4082-4088. DOI: 10.1039/C9SC00082H.

62. Liguori, P. F.; Russo, B.; Melicchio, A.; Golemme, G. Synthesis and gas sorption behaviour of ZIF-90 with large pore volume. *New Journal of Chemistry* **2017**, *41* (22), 13235-13239. DOI: 10.1039/C7NJ03192K.

63. Akimbekov, Z.; Katsenis, A. D.; Nagabhushana, G. P.; Ayoub, G.; Arhangelskis, M.; Morris, A. J.; Friščić, T.; Navrotsky, A. Experimental and theoretical evaluation of the stability of true MOF polymorphs explains their mechanochemical interconversions. *Journal of the American Chemical Society* **2017**, *139* (23), 7952-7957. DOI: 10.1021/jacs.7b03144.

64. Katsenis, A. D.; Puškarić, A.; Štrukil, V.; Mottillo, C.; Julien, P. A.; Užarević, K.; Pham, M.-H.; Do, T.-O.; Kimber, S. A. J.; Lazić, P.; et al. In situ X-ray diffraction monitoring of a mechanochemical reaction reveals a unique topology metal-organic framework. *Nature Communications* **2015**, *6* (1), 6662. DOI: 10.1038/ncomms7662.

65. Jian, M.; Liu, B.; Liu, R.; Qu, J.; Wang, H.; Zhang, X. Water-based synthesis of zeolitic imidazolate framework-8 with high morphology level at room temperature. *RSC Advances* **2015**, *5* (60), 48433-48441. DOI: 10.1039/C5RA04033G.

66. Carraro, F.; Velásquez-Hernández, M. d. J.; Astria, E.; Liang, W.; Twight, L.; Parise, C.; Ge, M.; Huang, Z.; Ricco, R.; Zou, X.; et al. Phase dependent encapsulation and release profile of ZIF-based biocomposites. *Chemical Science* **2020**, *11* (13), 3397-3404. DOI: 10.1039/C9SC05433B.

67. Liang, W.; Ricco, R.; Maddigan, N. K.; Dickinson, R. P.; Xu, H.; Li, Q.; Sumby, C. J.; Bell, S. G.; Falcaro, P.; Doonan, C. J. Control of structure topology and spatial distribution of biomacromolecules in protein@ZIF-8 biocomposites. *Chemistry of Materials* **2018**, *30* (3), 1069-1077. DOI: 10.1021/acs.chemmater.7b04977.

68. Chen, R.; Yao, J.; Gu, Q.; Smeets, S.; Baerlocher, C.; Gu, H.; Zhu, D.; Morris, W.; Yaghi, O. M.; Wang, H. A two-dimensional zeolitic imidazolate framework with a cushion-shaped cavity for CO2 adsorption. *Chemical Communications* **2013**, *49* (82), 9500-9502. DOI: 10.1039/C3CC44342F.

69. Yang, F.; Mu, H.; Wang, C.; Xiang, L.; Yao, K. X.; Liu, L.; Yang, Y.; Han, Y.; Li, Y.; Pan, Y. Morphological map of ZIF-8 crystals with five distinctive shapes: Feature of filler in mixed-matrix membranes on C3H6/C3H8 separation. *Chemistry of Materials* **2018**, *30* (10), 3467-3473. DOI: 10.1021/acs.chemmater.8b01073.

70. Venna, S. R.; Zhu, M.; Li, S.; Carreon, M. A. Knudsen diffusion through ZIF-8 membranes synthesized by secondary seeded growth. *Journal of Porous Materials* **2014**, *21* (2), 235-240. DOI: 10.1007/s10934-013-9768-1.

71. Maddigan, N. K.; Tarzia, A.; Huang, D. M.; Sumby, C. J.; Bell, S. G.; Falcaro, P.; Doonan, C. J. Protein surface functionalisation as a general strategy for facilitating biomimetic mineralisation of ZIF-8. *Chemical Science* **2018**, *9* (18), 4217-4223. DOI: 10.1039/C8SC00825F.

72. Estroff, L. A. Introduction: Biomineralization. *Chemical Reviews* **2008**, *108* (11), 4329-4331. DOI: 10.1021/cr8004789.

73. Liang, K.; Coghlan, C. J.; Bell, S. G.; Doonan, C.; Falcaro, P. Enzyme encapsulation in zeolitic imidazolate frameworks: a comparison between controlled co-precipitation and biomimetic mineralisation. *Chemical Communications* **2016**, *52* (3), 473-476. DOI: 10.1039/C5CC07577G.

74. Maddigan, N. K.; Linder-Patton, O. M.; Falcaro, P.; Sumby, C. J.; Bell, S. G.; Doonan, C. J. Influence of the synthesis and storage conditions on the activity of Candida antarctica lipase B ZIF-8 biocomposites. *ACS Applied Materials & Interfaces* **2021**. DOI: 10.1021/acsami.1c04785.

75. Knedel, T.-O.; Ricklefs, E.; Schlüsener, C.; Urlacher, V. B.; Janiak, C. Laccase encapsulation in ZIF-8 metal-organic framework shows stability enhancement and substrate selectivity. *ChemistryOpen* **2019**, *8* (11), 1337-1344. DOI: 10.1002/open.201900146.

76. Liang, J.; Liang, K. Multi-enzyme cascade reactions in metal-organic frameworks. *The Chemical Record* **2020**, *20* (10), 1100-1116. DOI: 10.1002/tcr.202000067.

77. Margoliash, E.; Novogrodsky, A.; Schejter, A. Irreversible reaction of 3-amino-1:2:4-triazole and related inhibitors with the protein of catalase. *Biochemical Journal* **1960**, *74* (2), 339-348. DOI: 10.1042/bj0740339.

78. Chelikani, P.; Fita, I.; Loewen, P. C. Diversity of structures and properties among catalases. *Cellular and Molecular Life Sciences* **2004**, *61* (2), 192-208. DOI: 10.1007/s00018-003-3206-5.

79. Ou, P.; Wolff, S. P. A discontinuous method for catalase determination at 'near physiological' concentrations of H2O2 and its application to the study of H2O2 fluxes within cells. *Journal of Biochemical and Biophysical Methods* **1996**, *31* (1), 59-67. DOI: 10.1016/0165-022X(95)00039-T.

80. Reid, T. J., 3rd; Murthy, M. R.; Sicignano, A.; Tanaka, N.; Musick, W. D.; Rossmann, M. G. Structure and heme environment of beef liver catalase at 2.5 A resolution. *Proc Natl Acad Sci U S A* **1981**, *78* (8), 4767-4771. DOI: 10.1073/pnas.78.8.4767.

81. Prakash, K.; Prajapati, S.; Ahmad, A.; Jain, S. K.; Bhakuni, V. Unique oligomeric intermediates of bovine liver catalase. *Protein Science* **2002**, *11* (1), 46-57. DOI: 10.1110/ps.20102.

82. Gao, H.; Wei, W.; Dong, L.; Feng, G.; Jiang, X.; Wu, R.; Lin, Z.; Li, W. Enhanced framework rigidity of a zeolitic metal-azolate via ligand substitution. *Crystals* **2017**, *7* (4), 99.

83. Duchamp, D. J.; Marsh, R. E. The crystal structure of trimesic acid (benzene-1,3,5-tricarboxylic acid). *Acta Crystallographica Section B: Structural Science, Crystal Engineering and Materials* **1969**, *25* (1), 5-19. DOI: doi:10.1107/S0567740869001713.

84. Li, P.; Ryder, M. R.; Stoddart, J. F. Hydrogen-bonded organic frameworks: A rising class of porous molecular materials. *Accounts of Materials Research* **2020**, *1* (1), 77-87. DOI: 10.1021/accountsmr.0c00019.

85. Yang, W.; Greenaway, A.; Lin, X.; Matsuda, R.; Blake, A. J.; Wilson, C.; Lewis, W.; Hubberstey, P.; Kitagawa, S.; Champness, N. R.; et al. Exceptional thermal stability in a supramolecular organic framework: Porosity and gas storage. *Journal of the American Chemical Society* **2010**, *132* (41), 14457-14469. DOI: 10.1021/ja1042935.

86. He, Y.; Xiang, S.; Chen, B. A microporous hydrogen-bonded organic framework for highly selective C2H2/C2H4 separation at ambient temperature. *Journal of the American Chemical Society* **2011**, *133* (37), 14570-14573. DOI: 10.1021/ja2066016.

87. Mastalerz, M.; Oppel, I. M. Rational construction of an extrinsic porous molecular crystal with an extraordinary high specific surface area. *Angewandte Chemie International Edition* **2012**, *51* (21), 5252-5255. DOI: 10.1002/anie.201201174.

88. Chen, T.-H.; Popov, I.; Kaveevivitchai, W.; Chuang, Y.-C.; Chen, Y.-S.; Daugulis, O.; Jacobson, A. J.; Miljanić, O. Š. Thermally robust and porous noncovalent organic framework with high affinity for fluorocarbons and CFCs. *Nature Communications* **2014**, *5* (1), 5131. DOI: 10.1038/ncomms6131.

89. Lin, R.-B.; He, Y.; Li, P.; Wang, H.; Zhou, W.; Chen, B. Multifunctional porous hydrogen-bonded organic framework materials. *Chemical Society Reviews* **2019**, *48* (5), 1362-1389. DOI: 10.1039/C8CS00155C.

90. Nandi, S.; Chakraborty, D.; Vaidhyanathan, R. A permanently porous single molecule H-bonded organic framework for selective CO2 capture. *Chemical Communications* **2016**, *52* (45), 7249-7252. DOI: 10.1039/C6CC02964G.

91. Ma, L.; Xie, Y.; Khoo, R. S. H.; Arman, H.; Wang, B.; Zhou, W.; Zhang, J.; Lin, R.-B.; Chen, B. An adaptive hydrogen-bonded organic framework for the exclusive recognition of p-xylene. *Chemistry – A European Journal* **2022**, *28* (11), e202104269. DOI: 10.1002/chem.202104269.

92. Liu, B.-T.; Pan, X.-H.; Nie, D.-Y.; Hu, X.-J.; Liu, E.-P.; Liu, T.-F. Ionic hydrogen-bonded organic frameworks for ion-responsive antimicrobial membranes. *Advanced Materials* **2020**, *32* (48), 2005912. DOI: 10.1002/adma.202005912.

93. Feng, J.-f.; Yan, X.-Y.; Ji, Z.-Y.; Liu, T.-F.; Cao, R. Fabrication of lanthanide-functionalized hydrogen-bonded organic framework films for ratiometric temperature sensing by electrophoretic deposition. *ACS Applied Materials & Interfaces* **2020**, *12* (26), 29854-29860. DOI: 10.1021/acsami.0c08354.

94. Wang, B.; Lin, R.-B.; Zhang, Z.; Xiang, S.; Chen, B. Hydrogen-bonded organic frameworks as a tunable platform for functional materials. *Journal of the American Chemical Society* **2020**, *142* (34), 14399-14416. DOI: 10.1021/jacs.0c06473.

95. Tang, Z.; Li, X.; Tong, L.; Yang, H.; Wu, J.; Zhang, X.; Song, T.; Huang, S.; Zhu, F.; Chen, G.; et al. A biocatalytic cascade in an ultrastable mesoporous hydrogen-bonded organic framework for point-of-care biosensing. *Angewandte Chemie International Edition* **2021**, *60* (44), 23608-23613. DOI: 10.1002/anie.202110351.

96. Chen, G.; Tong, L.; Huang, S.; Huang, S.; Zhu, F.; Ouyang, G. Hydrogen-bonded organic framework biomimetic entrapment allowing non-native biocatalytic activity in enzyme. *Nature Communications* **2022**, *13* (1), 4816. DOI: 10.1038/s41467-022-32454-2.

97. Tang, J.; Liu, J.; Zheng, Q.; Li, W.; Sheng, J.; Mao, L.; Wang, M. In-situ encapsulation of protein into nanoscale hydrogen-bonded organic frameworks for intracellular biocatalysis. *Angewandte Chemie International Edition* **2021**, *60* (41), 22315-22321. DOI: 10.1002/anie.202105634.

98. Luzuriaga, M. A.; Benjamin, C. E.; Gaertner, M. W.; Lee, H.; Herbert, F. C.; Mallick, S.; Gassensmith, J. J. ZIF-8 degrades in cell media, serum, and some - but not all - common laboratory buffers. *Supramolecular Chemistry* **2019**, *31* (8), 485-490. DOI: 10.1080/10610278.2019.1616089.

99. Velásquez-Hernández, M. d. J.; Ricco, R.; Carraro, F.; Limpoco, F. T.; Linares-Moreau, M.; Leitner, E.; Wiltsche, H.; Rattenberger, J.; Schröttner, H.; Frühwirt, P.; et al.

Degradation of ZIF-8 in phosphate buffered saline media. *CrystEngComm* **2019**, *21* (31), 4538-4544. DOI: 10.1039/C9CE00757A.

100. Spitsyna, A. S.; Poryvaev, A. S.; Sannikova, N. E.; Yazikova, A. A.; Kirilyuk, I. A.; Dobrynin, S. A.; Chinak, O. A.; Fedin, M. V.; Krumkacheva, O. A. Stability of ZIF-8 nanoparticles in most common cell culture media. *Molecules* **2022**, *27* (10). DOI: 10.3390/molecules27103240.

101. Gao, Y.; Doherty, C. M.; Mulet, X. A systematic study of the stability of enzyme/zeolitic imidazolate framework-8 composites in various biologically relevant solutions. *ChemistrySelect* **2020**, *5* (43), 13766-13774. DOI: 10.1002/slct.202003575.

102. Wang, H.; Jian, M.; Qi, Z.; Li, Y.; Liu, R.; Qu, J.; Zhang, X. Specific anion effects on the stability of zeolitic imidazolate framework-8 in aqueous solution. *Microporous and Mesoporous Materials* **2018**, *259*, 171-177. DOI: 10.1016/j.micromeso.2017.10.011.

103. Zhang, H.; Liu, D.; Yao, Y.; Zhang, B.; Lin, Y. S. Stability of ZIF-8 membranes and crystalline powders in water at room temperature. *Journal of Membrane Science* **2015**, *485*, 103-111. DOI: 10.1016/j.memsci.2015.03.023.

104. Sheng, L.; Yang, F.; Wang, C.; Yu, J.; Zhang, L.; Pan, Y. Comparison of the hydrothermal stability of ZIF-8 nanocrystals and polycrystalline membranes derived from zinc salt variations. *Materials Letters* **2017**, *197*, 184-187. DOI: 10.1016/j.matlet.2017.03.077.

105. Chen, L.; Zhang, B.; Chen, L.; Liu, H.; Hu, Y.; Qiao, S. Hydrogen-bonded organic frameworks: design, applications, and prospects. *Materials Advances* **2022**, *3* (9), 3680-3708. DOI: 10.1039/D1MA01173A.

106. Yang, C.; Wen, J.; Xue, Z.; Yin, X.; Li, Y.; Yuan, L. The accumulation and toxicity of ZIF-8 nanoparticles in Corbicula fluminea. *Journal of Environmental Sciences* **2023**, *127*, 91-101. DOI: 10.1016/j.jes.2022.03.020.

107. de Moura Ferraz, L. R.; Tabosa, A. É. G. A.; da Silva Nascimento, D. D. S.; Ferreira, A. S.; de Albuquerque Wanderley Sales, V.; Silva, J. Y. R.; Júnior, S. A.; Rolim, L. A.; de Souza Pereira, J. J.; Rolim-Neto, P. J. ZIF-8 as a promising drug delivery system for benznidazole: development, characterization, in vitro dialysis release and cytotoxicity. *Scientific Reports* **2020**, *10* (1), 16815. DOI: 10.1038/s41598-020-73848-w.

108. Hao, F.; Yan, Z.-Y.; Yan, X.-P. Recent advances in research on the effect of physicochemical properties on the cytotoxicity of metal–organic frameworks. *Small Science* **2022**, *2* (9), 2200044. DOI: 10.1002/smsc.202200044.

109. Liu, Y.; Xiao, W.; Yi, J. J.; Hu, C.; Park, S.-J.; Ward, M. D. Regulating the architectures of hydrogen-bonded frameworks through topological enforcement. *Journal of the American Chemical Society* **2015**, *137* (9), 3386-3392. DOI: 10.1021/jacs.5b00534.

110. White, N. G. Amidinium···carboxylate frameworks: predictable, robust, water-stable hydrogen bonded materials. *Chemical Communications* **2021**, *57* (84), 10998-11008. DOI: 10.1039/D1CC04782E.

111. Boer, S. A.; Morshedi, M.; Tarzia, A.; Doonan, C. J.; White, N. G. Molecular tectonics: A node-and-linker building block approach to a family of hydrogen-bonded frameworks. *Chemistry – A European Journal* **2019**, *25* (42), 10006-10012. DOI: 10.1002/chem.201902117.

112. Chen, G.; Huang, S.; Shen, Y.; Kou, X.; Ma, X.; Huang, S.; Tong, Q.; Ma, K.; Chen, W.; Wang, P.; et al. Protein-directed, hydrogen-bonded biohybrid framework. *Chem* **2021**. DOI: 10.1016/j.chempr.2021.07.003.

113. Wied, P.; Carraro, F.; Bolivar, J. M.; Doonan, C. J.; Falcaro, P.; Nidetzky, B. Combining a genetically engineered oxidase with hydrogen-bonded organic frameworks (HOFs) for highly efficient biocomposites. *Angewandte Chemie International Edition* **2022**, *61* (16), e202117345. DOI: 10.1002/anie.202117345.

CHAPTER 2

Improving the Activity of Sensitive Enzymes in ZIF-8

2.1 Chapter Overview

ZIF-8 has shown much potential as a support for enzyme immobilization. However, despite being the most frequently studied MOF for enzyme encapsulation, there remains several enzymes that lose function when immobilized in/on ZIF-8, such as catalase from bovine liver and alcohol oxidase from *Pichia pastoris*.[1, 2] It is thought that the loss of catalase activity is due to a change in the protein structure upon contact of catalase with the hydrophobic ZIF-8 surface, likely resulting in catalase aggregation.[1] We postulated that by utilizing some form of secondary barrier between the enzyme and the ZIF surface, we may be able to partially diminish this detrimental hydrophobic surface interaction and thus increase catalytic activity.

Two polymer-based methods were trialed to protect catalase from denaturation in/on ZIF-8. In **Section 2.2**, encapsulation of proteins in discrete single enzyme nanogels was investigated. The impact of these nanogels on the morphology and crystallinity of ZIF-8 was investigated, as well as the protection afforded to encapsulated catalase. In **Section 2.3,** conjugation of multiple catalase proteins to poly(acrylic acid) was performed as a method of protecting catalase from the hydrophobic ZIF-8 surface. This was followed by a review of the mechanism of catalase deactivation by ZIF-8 in **Section 2.4**, in which the impact of the constituents of ZIF-8 on catalase activity was investigated. The degradation of ZIF-8 under ambient storage conditions was also examined, to rationalize the lack of activity for catalase-on-ZIF-8 samples that were not exposed to the ZIF-8 synthesis conditions.

2.2 Single Enzyme Nanogels for the Protection of Sensitive Enzymes in ZIF-8

2.2.1 Background

Our first approach to creating a physical barrier between catalase and ZIF-8 utilized single enzyme nanogels (SENs). Single enzyme nanogels have been widely used for enzyme protection applications since they were first reported in 2006.[3-5] In an SEN, individual enzymes are encapsulated in a thin shell of polymer, either by in-situ polymerization or interaction with a pre-formed polymer.[4] This is effective at protecting enzymes from harsh environmental conditions such as high temperatures,[5, 6] organic solvents,[5, 6] proteolysis,[7] and pH changes.[3] The first reported SEN utilized polyacrylamide as the "shell", which was formed around the protein in-situ via radical polymerization. To anchor the polymer shell to the enzyme, chemical modification of the protein was needed to introduce surface vinyl groups, which could participate in the radical polymerization reaction (**Scheme 2.1**).[5]

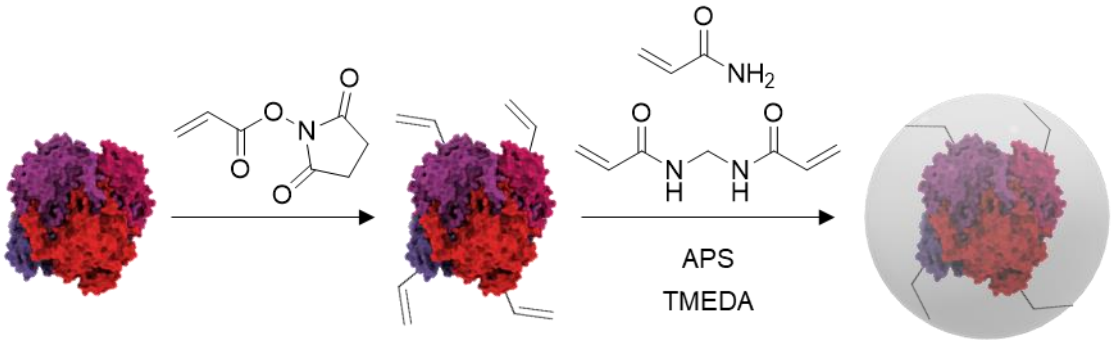

Scheme 2.1: General procedure for the synthesis of covalently anchored polyacrylamide single enzyme nanogels (SENs). Initial acryloylation reaction is carried out in boric acid buffer.

Protein surface modification is ultimately an undesirable requirement, as it adds additional complexity to an otherwise one-pot synthesis and risks denaturing the protein. A study in 2018 by Delaittre and co-workers showed that the surface modification can be avoided if a saccharide such as sucrose is included in the reaction mixture, which templates the formation of the polymer around the enzyme.[3] This study also showed that if the protein:monomer ratio was kept constant, increasing the amount of protein in the polymerization reaction increased the thickness of the resulting polymeric shell. As the shell thickness increased, the protection from pH extremes improved (**Figure 2.1B**),

however the turnover rate decreased for samples tested under ambient conditions (**Figure 2.1A**), likely due to slower diffusion through the polymer shell.[3] This allowed for the creation of SENs with tunable stability to harsh conditions, ideal for biocatalysis applications.

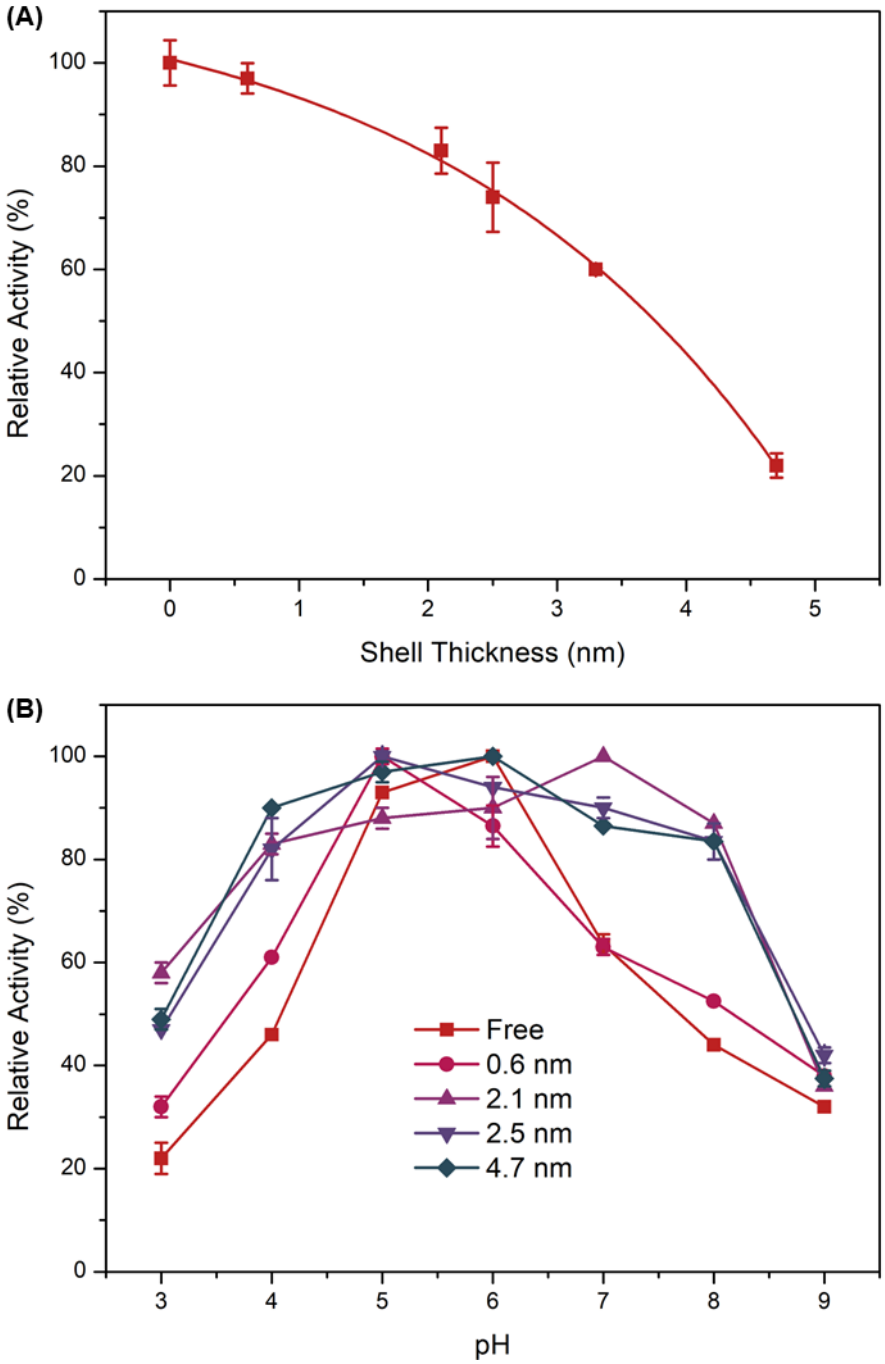

Figure 2.1: (**A**) Impact of SEN shell thickness on the activity of encapsulated glucose oxidase. (**B**) Relative activities of SEN samples when exposed to buffers of varying pH (figure adapted from ref. 3). As the shell size is increased, the activity of the enzyme decreases whilst the protection from harsh conditions is enhanced.

A small number of studies have previously investigated the synthesis of organic-inorganic SEN hybrids.[8, 9] For example, a study by Beloqui and co-workers investigated the synthesis of copper-based SEN hybrids. Briefly, the enzyme was first encapsulated in a polymeric coat synthesized *in situ*, which was then modified to introduce imidazole groups to the surface of the nanogel. Addition of $CuSO_4$ to these nanogels formed copper-SEN "nanosponges" of diameter 4-10 µm, which showed retained bioactivity under certain pH conditions (**Figure 2.2**).[9] Similarly, in a separate study, phosphate-decorated polyacrylamide was utilized to integrate cerium (III) on the surface of SENs. Glucose oxidase (GOx) was encapsulated within these SENs, to make a fluorescence-based glucose biosensor,[8] with potential application to the diagnosis and monitoring of diabetes mellitus.[10] These studies will not be discussed further, as they are not directly related to our work here. However, they demonstrate that SENs are compatible with metal-based systems, and so the synthesis of an SEN/MOF composite should be possible.

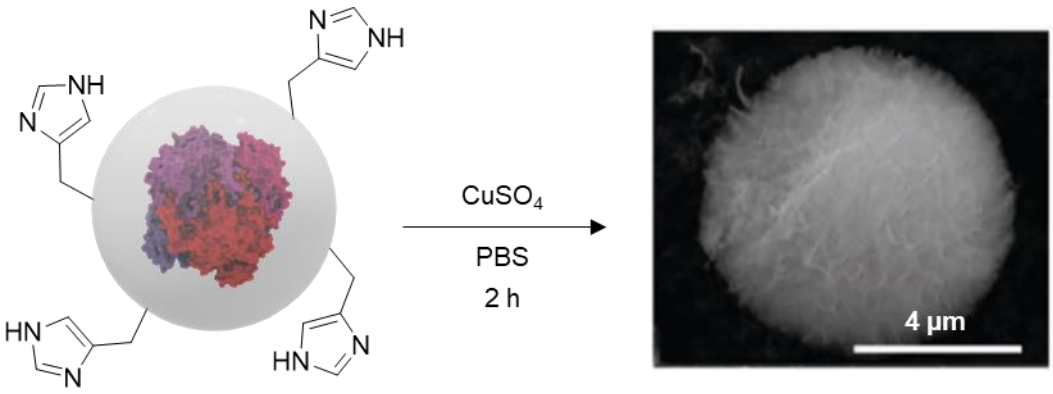

Figure 2.2: Synthesis of copper-SEN "nanosponges" from imidazole-grafted SENs (figure adapted from ref. 9).

In this section, we describe the synthesis of MOF/SEN composites, in which protein is first wrapped in a polymer shell and then encapsulated in ZIF-8. After performing initial SEN size control studies with BSA, we test the formation of ZIF-8 around polyacrylamide-based BSA@SENs. CAT@SEN@ZIF-8 samples are then prepared, and the catalytic activity assessed, to confirm if a thin polymer barrier is sufficient to protect enzymes from denaturing upon contact with the hydrophobic surface of ZIF-8. The synthesis of protein@SEN@ZIF-8 composites is summarized in **Scheme 2.2**.

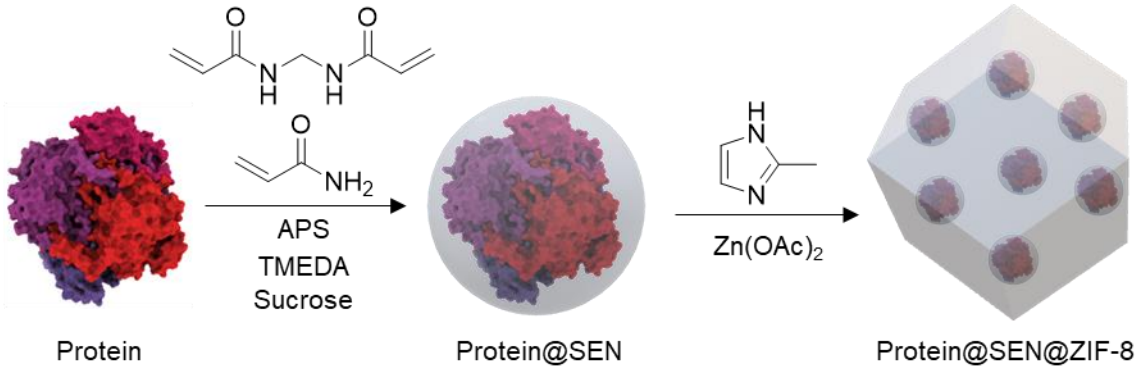

Scheme 2.2: Synthesis of protein@SEN@ZIF-8 biocomposites. SEN synthesis is carried out in sodium phosphate buffer.

2.2.2 Size control of polyacrylamide nanogels

To begin, the size control of SENs was investigated. This was important to the intended application, as SENs with a thicker shell would limit diffusion of substrate to the encapsulated enzyme, whilst thinner shells may not be sufficient to protect from the hydrophobic ZIF-8 surface. Size control has been previously reported for single enzyme nanogels,[3] and thus optimization of shell size was easily achieved. Initial experiments were carried out on bovine serum albumin (BSA). Though ultimately BSA was not of interest as it does not have catalytic activity, it is highly stable, readily abundant and inexpensive,[11] making it an ideal model protein. As surface modification of the protein is undesirable, a modified sucrose-templated polyacrylamide SEN synthesis was used (**Scheme 2.3**).[3] Previous reports on size control have held the monomer:protein ratio constant, and examined the effect of increasing the total concentration of all components on the shell size. In our studies, protein concentration was held constant, with the effect of increasing the concentration of only the polymer precursors and radical initiators assessed.

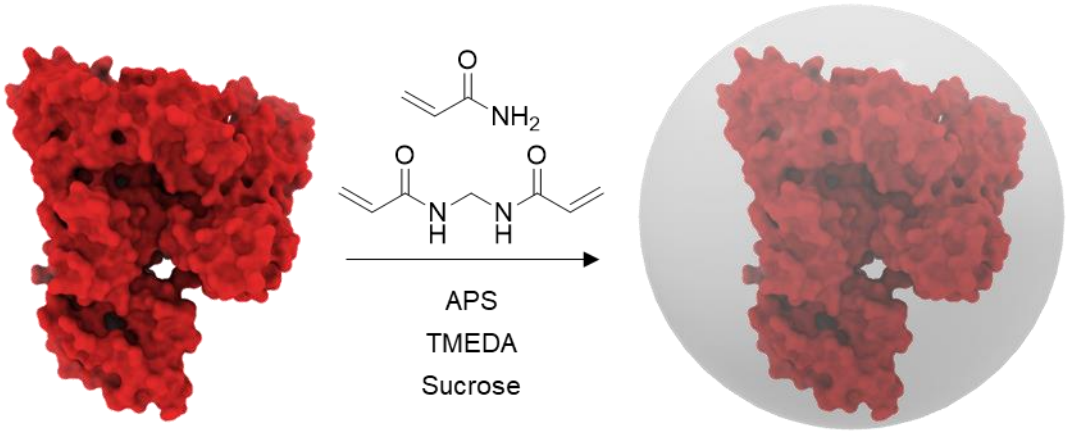

Scheme 2.3: Synthesis procedure for BSA@SEN samples. The reaction was carried out in pH 6 sodium phosphate buffer.

Six different monomer concentrations were tested for SEN synthesis: 22.5, 45, 90, 135, 180, and 360 mM, with the concentration of all other components except protein adjusted accordingly. All samples successfully formed SENs, however the 360 mM sample was highly viscous and unable to be adequately purified for analysis. UV/vis spectroscopy indicated increasing loss of protein at higher monomer concentrations, potentially due to polymerization continuing in the size-exclusion column, leading to unsuccessful elution for a portion of the protein.

Size distribution analysis was initially performed by referring to the intensity distribution of the BSA@SEN samples, measured by dynamic light scattering (DLS) (**Figure 2.3A**). Broad peaks at a diameter much larger than that of the protein are present in all samples, which may be caused by the presence of free polymer chains or minor protein aggregation. These peaks obscure the peaks corresponding to the protein nanogels, as particles with a larger size scatter a greater proportion of light and thus contribute far more significantly to the intensity distribution,[12] inhibiting insightful analysis of the nanogel size. To correct for this phenomenon, the distribution can be converted to a number distribution, which represents the size distribution as a proportion of the total number of particles (**Figure 2.3B**).[12] The number distribution for most samples remains broad, suggesting that the shell thickness was non-homogeneous within a sample and that some unencapsulated protein is present. In general, the size distribution of the SEN, both by number and intensity, shifts towards higher particle sizes as the monomer concentration is increased. The median size of the nanogel increases in a linear fashion as we increase the monomer:protein ratio (**Figure 2.4**), with shell thicknesses

ranging from 0.3-2.6 nm. Previous reports indicate that a shell thickness of 2.1 nm is sufficient to protect glucose oxidase from unfavorable pH conditions, whilst not significantly impacting diffusion of substrate to the enzyme.[3] Thus, it was reasoned that a sufficient shell had been produced to act as a barrier between encapsulated enzyme and the surface of ZIF-8.

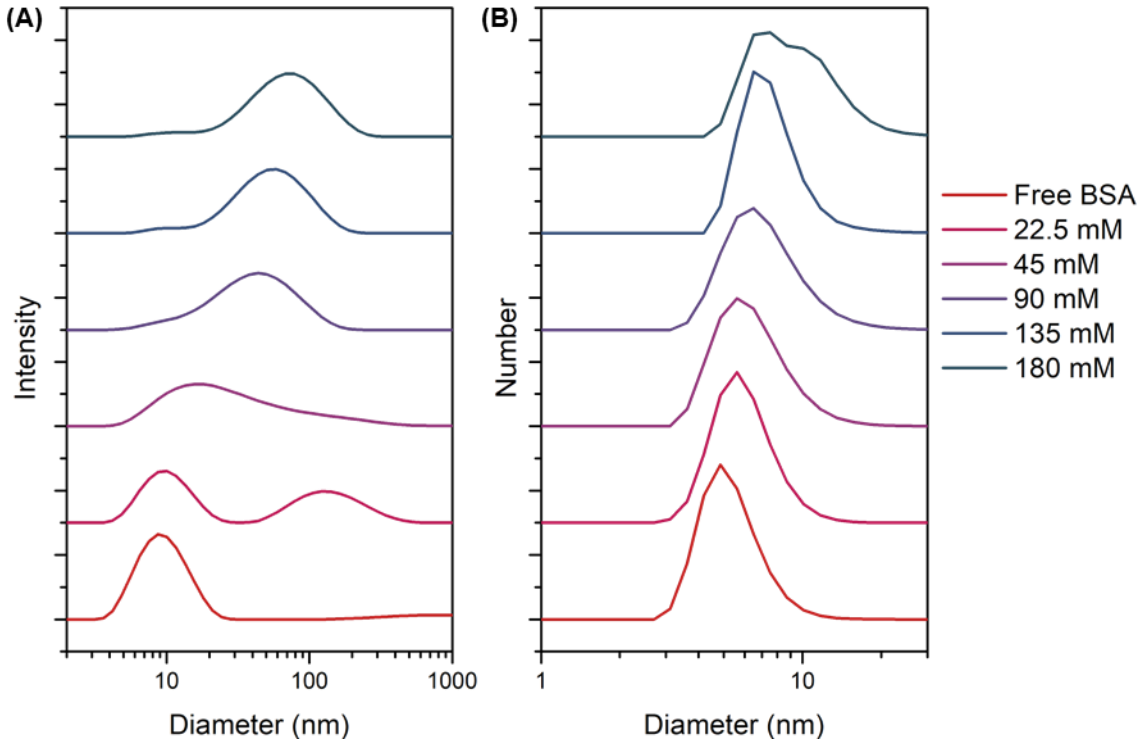

Figure 2.3: (**A**) Intensity and (**B**) number size distributions of BSA@SEN samples prepared using different acrylamide concentrations, as determined by dynamic light scattering (DLS). Samples were analyzed as a solution in tris buffer (100 mM, pH 7.4) and filtered through a 0.2 µm syringe filter prior to analysis. Distributions are an average of 2 independently prepared samples. SEN size distributions shift to larger diameters as the monomer concentration is increased.

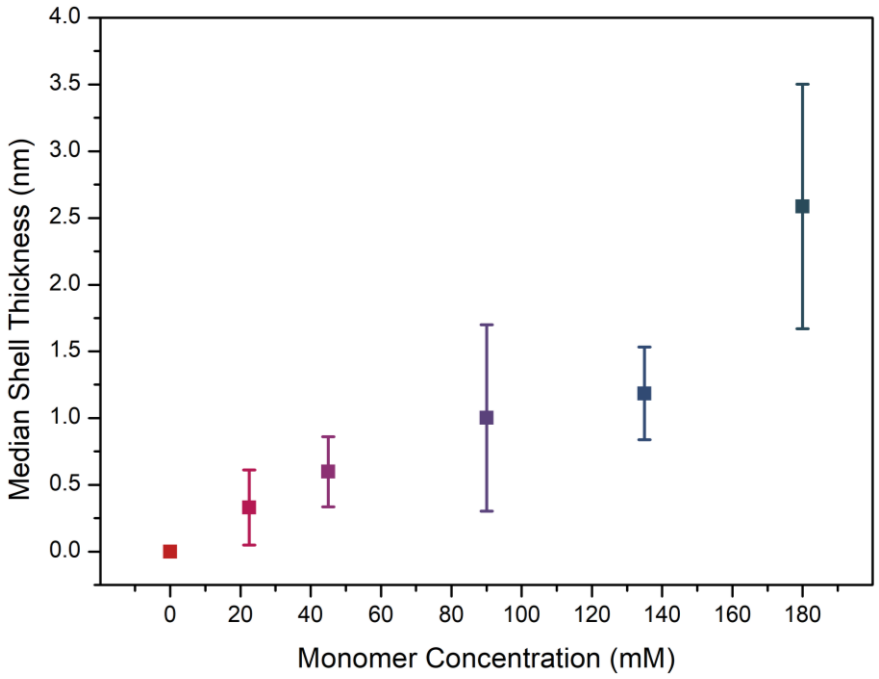

Figure 2.4: Effect of acrylamide concentration on the median thickness of the nanogel shell of BSA@SEN samples, determined from number distribution DLS data. Error bars represent the standard deviation in the median shell thickness of two independently prepared samples.

2.2.3 ZIF-8 formation around BSA@SEN

Before encapsulating an enzyme in an SEN, it was ensured that ZIF-8 could form around BSA@SEN samples. These experiments were conducted on the SEN synthesized using 180 mM acrylamide, denoted BSA@SEN-180, as a shell thickness of 2.6 nm would be expected to provide sufficient protection without significantly sacrificing permeability.[3]

Initially, ZIF-8 formation was trialed using a 40:640 ratio of $Zn(OAc)_2$:HmIM, which typically forms ZIF-8 even in the absence of protein. As expected, *sod*-ZIF-8 formed, as indicated by PXRD (**Figure 2.5**). Following this successful result, biomimetic mineralization of ZIF-8 around BSA@SEN-180 was attempted. Using a 20:80 ratio of $Zn(OAc)_2$:HmIM, the formation of sodalite ZIF-8 was observed. (**Figure 2.5**) This indicates that even with the polyacrylamide shell, biomimetic mineralization can occur. The formation of the solid is visibly slower for BSA@SEN samples when compared to samples of free BSA. This is likely because the diffusion of zinc ions to the protein

surface is slowed by the polymer capsule, slowing the accumulation of the metal and thus the mineralization process. Compared to encapsulation of free BSA, the biomimetic mineralization of ZIF-8 around BSA@SEN resulted in the formation of a monolithic structure when washed with ethanol and dried, which required extensive grinding prior to PXRD analysis.

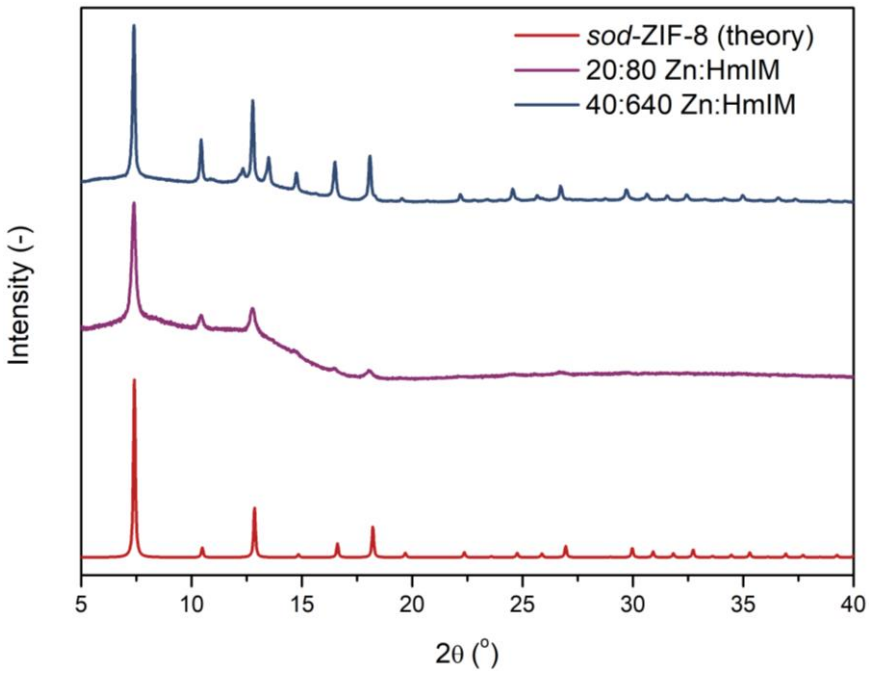

Figure 2.5: Powder X-Ray Diffraction (PXRD) patterns of ZIF-8 synthesized around BSA@SEN-180, by biomimetic mineralization (20:80 Zn:HmIM) and forced ZIF-8 precipitation (40:640 Zn:HmIM). Samples were washed twice with water and once with ethanol, and were air-dried and ground prior to analysis. Low peak height for the 20:80 Zn:HmIM sample relative to the baseline is likely a result of the limited amount of material available for analysis, in addition to contribution to the baseline by the amorphous polymer.

SEM analysis of ZIF-8 formed around single enzyme nanogels revealed that for a 40:640 ratio of $Zn(OAc)_2$:HmIM, crystals slightly different to the expected rhombic dodecahedral morphology formed. Compared to a sample of ZIF-8 synthesized around BSA under the same conditions, the particles were globular and had a more textured surface (**Figure 2.6**). The particle size was largely unchanged, with the average crystal size for BSA@ZIF-8 being 1.039 ± 0.020 μm whilst BSA@SEN-180@ZIF-8 had a size of 1.131 ± 0.024 μm (**Figure S2.2**). Meanwhile, samples synthesized using a biomimetic mineralization approach had a markedly different appearance. Rather than forming

discrete crystals, larger superstructures formed, as per the monolithic nature of the product prior to grinding. These superstructures have a textured surface, in which individual ZIF-8 rhombic dodecahedra can be clearly identified (**Figure 2.7**). This suggests that the SENs are somehow causing agglomeration of individual ZIF-8 particles.

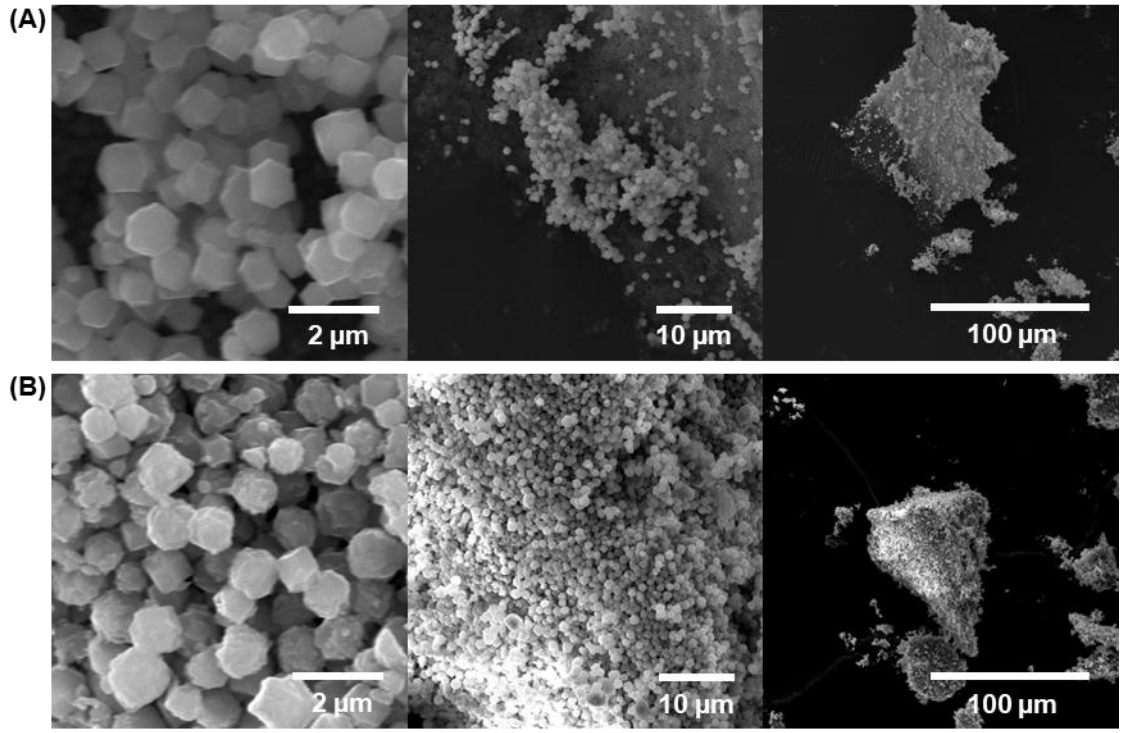

Figure 2.6: SEM images of (**A**) BSA and (**B**) BSA@SEN-180 encapsulated in ZIF-8 using a 40:640 $Zn(OAc)_2$:HmIM ratio. Samples were washed three times with water and dried under vacuum prior to analysis. BSA@ZIF-8 has the expected rhombic dodecahedron morphology, whilst BSA@SEN-180@ZIF-8 has less well-defined morphology.

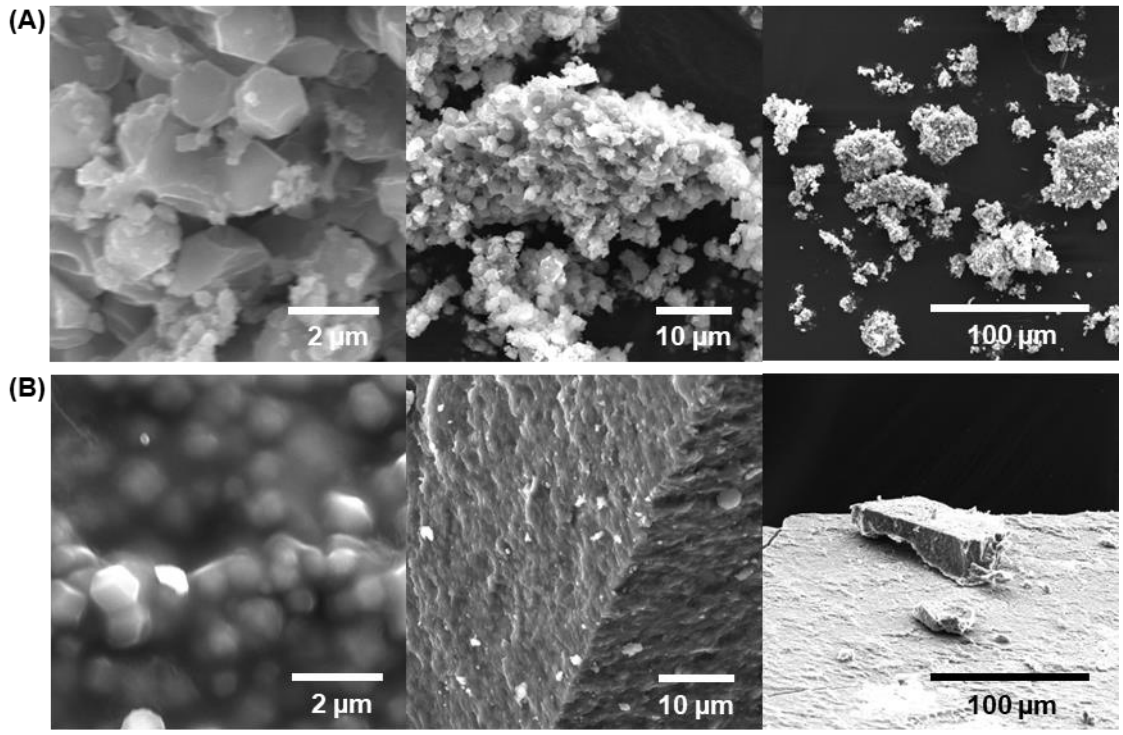

Figure 2.7: SEM images of (**A**) BSA and (**B**) BSA@SEN-180 encapsulated in ZIF-8 using a 20:80 $Zn(OAc)_2$:HmIM ratio. Samples were washed twice with water and once with ethanol, and air dried overnight. Grinding was required to fragment the sample for SEM analysis. BSA@ZIF-8 forms crystals with slightly deformed rhombic dodecahedron morphology, whilst BSA@SEN-180@ZIF-8 forms a monolithic structure in which individual ZIF-8 crystals can be identified.

The likely mechanism behind the formation of monoliths for the biomimetic mineralization of ZIF-8 around SENs consists of two simultaneous events, which occur during the ethanol wash of the composite. First, the SENs and free polymer chains precipitate out of solution upon addition of ethanol, to which polyacrylamide is known to be solvophobic.[13] Alongside this, the amorphous ZIF-8 precursor phase reforms to crystalline material on the surface of the polyacrylamide, similar to ZIF-8 coatings previously synthesized on the surface of polymer materials such as polyester fibres[14] and BPPO membranes.[15] This would lead to large, disordered composites containing a high proportion of crystalline material. However, as the size of the structure formed from the biomimetic mineralization procedure was quite large (several mm prior to grinding), the 20:80 $Zn(OAc)_2$:HmIM ratio was not pursued for enzymatic testing, as diffusion limitations could have a detrimental effect on composite activity.

2.2.4 Synthesis of CAT@SEN@ZIF-8

Given that an acrylamide concentration of 180 mM resulted in the formation of a nanogel which should be of sufficient thickness to protect BSA from harsh conditions, this monomer concentration was pursued for encapsulation of catalase. Since the size and oligomeric state of catalase (~250 kDa, 7.0 nm, tetramer) is significantly different to BSA (~66 kDa, 5.4 nm, monomer), treatment under the same conditions would not necessarily result in a nanogel of the same thickness. Thus, 60 mM and 120 mM acrylamide concentrations were also tested. Higher concentrations were not investigated as sample purification issues were encountered due to the viscosity of the product mixture.

Like for BSA, the thickness of SENs formed around catalase had a generally increasing trend as the monomer concentration was increased (**Figure 2.8, Figure S2.3**). The highest monomer concentration, 180 mM, resulted in a shell thickness of approximately 2.1 nm, compared to 2.6 nm for BSA. Meanwhile, the concentrations of 60 and 120 mM resulted in shell thicknesses of 0.5 and 0.3 nm, respectively. A shell thickness of greater than 2 nm was desired, and so only the largest sample was utilized for encapsulation in ZIF-8 and subsequent catalytic testing.

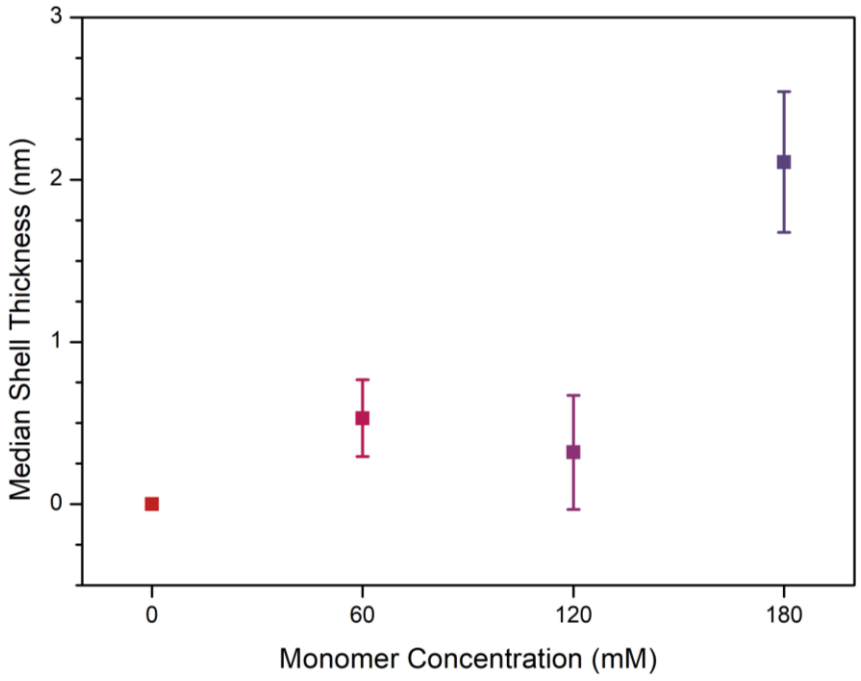

Figure 2.8: Effect of monomer concentration on the thickness of the nanogel coat of CAT@SEN samples, determined by DLS. Error bars represent the standard error in the median shell size of a sample upon repeat size measurements.

CAT@SEN-180 was encapsulated in ZIF-8 using the 40:640 ratio of $Zn(OAc)_2$:HmIM (**Figure 2.9**), as these conditions avoided the ZIF/polymer monoliths seen for BSA@SENs. Due to interference by the polymer in direct UV/vis spectroscopy, Bradford assay, and BCA assay, the initial dosage and loading of catalase in CAT@SEN-180@ZIF-8 samples could not be accurately determined, and so loading values will not be formally reported.

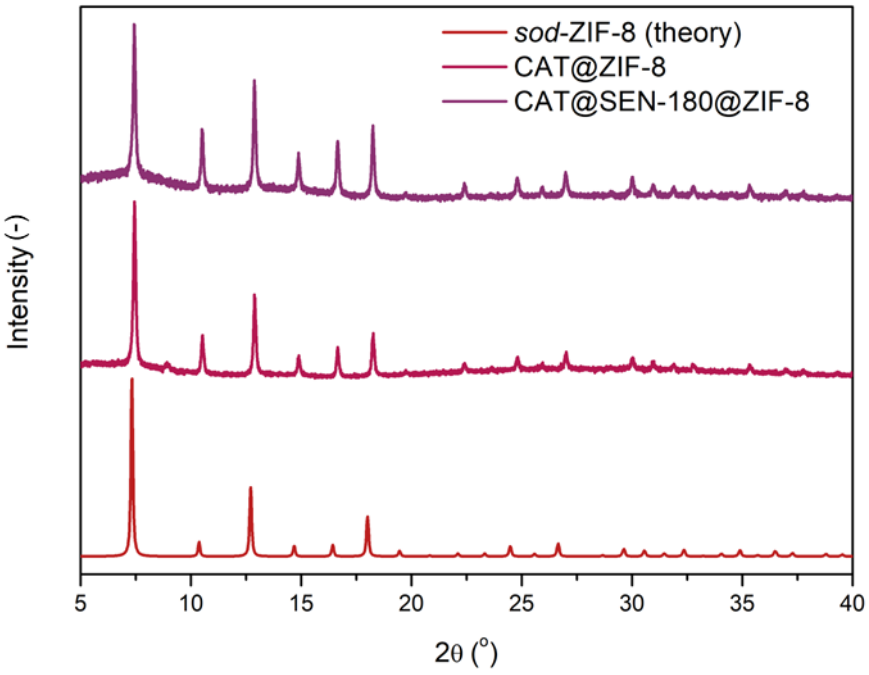

Figure 2.9: Powder X-Ray Diffraction (PXRD) patterns of ZIF-8 synthesized around CAT@SEN-180, by forced ZIF-8 precipitation. Samples were washed twice with water and once with ethanol, and were air-dried and ground prior to analysis. Low peak height relative to the baseline for the CAT@SEN-180@ZIF-8 sample is likely a result of the limited amount of material available for analysis, in addition to contribution to the baseline by the amorphous polymer.

The catalytic activity of CAT@SEN-180@ZIF-8 was investigated. Catalase is responsible for the breakdown of hydrogen peroxide to water and oxygen,[16] and thus to determine its activity either the breakdown of hydrogen peroxide or the evolution of oxygen may be measured. Activity studies were based on the breakdown of hydrogen peroxide, with the relative hydrogen peroxide concentration determined by FOX assay. In short, the FOX assay is based on the oxidation of Fe (II) to Fe (III) by peroxides under acidic conditions. Fe (III) then complexes to xylenol orange, forming a blue-purple complex that can be detected by UV/vis spectroscopy.[17] As the amount of this complex

formed is proportional to the amount of hydrogen peroxide present, the absorbance at 585 nm can be used to infer the hydrogen peroxide concentration and thus activity of catalase.

In activity testing, CAT@SEN-180 appeared to show greater activity than free catalase (**Figure S2.4**). This is likely due to inaccurate estimation of the stock concentration of CAT@SEN-180, as per the interference by the polymer mentioned above, and so the dosage of CAT@SEN-180 in the enzymatic reaction was different to the dosage of catalase. Unfortunately, when encapsulated in ZIF-8, both catalase and CAT@SEN-180 lost all activity, despite the presence of a 2.1 nm polymer shell for the SEN samples (**Figure 2.10**). This shell size has been previously reported to enable activity retentions of at least 60% when protein is exposed to pH 3-8, and thus was expected to provide sufficient protection from the hydrophobic ZIF-8 surface. Although a thicker nanogel may be desired, as sizes of approximately 5 nm are known to protect against conditions such as heating and exposure to organic solvents,[5] this could not be achieved due to the purification issues for larger shell sizes mentioned earlier. Control experiments for catalase and CAT@SEN-180 adsorbed on the surface of the ZIF also returned negligible activity, and thus the inactivation of catalase was not due to diffusion limitations or exposure of the enzyme to harsh synthesis conditions. Overall, it was concluded that the synthesized SENs were unable to protect catalase from the hydrophobic ZIF-8 surface, either due to insufficient shell thickness or due to contribution by other detrimental factors which the nanogel could not protect against.

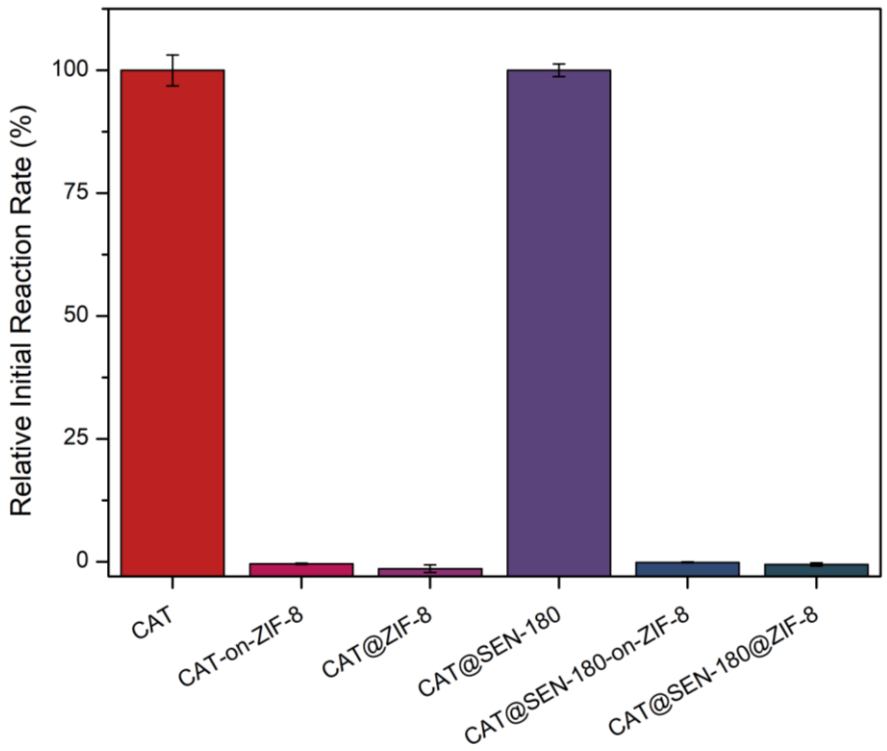

Figure 2.10: Relative initial H_2O_2 decomposition rates of catalase and CAT@SEN-180 when encapsulated in, or bound to the surface of, ZIF-8, synthesized using 40:640 $Zn(OAc)_2$:HmIM. Samples are normalized relative to the corresponding ZIF-free control, due to difficulties estimating the stock concentration of CAT@SEN-180. Error bars represent the standard error in the slope of the linear regression of **Figure S2.4** from which the relative initial reaction rate was derived. Catalase lost all activity in/on ZIF-8, including when encapsulated in an SEN.

2.2.5 Summary

Single enzyme nanogels were unable to protect catalase from the hydrophobic surface of ZIF-8. Initial studies with BSA revealed that polyacrylamide nanogels of controllable size could be synthesized by varying the concentration of the polymer precursors. These SENs could then be encapsulated in ZIF-8, either by biomimetic mineralization or by forced co-precipitation. Biomimetic mineralization resulted in the formation of unusual monolithic ZIF-8 structures, with individual ZIF-8 crystals adhered to the surface of larger polymer masses. These polymer-enzyme-ZIF composites may have interesting properties that could be further investigated; however they were not used for catalysis as the low surface area would have a detrimental impact on catalytic activity.

Forced precipitation of ZIF-8 returned discrete crystals, albeit with slight deformation to the expected rhombic dodecahedron morphology. CAT@SENs were then synthesized, of comparable size to that synthesized around BSA under identical conditions. Unfortunately, upon encapsulation in, or adsorption on, ZIF-8, CAT@SEN lost all activity. Thus, the polyacrylamide shell was unable to protect catalase from the hydrophobic surface interaction with ZIF-8.

2.3 Polymer Conjugates for the Protection of Sensitive Enzymes in ZIF-8

2.3.1 Background

With attempts at protecting sensitive enzymes from the hydrophobic surface of ZIF-8 using single enzyme nanogels proving fruitless, we decided to trial an alternative method of protecting catalase that may prove more successful. Rather than protecting individual enzymes within their own shell, we pursued a method of linking multiple proteins into a single, highly protected unit. By having multiple enzymes in a single cluster, some enzymes could be more distanced from the ZIF-8 surface than others. If the lack of protection afforded to the catalase by SEN encapsulation was due to the shell thickness being insufficient, this would provide greater protection from the hydrophobic ZIF-8 surface.

Our approach bears similarity to cross-linked enzyme aggregates (CLEAs), a common method of enzyme immobilization. CLEAs are constructed from individual enzymes linked together using a bifunctional reagent, such as glutaraldehyde, to create large, insoluble aggregates.[18] These aggregates are composed of nearly entirely enzyme, and thus are effectively carrier-free.[19] However, CLEAs are not useful for encapsulation in ZIF-8, as they are by definition insoluble and so are unlikely to be successfully encapsulated. Instead, the chosen approach utilized polyacrylic acid (PAA) as a support, which retains solubility when attached to proteins. Conjugation to PAA (**Scheme 2.4**) has been used previously to protect catalase from a variety of harsh conditions. Kumar and co-workers reported that catalase-PAA conjugates retained activity even after exposure to high temperatures (~85 ^{o}C), long term storage (10 weeks at 8 ^{o}C), trypsin digestion, and exposure to negatively charged inhibitors, whilst unmodified catalase lost activity.[20] In this study, the conjugation was carried out at a variety of different mole ratios and pH conditions, which were shown to have an impact on the activity of the product and its resistance to certain conditions. The tunability of the synthesis allowed conjugates designed for certain conditions to be synthesized.

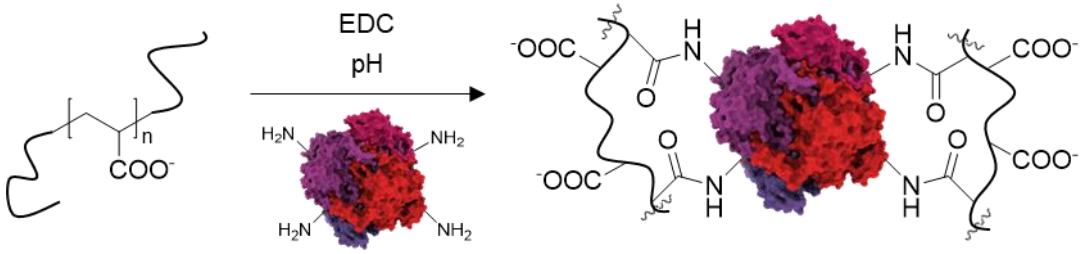

Scheme 2.4: Conjugation of catalase to poly(acrylic acid) (figure adapted from ref. [20]). The reaction was carried out in sodium phosphate buffer.

Polymer conjugation was chosen as a method of protecting catalase from the ZIF-8 surface for several reasons. Firstly, existing literature utilized catalase, the model enzyme intended for protection inside ZIF-8 in this work. Thus, the reported optimization and preliminary testing of the polymer-enzyme composite could be directly applied to our system. Secondly, PAA is negatively charged, and so it was expected that a conjugate that is composed of mostly PAA to also be negatively charged. This would allow the biomimetic mineralization procedure for ZIF-8 to be used, as negatively charged macromolecules are able to nucleate the growth of ZIF-8.[21] This requires a lower amount of precursors, providing an economic benefit, and ensures that the protein is encapsulated within the framework. With this combination of desirable characteristics, it was hoped that conjugation to PAA would be sufficient to protect catalase from denaturing in ZIF-8.

2.3.2 Synthesis and characterization of catalase-PAA conjugates

Attachment of catalase to poly(acrylic acid) required a carbodiimide conjugation reaction, using EDC (**Scheme 2.4**). Previous reports have indicated that pH and mole ratio have an impact on the catalytic activity and protection of catalase. The combination of conditions chosen were pH 7 and a 1:500 mole ratio of catalase:PAA, as this combination resulted in a conjugate with well-retained catalase activity and appreciable resistance to proteolysis.[20] After synthesis, the reaction mixture was passed through a 10 kDa filter and the filtrate discarded, thus removing of the majority of the unreacted PAA (MW 8000 Da).

Successful conjugation of catalase to PAA was verified by DLS (**Figure 2.11**). For catalase alone, a sole peak at 7.0 nm is present, corresponding to free, tetrameric

catalase. Upon the conjugation to PAA, this peak disappears, and instead there is a peak at 128 nm, indicating that the majority of, if not all, catalase in the sample successfully conjugated to PAA. It is important to note that PAA does not fit the spherical assumption for processing of DLS data, and as a result this size is merely an estimate. Nonetheless, it provides evidence that the conjugation reaction was successful.

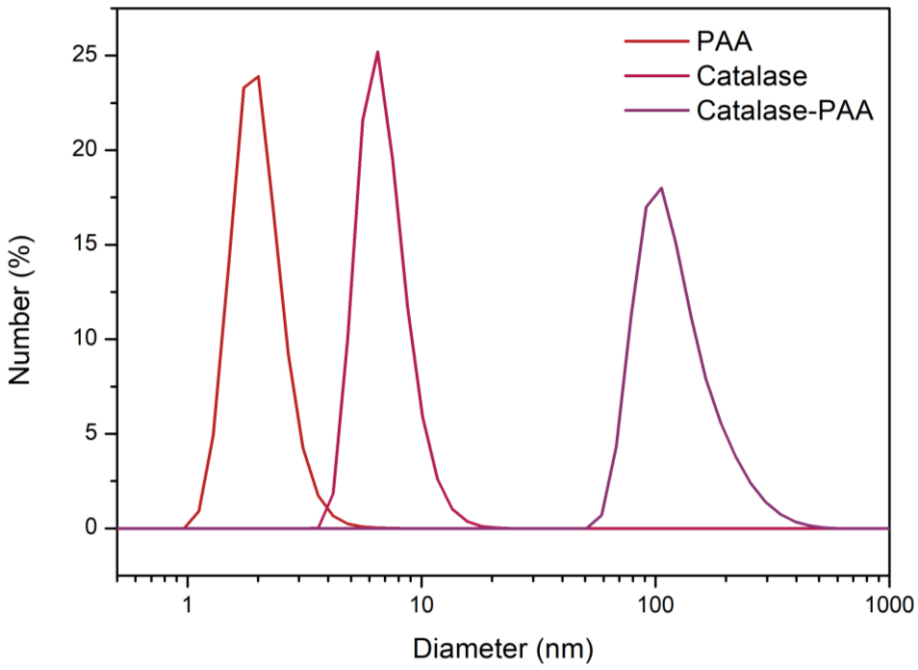

Figure 2.11: DLS size distributions of PAA, catalase, and catalase conjugated to PAA. Samples were analyzed as a solution in tris buffer (100 mM, pH 7.4). The particles formed upon conjugation are significantly larger than the constituent catalase and PAA. PAA does not fulfill the spherical assumption for processing of DLS data, and so the size distributions presented are an estimate.

TEM imaging of the polymer/protein composite also indicated that conjugation was successful (**Figure 2.12**). In TEM images prior to conjugation, the uranyl acetate used for grid staining localized with the PAA. Given that there is no inaccessible core of the PAA, this led to large, dark clusters in the TEM. However, the sample changed considerably upon the conjugation of catalase to PAA. Light-colored circles of average diameter 11.2 ± 1.7 nm are seen amongst the stained PAA. Given that catalase has a modal diameter of 7.0 nm (measured by number distribution DLS), with literature dimensions of 9.0 × 8.0 × 6.0 nm,[22] it is likely that these light-colored spots correspond to individual catalase macromolecules conjugated to the surface of the PAA. These spots occur as the core of the protein is inaccessible to the dye, and thus the stain localizes with

the PAA and adheres to the surface of the grid except for where catalase is located. The wt.% catalase in the conjugate was determined to be 4.47% by UV/vis spectroscopy, with only a slight loss of catalase loading in the purification procedure (**Table 2.1**). This further confirms that a successful conjugation reaction occurred.

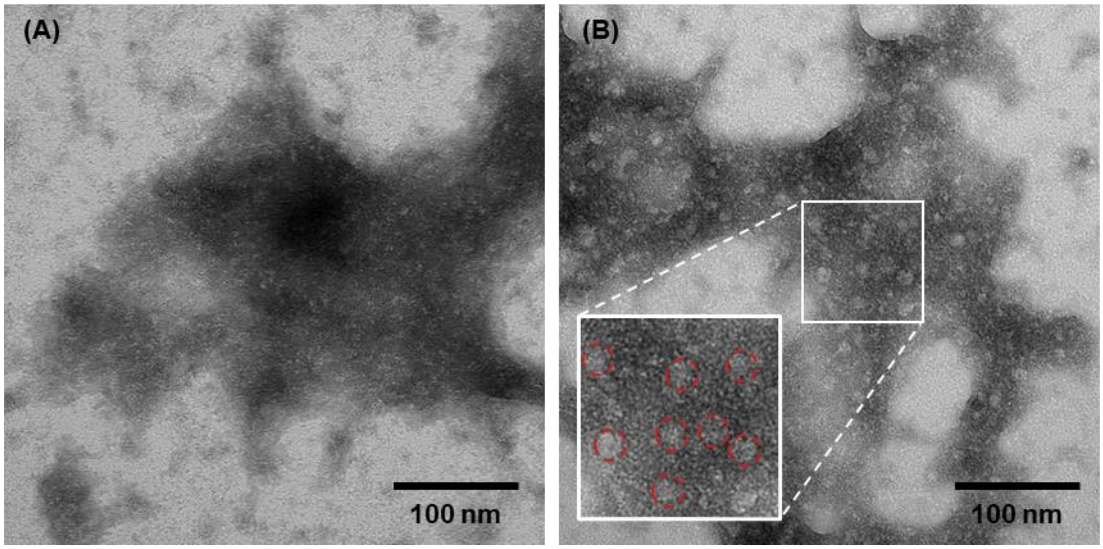

Figure 2.12: TEM images of (**A**) PAA, and (**B**) catalase conjugated to PAA, stained with uranyl acetate. Light spots of diameter 11.2 ± 1.7 nm correspond to individual catalase macromolecules.

Table 2.1: Loading of enzyme in catalase-PAA conjugates

CAT-PAA Sample	wt.% Catalase
Theoretical loading (100% conjugation)	5.50%
As-synthesized	4.47%

2.3.3 Encapsulation of catalase-PAA in ZIF-8

The catalase-PAA conjugate was then encapsulated in ZIF-8. Given that the conjugate was of a significantly larger size than free catalase (128 nm by DLS, up to 1 μm by TEM), it was reasoned that a procedure intended for the encapsulation of proteins would not be applicable, and that a procedure intended for the encapsulation of larger species may be required. Thus, a modified procedure previously reported for the encapsulation of yeast cells was used,[23, 24] which are of a more comparable size to the catalase-PAA conjugates, with a typical yeast cell having a diameter of ~8 μm at room temperature.[25] Unfortunately, ZIF-8 did not form around the conjugates under these

conditions. Though a white solid formed, analysis by PXRD revealed the solid to be amorphous (**Figure 2.13**). Equivalent catalase-only controls resulted in the formation of *dia*-ZIF-8, a known ZIF-8 topology. This topology likely formed due to the significant effect ZIF-8 precursor concentrations have on the polymorph distribution, which has been investigated extensively in the past.[26] As the intended *sod*-ZIF-8 product did not form, this ZIF-8 synthesis was abandoned, and the original biomimetic mineralization approach was utilized.

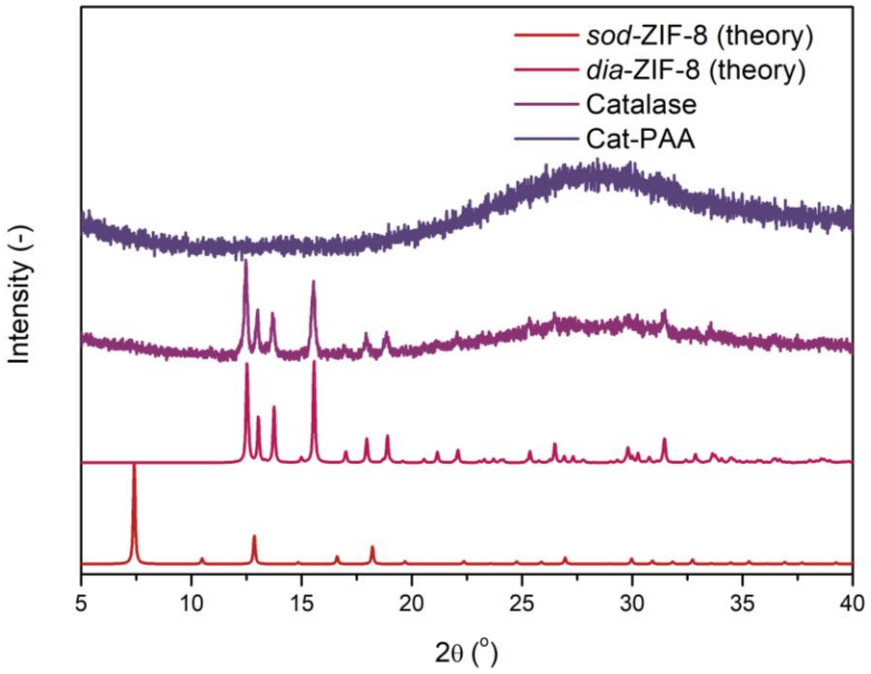

Figure 2.13: Powder X-Ray Diffraction (PXRD) patterns of attempted ZIF-8 synthesis around catalase and PAA conjugated catalase using procedure for yeast cell encapsulation, compared to theoretical sodalite and diamondoid ZIF-8. Samples were washed three times with water and analyzed in water.

Synthesis of ZIF-8 around catalase-PAA under biomimetic mineralization conditions (20:80 HmIM:$Zn(OAc)_2$) returned promising results. A white solid formed, and after washing with ethanol returned a PXRD characteristic of ZIF-8 (**Figure 2.14**). This was expected, as conjugated PAA has a significant negative charge, and so could promote the accumulation of zinc ions which initiates the biomimetic mineralization of ZIF-8.[21, 27] Previous studies have indicated that use of lower $Zn(OAc)_2$:HmIM ratios can lead to *Candida antarctica* Lipase B@ZIF-8 composites with higher activity, attributed to a combination of lower particle size and larger pore size as the precursor ratio is decreased.[28] Thus, in hopes of obtaining a material with high activity, this catalase-PAA@ZIF-8 composite was used in catalytic testing.

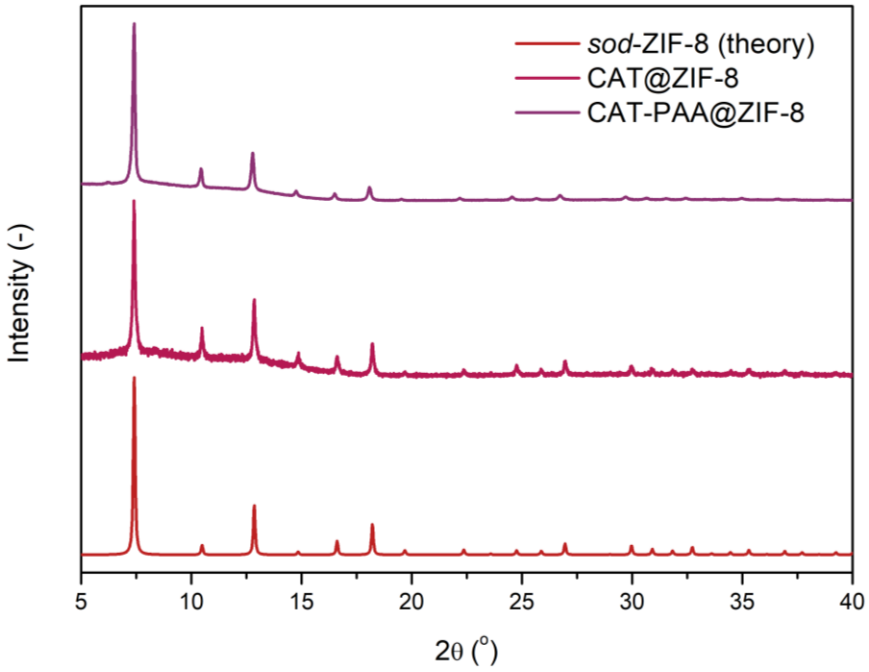

Figure 2.14: Powder X-Ray Diffraction (PXRD) patterns of ZIF-8 synthesized around catalase and PAA conjugated catalase using 20:80 $Zn(OAc)_2$:HmIM. Samples were washed twice with water and once with ethanol, and were air-dried and ground prior to analysis.

2.3.4 Catalytic testing

With the catalase-PAA@ZIF-8 composite synthesized, catalytic testing of the composite was performed. Initially, the activity of unencapsulated catalase-PAA was determined, with the conjugate returning an activity of approximately 6% of free catalase. The decrease in activity is likely a result of the covalent attachment to PAA, which may have changed the conformation of the protein and thus altered the enzymatic activity. Further to this, the proximity of PAA could change the chemical environment around catalase, altering folding and the interaction with substrate/product molecules. When encapsulated in ZIF-8, activity for both free catalase and catalase-PAA was lost (**Figure 2.15**). The complete loss of activity may have been due to insufficient protection provided by the PAA conjugate, as specific protection from hydrophobic surface contact has not been previously demonstrated for such systems. Alternatively, as two barrier-based protection methods proved unsuccessful, it was possible that additional factors were contributing to the deactivation of catalase by ZIF-8. These factors are further investigated in the following section.

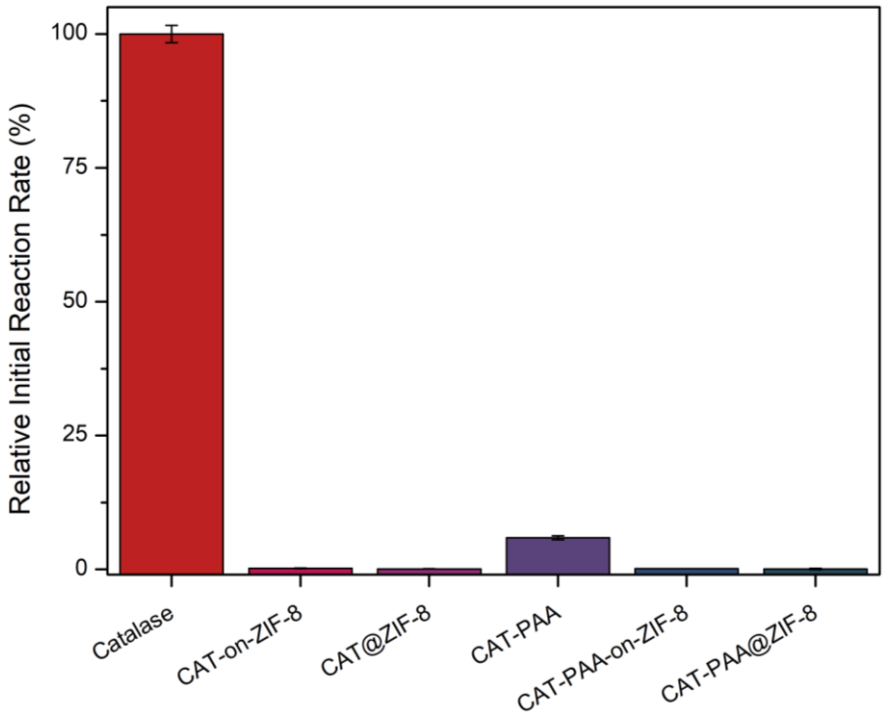

Figure 2.15: Relative initial H_2O_2 decomposition rates of catalase and catalase-PAA samples when encapsulated in ZIF-8, synthesized using 20:80 $Zn(OAc)_2$:HmIM. Samples are normalized relative to free catalase. Error bars represent the standard error in the slope of the linear regression of **Figure S2.5** from which the relative initial reaction rate was derived. Catalase-PAA exhibits significantly lower activity than free catalase, whilst both catalase and catalase-PAA completely lose activity in/on ZIF-8.

2.3.5 Summary

Akin to the single enzyme nanogels synthesized in the previous section, conjugation of catalase to poly(acrylic acid) was unable to prevent activity loss when encapsulated in, or bound to the surface of, ZIF-8. Catalase was successfully conjugated to 8 kDa poly(acrylic acid) with a wt.% loading of 4.47%, verified by TEM and DLS. Biomimetic mineralization of ZIF-8 around the catalase-PAA conjugates was successful, due to the significant negative charge possessed by the polymer. Unfortunately, a reduction of activity compared to free catalase was observed for these conjugates, which was reduced to zero when encapsulated in ZIF-8. Thus, it was concluded that tuning the enzyme-MOF interface using a physical barrier around catalase is insufficient to protect from denaturation. This indicates that there may be other factors which contribute to the loss of activity of catalase, and other enzymes, when immobilized in- or on-ZIF-8.

2.4 Revisiting the Mechanism of Deactivation of Catalase by ZIF-8

2.4.1 Background

Using a physical barrier to protect catalase from the hydrophobic surface of ZIF-8 proved consistently ineffective, thus we refocused our attention towards further probing the mechanism behind the deactivation of catalase by ZIF-8. In 2019, it was proposed that the deactivation of catalase by ZIF-8 was due to unfolding upon adsorption to the hydrophobic framework surface.[1] However, our results indicate that there may be more elements that contribute to the deactivation of the enzyme than framework surface chemistry alone. This formed the final part of our investigation into enzyme@MOF biocomposites.

It is widely known that the adsorption of proteins on a surface can induce conformational changes. However, this is not always detrimental to enzyme activity, and is partially responsible for the stabilization of proteins on supports.[29] Rather, a combination of factors are responsible for the impact that surface adsorption has on protein unfolding. For example, at dilute concentrations, enzymes tend to be stabilized when immobilized on a surface, whilst at higher concentration denaturation can result.[29] Generally, unfolding of a protein on contact with a hydrophobic surface is facilitated for two reasons. Firstly, at the surface, the local concentration of protein is higher, which often decreases the stability of the folded state (depending on additional environmental factors). Secondly, the hydrophobic surface lowers the energy barrier for unfolding, leading to denaturation and or/aggregation.[29] Computational studies have revealed that secondary protein structures are predictably altered on contact with a moderately hydrophobic surface. Consistently, α-helices begin to "spread" into an elliptical shape as they approach a hydrophobic surface. β-sheets, on the other hand, have higher hydrophobicity, and so unfold into random coils and some structured conformations.[30] Given the extreme hydrophobicity of ZIF-8, as indicated by its high water contact angle of 142°,[31] the deactivation of catalase on contact with the surface is unsurprising. IR studies have shown that catalase denatures when encapsulated in or immobilized on ZIF-8 (**Figure 2.16**).[1, 32] Notably, peaks corresponding to β-sheets of catalase shift on contact with ZIF-8, with the new peak position being characteristic of protein aggregates. This change in the IR spectra is not evident when catalase is encapsulated in MAF-7 or ZIF-

90, providing good evidence that the hydrophobicity of the framework is responsible for catalase denaturation and aggregation.

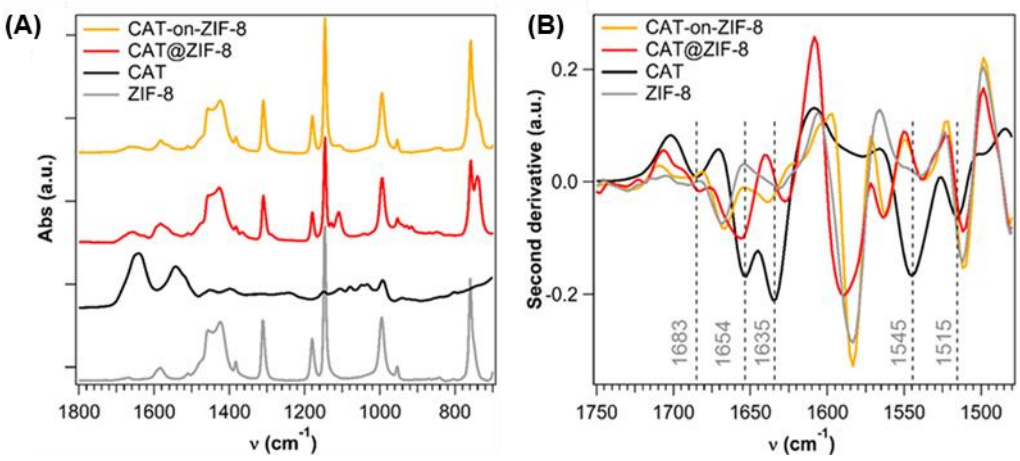

Figure 2.16: (**A**) As-recorded and (**B**) second derivative IR spectra of ZIF-8, catalase, CAT@ZIF-8, and catalase-on-ZIF-8. Dashed lines in the second derivative spectrum indicate the spectral vibrations of the amide I (1683, 1654 and 1635 cm^{-1}, corresponding to α-helices, β-sheets, and turns and loops, respectively) and amide II (1545 and 1515 cm^{-1}, corresponding to α-helices and β-sheets). The shift in the position of peaks corresponding to β-sheets of catalase is characteristic of protein aggregates (figure sourced from ref. 1).

However, our results indicate that other factors may be impacting catalase activity in addition to the hydrophobic surface interaction. There are several other variables that may contribute to diminished enzymatic activity in a support, including synthesis pH, presence of inhibitors, and diffusion limitations of substrates/products. As catalase-on-ZIF-8 samples show no activity, diffusion limitations are not fully responsible for the loss of activity. Given that the barrier around the enzyme was permeable to small molecules, our attention was drawn towards the ZIF-8 precursors. Certain molecules with structural similarity to 2-methylimidazole are known inhibitors of catalase, such as 3-amino-1,2,4-triazole (**Figure 2.17**).[33] Schejter and co-workers investigated a variety of potential catalase inhibitors, and found that exposure to 20 mM 3-amino-1,2,4-triazole for 2 hours caused the activity to drop to 7% of its original value, with several carbazides showing similar impact. Intriguingly, data indicated that the inhibitors interacted with the polypeptide itself and not the heme iron.[33] Thus, potentially, the deactivation of catalase upon encapsulation in ZIF-8 may arise not only due to the interaction with the hydrophobic framework surface, but also due to exposure to high concentrations of

HmIM. Further to this, catalase is sensitive to alkaline solutions. It has been previously shown that when exposed to a solution with pH >11.5 and low ionic strength, catalase dissociates into monomers, completely losing activity and some α-helical structure.[34] These studies also showed that as the pH is increased past 9.5, the activity decreases, with near complete activity loss at pH 11 and above.[34] Thus, there is considerable potential for the synthesis conditions of ZIF-8 to contribute towards the deactivation of catalase.

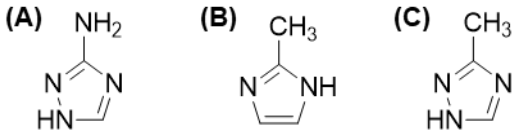

Figure 2.17: Comparison of structures of (**A**) known catalase inhibitor 2-amino-1,2,4-triazole to (**B**) HmIM for ZIF-8 synthesis and (**C**) Hmtz for MAF-7 synthesis.

In this section, the explanation behind our unsuccessful protection results is explored. We commence by investigating the impact that 2-methylimidazole has on catalase activity, as similarly structured molecules are known inhibitors of catalase. The pH sensitivity of catalase is then assessed, as the synthesis conditions for ZIF-8 are highly alkaline. Finally, the properties of ZIF-8 suspensions are assessed and used to rationalize the deactivation of catalase for on-ZIF samples, which are not exposed to the synthesis conditions.

2.4.2 Deactivation of catalase by 2-methylimidazole

To assess if 2-methylimidazole was impacting catalase activity, catalase was exposed to a variety of concentrations of HmIM overnight, and then its catalytic activity was tested (**Figure 2.18**). The effect of the 2-methylimidazole on catalase was indisputable, with the catalase completely losing activity when exposed to the synthesis concentration of HmIM. Even the lowest concentration of HmIM tested, 5 mM, resulted in an approximately 40% decrease in catalase activity. This suggests that the deactivation of catalase is at least in part due to exposure of the enzyme to 2-methylimidazole, for CAT@ZIF-8 samples.

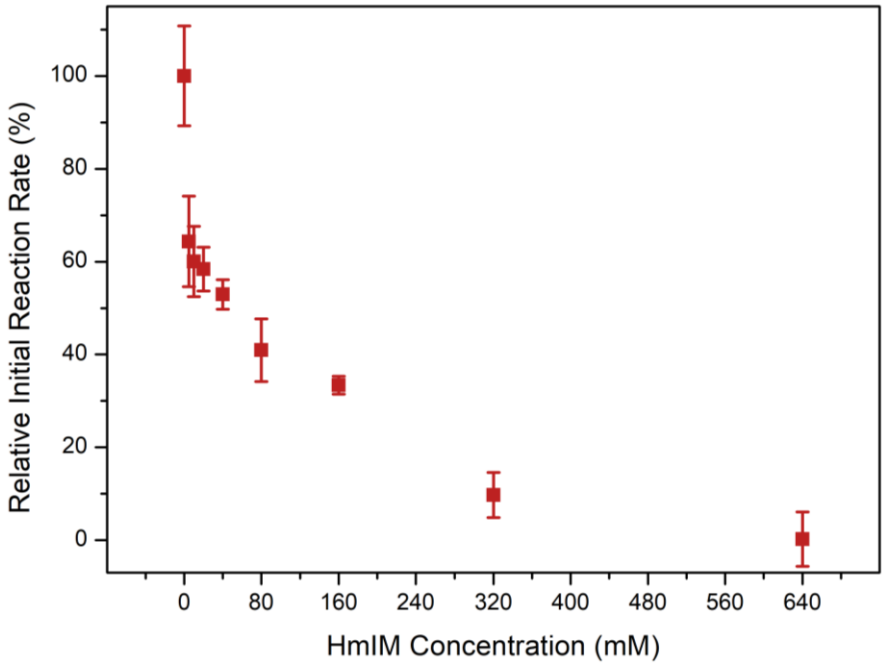

Figure 2.18: Effect of 2-methylimidazole exposure on initial rate of H_2O_2 decomposition by catalase, as determined by FOX assay. Catalase was exposed to each methylimidazole concentration at ambient conditions for 16 hours, and then diluted in 50 mM tris buffer prior to catalytic testing. The enzyme concentration in the reaction was 20 nM. Samples are normalized relative to catalase stored in ultrapure water at ambient conditions for 16 hours. Error bars represent the standard error in the slope of the linear regression of **Figure S2.6** from which the relative initial reaction rate was derived. All samples containing HmIM exhibited an initial rate loss of over 35%, with catalase losing all activity after exposure to 640 mM HmIM.

However, it is noteworthy that the structure of 3-methyl-1,2,4-triazole, the linker required to synthesize MAF-7, even more closely resembles the structure of the known 3-amino-1,2,4-triazole catalase inhibitor, differing only by the identity of the substituent on the triazole. Thus, it would be expected to be equally, if not more, detrimental to catalase activity when compared to HmIM. However, overnight exposure of catalase to the synthesis concentration of Hmtz had no effect on the catalase activity, whilst exposure to deprotonated Hmtz, as used in MAF-7 synthesis, resulted in a ~70% decrease in activity (**Figure 2.19**). This suggests that the deactivation of catalase may not be a direct result of interaction with the linker, but rather is due to the impact the linkers have on the pH of the solution.

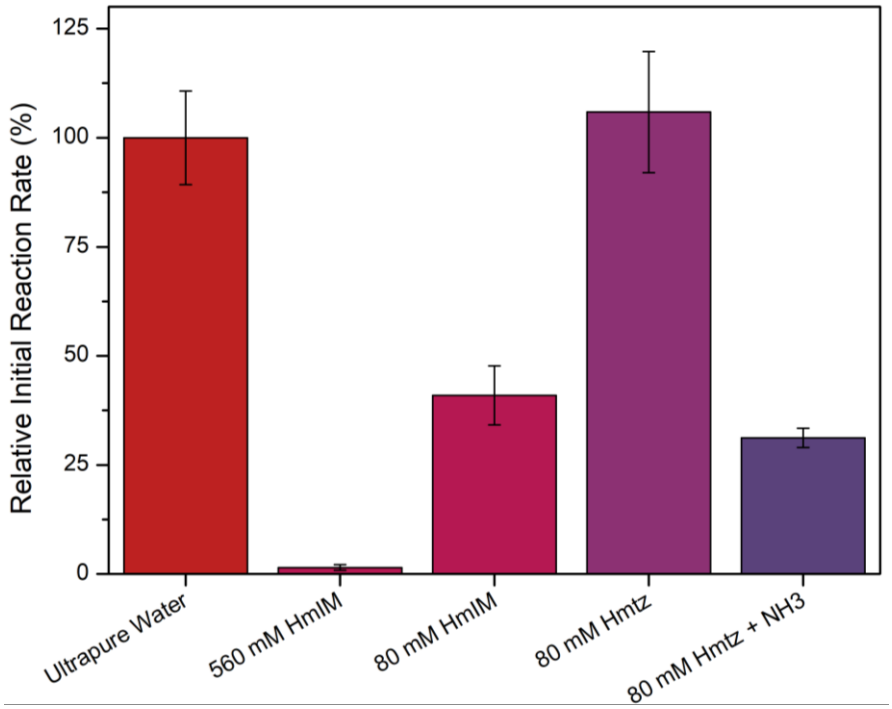

Figure 2.19: Effect of 16-hour exposure to synthesis concentrations of linkers for ZIF-8 (HmIM) and MAF-7 (Hmtz) on catalase activity. To replicate the synthesis conditions, the MAF-7 linker with a stoichiometric quantity of ammonia was also tested. Samples are normalized relative to catalase stored in ultrapure water at ambient conditions for 16 hours. Error bars represent the standard error in the slope of the linear regression from which the relative initial reaction rate was derived. Catalase loses all activity when exposed to the synthesis concentration of HmIM for forced ZIF-8 precipitation, whilst 60% activity loss is observed under biomimetic mineralization conditions. Hmtz has negligible impact on catalase activity, except in the presence of ammonia.

Previous reports have suggested that catalase is highly sensitive to alkaline conditions.[34] HmIM solutions are significantly more alkaline than Hmtz solutions, which could provide alternative explanation for why catalase is deactivated in ZIF-8 but not MAF-7. The pH of a variety of solutions relevant to ZIF-8 and MAF-7 synthesis is presented in **Table 2.2**. The pH of many of these solutions is within the range in which catalase would be expected to lose activity, although exposure to the single-component solutions prior to mixing would only be brief (<10 min). To assess if this was what was causing catalase deactivation, catalase was exposed overnight to a variety of pH conditions and its activity measured (**Figure 2.20**). Activity dropped from 100% at pH 7 to 89%, 56%, and 3% for pH 9, 11, and 13, respectively. Given that an overnight exposure to pH 11 decreases catalase activity by only 44%, it is unlikely that the brief exposure of

catalase to a ZIF-8 component prior to synthesis is responsible for activity loss. An exception to this is the HmIM solution for the forced ZIF-8 precipitation, as a pH of 11.8 may be sufficient to cause some impact on catalase activity even after brief exposure. Catalase is exposed overnight to pH 9.7 for the forced ZIF-8 precipitation, 8.0 for biomimetic mineralization, and 7.4 for MAF-7 synthesis. Over this extended period, some activity loss (~30%) would be expected for CAT@ZIF-8 synthesized using forced ZIF-8 precipitation. Though this is well below the 100% loss of activity seen for CAT@ZIF-8 samples in the past, it indicates that pH contributes towards the deactivation of catalase upon encapsulation in ZIF-8.

Table 2.2: pH of solutions relevant to the synthesis of ZIF-8 and MAF-7.

Synthesis procedure	**pH of linker**	**pH of Zn**	**pH upon mixing**
Forced ZIF-8 precipitation (40:640 Zn:HmIM)	11.8	5.5	9.7
Biomimetic mineralization of ZIF-8 (20:80 Zn:HmIM)	11.3	6.2	8.0
MAF-7 synthesis	10.7*	6.0	7.4

*deprotonated with stoichiometric quantity of NH_3

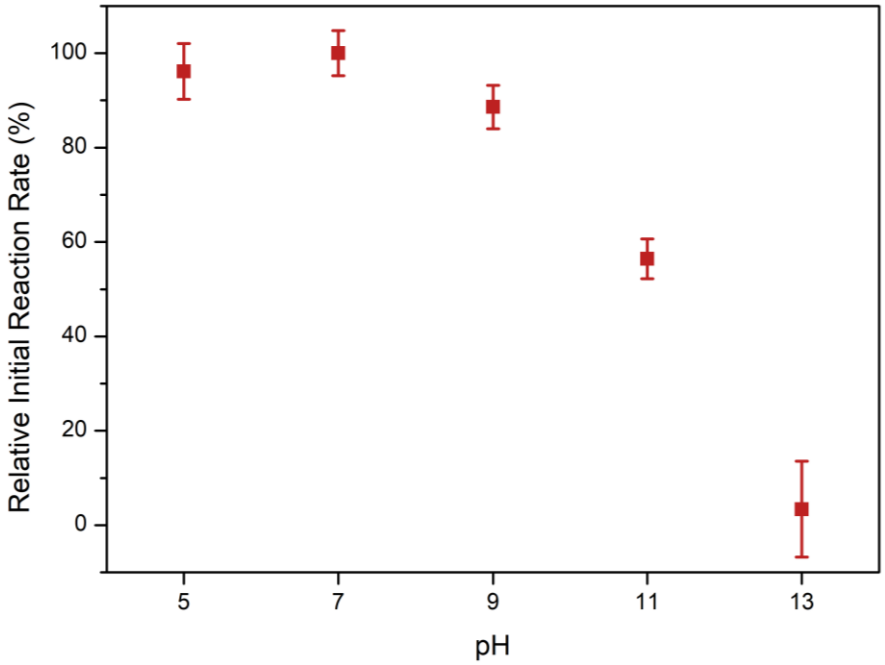

Figure 2.20: Impact of pH on catalase activity. Catalase was exposed to each pH at ambient conditions for 16 hours, and then diluted in 50 mM tris buffer prior to catalytic testing. The enzyme concentration in the reaction was 20 nM. Samples are normalized relative to catalase stored in ultrapure water at ambient conditions for 16 hours. Error bars represent the standard error in the slope of the linear regression of **Figure S2.7** from which the relative initial reaction rate was derived. Catalase activity decreases as the pH is increased past 9, reaching a minimum of 3% at pH 13.

With the above considered, the activity loss of catalase encapsulated in ZIF-8 is not solely due to exposure to the hydrophobic framework surface. Rather, it is due to a combination of factors, including the hydrophobicity of ZIF-8, substrate diffusion limitations, and high synthesis pH. Though encapsulation in an SEN and conjugation to PAA should partially protect catalase from these conditions, the combination of the three is likely too overwhelming for the nanogel to provide sufficient protection.

2.4.3 Release of 2-methylimidazole from ZIF-8

Given that the presence of 2-methylimidazole during ZIF-8 synthesis impacts the activity of catalase, either directly or indirectly via the associated alkaline pH, it was possible that the release of small amounts of HmIM from ZIF-8 in storage could also be impacting catalase activity. This could provide some explanation for why protected

catalase-on-ZIF samples showed no activity, as these samples were not exposed to the synthesis conditions for ZIF-8.

Though ZIF-8 maintains bulk crystallinity in water, it has been widely published that ZIF-8 exhibits some instability in certain solvents. For example, common buffers including PBS,[35-38] bis-tris,[39] bicarbonate,[35, 39, 40] phosphate,[28, 35, 39, 40] and citrate,[37] are known to cause protein leaching, surface etching, or loss of crystallinity for ZIF-8. Even exposure to mild concentrations of a secondary protein in solution, or certain free amino acids, can cause leaching of enzyme from ZIF-8.[39] Finally, some studies suggest that ZIF-8 exhibits mild instability in pure water,[40-42] with the degradation of ZIF-8 becoming inhibited once an equilibrium concentration of HmIM in solution is reached.[41] This would be accompanied with an increase in pH as shown in **Scheme 2.5**.

$$[Zn(mIM)_2]_{(s)} + 2H_2O_{(l)} \rightleftharpoons 2OH^-_{(aq)} + Zn^{2+}_{(aq)} + 2HmIM_{(aq)}$$

Scheme 2.5: Degradation of ZIF-8 in water (adapted from refs. 38, 41).

The release of HmIM from ZIF-8 could have a detrimental impact on surface-bound or encapsulated catalase. Though the resulting concentration of HmIM and pH would be milder than the synthesis conditions, the exposure period would be indefinite as the biocomposites were stored as an aqueous suspension. To assess the stability of ZIF-8, pure ZIF-8 was synthesized and stored identically to previously prepared biocomposites. The sample maintained bulk crystallinity after 2-week storage in water, although small peaks in the PXRD pattern at 12.08° and 13.26° indicate the formation of a small amount of a second MOF phase (**Figure 2.21**). These peaks match those of katsenite topology ZIF-8,[43] however they are insufficient to distinguish from other potential topologies such as diamondoid.[26] SEM indicates some changes in the morphological distribution of ZIF-8 particles after 2-week storage, with larger, rounded particles beginning to appear (**Figure 2.22**), which may the second phase observed in the PXRD. The average size of the rhombic dodecahedron crystals also decreases from 1.515 ± 0.024 μm to 1.069 ± 0.026 μm (**Figure 2.23**), suggesting the removal of some surface layers of the ZIF.

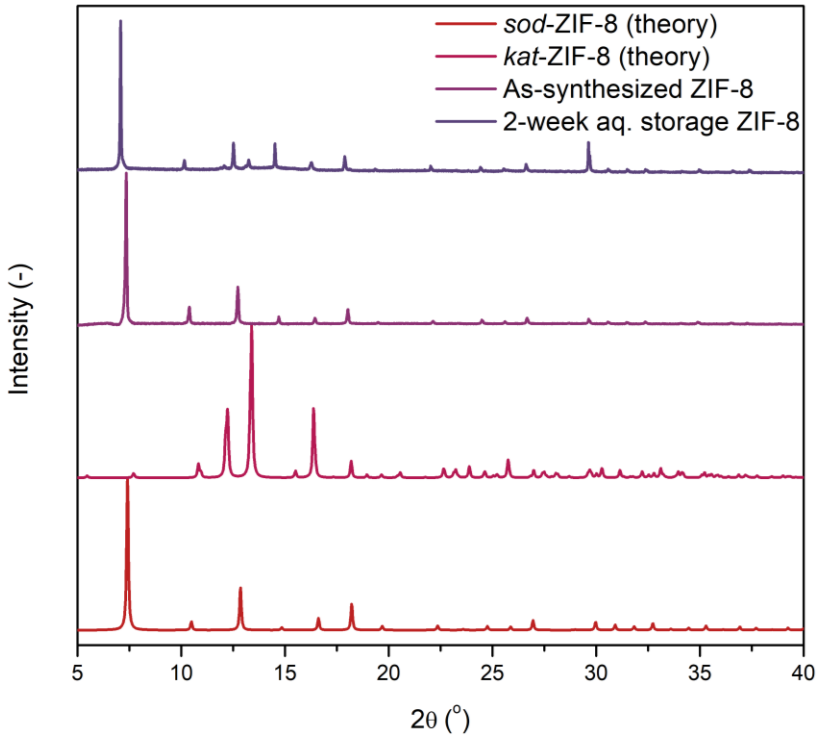

Figure 2.21: PXRD patterns of ZIF-8 after storage in ultrapure water for 2 weeks. Analysis was performed on a wet sample in the storage supernatant. The sample maintains bulk crystallinity after storage, however additional small peaks at 12.08° and 13.26° appear, which may correspond to the formation of a small amount of *kat*-ZIF-8 or other non-sodalite topology.

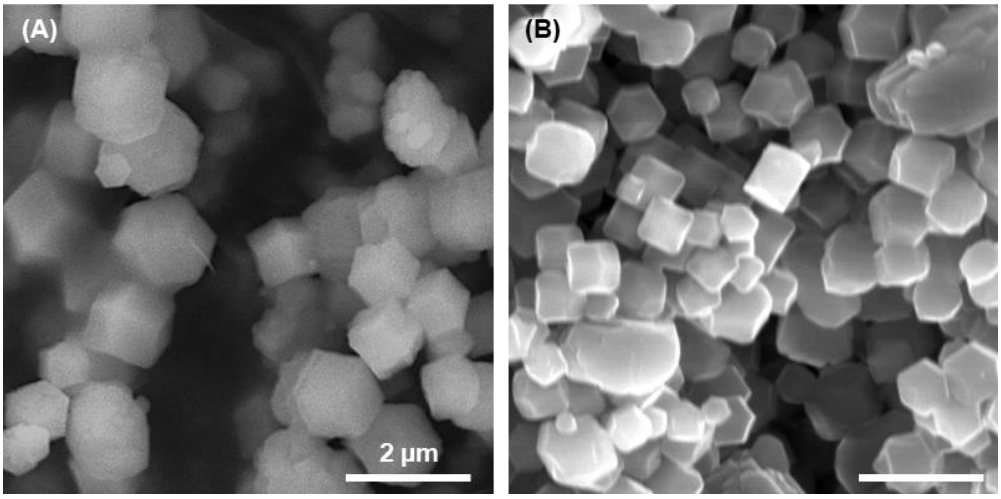

Figure 2.22: SEM images of (**A**) as-synthesized ZIF-8 and (**B**) ZIF-8 stored in ultrapure water for 2 weeks. Samples were synthesized using 40:640 $Zn(OAc)_2$:HmIM and dried under vacuum prior to analysis. The rhombic dodecahedron crystals decrease slightly in size during storage, whilst some larger rounded particles begin to appear, potentially corresponding to an additional ZIF-8 phase.

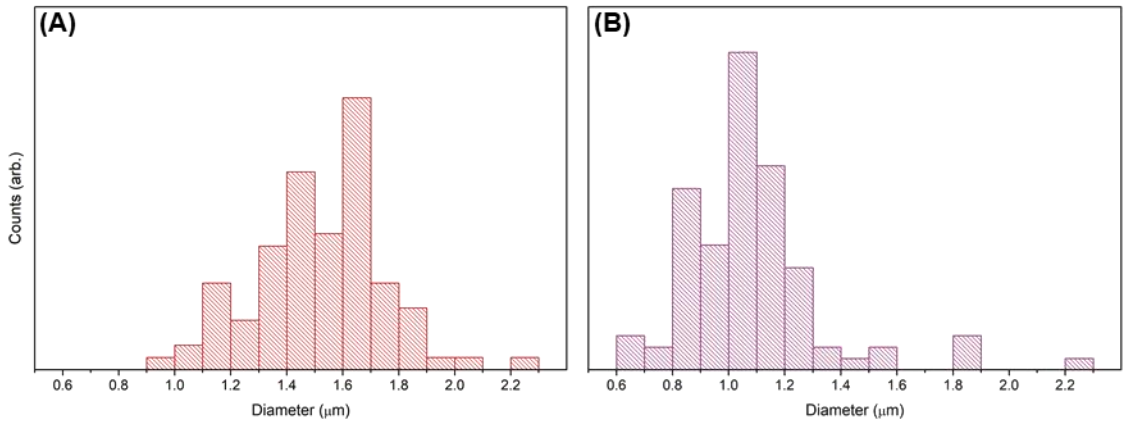

Figure 2.23: Particle size distributions of (**A**) as-synthesized ZIF-8 and (**B**) ZIF-8 stored in ultrapure water for 2 weeks. Samples were synthesized using 40:640 $Zn(OAc)_2$:HmIM and dried under vacuum prior to analysis. Mean particle sizes were calculated to be (**A**) 1.515 ± 0.024 μm and (**B**) 1.069 ± 0.026 μm.

To confirm the loss of 2-methylimidazole from ZIF-8 during storage, UV/vis spectroscopy was used, with the HmIM absorbance at 207 nm compared to a calibration curve of known concentrations of HmIM. It was found that the concentration of HmIM in the solution was low immediately after washing, however over time increased until it settled to a value of approximately 20 mM (**Figure 2.24**, **Figure S2.8**). In conjunction with this, the pH of the supernatant after the two-week storage period was 10.0, further validating the release of HmIM. Based on the catalase activity in 20 mM HmIM of 58% (**Figure 2.18**) and the anticipated activity in pH 10 of roughly 70% (**Figure 2.20**), it is reasonable to expect a 30-40% decrease in CAT@/on-ZIF-8 for each day of storage. Further to this, the concentration of HmIM at the surface of the ZIF may be higher than in the bulk solution, resulting in larger impacts on activity than predicted here. Overall, this indicates that, in the long term, CAT@ZIF-8 composites would lose all activity, regardless of the presence of permeable polymer shells to protect from the hydrophobic ZIF-8 surface. Potentially, a buffered solvent system could be used in conjunction with protective polymer shells to create a functional CAT@ZIF-8 system, although this requires further research and will be discussed in **Chapter 4**.

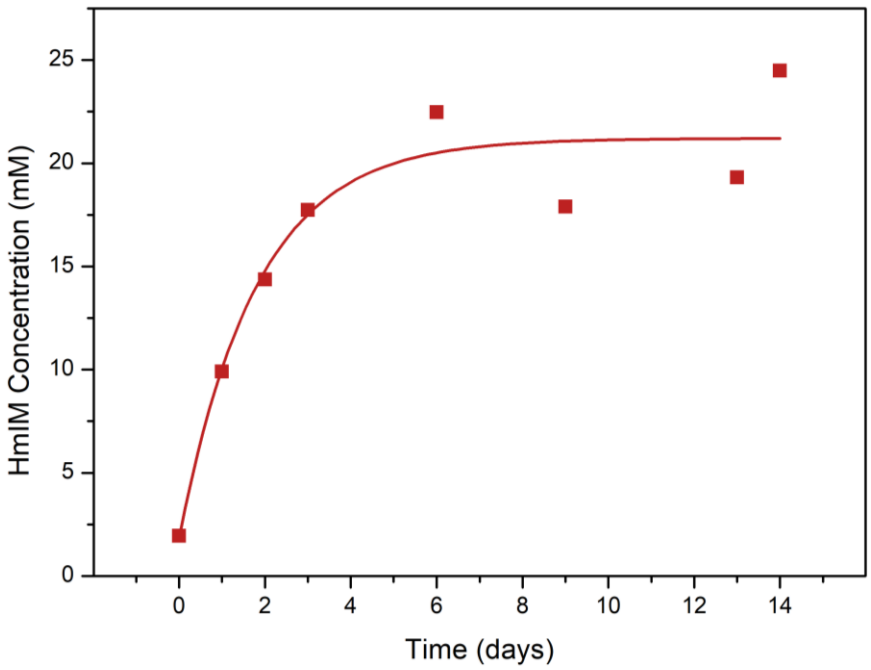

Figure 2.24: Release of HmIM from ZIF-8 stored in ultrapure water. Aliquots of the supernatant were analyzed by UV/vis spectroscopy, and the HmIM concentration determined from the 207 nm absorbance peak. Inconsistent concentration values after a longer time are likely due to difficulties separating ZIF-8 particles from the supernatant.

2.4.4 Summary

Alternative factors which may contribute to the loss of catalase activity in/on ZIF-8 were assessed. It was found that catalase is highly sensitive to 2-methylimidazole and alkaline pH, both of which are present in ZIF-8 synthesis. Although the overnight exposure to the synthesis conditions was unlikely to cause the complete activity loss seen for CAT@ZIF-8 composites, storage as an aqueous suspension led to extended exposure of catalase to mildly basic pH and moderate concentrations of HmIM, due to the instability of ZIF-8 in water. Thus, regardless of the success of catalase protection from the hydrophobic surface of ZIF-8, activity loss would result during storage. Polymer/enzyme composites are therefore an ineffective method of preventing catalase denaturation in ZIF-8, although further investigation with storage in buffer could provide more promising results.

2.5 Conclusions

Single enzyme nanogels and enzyme-polymer conjugates were trialed as materials for the protection of catalase inside ZIF-8, intending to prevent the detrimental interaction with the ZIF-8 surface which causes enzyme deactivation. In both cases, no catalase activity was observed in- or on-ZIF-8, suggesting that additional factors may contribute to enzyme deactivation in ZIF-8. Studies on the stability of ZIF-8 revealed the framework releases small amounts of 2-methylmidazole during storage in ultrapure water, raising the concentration of free 2-methylimidazole in solution. This was insufficient to disrupt bulk crystallinity, but could negatively impact catalase activity, either by direct interaction of the linker with catalase or indirectly by raising the pH of the solution. To protect catalase from denaturation upon encapsulation in ZIF-8, storage in a buffer combined with polymer-based protection methods may prove promising.

2.6 Experimental

2.6.1 Materials & characterization

Materials

All materials were purchased from Merck unless otherwise stated. Catalase from bovine liver (C9322) was purchased from Sigma Aldrich as a Lyophilized powder and the concentration of solutions of catalase assessed by measuring the UV/vis absorbance at 280 nm. Bovine serum albumen (BSA, A6003) was used as received and 100% purity was assumed. Ultrapure Milli-Q water with resistivity of >18 MΩ cm-1 (Merck Millipore purification system) was used for all syntheses, wash protocols and buffer preparations.

Powder x-ray diffraction (PXRD)

PXRD data of dry samples were collected on a Bruker D4 Endeavor x-ray diffractometer. A Co anode was used to produce K_α radiation (λ = 1.78897 Å). Flat plate diffraction data was collected over the range 2θ =5−40°. The PXRD data were converted by PowDLL converter (version 2.97.0.0) and presented as the Cu-source irradiated patterns (λ = 1.54056 Å).

PXRD data of wet samples were collected on a Bruker D8 Advanced X-ray powder diffractometer using a Cu Kα λ=1.5418 Å radiation source, using 1.0 mm glass capillaries. Data were collected for between 2θ of 2° to 52.94° with Phi rotation at 20 rotations per min at 1-second exposure per step at 5001 steps.

Transmission electron microscopy (TEM)

TEM images were collected on a FEI Tecnai G2 Spirit TEM. Samples were drop-cast onto a 3 mm TEM grids and the excess solution blotted away with a piece of filter paper, leaving a thin layer of solution on the grid. The samples were air dried and then stained with uranyl acetate prior to analysis.

Scanning electron microscopy (SEM)

SEM images were collected on a FEI Quanta 450 FEG Environmental Scanning Electron Microscope (ESEM), operating at 10.0 kV with a spot size of 3.0, and under

ultrahigh vacuum (10 7 – 10-12 hPa) conditions. Samples were dried and loaded onto 12 mm carbon tabs on aluminium stages and sputter-coated with carbon prior to analysis.

Dynamic light scattering (DLS) & zeta potential

DLS and zeta potential measurements were taken on a Malvern Zetasizer Nano ZSP dynamic light scattering instrument. Data were analyzed using Malvern Zetasizer software (version 8.01.4906).

Dynamic light scattering of proteins was performed using 12 mm polystyrene cuvettes. Proteins were dissolved to a concentration of ~1 mg/mL in 1 x PBS and passed through a 0.2 µm syringe filter prior to analysis. Measurements were performed in triplicate, with each measurement consisting of 15 runs of 10 s each, with a 120 s prior incubation period. The following measurement parameters were used: Temperature = 25.0 ^{o}C, material RI = 1.450, dispersant RI = 1.332, dispersant viscosity = 0.9082 cP.

UV/visible spectroscopy

UV/vis spectroscopy data were collected on a Shimadzu UV-3600 Plus spectrophotometer. UV/vis absorption measurements for the purposes of assays were performed in polystyrene cuvettes, whilst UV/vis absorption measurements of pure proteins or 2-methylimidazole were performed in quartz cuvettes. The wavelength of the incident light varied by experiment and is specified in the text.

2.6.2 Single enzyme nanogels & ZIF-8 syntheses

Single enzyme nanogel synthesis

During SEN synthesis, the AAm:BIS:APS:TMEDA concentration ratio was held constant at 12:2:1:1, and the acrylamide concentration adjusted as specified in the text. The amount of protein and sucrose was held constant across all experiments.

For the synthesis of protein@SENs, protein (7.98 mg), sucrose (0.2 g) and acrylamide were dissolved in sodium phosphate buffer (50 mM, pH 6.1, 3.6 mL). N,N'-methylenebisacrylamide in DMSO (0.4 mL) was added and the mixture degassed with nitrogen for 45 minutes. Whilst degassing with nitrogen, ammonium persulphate then tetramethylethylenediamine were added. The reaction was kept under nitrogen and stirred at room temperature for 2 hours. The mixture was passed through a Sephadex G-25

column and fractions collected. Fractions were analyzed by UV-vis spectroscopy to determine which fractions contained BSA (i.e. those with an absorbance at ~280 nm). The BSA-containing fractions were concentrated and rinsed with water by centrifugation through a 10 kDa filter. Protein@SEN samples were stored as a concentrated solution in water at 4 °C. The concentration of protein in the sample was estimated from the 280 nm protein absorbance in UV/vis spectroscopy, with the predicted contribution of the polymer to the absorbance subtracted.

ZIF-8 syntheses

For the synthesis of pure ZIF-8, final concentrations of 640 mM 2-methylimidazole (HmIM) and 40 mM $Zn(OAc)_2$ were used. Briefly, $Zn(OAc)_2$ (600 mM, 0.2 mL) was added to a solution of HmIM (685 mM, 2.8 mL). The reaction mixture was left under ambient conditions for 16 hours, and then the solid washed three times with water. Samples for catalytic testing were resuspended in water and stored at 4 °C. Samples for PXRD were dried under vacuum overnight.

For forced ZIF-8 precipitation in the presence of protein, final concentrations of 640 mM 2-methylimidazole (HmIM) and 40 mM $Zn(OAc)_2$ were used. Briefly, $Zn(OAc)_2$ (600 mM, 0.2 mL) was added to a solution of HmIM (685 mM, 2.8 mL) containing protein/SEN (2 mg). The reaction mixture was left under ambient conditions for 16 hours, and then washed three times with water. Samples for catalytic testing were resuspended in water and stored at 4 °C. Samples for PXRD were dried under vacuum overnight.

For biomimetic mineralization of ZIF-8, final concentrations of 80 mM 2-methylimidazole (HmIM) and 20 mM $Zn(OAc)_2$ were used. Briefly, $Zn(OAc)_2$ (40 mM, 2 mL) was added to a solution of HmIM (160 mM, 2 ml) containing protein/SEN (2 mg). The reaction mixture was left under ambient conditions for 16 hours, and then washed twice with water and once with ethanol. Samples for catalytic testing were resuspended in water and stored at 4 °C. Samples for PXRD were air dried overnight at ambient temperature and pressure.

Protein-on-ZIF-8 synthesis

For protein-on-ZIF-8 synthesis, a sample of pure ZIF-8 was prepared as per the procedure above. This sample was then resuspended in water (3 mL) with protein (2 mg),

and the mixture stirred for 2 hours. The sample was then washed three times with water, resuspended in water and stored at 4 °C.

Catalase purification procedure

Catalase (100 mg) was dissolved in tris buffer (50 mM, pH 7.5, 50 mL) and the supernatant isolated by centrifugation (3823 g, 8 min). The supernatant was removed and passed through a 0.22 µm syringe filter membrane into a HiTrap SP HP cation exchange column pre-equilibrated with tris buffer. Tris buffer with sodium chloride (75 mM) was passed through the column and slowly eluted a red band. 100 and 125 mM NaCl in tris resulted in no further elution, whilst 150 mM NaCl resulted in the elution of a second band. Fractions were collected and fractions with a UV vis ratio of absorbances 405 nm / 280 nm greater than 0.3 were combined and exchanged into sodium phosphate buffer (50 mM, pH 6.1) using a PD-10 column.

Loading quantification

Loading of catalase/SEN in/on ZIF-8 was quantified by Bradford assay of the supernatant/washings. A 100 µL sample of the supernatant/washing mixture was taken (diluted where necessary) and mixed with 3 mL of Bradford reagent. Samples were incubated at room temperature for 5 minutes and the absorbance at 595 nm measured by UV/vis spectroscopy. This was compared to a calibration curve of known concentrations of catalase/SEN to determine the concentration of catalase/SEN in the washings, from which the loading in/on ZIF-8 could be inferred.

Catalytic testing

The Ferrous Oxidation in Xylenol orange (FOX) assay was used to assess the activity of catalase-containing samples. The FOX reagent is composed of 100 mM sorbitol, 25 mM H_2SO_4, 250 µM ammonium ferrous sulfate, and 100 µM xylenol orange.

In activity testing, catalase, CAT@SEN, CAT@ZIF, or CAT@SEN@ZIF was stirred in tris buffer (0.05 M, pH 7.4, 500 µL), followed by the addition of hydrogen peroxide (160 µM, 500 µL). The catalase concentration in the enzymatic reaction varied by experiment and is specified in the text. At defined time intervals, 50 µL samples of the reaction mixture were taken and mixed with 950 µL of FOX reagent. After incubation for at least 30 minutes at room temperature, the UV/vis absorbance at 585 nm was recorded to assess the breakdown of hydrogen peroxide by catalase.

2.6.3 Protein-polymer conjugates

Catalase-PAA synthesis

A solution of 8000 Da PAA (10 wt.%, 2 mL) in water was added to sodium phosphate buffer (200 mM, pH 7, 0.5 mL). EDC solution (200 mM, 2.5 mL) was then added and stirred for 10 minutes. Catalase solution (5 mg/mL, 2.33 mL) was added dropwise and the mixture stirred at room temperature for 4 hours. Unreacted precursors and by-products were removed by repeated centrifugation through a 10 kDa filter (3823 g). Samples were stored as an aqueous solution at 4 °C.

Alternative ZIF-8 synthesis procedure (for larger particles)

For the synthesis of ZIF-8 around catalase-PAA, a modified procedure to that reported by Falcaro and co-workers for the encapsulation of yeast cells was initially trialed.[24] $Zn(OAc)_2$ (40 mM, 5 mL) was added to either catalase or catalase-PAA (2 mg) in HmIM (640 mM, 5 mL). The reaction mixture was shaken for 2 hours, and then washed three times with water. PXRD was performed on wet samples.

Quantification of wt.% catalase in PAA conjugates

The amount of catalase in 500 µL of a sample of catalase-PAA was determined by measurement of the 280 nm peak of catalase. The sample was then freeze dried and weighed to determine the total mass of conjugate present, from which the wt.% loading could be determined.

2.6.4 Studies on deactivation of catalase

Overnight exposure of catalase to HmIM and Hmtz

Catalase (2 mg) was dissolved in various concentrations of HmIM in water (640, 560, 320, 160, 80, 40, 20, 10, 5 mM). 80 mM Hmtz, with and without deprotonation with a stoichiometric quantity of ammonia, was also tested as a comparison to the MAF-7 synthesis conditions. The samples were left undisturbed at room temperature for 16 hours, and were then diluted in tris buffer to a catalase concentration of 40 nM. Catalytic testing was performed as described previously, at a catalase concentration of 20 nM.

Overnight exposure of catalase to solutions of varying pH

Samples of ultrapure water were pH adjusted to integer values 2-14 by use of either NaOH or HCl. Catalase (2 mg) was then added to each sample. The samples were left undisturbed at room temperature for 16 hours, after which the final pH was measured to the nearest integer unit. The samples were then diluted in tris buffer to a catalase concentration of 40 nM. Catalytic testing was performed as described previously, at a catalase concentration of 20 nM.

Monitoring the degradation of ZIF-8 by UV/vis spectroscopy

ZIF-8 was synthesized and washed using the forced precipitation approach described previously. The ZIF was then resuspended in water (3 mL). To determine the concentration of HmIM released at each time interval,100 µL of the sample was taken and the supernatant isolated by centrifugation (6000 g, 10 mins). The supernatant was diluted twenty-fold, and then the absorbance at 207 nm determined by UV/vis spectroscopy. The concentration of HmIM in the solution was determined by comparison to a calibration curve of known HmIM concentrations.

2.7 References

1. Liang, W.; Xu, H.; Carraro, F.; Maddigan, N. K.; Li, Q.; Bell, S. G.; Huang, D. M.; Tarzia, A.; Solomon, M. B.; Amenitsch, H.; et al. Enhanced activity of enzymes encapsulated in hydrophilic metal–organic frameworks. *Journal of the American Chemical Society* **2019**, *141* (6), 2348-2355. DOI: 10.1021/jacs.8b10302.

2. Liang, W.; Carraro, F.; Solomon, M. B.; Bell, S. G.; Amenitsch, H.; Sumby, C. J.; White, N. G.; Falcaro, P.; Doonan, C. J. Enzyme encapsulation in a porous hydrogen-bonded organic framework. *Journal of the American Chemical Society* **2019**, *141* (36), 14298-14305. DOI: 10.1021/jacs.9b06589.

3. Beloqui, A.; Kobitski, A. Y.; Nienhaus, G. U.; Delaittre, G. A simple route to highly active single-enzyme nanogels. *Chemical Science* **2018**, *9* (4), 1006-1013. DOI: 10.1039/C7SC04438K.

4. Chapman, R.; Stenzel, M. H. All wrapped up: Stabilization of enzymes within single enzyme nanoparticles. *Journal of the American Chemical Society* **2019**, *141* (7), 2754-2769. DOI: 10.1021/jacs.8b10338.

5. Yan, M.; Ge, J.; Liu, Z.; Ouyang, P. Encapsulation of single enzyme in nanogel with enhanced biocatalytic activity and stability. *Journal of the American Chemical Society* **2006**, *128* (34), 11008-11009. DOI: 10.1021/ja064126t.

6. Ge, J.; Lu, D.; Wang, J.; Liu, Z. Lipase nanogel catalyzed transesterification in anhydrous dimethyl sulfoxide. *Biomacromolecules* **2009**, *10* (6), 1612-1618. DOI: 10.1021/bm900205r.

7. Yan, M.; Du, J.; Gu, Z.; Liang, M.; Hu, Y.; Zhang, W.; Priceman, S.; Wu, L.; Zhou, Z. H.; Liu, Z.; et al. A novel intracellular protein delivery platform based on single-protein nanocapsules. *Nature Nanotechnology* **2010**, *5* (1), 48-53. DOI: 10.1038/nnano.2009.341.

8. Sánchez-deAlcázar, D.; Rodriguez-Abetxuko, A.; Beloqui, A. Metal–organic enzyme nanogels as nanointegrated self-reporting chemobiosensors. *ACS Applied Materials & Interfaces* **2022**, *14* (24), 27589-27598. DOI: 10.1021/acsami.2c04385.

9. Rodriguez-Abetxuko, A.; Morant-Miñana, M. C.; López-Gallego, F.; Yate, L.; Seifert, A.; Knez, M.; Beloqui, A. Imidazole-grafted nanogels for the fabrication of organic–inorganic protein hybrids. *Advanced Functional Materials* **2018**, *28* (35), 1803115. DOI: 10.1002/adfm.201803115.

10. Baca, J. T.; Finegold, D. N.; Asher, S. A. Tear glucose analysis for the noninvasive detection and monitoring of diabetes mellitus. *The Ocular Surface* **2007**, *5* (4), 280-293. DOI: 10.1016/S1542-0124(12)70094-0.

11. Doumas, B. T. Standards for total serum protein assays - a collaborative study. *Clin Chem* **1975**, *21* (8), 1159-1166.

12. Wishard, A.; Gibb, B. C. Dynamic light scattering – an all-purpose guide for the supramolecular chemist. *Supramolecular Chemistry* **2019**, *31* (9), 608-615. DOI: 10.1080/10610278.2019.1629438.

13. Wu, S.; Shanks, R. A. Solubility study of polyacrylamide in polar solvents. *Journal of Applied Polymer Science* **2004**, *93* (3), 1493-1499. DOI: 10.1002/app.20608.

14. Zhang, Y.; Jia, Y.; Hou, L. a. Synthesis of zeolitic imidazolate framework-8 on polyester fiber for PM2.5 removal. *RSC Advances* **2018**, *8* (55), 31471-31477. DOI: 10.1039/C8RA06414H.

15. Shamsaei, E.; Lin, X.; Low, Z.-X.; Abbasi, Z.; Hu, Y.; Liu, J. Z.; Wang, H. Aqueous phase synthesis of ZIF-8 membrane with controllable location on an asymmetrically porous polymer substrate. *ACS Applied Materials & Interfaces* **2016**, *8* (9), 6236-6244. DOI: 10.1021/acsami.5b12684.

16. Chelikani, P.; Fita, I.; Loewen, P. C. Diversity of structures and properties among catalases. *Cellular and Molecular Life Sciences* **2004**, *61* (2), 192-208. DOI: 10.1007/s00018-003-3206-5.

17. Nourooz-Zadeh, J. Ferrous ion oxidation in presence of xylenol orange for detection of lipid hydroperoxides in plasma. In *Methods in Enzymology*, Vol. 300; Academic Press, 1999; pp 58-62.

18. Sheldon, R. A. Cross-linked enzyme aggregates as industrial biocatalysts. *Organic Process Research & Development* **2011**, *15* (1), 213-223. DOI: 10.1021/op100289f.

19. Cao, L.; Langen, L. v.; Sheldon, R. A. Immobilised enzymes: carrier-bound or carrier-free? *Current Opinion in Biotechnology* **2003**, *14* (4), 387-394. DOI: 10.1016/S0958-1669(03)00096-X.

20. Riccardi, C. M.; Cole, K. S.; Benson, K. R.; Ward, J. R.; Bassett, K. M.; Zhang, Y.; Zore, O. V.; Stromer, B.; Kasi, R. M.; Kumar, C. V. Toward "stable-on-the-table" enzymes: Improving key properties of catalase by covalent conjugation with poly(acrylic acid). *Bioconjugate Chemistry* **2014**, *25* (8), 1501-1510. DOI: 10.1021/bc500233u.

21. Maddigan, N. K.; Tarzia, A.; Huang, D. M.; Sumby, C. J.; Bell, S. G.; Falcaro, P.; Doonan, C. J. Protein surface functionalisation as a general strategy for facilitating biomimetic mineralisation of ZIF-8. *Chemical Science* **2018**, *9* (18), 4217-4223. DOI: 10.1039/C8SC00825F.

22. Reid, T. J., 3rd; Murthy, M. R.; Sicignano, A.; Tanaka, N.; Musick, W. D.; Rossmann, M. G. Structure and heme environment of beef liver catalase at 2.5 A resolution. *Proc Natl Acad Sci U S A* **1981**, *78* (8), 4767-4771. DOI: 10.1073/pnas.78.8.4767.

23. Liang, K.; Richardson, J. J.; Cui, J.; Caruso, F.; Doonan, C. J.; Falcaro, P. Metal–organic framework coatings as cytoprotective exoskeletons for living cells. *Advanced Materials* **2016**, *28* (36), 7910-7914. DOI: 10.1002/adma.201602335.

24. Gan, L.; Velásquez-Hernández, M. d. J.; Emmerstorfer-Augustin, A.; Wied, P.; Wolinski, H.; Zilio, S. D.; Solomon, M.; Liang, W.; Doonan, C.; Falcaro, P. Multi-layered ZIF-coated cells for the release of bioactive molecules in hostile environments. *Chemical Communications* **2022**, *58* (72), 10004-10007. DOI: 10.1039/D2CC03072A.

25. Zakhartsev, M.; Reuss, M. Cell size and morphological properties of yeast Saccharomyces cerevisiae in relation to growth temperature. *FEMS Yeast Research* **2018**, *18* (6). DOI: 10.1093/femsyr/foy052.

26. Liang, W.; Ricco, R.; Maddigan, N. K.; Dickinson, R. P.; Xu, H.; Li, Q.; Sumby, C. J.; Bell, S. G.; Falcaro, P.; Doonan, C. J. Control of structure topology and spatial distribution of biomacromolecules in protein@ZIF-8 biocomposites. *Chemistry of Materials* **2018**, *30* (3), 1069-1077. DOI: 10.1021/acs.chemmater.7b04977.

27. Maddigan, N. K. Enzyme immobilisation using porous frameworks. University of Adelaide, Adelaide, 2020. https://hdl.handle.net/2440/126087.

28. Maddigan, N. K.; Linder-Patton, O. M.; Falcaro, P.; Sumby, C. J.; Bell, S. G.; Doonan, C. J. Influence of the synthesis and storage conditions on the activity of Candida antarctica lipase B ZIF-8 biocomposites. *ACS Applied Materials & Interfaces* **2021**. DOI: 10.1021/acsami.1c04785.

29. Sharma, S.; Berne, B. J.; Kumar, S. K. Thermal and structural stability of adsorbed proteins. *Biophysical Journal* **2010**, *99* (4), 1157-1165. DOI: 10.1016/j.bpj.2010.05.030.

30. Moskovitz, Y.; Srebnik, S. Conformational changes of globular proteins upon adsorption on a hydrophobic surface. *Physical Chemistry Chemical Physics* **2014**, *16* (23), 11698-11707. DOI: 10.1039/C4CP00354C.

31. Sann, E. E.; Pan, Y.; Gao, Z.; Zhan, S.; Xia, F. Highly hydrophobic ZIF-8 particles and application for oil-water separation. *Separation and Purification Technology* **2018**, *206*, 186-191. DOI: 10.1016/j.seppur.2018.04.027.

32. Shivu, B.; Seshadri, S.; Li, J.; Oberg, K. A.; Uversky, V. N.; Fink, A. L. Distinct β-sheet structure in protein aggregates determined by ATR–FTIR spectroscopy. *Biochemistry* **2013**, *52* (31), 5176-5183. DOI: 10.1021/bi400625v.

33. Margoliash, E.; Novogrodsky, A.; Schejter, A. Irreversible reaction of 3-amino-1:2:4-triazole and related inhibitors with the protein of catalase. *Biochemical Journal* **1960**, *74* (2), 339-348. DOI: 10.1042/bj0740339.

34. Prajapati, S.; Bhakuni, V.; Babu, K. R.; Jain, S. K. Alkaline unfolding and salt-induced folding of bovine liver catalase at high pH. *European Journal of Biochemistry* **1998**, *255* (1), 178-184. DOI: 10.1046/j.1432-1327.1998.2550178.x.

35. Luzuriaga, M. A.; Benjamin, C. E.; Gaertner, M. W.; Lee, H.; Herbert, F. C.; Mallick, S.; Gassensmith, J. J. ZIF-8 degrades in cell media, serum, and some - but not all - common laboratory buffers. *Supramolecular Chemistry* **2019**, *31* (8), 485-490. DOI: 10.1080/10610278.2019.1616089.

36. Velásquez-Hernández, M. d. J.; Ricco, R.; Carraro, F.; Limpoco, F. T.; Linares-Moreau, M.; Leitner, E.; Wiltsche, H.; Rattenberger, J.; Schröttner, H.; Frühwirt, P.; et al. Degradation of ZIF-8 in phosphate buffered saline media. *CrystEngComm* **2019**, *21* (31), 4538-4544. DOI: 10.1039/C9CE00757A.

37. Spitsyna, A. S.; Poryvaev, A. S.; Sannikova, N. E.; Yazikova, A. A.; Kirilyuk, I. A.; Dobrynin, S. A.; Chinak, O. A.; Fedin, M. V.; Krumkacheva, O. A. Stability of ZIF-8 nanoparticles in most common cell culture media. *Molecules* **2022**, *27* (10). DOI: 10.3390/molecules27103240.

38. Butonova, S. A.; Ikonnikova, E. V.; Sharsheeva, A.; Chernyshov, I. Y.; Kuchur, O. A.; Mukhin, I. S.; Hey-Hawkins, E.; Vinogradov, A. V.; Morozov, M. I. Degradation kinetic study of ZIF-8 microcrystals with and without the presence of lactic acid. *RSC Advances* **2021**, *11* (62), 39169-39176. DOI: 10.1039/D1RA07089D.

39. Gao, Y.; Doherty, C. M.; Mulet, X. A systematic study of the stability of enzyme/zeolitic imidazolate framework-8 composites in various biologically relevant solutions. *ChemistrySelect* **2020**, *5* (43), 13766-13774. DOI: 10.1002/slct.202003575.

40. Wang, H.; Jian, M.; Qi, Z.; Li, Y.; Liu, R.; Qu, J.; Zhang, X. Specific anion effects on the stability of zeolitic imidazolate framework-8 in aqueous solution. *Microporous and Mesoporous Materials* **2018**, *259*, 171-177. DOI: 10.1016/j.micromeso.2017.10.011.

41. Zhang, H.; Liu, D.; Yao, Y.; Zhang, B.; Lin, Y. S. Stability of ZIF-8 membranes and crystalline powders in water at room temperature. *Journal of Membrane Science* **2015**, *485*, 103-111. DOI: 10.1016/j.memsci.2015.03.023.

42. Sheng, L.; Yang, F.; Wang, C.; Yu, J.; Zhang, L.; Pan, Y. Comparison of the hydrothermal stability of ZIF-8 nanocrystals and polycrystalline membranes derived from zinc salt variations. *Materials Letters* **2017**, *197*, 184-187. DOI: 10.1016/j.matlet.2017.03.077.

43. Katsenis, A. D.; Puškarić, A.; Štrukil, V.; Mottillo, C.; Julien, P. A.; Užarević, K.; Pham, M.-H.; Do, T.-O.; Kimber, S. A. J.; Lazić, P.; et al. In situ X-ray diffraction monitoring of a mechanochemical reaction reveals a unique topology metal-organic framework. *Nature Communications* **2015**, *6* (1), 6662. DOI: 10.1038/ncomms7662.

2.8 Supporting Information

2.8.1 Single enzyme nanogels

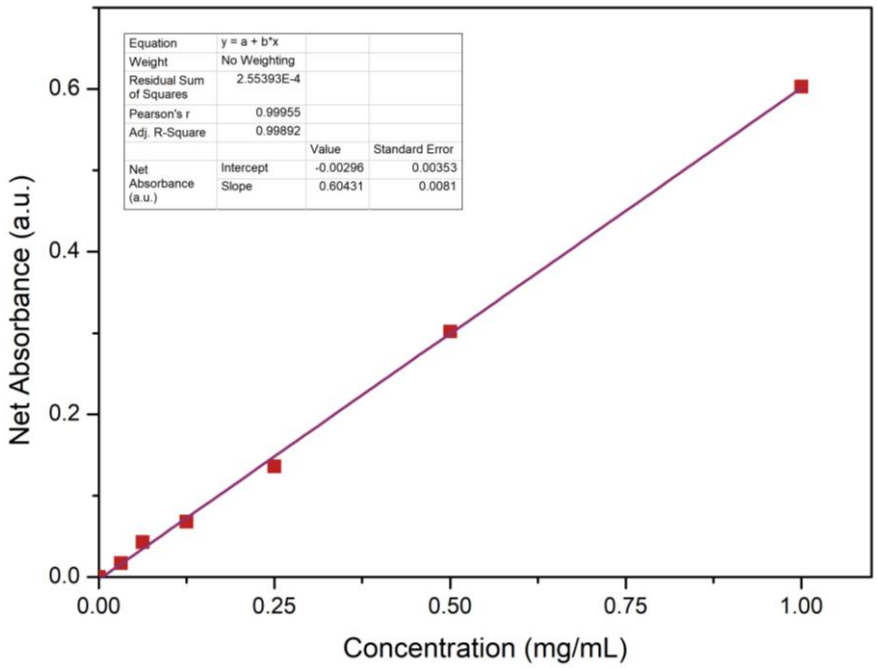

Figure S2.1: Example Bradford calibration curve for the determination of protein concentration in washings/supernatant of ZIF-8. Example curve was prepared using catalase, with the absorbance measured at 595 nm.

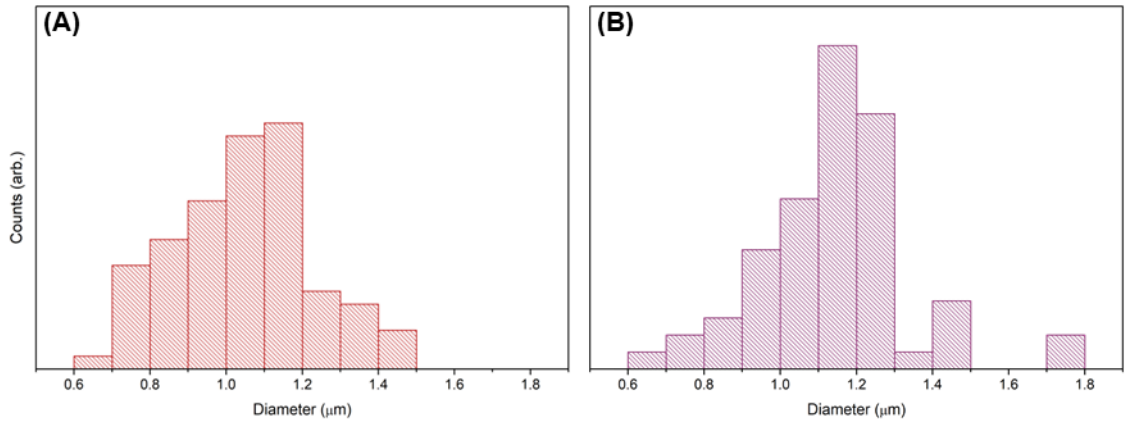

Figure S2.2: Particle size distributions of (**A**) BSA@ZIF-8 and (**B**) BSA@SEN-180@ZIF-8, synthesized using 40:640 $Zn(OAc)_2$:HmIM. Samples were washed three times with water and dried under vacuum prior to analysis. Mean particle sizes were calculated to be (**A**) 1.039 ± 0.020 µm and (**B**) 1.131 ± 0.024 µm.

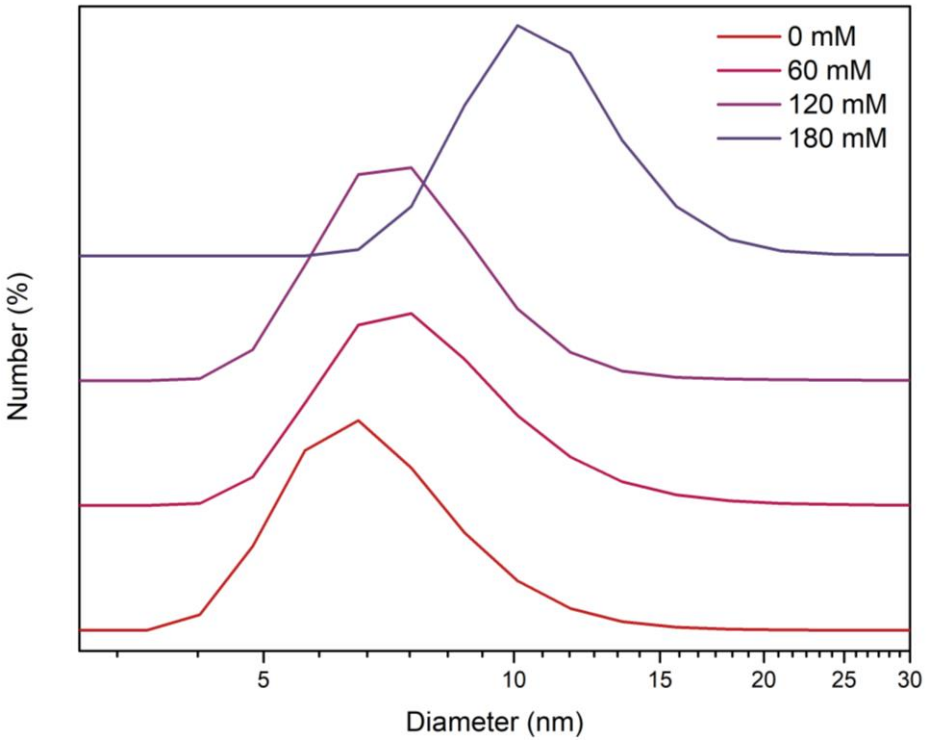

Figure S2.3: Number size distributions of CAT@SEN samples prepared using different acrylamide concentrations, as determined by dynamic light scattering (DLS). Samples were analyzed as a solution in tris buffer (100 mM, pH 7.4) and filtered through a 0.2 µm syringe filter prior to analysis.

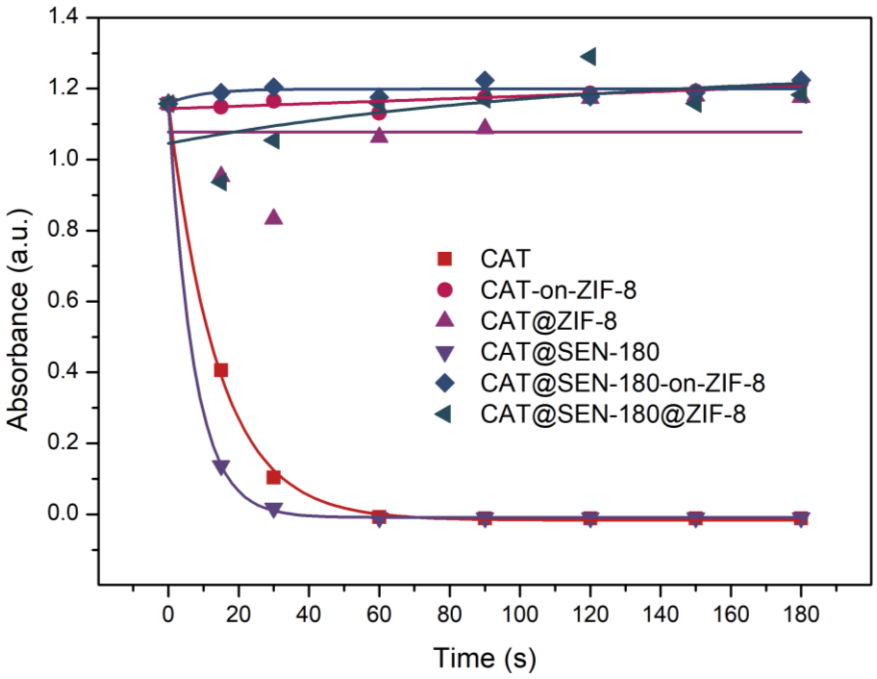

Figure S2.4: Breakdown of hydrogen peroxide by catalase and CAT@SEN-180 samples when encapsulated in ZIF-8, synthesized using 40:640 $Zn(OAc)_2$:HmIM. Samples were taken from the reaction vessel and mixed with FOX reagent, leading to an absorbance at 585 nm proportional to the amount of hydrogen peroxide present.

2.8.2 Protein-polymer conjugates

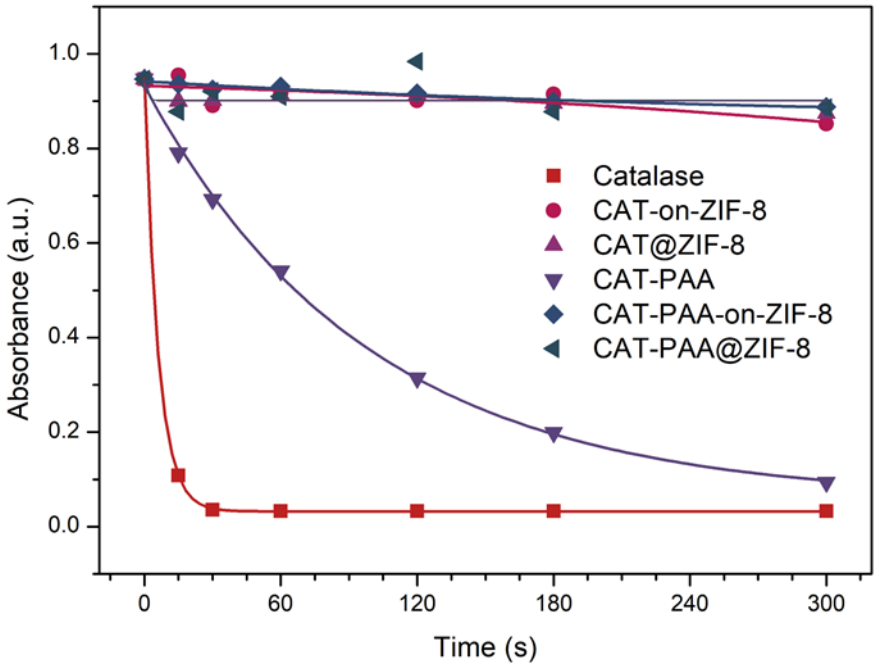

Figure S2.5: Breakdown of hydrogen peroxide by catalase and catalase-PAA samples when encapsulated in ZIF-8, synthesized using 20:80 Zn(OAc)2:HmIM. The enzyme concentration in the reaction was 100 nM. Samples were taken from the reaction vessel and mixed with FOX reagent, leading to an absorbance at 585 nm proportional to the amount of hydrogen peroxide present.

2.8.3 Studies on the deactivation of catalase

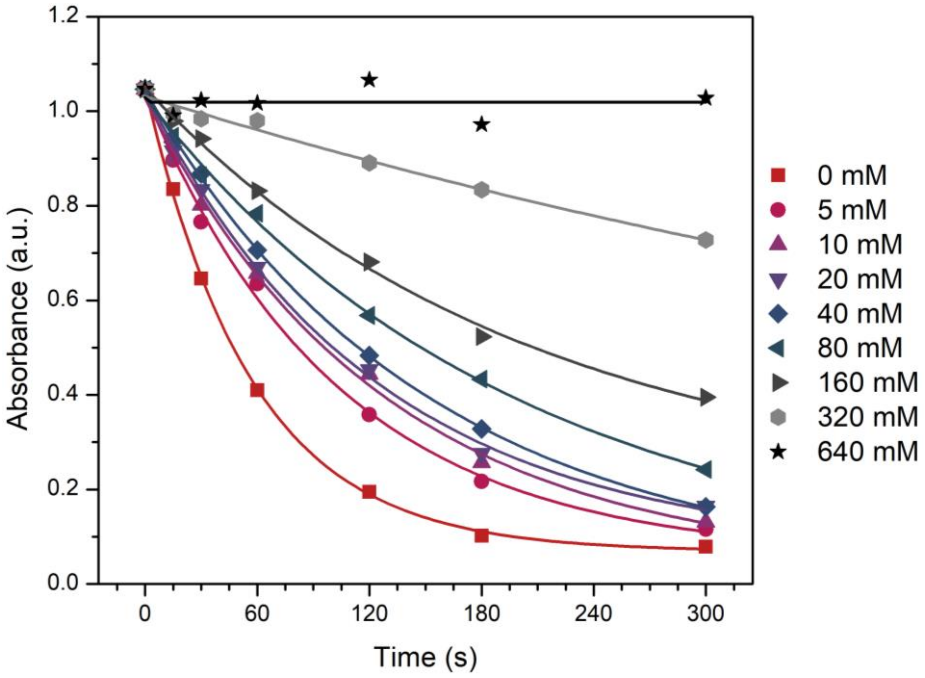

Figure S2.6: Raw data for the catalytic testing of catalase after overnight exposure to various concentrations of 2-methylimidazole. The enzyme concentration in the reaction was 20 nM.

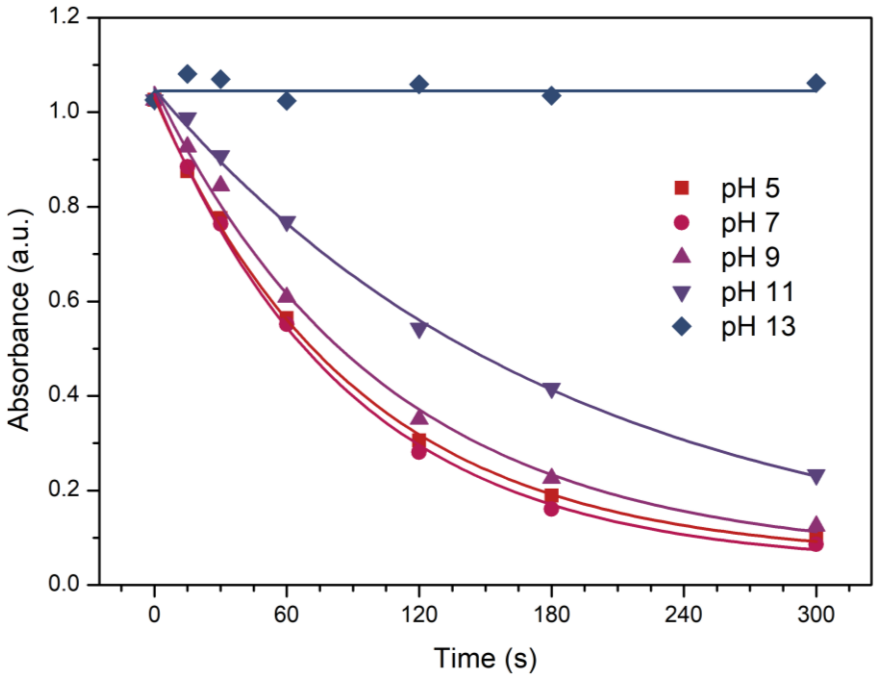

Figure S2.7: Raw data for the catalytic testing of catalase after overnight exposure to solutions of varying pH. The enzyme concentration in the reaction was 20 nM.

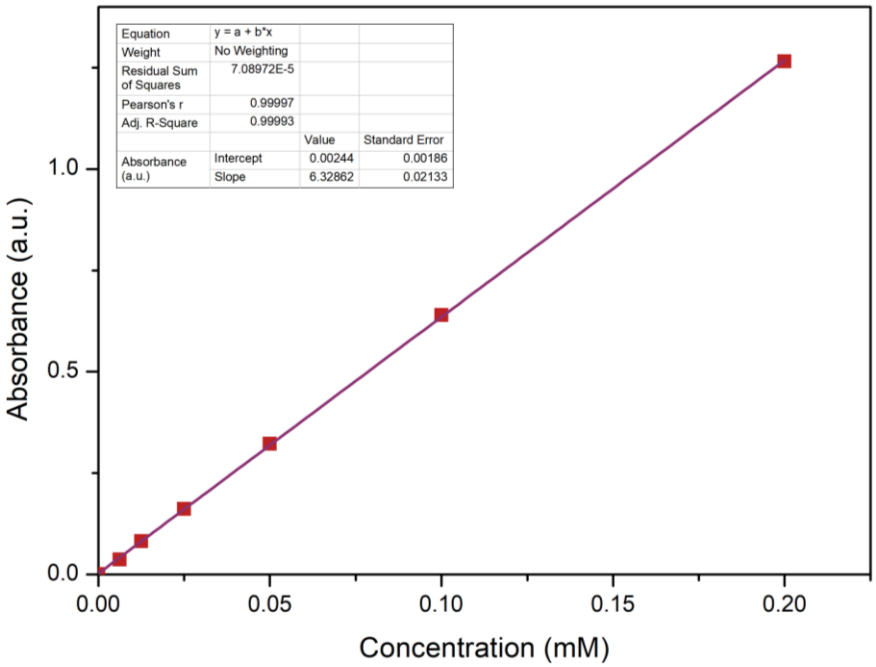

Figure S2.8: UV/vis absorption calibration curve for the determination of 2-methylimidazole concentration in solution, with absorbance measured at 207 nm.

CHAPTER 3

Controlling the Spatial Distribution of Proteins in BioHOF-1

3.1 Chapter Overview

BioHOF-1 was the first hydrogen bonded organic framework (HOF) reported for the encapsulation of biomolecules, consisting of tetrahedral amidinium and carboxylate linkers. When sodium 4,4',4",4"'-methanetetrayltetrabenzoate (tetra-carboxylate) and 4,4',4",4"'-methanetetrayltetrabenzimidamide hydrochloride (tetra-amidinium) are combined in the presence of protein, it enables the formation of a charge-assisted HOF around the protein. As opposed to ZIF-8, the protein does not actively nucleate HOF growth, rather it is randomly incorporated into the framework through particle aggregation.[1] As the protein is not directly involved in the nucleation process, complete protein encapsulation is unlikely, and thus investigation into the loading of protein in BioHOF-1 is necessary.

Techniques for accurately evaluating the encapsulation of proteins in BioHOF-1, both quantitatively and qualitatively, are established in **Section 3.2**. These techniques were used to investigate methods of increasing protein loading in BioHOF-1. In **Section 3.3**, the effect of protein surface chemistry on encapsulation of BioHOF-1 was assessed. This revealed a significant preference for protein to adsorb to the surface of the HOF regardless of surface chemistry. In **Section 3.4**, slowing the HOF framework growth using modulators was trialed as a method of overcoming the preference for surface adsorption, aiming for protein loading to increase by allowing more time for the protein to adhere to the surface of the growing HOF crystals. Promoting hydrogen bonding between the protein and the HOF precursors was also trialed in **Section 3.5**, by adhering a guanidinium-decorated polymer to the protein surface prior to encapsulation. The significant amount of surface-bound protein for all HOF composites led to the investigation of layer-by-layer polyelectrolyte coating as a method of providing additional protection to surface-bound protein, detailed in **Section 3.6**.

3.2 Establishing Methods for Loading Quantification and Visualization

3.2.1 Background

The amount of protein immobilized in/on a material is important in the field of biocatalysis, as higher protein incorporation uses framework precursors more efficiently and yields composites with higher activity per unit weight. Two values are often used to quantify how much protein is immobilized in/on porous frameworks: encapsulation efficiency and weight/weight loading. In the ensuing chapter, these two terms will be frequently used, and thus formal definitions are required. Encapsulation efficiency refers to the percentage of the original dosage of protein encapsulated within the framework. Encapsulation efficiency is calculated after a washing procedure and is often based on the protein concentration in the synthesis supernatant/washings, from which the amount of immobilized protein can be inferred (**Equation 1**). Meanwhile, weight/weight loading considers how much of the final dry composite mass is protein. Loading can be inferred from the protein concentration in the synthesis supernatant/washings, however is also commonly calculated by digesting a known mass of framework and determining how much protein was present in the sample (**Equation 2**).

$$\text{encapsulation efficiency} = \frac{P_{\text{immobilized}}}{P_{\text{total}}} \times 100\% \quad (\mathbf{1})$$

$$\text{wt.\% loading} = \frac{P_{\text{immobilized}}}{H_{\text{total}}} \times 100\% \quad (\mathbf{2})$$

Where $P_{\text{immobilized}}$ is the mass of immobilized protein, P_{total} is the mass of protein used in the synthesis, and H_{total} is the total mass of the protein/HOF composite.

In existing literature, either of these two values is typically reported to quantify the success of encapsulation of protein in a framework. It is important to note that a high encapsulation efficiency does not necessarily imply a high wt.% loading, and vice versa (**Figure 3.1**). For example, a large excess of framework precursors could be used to ensure that all protein is encapsulated, leading to exceptional encapsulation efficiency. However, the mass of composite formed would also increase, leading to a lower wt.% loading value.

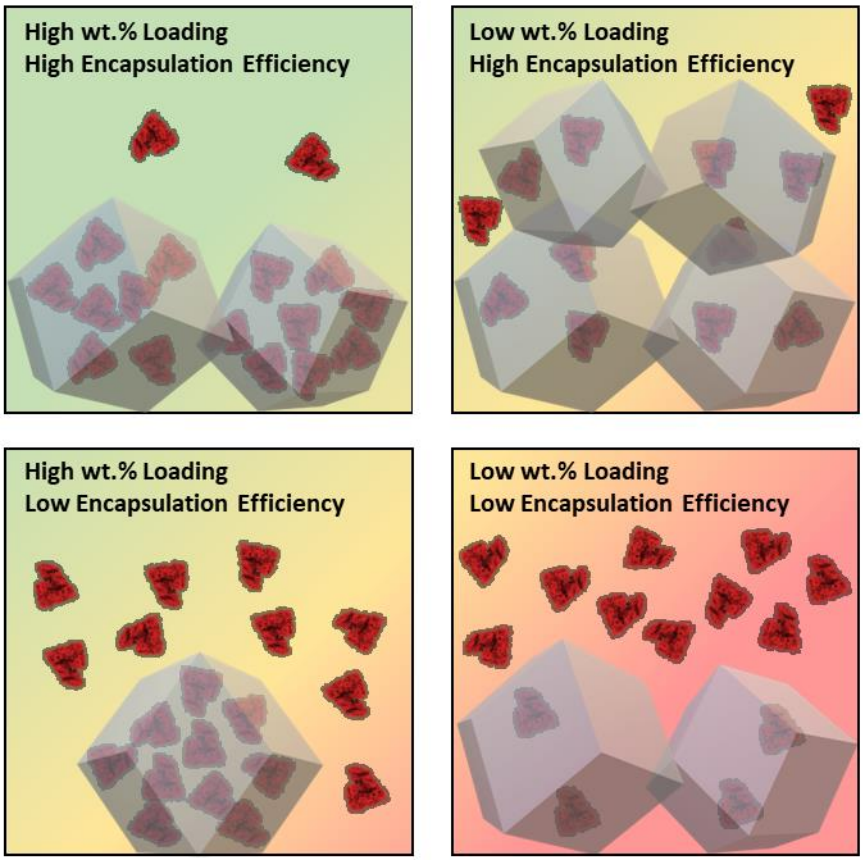

Figure 3.1: Simplified diagram representing the difference between encapsulation efficiency and weight/weight loading. Wt.% loading refers to how much of the mass of the final composite is composed of protein, whilst encapsulation efficiency refers to the proportion of the initial protein dosage incorporated into the framework.

Ideally, a biocomposite would possess high wt.% loading and encapsulation efficiency, although depending on the application one of these values may be preferentially targeted. For example, ZIF-8 can achieve encapsulation efficiencies of up to 100% depending on the biomolecule.[2] Though the weight/weight loading is often not notably high (e.g. 3.3 wt.% for catalase@ZIF-8[3]), arguably this is non-critical as the starting materials are far less valuable than the species being encapsulated. On the contrary, BioHOF-1 is made from linkers that have limited commercial availability, and as such it is within best interest to ensure a high wt.% loading to minimize the amount of framework precursors required to make a composite with appreciable activity.

Currently, other HOFs outcompete BioHOF-1 from a weight/weight loading and encapsulation efficiency standpoint. A series of single-component frameworks reported by Ouyang and co-workers, for example, reported loadings as high as 67.4 wt.% with

encapsulation efficiencies of ~80%.[4] This is significantly greater than the highest loading reported for an unmodified enzyme in BioHOF-1 of 6.0 wt.%.[1] However, neither of these studies thoroughly investigated the spatial location of the protein in the framework. Proteins situated on the surface of the framework are not as well protected as encapsulated protein,[1, 3] and thus evaluation of protein location is crucial to understanding how viable the composite is for biocatalysis.

Most studies utilize confocal laser scanning microscopy (CLSM) to identify the location of protein in/on the framework.[1, 3, 5-8] Though this gives some information on if a protein is surface bound or encapsulated, it does not allow individual protein macromolecules to be identified, nor does it provide reliable comparison of protein content between samples. Recent studies have utilized gold nanoclusters conjugated to the protein surface, which allows the spatial location of proteins to be visualized by TEM.[4, 9] These metal nanoparticles are prepared using the natural sequestering and reducing abilities of BSA, which localizes gold atoms within the protein and then reduces them to form nanoclusters.[10] However, this modifies the surface chemistry of the protein, which can impact how the protein interacts with the framework and thus change the loading. Ultimately, more robust methods of visualizing proteins in HOFs are desired, which could be used in combination with existing techniques.

In this section, the approaches used to optimize the loading of proteins in BioHOF-1 are established. First, we discuss potential methods of quantifying the loading of proteins in BioHOF-1, as the BioHOF-1 precursors exhibit interference in a variety of common assays. Following this, methods of visualizing the spatial distribution of proteins in BioHOF-1 are established. Using these techniques, washing procedures to remove surface-bound protein from BioHOF-1 are developed, ensuring that the protein loading values reflect encapsulated protein and not surface-bound protein. These methods are then utilized in the ensuing sections to trial various methods of increasing the protein loading in BioHOF-1.

3.2.2 Trialling methods of protein quantification

To thoroughly investigate the factors that impact the encapsulation of protein in BioHOF-1, a sensitive and accurate method of measuring protein concentration was required, which could be performed on either the supernatant/washings from the HOF

biocomposite synthesis or a decomposed HOF sample. Previously, quantification of protein loading in BioHOF-1 was conducted by ICP-MS, using sulfur content to determine the amount of protein present by reference to a calibration curve of known protein concentrations.[1] However, this process is expensive and time-consuming, and thus to optimize protein loading a faster and less costly method is highly desirable.

One of three methods is typically used for determining the loading of proteins in ZIFs: Direct UV/vis spectroscopy, Bradford assay, or fluorescence spectroscopy. For BioHOF-1, each of these three methods proved ineffective at accurately determining protein loading. Direct UV/vis spectroscopy was initially trialled as a method of loading determination, which allows the concentration of protein to be determined by measurement of the ~280 nm absorption peak, caused by contributions from Tryptophan, Tyrosine and Phenylalanine amino acid residues.[11] However, it became immediately apparent that the absorbance due to the aromatic rings of the HOF precursors shrouds the 280 nm protein peak entirely, preventing any insight into the protein loading (**Figure S3.1**). The Bradford assay proved similarly impractical, as the tetra-carboxylate acid linker induced a strong absorbance from the Bradford reagent (**Figure S3.2**). This is likely due to binding of the HOF linkers to the Bradford reagent, inducing the absorbance shift to 595 nm even without protein present.[12] Finally, fluorescence spectroscopy of FITC-labelled protein was considered as a method of loading quantification. However, fluorescence intensity can vary with pH[13] and presence of organic solvents,[14] which does not suit the breakdown conditions for the HOF nor the presence of acidic/basic HOF linkers. Thus, none of the above methods were able to be utilized in loading studies.

The method decided upon for the quantification of protein encapsulation was the bicinchoninic acid (BCA) assay. This assay involves the addition of copper (II) sulfate in an alkaline buffer containing bicinchoninic acid to a solution of protein. The protein induces the alkaline reduction of Cu(II) to Cu(I), which forms a complex with bicinchoninic acid with an absorbance at 562 nm.[15-17] This technique is typically less sensitive to detergents and buffers as other protein quantification procedures,[16, 17] and thus we were hopeful that BioHOF-1 would not interfere with the assay. Initial trials using a digested sample of BioHOF-1 and an hour-long incubation at 70 °C were not promising, with the HOF forming a large amount of precipitate and exhibiting some interference in the assay (**Figure S3.3**). However, when the incubation conditions were altered to overnight at room temperature, no precipitate formed, and minimal UV/vis

absorbance was observed (**Figure S3.4**). Though the absorbance was not low enough for it to be considered a negligible impact, it was sufficient to use this method to determine the protein concentration, with a minor correction to the value to account for the absorbance due to the HOF precursors. Further, the chosen degradation conditions of 0.01 M NaOH with 10% DMSO allowed serviceable calibration curves to be produced for BSA and ferritin (**Figure S3.5**). Since deciding on this as the quantification method, a study was published using the BCA assay to determine protein loading in BioHOF-1,[18] verifying the validity of this assay for studies on BioHOF-1.

3.2.3 Visualization of spatial distribution of proteins in/on HOFs

We sought to not only determine the loading of protein in BioHOF-1, but also ensure that the loading reflected the encapsulated protein content and not surface bound or aggregated protein. Thus, a method of visualizing the localization of protein in/on the HOF was also required. This can be achieved using confocal laser scanning microscopy (CLSM),[1, 3, 5-8] though a higher resolution method that allows the identification of individual protein macromolecules is desired. Previously, some studies have grown metal nanoparticles within proteins,[4, 9] which are dense enough to visualize by transmission electron microscopy (TEM). Such methods, however, may change the protein structure, which is undesirable as it can alter the loading of protein in the framework. Instead, ferritin (FER) was chosen as a model protein. Ferritin is a 24-mer, with the subunits arranging themselves to create a large core for iron storage (**Figure 3.2**).[19, 20] As many as 4500 iron atoms can be stored inside this core as a hydrous ferric oxide-phosphate complex, with a maximum diameter of approximately 80 Å.[20] Due to the abundance of iron, ferritin can be visualized inside HOFs using TEM. Thus, use of ferritin as a model protein allows the spatial location of individual proteins to be identified without the need for additional modification.

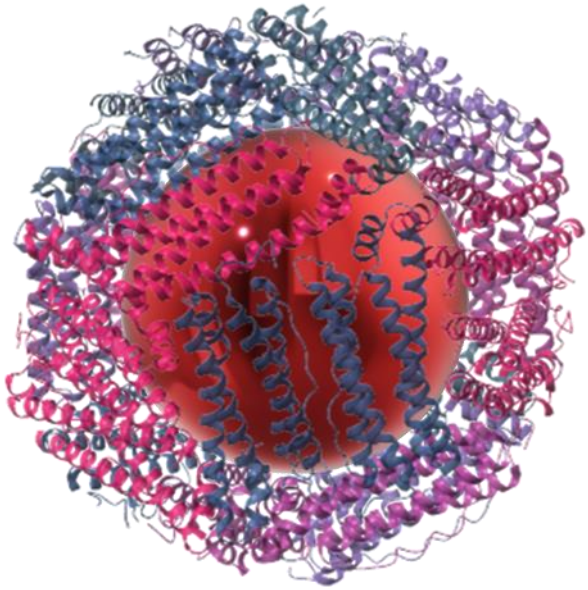

Figure 3.2: Structure of equine ferritin. Ferritin is a homo-24-mer with a molecular weight of approximately 470 kDa,[21] with a large (~ 80 Å)[20] hollow core for iron storage (figure adapted from ref. 21).

To distinguish between surface-immobilized and encapsulated ferritin, a washing procedure was established that would remove surface-bound ferritin. To assess if all surface-bound protein was removed, controls were performed in which as-synthesized BioHOF-1 was mixed with ferritin and then washed using specific protocols. Removal of ferritin when comparing the TEMs of the initial surface-bound ferritin sample and the washed sample indicated a successful washing procedure. 10% SDS appeared successful at removing ferritin from the surface of BioHOF-1 (**Figure 3.3**), and so this washing procedure was used for encapsulation studies. Importantly, SDS, when appropriately diluted, does not interfere with the BCA assay,[15] and so loading can be determined quantitatively for washed samples without risk of SDS contributing to the loading value. It is important to note that long-term incubation studies of BioHOF-1 in 10% SDS revealed that the framework degrades over the course of an hour. For this reason, washing procedures were carried out for a short timeframe (<5 minutes) with only mild agitation.

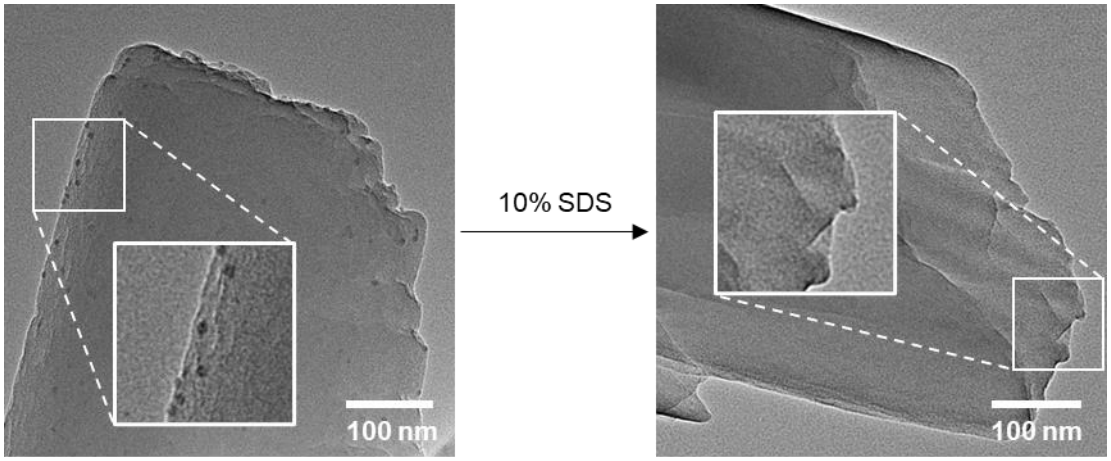

Figure 3.3: Washing of ferritin from the surface of ferritin-on-BioHOF-1 samples using 10% aqueous SDS. The sample pictured on the left was washed with water (× 2) and ethanol, whilst the sample pictured on the right was further washed with 10% SDS, then water (× 2) and ethanol. Black spots correspond to the iron core of individual ferritin macromolecules.

3.2.4 Summary

The loading quantification and visualization procedures for encapsulation of protein in BioHOF-1 were formally established. Breakdown of the framework using 10% DMSO with 0.01 M sodium hydroxide was able to release encapsulated enzyme into the solution, which could then be quantified by use of a BCA assay. To visualize the spatial location of protein in the framework, ferritin was used as a model protein, which could be visualized using TEM. Combined with a washing procedure using 10% SDS, the loading of ferritin encapsulated in BioHOF-1 could be efficiently and accurately evaluated.

3.3 Effect of Protein Surface Chemistry on Loading in BioHOF-1

3.3.1 Background

Protein surface chemistry is known to impact the incorporation of proteins into porous frameworks. ZIF-8, as discussed earlier, can undergo biomimetic mineralization around proteins, however only if the protein is of a sufficiently negative charge.[22] There are also certain HOFs that are known to have protein loading impacted by protein surface chemistry. Ouyang and co-workers reported the synthesis of single-component HOFs in water, from pyrene-based tetra-carboxylic acids, which only formed in the presence of protein.[4] The formation of the framework was postulated to be initiated by hydrogen bonding to the peptide backbone, followed by propagation by π-π stacking between adjacent linkers, forming a crystalline assembly. A variety of different proteins were encapsulated in this HOF, including BSA, catalase, horseradish peroxidase, and cytochrome C, amongst others, with each protein producing different amounts of framework with varying loading values. Importantly, the authors showed that increasing the positive charge on BSA by amination resulted in increased encapsulation efficiency, changing from 79.7% to 98.0%, indicating that protein surface chemistry plays an important role for incorporation into the framework.[4] Our own studies on this framework revealed that not all proteins initiate framework growth, for example no precipitate forms when ferritin is used as the protein for encapsulation. This indicates that HOFs can exhibit surface chemistry-dependent growth, in the same vein as ZIF-8.

Though BioHOF-1 does not exhibit a biomimetic mineralization mechanism of framework growth, there is some evidence that protein charge has an impact on incorporation into the framework. Studies using a modified D-amino acid oxidase linked to a highly positively charged N-terminal group have achieved significantly higher loading in BioHOF-1 (e.g. 55 wt. %) than has been reported for unmodified proteins. However, in these studies, digestion with trypsin resulted in a >90% activity loss, suggesting that the majority of protein was immobilized on the surface and not truly encapsulated.[18] Regardless, it suggests that protein charge impacts how the protein interacts with BioHOF-1. Interaction between the HOF linkers and protein has been previously established in DLS studies, in which the median particle size of a protein increased if the protein was combined with either HOF linker, indicating a secondary

shell of linker forms around the protein.[1] This interaction arises as the linkers bear functional groups natively possessed by certain amino acids; glutamate and aspartate possess carboxylate groups whilst arginine has amidinium-like guanidinium groups. Proteins would thus be expected to interact with the linkers via the same hydrogen bonding motif as between linkers. Therefore, changing the proportion of surface carboxylates and/or amines could alter the interaction between the protein and the HOF linkers, thus changing the incorporation of protein into the framework.

In this section, surface modification of ferritin is investigated as a method of altering the loading of proteins in BioHOF-1. Amination and succinylation are used to increase the surface positive and negative charge on the protein, respectively. Modified ferritins are then encapsulated in BioHOF-1, and the loadings determined by BCA assay and TEM.

3.3.2 Surface modification of ferritin

To systematically study the effect of protein surface chemistry on loading in BioHOF-1, two different surface modifications were performed on the protein (**Scheme 3.1**). The first of these two modifications was amination, whereby the side chains of glutamate and aspartate residues were coupled to ethylenediamine, changing the terminal carboxylate to a terminal amine. The second was succinylation, in which the terminal amine groups of lysine residues were converted to carboxylate groups, by reaction with succinic anhydride. This approach has been previously used to promote the biomimetic mineralization of ZIF-8 around proteins that otherwise to do not induce ZIF-8 formation.[22] Success of protein surface modification was monitored by measuring the protein's zeta potential, which at a fixed pH can be regarded as a measure of relative surface charge.[23, 24] Thus, for amination reactions an increase in zeta potential is expected, whilst a decrease in zeta potential (i.e. more negative) is expected for succinylation.

The zeta potential of unmodified ferritin is approximately -16 mV (**Table 3.1, Figure S3.6**), due to the abundance of negatively charged amino acids (624 residues) when compared to positively charged amino acids (456 residues, excluding histidine). This aligns with the isoelectric point of ferritin of 4.4,[25] which indicates that an acidic medium is required to bring the macromolecule to a net neutral charge. Upon amination, the zeta potential of ferritin increases to +17 mV, owing to the conversion of all

negatively charged carboxylates to amines. Meanwhile, succinylation affords a zeta potential of -33 mV. The impact of succinylation on the zeta potential is lower in magnitude than for amination, potentially owing to the modification only converting lysine residues and not all basic amino acids. The magnitude of the change in surface charge is also reflected in the change in theoretical pI of ferritin (**Table 3.1**). Importantly, the median diameter of ferritin does not change significantly following modification, suggesting that the protein remains in its native oligomeric state and has not aggregated or disassociated into its constituent subunits. Thus, surface modification was regarded as successful.

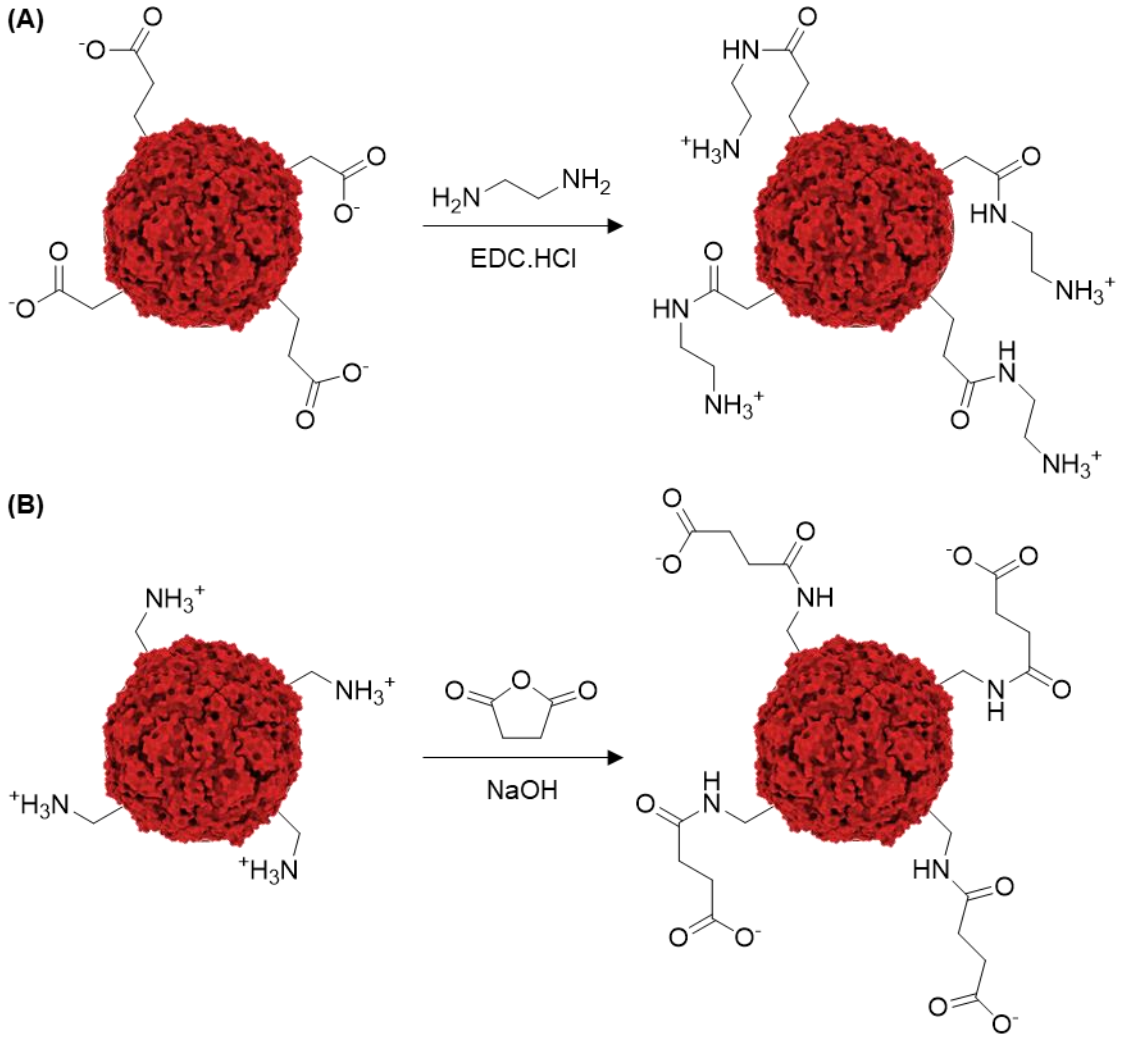

Scheme 3.1: Procedures for (A) amination and (B) succinylation of ferritin. Succinylation reaction was carried out in PBS (pH 8). Amination increases the positive charge on the protein by the conversion of the carboxylate groups of glutamate and aspartate residues to amines. Succinylation increases the negative charge on the protein by the conversion of the amine groups of lysine residues to carboxylates.

Table 3.1: Zeta potentials, theoretical isoelectric points, and median diameters of ferritin following surface modification reactions. Zeta potential measurements were recorded in 10 mM KCl, whilst size measurements were recorded in 1x PBS.

Modification	Zeta Potential (mV)	Theoretical pI [26]	Median Diameter (nm)
Unmodified	-15.7 ± 5.5	5.37	10.0 ± 2.6
Amination	+17.1 ± 5.6	11.71	10.6 ± 2.7
Succinylation	-33.0 ± 9.4	4.26	9.4 ± 2.6

3.3.3 Loading of modified ferritin in BioHOF-1

BioHOF-1 was synthesized in the presence of the modified variants of ferritin. Preliminary tests revealed that ferritin was prone to forming insoluble protein aggregates in the presence of the tetra-amidinium linker over time, likely due to joining of individual ferritin macromolecules via hydrogen bonding to the linker. Intriguingly, aminated ferritin did not aggregate with the tetra-amidinium linker, but rather with the tetra-carboxylate linker. This is due to aminated ferritin possessing a significant positive charge, and thus interaction with the tetra-carboxylate is more favourable. For consistency, all FER@BioHOF-1 samples were prepared by addition of protein to a solution of the tetra-amidinium, followed by addition of the tetra-carboxylate. However, the time in solution with the tetra-amidinium link was kept to a minimum to ensure that aggregate formation did not skew loading results.

TEM imaging of FER@BioHOF-1 samples initially indicates that amination is effective at increasing protein loading (**Figure 3.4**). Compared to the unmodified ferritin control, an increase in the number of ferritin nanoparticles in the TEM is observed. Meanwhile, succinylation appears to have minimal impact on the protein loading. This could suggest that the interaction between positively charged residues of the protein and the tetra-carboxylate linker is more crucial for the incorporation of protein into the HOF than interactions from negatively charged residues. However, when considering that the beam in TEM transmits through the entire sample, the loading remains considerably lower than other reported values. This is supported by BCA assay data of degraded HOF

samples, which suggests that the loading of ferritin remains below 4 wt.% for all samples (**Figure 3.5**). Aminated ferritin has a marginally higher loading of 3.0% compared to 2.0% for ferritin and 1.4% for succinylated ferritin, however all well below the >50% loadings reported for single component frameworks. Comparison to the BCA data prior to SDS washing reveals that the low loading is due to a significant portion of the protein adhering to the surface of the HOF or aggregating, with loadings of 15-20% being observed without an SDS wash. This indicates that as little as 8% of the total immobilized protein content is truly encapsulated, with even the aminated ferritin sample having only 16% of the immobilized protein encapsulated. This larger protein loading prior to SDS washing, as well as the formation of large ferritin aggregates, is reflected in TEM images (**Figure S3.7**). PXRD indicates that all samples are BioHOF-1 (**Figure 3.6**), and thus variation in loading is not a result of different framework topologies. Overall, data indicates that the low loadings of ferritin in BioHOF-1 are due to ferritin preferentially adsorbing to the surface of the HOF or aggregating, rather than being incorporated into the framework, which occurs regardless of surface modification.

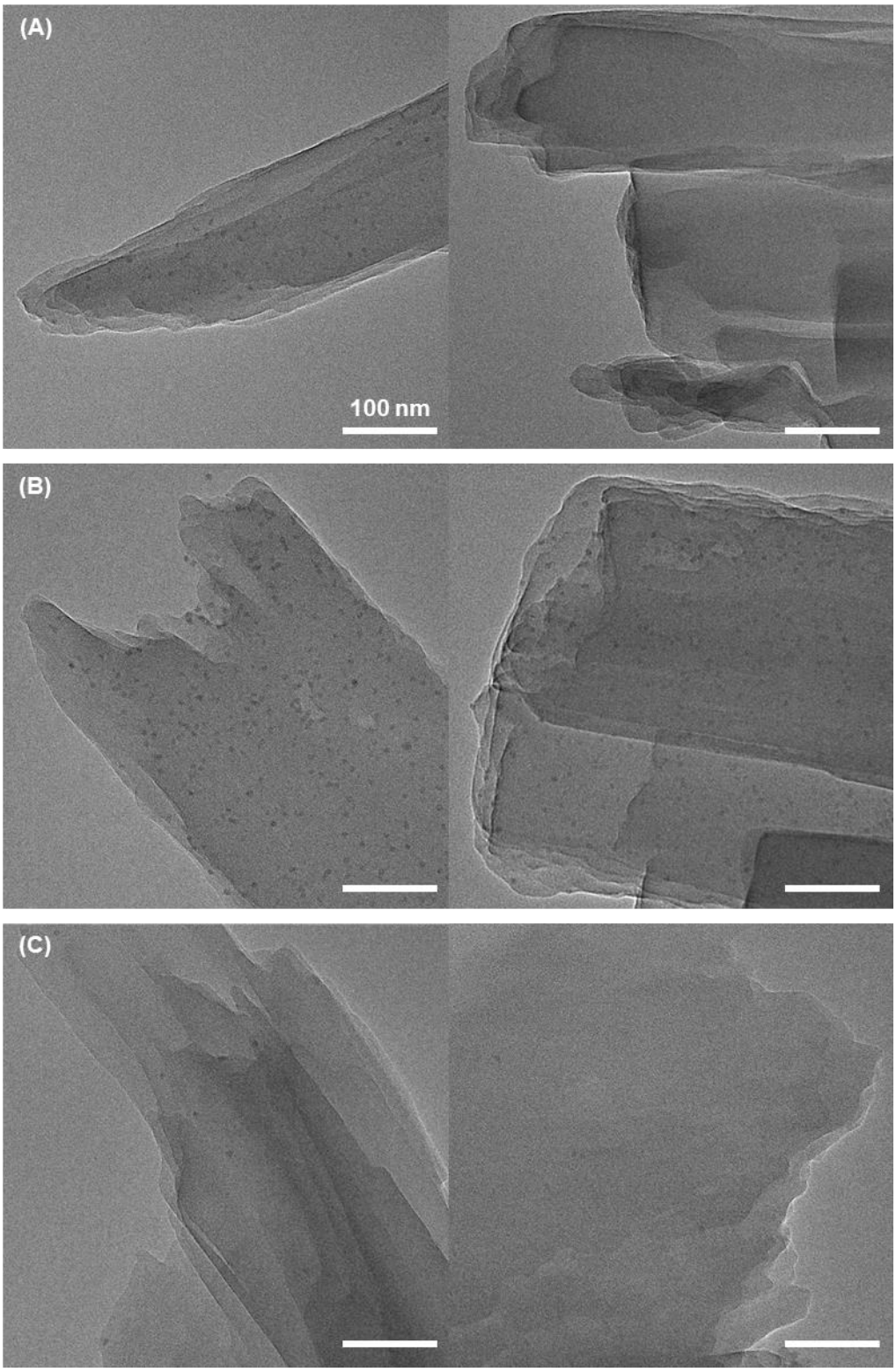

Figure 3.4: TEM images of BioHOF-1 synthesized in the presence of (**A**) unmodified, (**B**) aminated, and (**C**) succinylated ferritin. Samples were washed with 10% SDS prior to imaging to ensure only encapsulated protein was visible. Black spots correspond to the iron core of individual ferritin macromolecules.

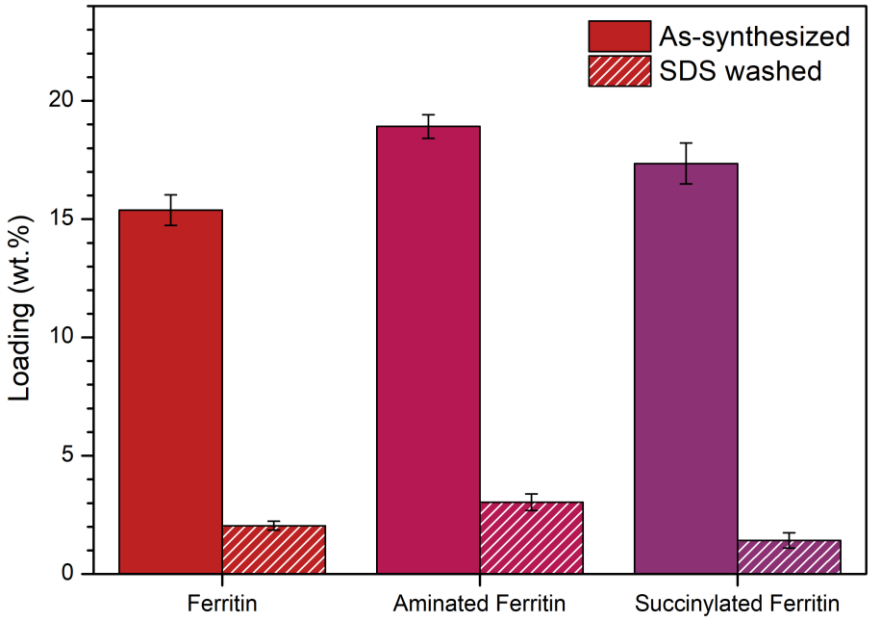

Figure 3.5: Effect of amination and succinylation on ferritin loading in BioHOF-1, determined by BCA assay. As-synthesized samples were not washed with SDS, and thus the loading values include aggregated and surface-immobilized protein. SDS-washed samples were washed with 10% SDS for 5 minutes, and so only encapsulated protein is present. Error bars represent the standard error in the loading of the sample determined from triplicate assay measurements. Amination slightly increases the loading of ferritin in BioHOF-1, however all forms of ferritin show a significant preference to adsorb to the surface of the HOF or aggregate.

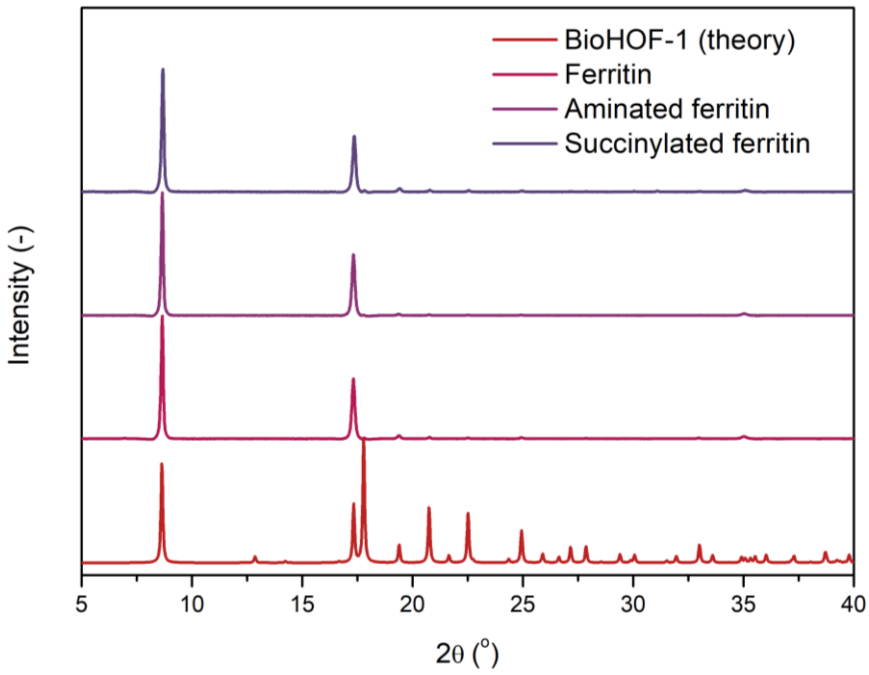

Figure 3.6: PXRD patterns of BioHOF-1 synthesized in the presence of ferritin, aminated ferritin, and succinylated ferritin. Samples were washed with water (x 2), ethanol, 10% SDS, water (x 2) and ethanol, and were dried under vacuum prior to analysis.

It is noteworthy that, in general, the loading values are significantly lower than for a single-component carboxylic acid HOF, which have reported loadings of up to 67.4 wt.%. There are several potential explanations for why BioHOF-1 does not exhibit the same loading behaviours as for single-component frameworks. BioHOF-1 is a two component HOF, and as such any modification that enhances the interaction with one linker could also lessen the interaction with the other linker. Amination, for example, could promote the interaction between the protein and the negatively charged tetra-carboxylate linker, whilst simultaneously hindering the interaction with the positively charged tetra-amidinium. Thus, there may be a delicate balance between the interactions with each linker required for successful encapsulation. For a single-component framework, however, there is a more limited range of interactions that the protein can experience with the linker. Intuitively, if the linker interacts with the protein near-exclusively via hydrogen bonding with surface amine groups, increasing the number of surface amine residues would promote interaction of the protein with the framework precursor, encouraging nucleation.[4] Without a second linker, there is no competing interactions to be considered.

Furthermore, the mechanism of encapsulation of protein in BioHOF-1 varies from single-component HOFs. Encapsulation of proteins in BioHOF-1 occurs by particle aggregation.[1] Since the protein disrupts what would otherwise be a pristine crystalline material, the encapsulation of protein could be regarded as unfavourable for crystal growth. On the other hand, the growth of single-component HOFs is believed to be nucleated by protein.[4] Since the protein is actively involved in the crystallization mechanism, the incorporation into the framework is more favourable. This may lead to higher loading composites than for BioHOF-1.

Finally, and perhaps most importantly, the existing literature on encapsulation of proteins in HOFs has not adequately distinguished between surface-bound and encapsulated protein. Washing of composites in literature is conducted using only water or ethanol,[1, 4, 7, 27, 28] and thus complete removal of surface-bound protein is unlikely. For a similar washing procedure performed on FER@BioHOF-1, a loading of 15.4 wt.% is obtained (**Figure 3.5**), which is more comparable to literature values. It is plausible that a significant portion of the immobilized protein for single-component HOFs is surface bound, much like for BioHOF-1, and thus the true encapsulated protein loading is lower than reported values. Thus, aiming for loadings of >50% as reported in the literature may not be a realistic objective. Nonetheless, loadings of <3% are well below what is desired for biocatalysis applications, and thus optimization of protein loading remains necessary.

3.3.4 Summary

Surface modification of ferritin was performed to probe the impact that protein surface chemistry has on incorporation in BioHOF-1. Both aminated and succinylated ferritin were prepared, to trial the encapsulation of a protein with a higher positive and a higher negative charge, respectively. Unfortunately, surface modification had little impact on the loading of protein, with all ferritin variants returning loadings of <3 wt.%. Loading analysis prior to SDS washing revealed that most of the protein was surface bound or aggregated, indicating that the protein prefers surface adsorption over encapsulation in the framework. Thus, alternative approaches for increasing loading in BioHOF-1 will be investigated, which attempt to overcome this adsorption preference.

3.4 Effect of Slowed Framework Growth on Protein Loading in BioHOF-1

3.4.1 Background

With the surface modification of ferritin proving unsuccessful at improving loading, alternative methods of increasing protein loading were investigated. Data from surface modification experiments indicated that ferritin prefers surface-binding over encapsulation within the framework, regardless of surface chemistry. Thus, to increase the loading, this preference for surface-binding needed to be shifted towards encapsulation.

BioHOF-1 forms extremely rapidly in water, which may disfavour protein encapsulation. UV/vis spectroscopy studies reveal that transmittance of light during BioHOF-1 synthesis reaches 5% merely 2 seconds after addition of the second linker, settling at 0.1% after 30 seconds (**Figure 3.7**). The rapid formation of the framework is likely caused by extremely favourable pi-stacking between the linkers, in combination with the strong amidinium-carboxylate interaction. As the protein does not actively nucleate HOF growth, the rapid growth likely does not allow the protein to interact with the framework, leading to low protein encapsulation. However, results in the previous section indicate that ferritin, though not encapsulated, interacts strongly with the framework surface. We postulated that by slowing the growth rate of the HOF, protein may adsorb onto the surface of the growing framework, leading to increased loading.

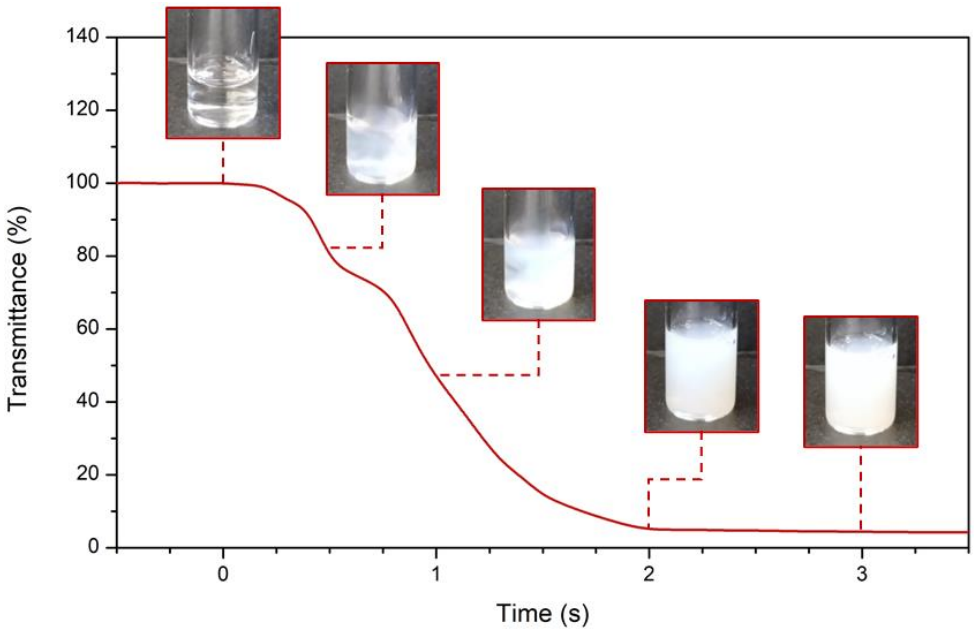

Figure 3.7: Time course UV/vis transmittance of BioHOF-1 formation, measured at 700 nm. The zero timepoint represents the point at which the tetra-carboxylate solution first contacts the tetra-amidinium solution. The solution reaches near-complete opacity within two seconds of the addition of the second linker, indicating rapid HOF growth. In the time following the data presented here, the transmittance gradually decreases until settling on a value of 0.1% after 30 seconds.

There are several methods that could be utilized to slow the growth of BioHOF-1. One of the simplest approaches that could be taken to slowing the growth of the framework is decreasing the concentration of the linker solutions. However, previous studies on similar amidinium-carboxylate frameworks have shown that even at low linker concentrations, HOF growth is rapid and results in extremely small needle crystals.[29] Furthermore, previous experiments within our lab indicate that the growth rate of BioHOF-1 is not visibly impacted by diluting the precursor solutions. Alternatively, modulators could be used as a method of slowing HOF growth. A modulator that has been previously demonstrated to be effective at slowing the growth of amidinium/carboxylate frameworks is sodium sulfate. White and co-workers used sodium sulfate to slow the growth of a framework consisting of tetra-amidinium cations and diazobenzene-based dicarboxylate anions.[29] They found that in the presence of 10 equivalents of sodium sulfate the size of the crystals increased, with a further size increase with 100 equivalents of sodium sulfate. This occurs as the sulfate anion is able to competitively interact with the amidinium groups of the linker (**Figure 3.8**), preventing

hydrogen bonding to carboxylates and thus slowing HOF growth. We sought to investigate if modulators could also be used to increase the loading of proteins in BioHOF-1.

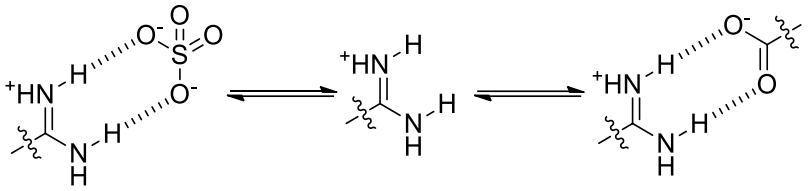

Figure 3.8: Mechanism of modulation of HOF growth by sodium sulfate. Sodium sulfate hydrogen bonds competitively to the amidinium cation, preventing bonding to the carboxylate anion.

3.4.2 Effect of sodium sulfate on ferritin encapsulation

BioHOF-1 was synthesized in the presence of 0, 20, and 100 equivalents of sodium sulfate, relative to the number of moles of linker. Visually, all samples continued to form BioHOF-1 extremely rapidly, with the mixture becoming fully opaque in <3 seconds. Furthermore, investigation of the crystals by SEM indicated no significant increase in the crystal size with the inclusion of sodium sulfate (**Figure S3.8**). Due to extensive crystal breakage rendering it difficult to accurately measure crystal length/width, detailed statistical analysis of the crystal size could not be performed. Nonetheless, the effect of sodium sulfate on the crystal size was minimal compared to literature examples for tetra-amidinium/di-carboxylate frameworks, as increased crystal size could be clearly seen in SEM images for such frameworks.[29] Intriguingly, though the growth of the HOF was not significantly impacted by sodium sulfate, the loading of ferritin varied between samples. TEM of SDS-washed samples revealed that sodium sulfate increased the ferritin loading (**Figure 3.9**), with samples with no sodium sulfate having no ferritin encapsulated, whilst samples with sodium sulfate had an abundance of ferritin. To quantify the change in loading, the bicinchoninic acid (BCA) assay was used. The sample with no sodium sulfate present returned a relatively low loading of 2.2%, which increased to 8.7% and 5.8% for 20 and 100 equivalents of sodium sulfate, respectively (**Figure 3.10**). PXRD indicated that all samples formed crystalline BioHOF-1, and thus topological variation was not the cause of the increased encapsulation (**Figure 3.11**). Thus, sodium sulfate was effective at increasing the loading of ferritin in BioHOF-1. However, this does not imply that sodium sulfate would increase the loading of all

proteins in BioHOF-1, as the mechanism of loading enhancement was not slowed framework growth as intended. Thus, other proteins were tested to assess the broad applicability of this approach.

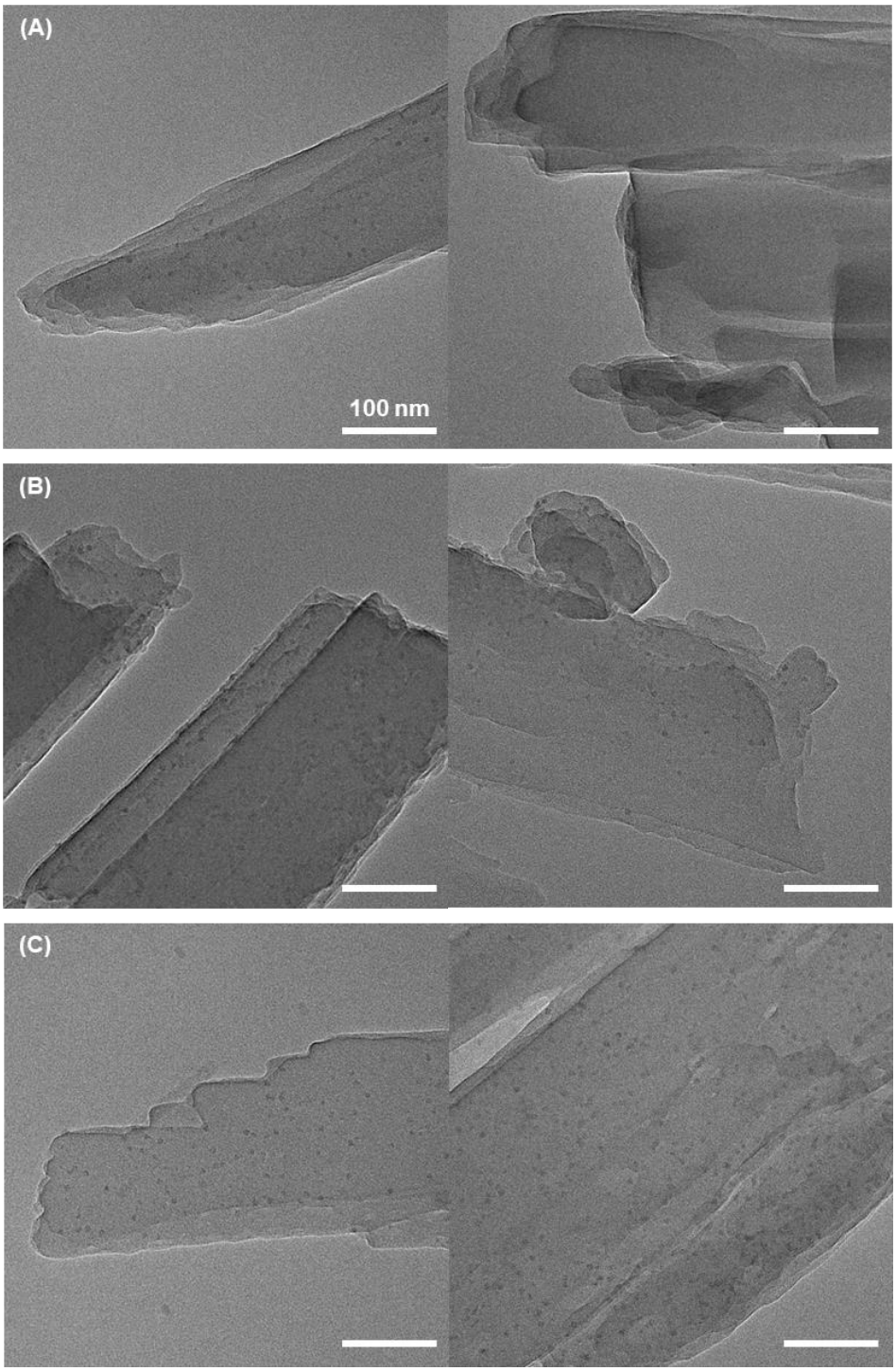

Figure 3.9: TEM images of FER@BioHOF-1 synthesized in the presence of (A) 0, (B) 20, and (C) 100 equivalents of sodium sulfate. Samples were washed with 10% SDS prior to imaging to ensure only encapsulated protein was visible. Black spots correspond to the iron core of individual ferritin macromolecules.

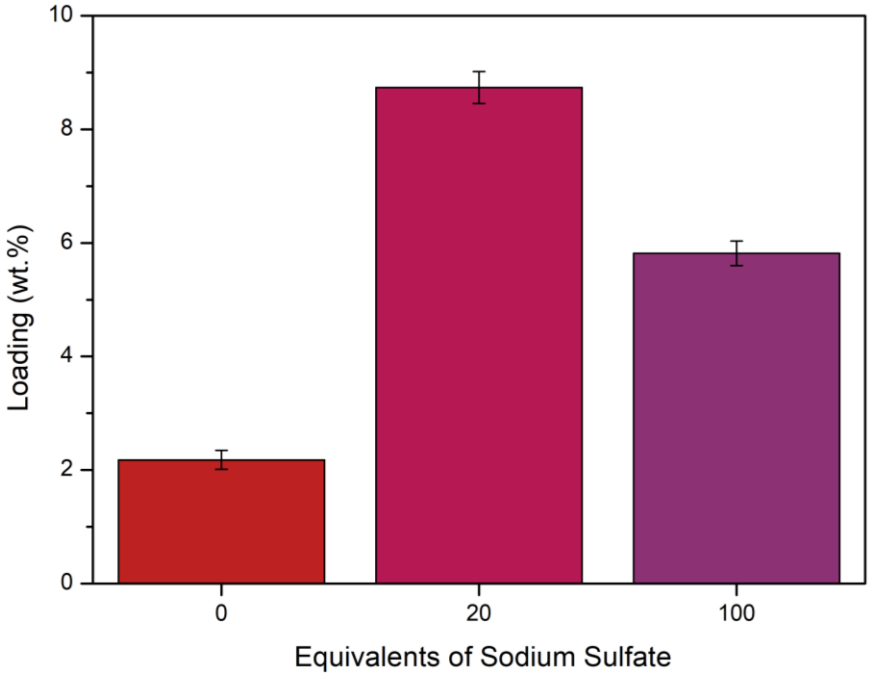

Figure 3.10: Effect of sodium sulfate on the loading of ferritin in BioHOF-1, determined by BCA assay. Samples were washed with 10% SDS prior to analysis to ensure only encapsulated protein was included in the loading value. Error bars represent the standard error in the loading of the sample determined from triplicate assay measurements. 20 equivalents of sodium sulfate achieves the highest ferritin loading.

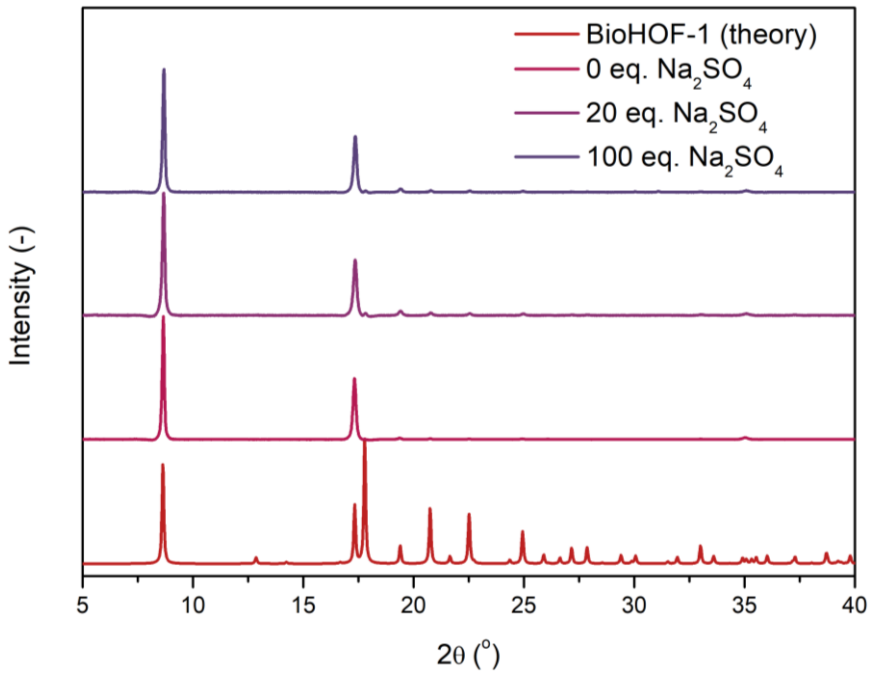

Figure 3.11: PXRD patterns of BioHOF-1 synthesized in the presence of ferritin and different equivalents of sodium sulfate. Samples were washed with water (x 2), ethanol, 10% SDS, water (x 2) and ethanol, and were dried under vacuum prior to analysis.

3.4.3 Extension to other proteins

We sought to increase the loading of all proteins in BioHOF-1, not solely ferritin. Thus, BSA was investigated as a second model protein, which has substantially different size and surface chemistry to ferritin. Whilst ferritin has a significant negative charge and a relatively large size of 470 kDa, BSA has only a slight negative charge of -3.6 ± 3.7 mV, and a much smaller molecular weight of 66 kDa. As BSA lacks the iron core of ferritin, the protein was labelled with FITC, which can be visualized by CLSM. Although this technique lacks the ability to identify individual protein macromolecules as can be done using ferritin, it serves as a basic check that the protein is encapsulated and not surface-bound.

CLSM data indicates that despite 10% SDS washing, FITC-tagged BSA (F-BSA) is retained on the surface of the HOF (**Figure 3.12**). For samples synthesized in the presence of 20 and 100 equivalents of sodium sulfate, it is evident that the core of the crystals contains little protein, with most protein present on the crystal surface. Further to this, even with protein retained on the surface for sodium sulfate containing samples, BCA data reveals that the loading of protein decreased as the sodium sulfate concentration increased, contrary to what is observed for ferritin. For F-BSA, the loading initially starts at 5.7%, and then drops to 4.5% and 1.1% for 20 and 100 equivalents of sodium sulfate, respectively (**Figure 3.13**). Thus, sodium sulfate was not effective as a general method for increasing protein loading in BioHOF-1.

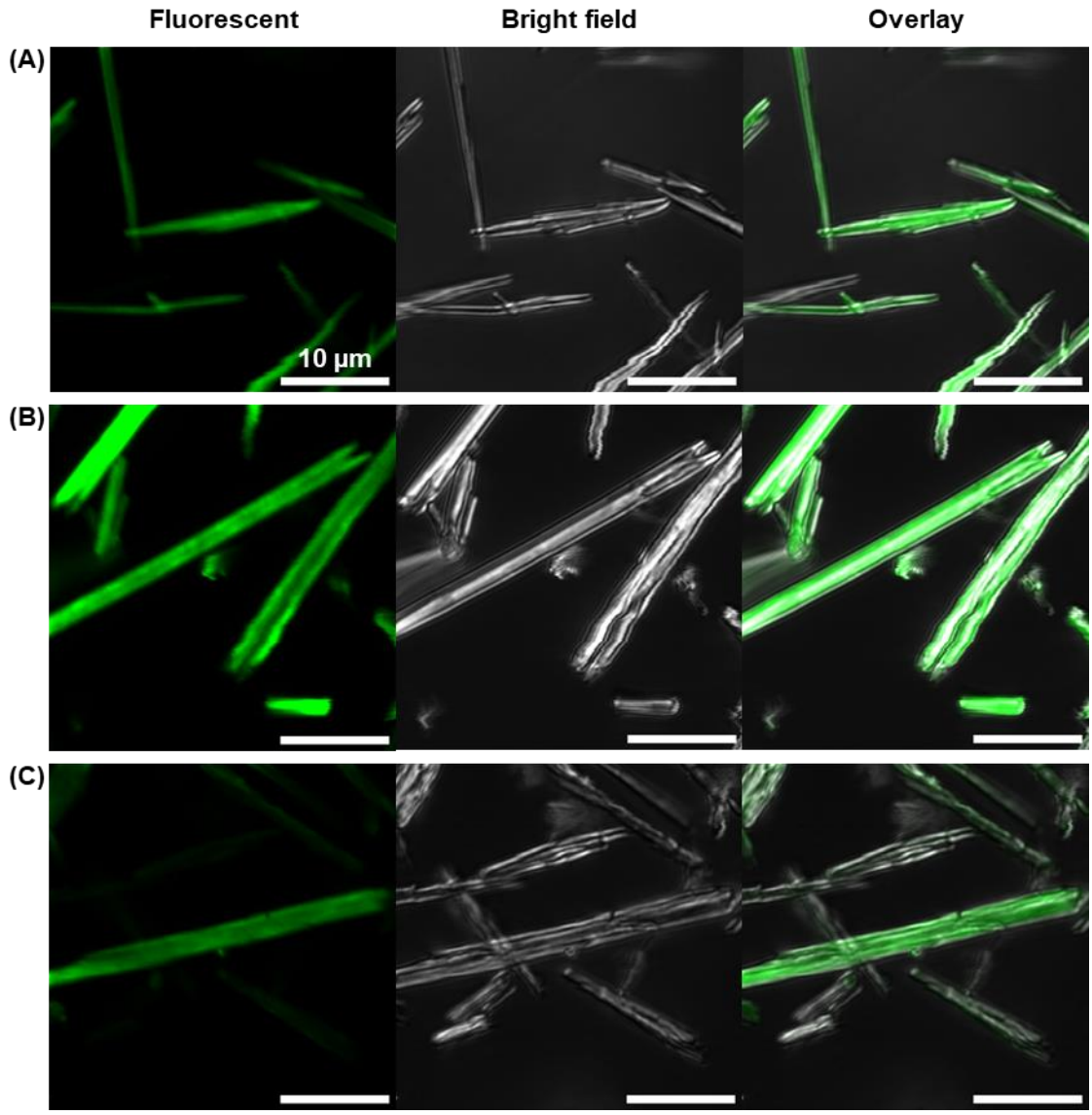

Figure 3.12: Confocal laser scanning microscopy (CLSM) images of BioHOF-1 synthesized with FITC-tagged BSA and (A) 0, (B) 20, and (C) 100 equivalents of sodium sulfate. Samples were washed with 10% SDS prior to imaging, and excited at 488 nm. Localization of fluorescence towards the edges of the crystals indicates that surface-bound protein is present.

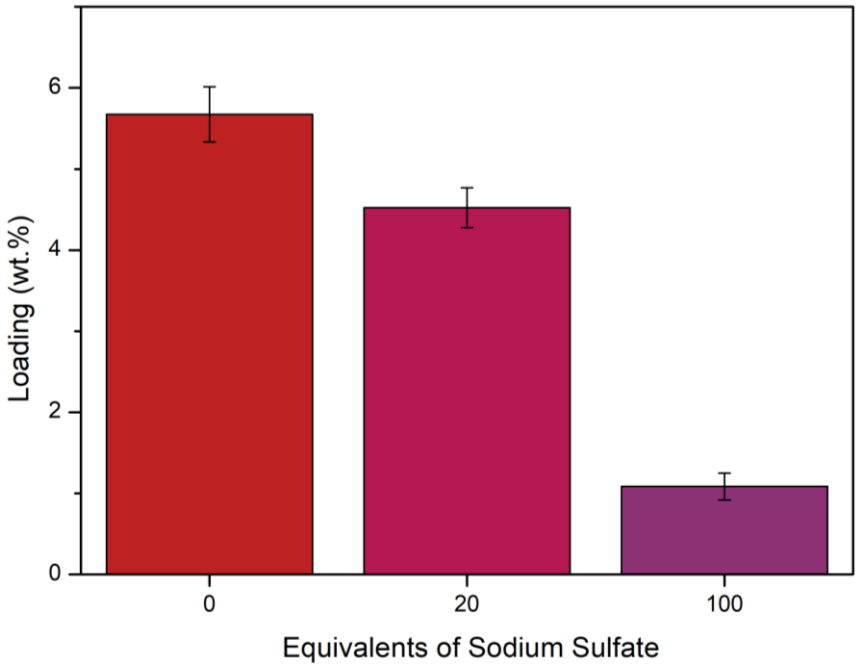

Figure 3.13: Effect of sodium sulfate on incorporation of FITC-tagged BSA into BioHOF-1, determined by BCA assay. Samples were washed with 10% SDS prior to analysis to ensure only encapsulated protein was included in the loading value. Error bars represent the standard error in the loading of the sample determined from triplicate assay measurements. Sodium sulfate has a detrimental impact on the loading of F-BSA in BioHOF-1, contrary to previous observations for ferritin.

3.4.4 Protein aggregation in the presence of sodium sulfate

Sodium sulfate impacted protein loading in BioHOF-1, however the effect was inconsistent depending on the identity of the protein. Potentially, the concentration of sodium sulfate could be manipulated to increase loading depending on the properties of the protein. Thus, the cause of altered protein loading in BioHOF-1 in the presence of sodium sulfate was investigated.

When conducting loading experiments, it was evident that ferritin was prone to forming a precipitate when mixed with the tetra-amidinium link, with DLS studies revealing the formation of particles with median size of approximately 4.5 μm (**Figure 3.14).** Furthermore, TEM images of non-SDS washed FER@BioHOF-1 samples reveal that ferritin forms large, amorphous aggregates during BioHOF-1 synthesis (**Figure 3.15**). These aggregates are likely a result of the interaction between carboxylate residues

of the protein and the amidinium groups of the linker, resulting in the linking of individual ferritin units. Such aggregates are too large to be incorporated into the HOF, and wash away with 10% SDS, thus decreasing the amount of available ferritin for encapsulation. When sodium sulfate is present, however, aggregation is not as prevalent, and again free ferritin is present in the DLS size distribution (**Figure 3.14)**. This is potentially a result of the modulating capacity of sodium sulfate, which prevents the strong interaction between the ferritin carboxylates and tetra-amidinium from forming aggregates. Alternatively, it could be a non-specific interaction owing to the general increase in ionic strength of the solution. In either case, more ferritin is available for encapsulation in the HOF, leading to an increase in loading.

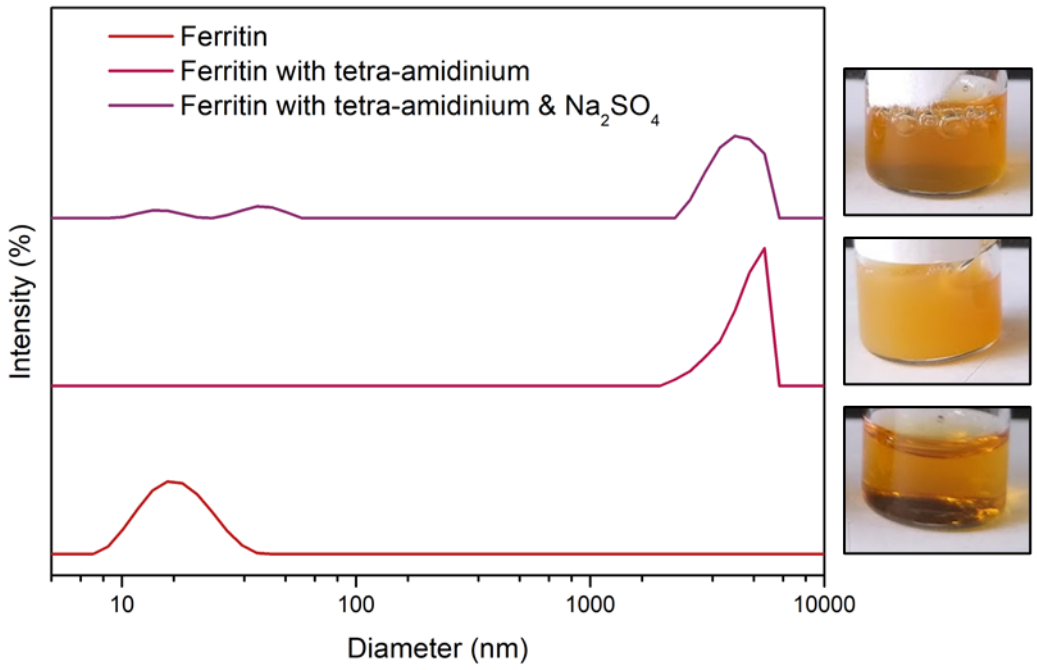

Figure 3.14: Effect of sodium sulfate on the oligomeric state of ferritin in the presence of the tetra-amidinium linker, measured by DLS. Samples were measured in ultrapure water. The tetra-amidinium linker promotes ferritin aggregation, however aggregate formation is lessened in the presence of sodium sulfate.

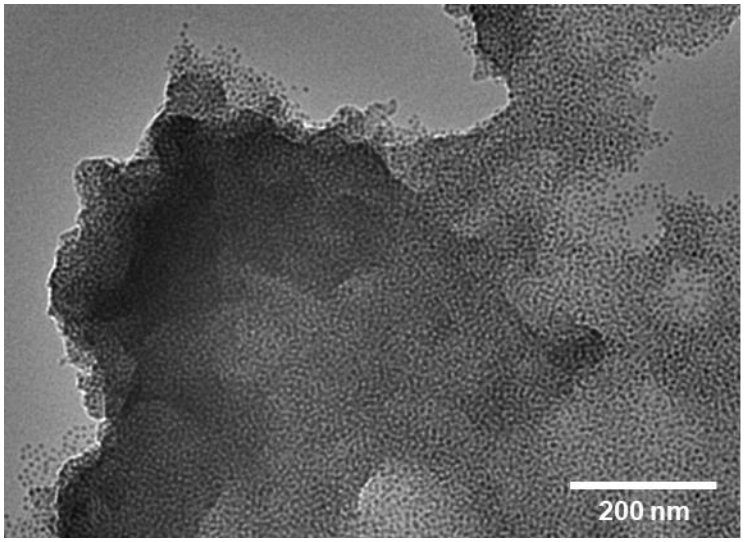

Figure 3.15: TEM image of ferritin aggregates formed during BioHOF-1 synthesis, prior to 10% SDS washing. Black spots correspond to the iron core of individual ferritin macromolecules.

Conversely, BSA forms minimal precipitate when mixed with the tetra-amidinium linker, regardless of the presence of sodium sulfate. DLS reveals that although some aggregation occurs, a portion of BSA remains in its free, monomeric form when mixed with the tetra-amidinium (**Figure 3.16**). This may be because the zeta potential of BSA is -3.6 ± 3.7 mV, significantly less negative than the zeta potential of -15.7 ± 5.5 mV for ferritin, owing to a similar number of acidic (198) and basic (164 excluding histidine) amino acid residues. As the surface charge on BSA is of significantly lower magnitude, the ability for the positively charged tetra-amidinium to surround and induce aggregation of the protein is less. Thus, sodium sulfate is not as paramount for ensuring BSA remains in its soluble form during the encapsulation procedure, when compared to ferritin. However, this does not provide an explanation for why the loading decreased in the presence of sodium sulfate for F-BSA. A possible reason for this occurrence links back to how sodium sulfate interferes with the amidinium/carboxylate interaction. Potentially, interaction between the protein carboxylates and the tetra-amidinium is needed for efficient encapsulation. Sodium sulfate may decrease the magnitude of this interaction, whilst the HOF is still able to form due to the strong pi-pi stacking interactions that are unaffected by the modulator. Thus, if the sodium sulfate does not have an active role in minimizing protein aggregation, the diminished amidinium/carboxylate interaction has a negative effect on the incorporation of protein into the framework. This may mean that sodium sulfate can be used selectively to increase

loading of proteins that are prone to aggregation with the tetra-amidinium and/or tetra-carboxylate linker.

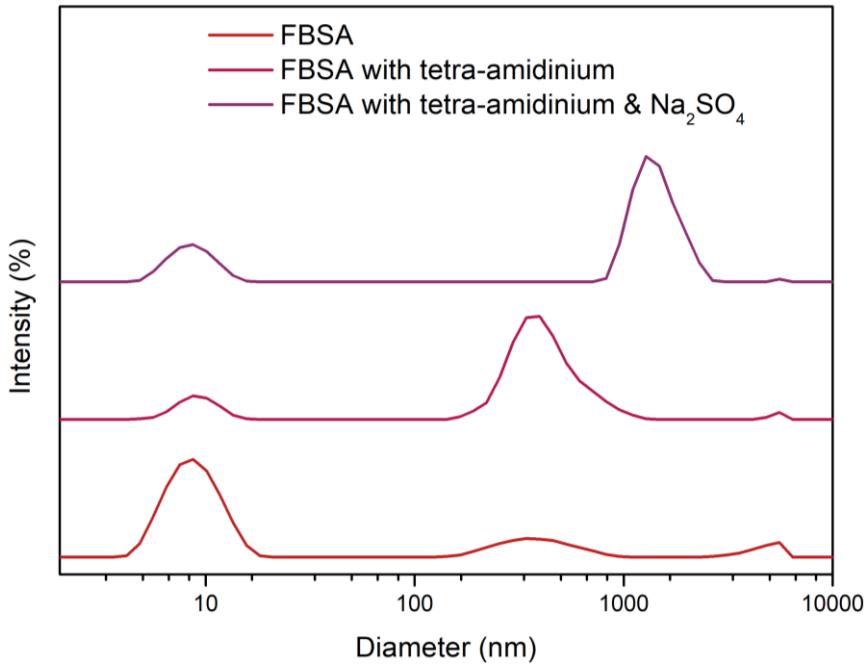

Figure 3.16: Effect of sodium sulfate on the oligomeric state of FITC-tagged BSA in the presence of the tetra-amidinium linker, measured by DLS. Samples were measured in ultrapure water. Some monomeric, unaggregated F-BSA is present all in samples.

Another potential reason for the inconsistent impact of sodium sulfate on loading is the inability for 10% SDS to completely wash BSA from the surface of the HOF. This is intriguing, as SDS washing causes the surface layers of the framework to wash away, with complete degradation of the framework possible for extended (~1 hr) SDS exposure, and so removal of protein from the surface of the framework would be expected. Surface-bound BSA may be exhibiting some form of protective effect on the HOF, preventing SDS from accessing the framework. Thus, the loading values do not reflect the encapsulated protein, but also include surface-bound protein. The true relationship between sodium sulfate and protein encapsulation may therefore not be reflected by the calculated loading values. Regardless, as loadings remained low for all samples, and the mechanism of loading enhancement was not generalizable, sodium sulfate was not further pursued as a method of increasing protein loading in BioHOF-1.

3.4.5 Summary

Sodium sulfate was trialled as an additive for the enhancement of protein loading in BioHOF-1, by slowing the growth of the framework and thus allowing time for protein to adhere to and incorporate into the growing framework. Though this increased the loading of ferritin in BioHOF-1, it had a detrimental impact on the loading of FITC-tagged BSA. This is likely a result of the modulator preventing the aggregation of ferritin with the tetra-amidinium link, whilst FBSA is not as prone to aggregation. Further experiments are necessary to determine the properties of proteins and/or HOF linkers for which addition of sodium sulfate is an effective method of increasing loading.

3.5 Functionalized Polymers for Increased Protein Loading in BioHOF-1

3.5.1 Background

With our attempts at using surface modification and modulators to increase loading proving largely unsuccessful, one final approach was trialled for increasing the loading of proteins in BioHOF-1. Although surface modification was tested as a method of increasing loading, this primarily probed the broad effect of surface charge on the incorporation of proteins into BioHOF-1, rather than the presence of specific hydrogen bonding groups. Even with surface modification, a protein would be expected to have a far lower proportion of hydrogen bonding groups per unit weight than the HOF, and so inclusion into the framework would be enthalpically unfavourable as it lowers the total number of hydrogen bonding interactions. To increase the loading of protein in BioHOF-1, a dramatic enhancement in the number of surface hydrogen-bonding groups may be required, which cannot be achieved by surface modification. Thus, we chose to investigate wrapping the protein in a functionalized polymer, which may be able to promote the nucleation of HOF growth around the protein, thereby increasing protein loading.

This polymer-wrapping approach was inspired by molecular glues, which are discrete molecules that can adhere strongly to the surface of proteins and force them into close proximity of each other.[30] Physical proximity plays an important role in a variety of cellular processes, such as protein degradation,[30] initiation of apoptosis, protein transport and folding, and gene activation.[31] Though molecular glues have many different forms, our attention was drawn towards guanidinium-terminated dendrimers and polypeptides (**Figure 3.17**), which have been investigated extensively by Aida and co-workers.[32, 33] These specific molecular glues adhere to proteins via salt bridges, as guanidinium ions are known to interact with oxyanions present in proteins.[33] Although the guanidinium-anion interaction alone is insufficient to enable strong binding, the connection of multiple guanidinium groups via a flexible spacer enables multivalency of the interaction and thus increases the binding strength.[33] These glues have been used for a variety of applications. For example, a photocleavable guanidinium dendrimer has been developed that can cover a protein surface, preventing intermolecular protein-protein interactions. Exposure to UV light causes certain linkages within the dendrimer to be

cleaved, decreasing the multivalency of the interaction and freeing the protein from the molecular glue. This enables protein-protein interactions to be controllably switched on by exposure to UV light, which could have a variety of therapeutic applications.[34]

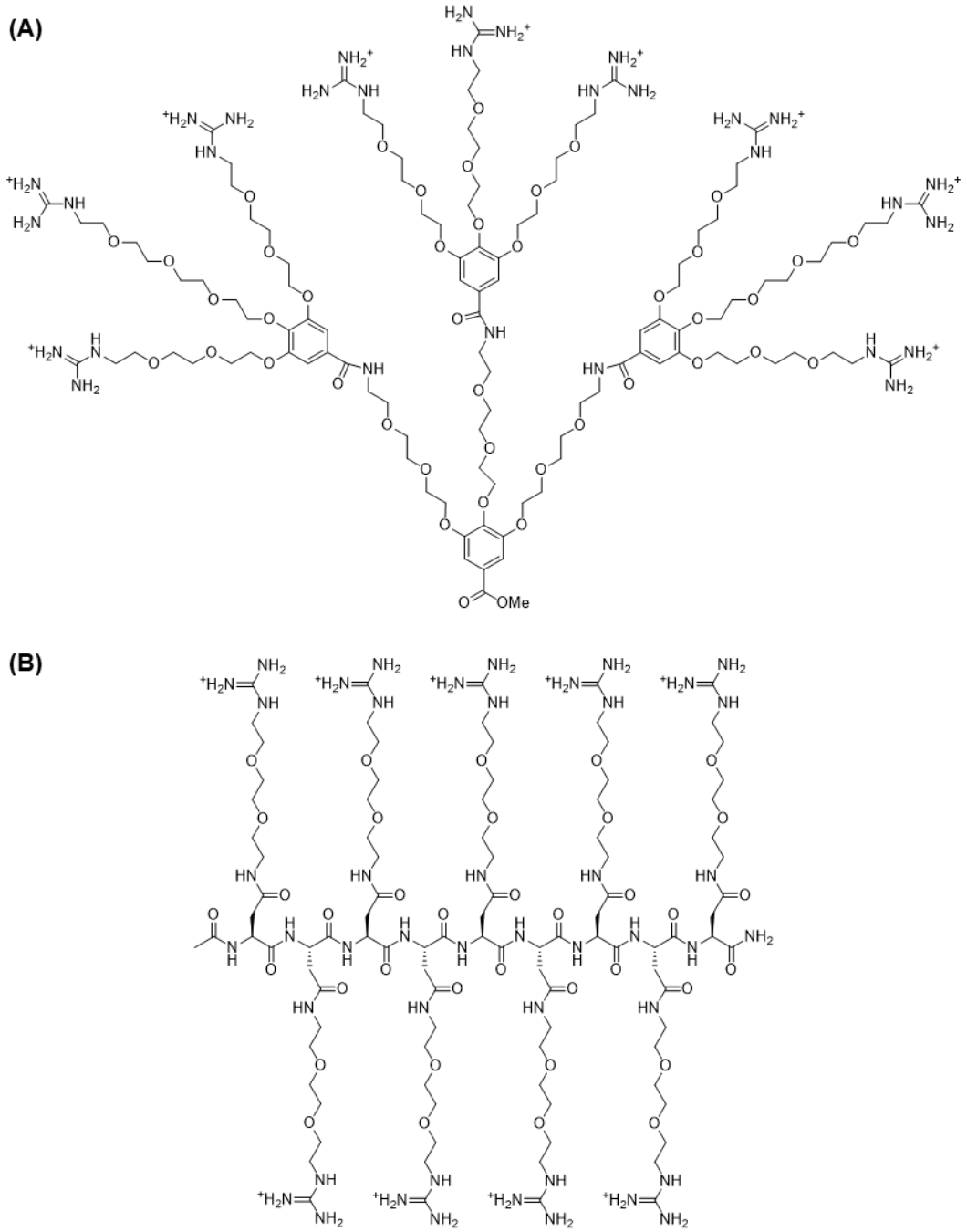

Figure 3.17: Examples of guanidinium-terminated molecular glues (A) G1(Gu^+)$_9$OMe and (B) Asn(TEG-Gu^+)$_9$, previously demonstrated to strongly adhere to proteins (figure adapted from ref. 33).

The reason for our interest in these guanidinium-terminated dendrimers and polypeptides, over other forms of molecular glues, was simple: Guanidinium groups bear similarity to the amidinium groups of the positively charged BioHOF-1 linker. Thus, the tetra-carboxylate linker could form salt bridges with the guanidinium ions of the molecular glue, promoting the nucleation of HOF growth around proteins with surface-adhered dendrimer. However, the complexity of these dendrimers means that they require a lengthy synthesis and are thus ultimately not economical as an additive for improving loading in BioHOF-1. Instead, guanidinium-modified poly(ethyleneimine) (G-PEI) was used (**Figure 3.18**), which could carry the benefits of a multivalent amidinium-based molecular glue but without a lengthy and costly synthesis required.

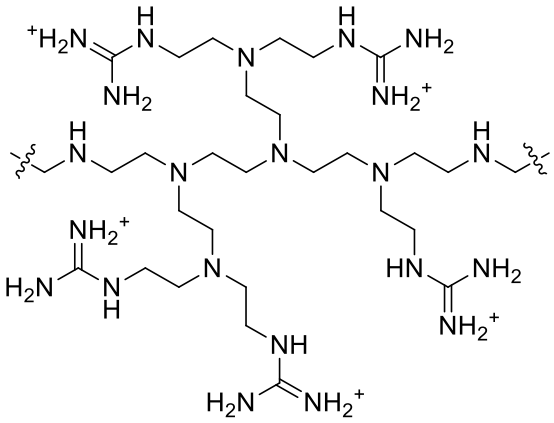

Figure 3.18: Example structure of guanidinium-modified poly(ethyleneimine) (G-PEI). G-PEI is expected to have properties similar to a molecular glue.

Unmodified poly(ethyleneimine) has been previously shown to interact with proteins, further validating its use in this work. It is widely used as a method of precipitating proteins for purification.[35], particularly negatively charged proteins.[35, 36] The amount of polymer required to cause precipitation of the protein typically increases as the surface charge density increases in negativity.[37] The mechanism behind protein precipitation by polyelectrolytes consists of several steps. First, protein-polyelectrolyte complexes are formed, due to a variety of interactions experienced between the protein and the PEI including electrostatic attraction, hydrogen bonding, and hydrophobic interactions. These complexes aggregate to form primary particles, which then further aggregate to form flocs.[38] Though aggregation of proteins has been shown in the previous chapter to be detrimental to encapsulation in BioHOF-1, careful manipulation of the polymer and protein concentrations may allow surface-binding of the G-PEI without

causing complete aggregation. This surface-bound G-PEI may then facilitate interaction with the tetra-carboxylate linker, leading to encapsulation in BioHOF-1.

3.5.2 Studies on protein/polymer interaction

Prior to encapsulation experiments, studies on G-PEI adhesion to ferritin were performed. G-PEI is a random, non-directional polymer, and thus it would be expected to adhere to multiple proteins and cause aggregation,[38] as opposed to guanidinium dendrimers which are designed to prevent protein-protein interactions or form more discrete complexes.[33, 34] Studies in the previous section with sodium sulfate suggested that protein aggregation had a detrimental impact on the incorporation of protein into BioHOF-1. Thus, studies were performed to assess at which concentrations G-PEI causes protein aggregation, as it was sought to interact with the protein but not cause complete aggregation. Interestingly, in the presence of remarkably small amounts of polymer (e.g. 20 µg/mL), aggregates formed, as indicated visually and by DLS analysis (**Figure 3.19**). As the polymer concentration was increased, aggregate formation diminished, until only a small peak of median size 206 nm was present in the intensity distribution alongside the ferritin peak. This is indicative of some form of interaction between ferritin and G-PEI.

Decreased aggregation at high G-PEI concentrations is an intriguing result, as in the literature it is noted that increasing unmodified PEI concentration tends to facilitate protein aggregation.[37] Aggregation of protein with polyelectrolytes is thought to be limited by two modes of interaction. Charge neutralization of the protein by the polymer leads to diminished electrostatic repulsion, facilitating aggregation through van der Waals attraction. Accompanying this is polymer bridging, in which the polymer adsorbed on one protein particle may interact with a bare patch on an adjacent protein, further promoting aggregation.[39] It is currently unclear why higher G-PEI concentrations diminish ferritin aggregation. A potential explanation for this occurrence is that G-PEI, at exceptionally high concentrations, completely surrounds the protein, with excess guanidinium groups facing outwards into the bulk solution. With all protein surrounded, these free guanidinium groups are unable to interact with neighbouring protein, whilst charge-charge repulsion from the large excess of G-PEI keeps proteins from aggregating. However, our evidence to support this mechanism of action is insufficient. Regardless,

these studies indicate that G-PEI interacts strongly with ferritin, with complete aggregation avoided at higher polymer concentrations.

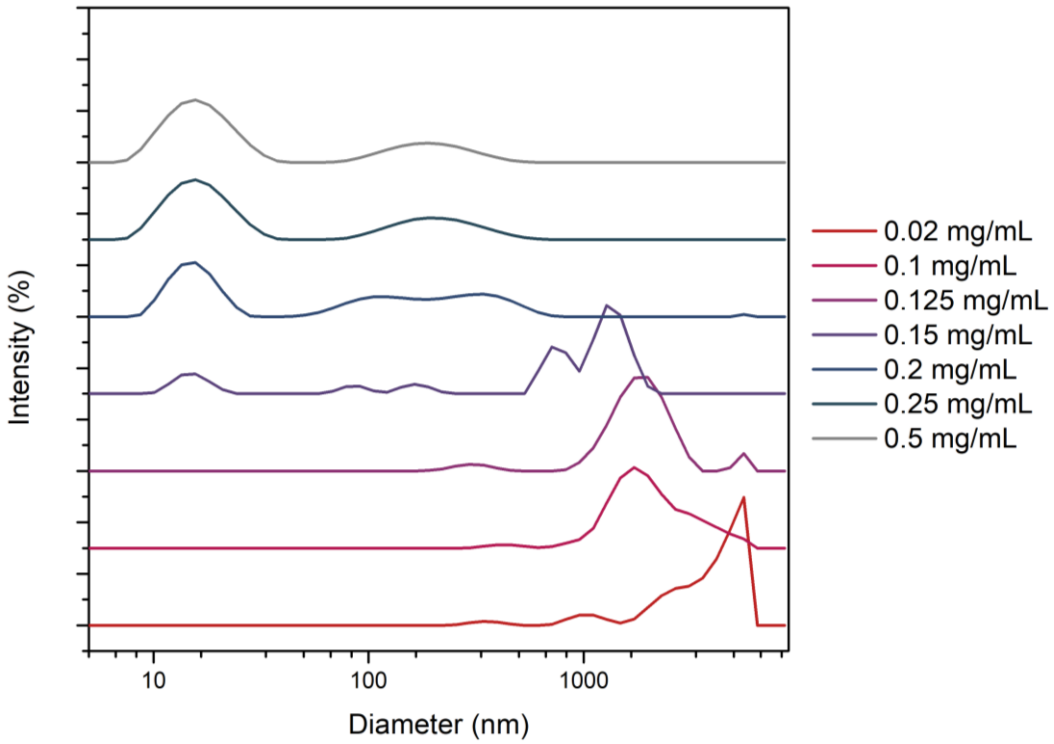

Figure 3.19: Effect of guanidinium-modified poly(ethyleneimine) concentration on the aggregation of ferritin. Measurements were made in water at a ferritin concentration of 1 mg/mL, and are presented as an intensity distribution. Lower G-PEI concentrations cause ferritin aggregation, as indicated by the disappearance of the peak at ~16 nm and the appearance of particles >300 nm in diameter.

Based on the results from aggregation studies, the chosen concentration of polymer to be incubated with ferritin prior to BioHOF-1 synthesis was 0.25 mg/mL, as it was the lowest concentration of polymer that showed no evidence of ferritin aggregation. Interaction between ferritin and G-PEI at this concentration was further verified by measuring the zeta potential of the protein, which changes from -15.7 mV to +14.7 mV upon incubation with the polymer (**Figure 3.20**). The zeta potential distribution broadens significantly with G-PEI present, likely due to the extent of surface coverage varying between ferritin macromolecules. Regardless, this indicates successful surface coverage of G-PEI on ferritin, which should promote interaction with the BioHOF-1 tetra-carboxylate linker.

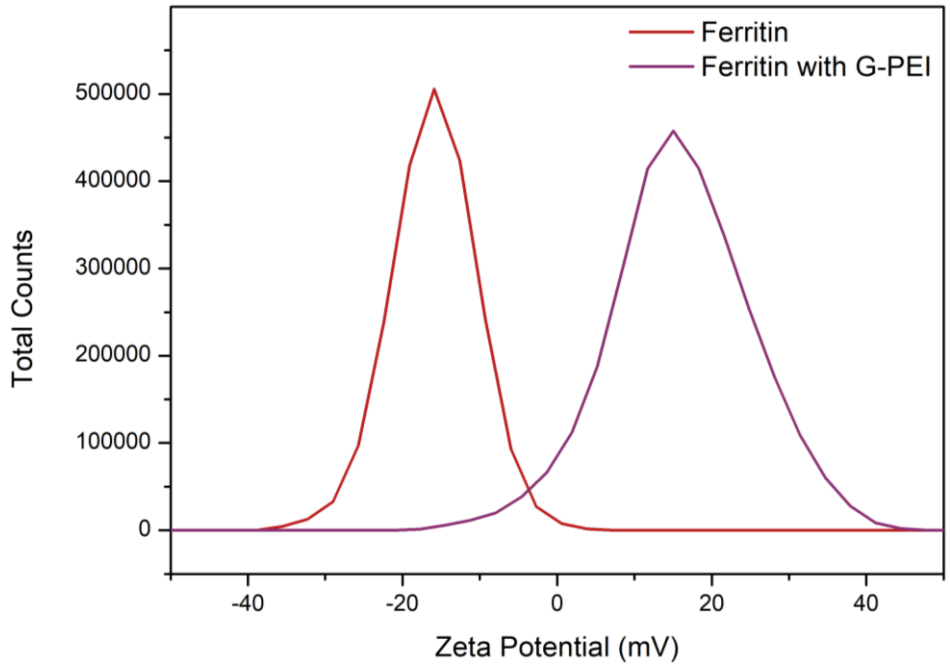

Figure 3.20: Zeta potential distribution of 1 mg/mL ferritin before and after incubation with 0.25 mg/mL poly(ethyleneimine). Measurements were made in water. G-PEI adheres to the surface of ferritin, causing the charge on ferritin to become more positive.

3.5.3 Effect of polymer on ferritin encapsulation in BioHOF-1

In addition to causing aggregation of ferritin, early attempts to encapsulate a ferritin/G-PEI mixture in BioHOF-1 revealed that G-PEI forms an amorphous precipitate when mixed with the tetra-carboxylate link. This is unsurprising, as carboxylate and guanidinium ions are known to form strong salt bridges with each other. Introduction of the tetra-carboxylate into a solution of the polymer may allow the linking of guanidinium groups of separate polymer strands together via the tetra-carboxylate link. The combination of charge neutralization and formation of larger polymer networks would decrease the solubility of the polymer and cause it to precipitate. This could remove ferritin/G-PEI from solution, preventing encapsulation in BioHOF-1. Thus, it was decided that both orders of formation of the HOF would be tested, to assess if the precipitation of the polymer with the tetra-carboxylate link could have a beneficial impact on protein encapsulation.

The effect of G-PEI incubation on encapsulation of ferritin in BioHOF-1 was assessed. TEM imaging revealed that ferritin encapsulation was slightly improved, with

little ferritin present in samples without polymer, and a slight improvement in ferritin encapsulation for samples containing polymer (**Figure 3.21**). BCA data confirmed a slightly improved loading with polymer present (**Figure 3.22**). Unfortunately, the G-PEI polymer contributed to the BCA absorbance, as does PEI to all common methods of protein quantification,[40] and so the wt.% loading values assume ferritin and G-PEI were incorporated into the framework in the same ratio as were initially administered. As such, these values should be regarded as an upper estimate. Intriguingly, the amount of ferritin increased slightly for BioHOF-1 synthesized with the addition of the tetra-carboxylate linker to the G-PEI/ferritin mixture prior to the tetra-amidinium linker, with this order of addition returning a maximum loading of 4.4% compared to 3.0% for the opposite order. This is contrary to what was expected, as this sample experienced precipitation of the tetra-carboxylate with the G-PEI/ferritin composite. Polyelectrolyte aggregates are known to be resolubilized in solutions containing higher salt concentration,[41] and so potentially the addition of the tetra-amidinium linker may help resolubilize the polymer, protein and tetra-carboxylate. This would enable the HOF to form from the constituents of the aggregates as they redissolve, leading to higher loading as the protein is localized at the site of framework formation.

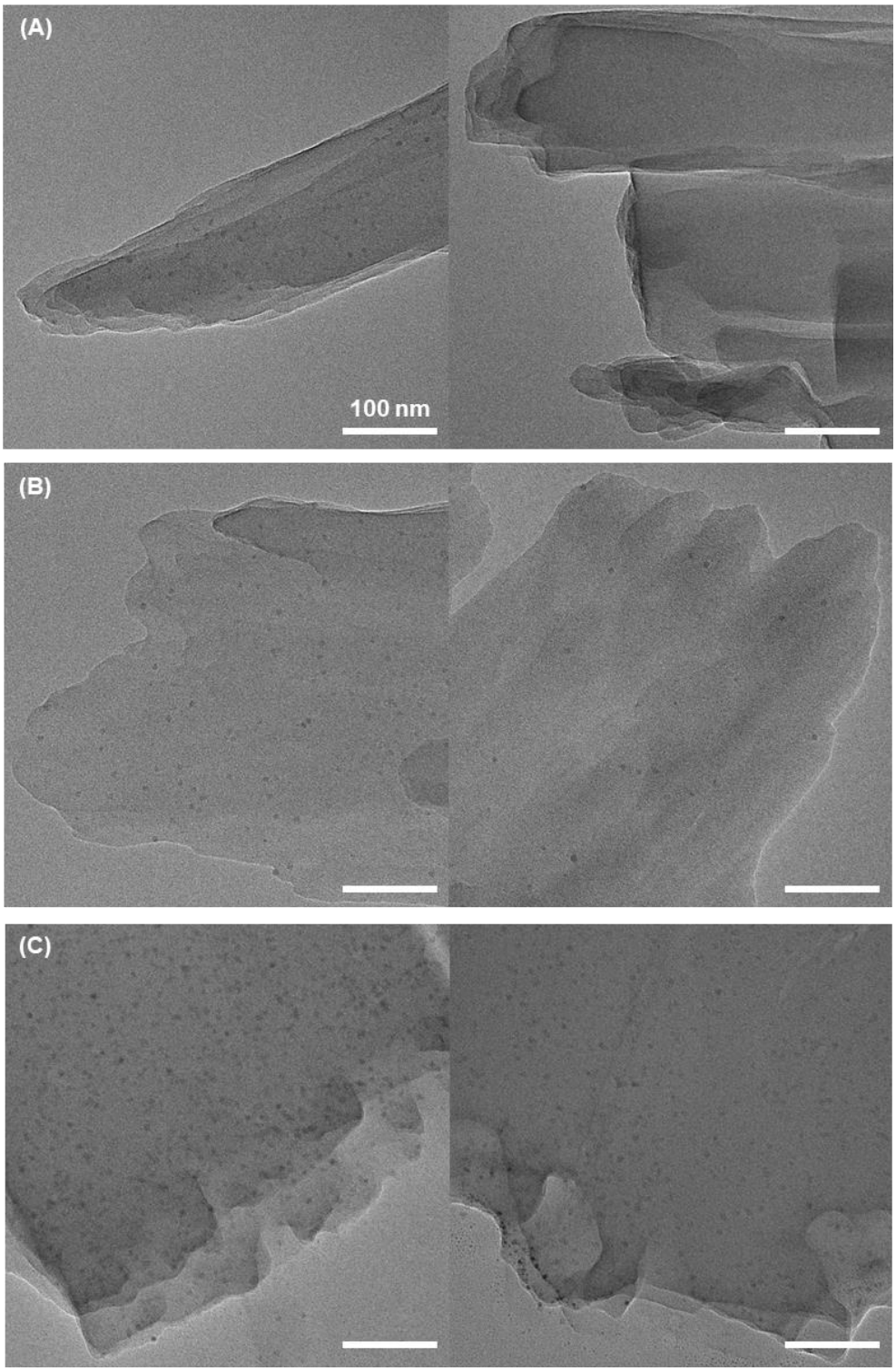

Figure 3.21: TEM images of (**A**) as-synthesized FER@BioHOF-1, (**B**) FER/G-PEI@BioHOF-1 synthesized by addition of the tetra-amidinium linker first, and (**C**) FER/G-PEI@BioHOF-1 synthesized in the presence of the tetra-carboxylate linker first. Samples were washed with 10% SDS prior to imaging to ensure only encapsulated protein was visible. Black spots correspond to the iron core of individual ferritin macromolecules.

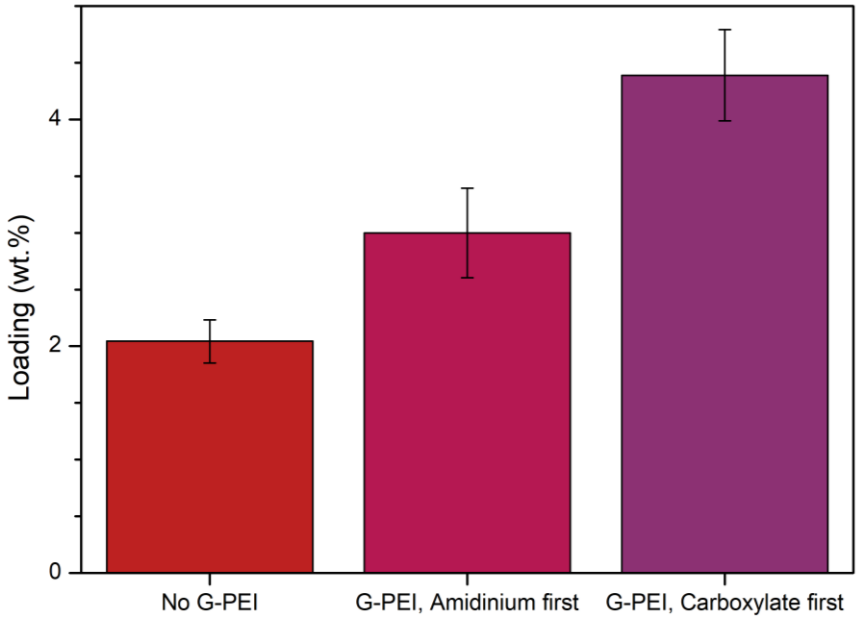

Figure 3.22: Effect of G-PEI and order of linker addition on loading of ferritin in BioHOF-1. Samples were washed with 10% SDS prior to analysis to ensure only encapsulated protein was included in the loading value. Error bars represent the standard error in the loading of the sample determined from triplicate assay measurements. Pre-incubation with G-PEI increases the loading of ferritin in BioHOF-1, with different loadings resulting depending on the order of addition of the HOF linkers. G-PEI contributes to the assay absorbance and thus the values above should be regarded as an upper estimate of loading.

PXRD indicates that despite the presence of the amorphous G-PEI polymer, the precipitates formed are crystalline BioHOF-1 (**Figure 3.23**). However, SEM indicates that the crystals are more deformed than pure FER@BioHOF-1, with crystals forming clumps rather than individual, discrete crystals (**Figure 3.24**). Of the two orders of addition, forming the HOF with the tetra-carboxylate added first appears to form larger, intergrown masses of crystals. This is likely a result of the prior precipitation of the tetra-carboxylate with the G-PEI/ferritin, which the HOF may grow from upon the introduction of the tetra-amidinium. The presence of loose polymer chains of G-PEI may also be increasing the number defect sites within BioHOF-1. This could have some potential benefits for the activity of encapsulated enzymes, as defects accompany an increased pore size distribution,[42] which could promote the diffusion of substrates/products to and from the enzyme. Nonetheless, use of a guanylated polymer proved to only have a minor

impact on the encapsulation of ferritin in BioHOF-1, and thus did not achieve our intended loading enhancement.

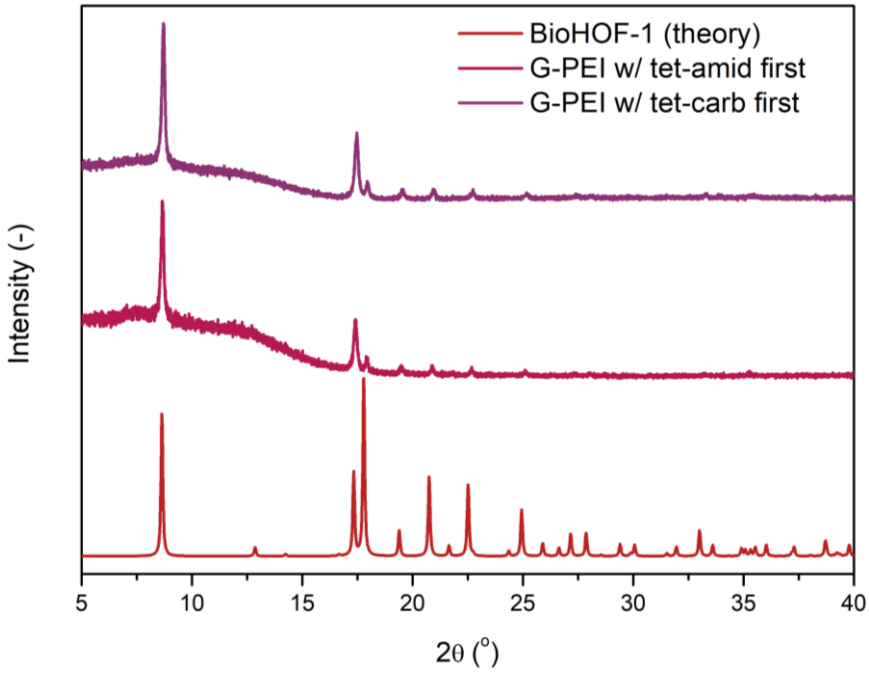

Figure 3.23: PXRD of BioHOF-1 synthesized in the presence of 1 mg/mL ferritin and 0.25 mg/mL G-PEI. Samples were washed with water (x 2), ethanol, 10% SDS, water (x 2) and ethanol, and were dried under vacuum prior to analysis. Low peak height relative to the baseline is likely a result of the limited amount of material available for analysis, in addition to contribution to the baseline by the amorphous polymer.

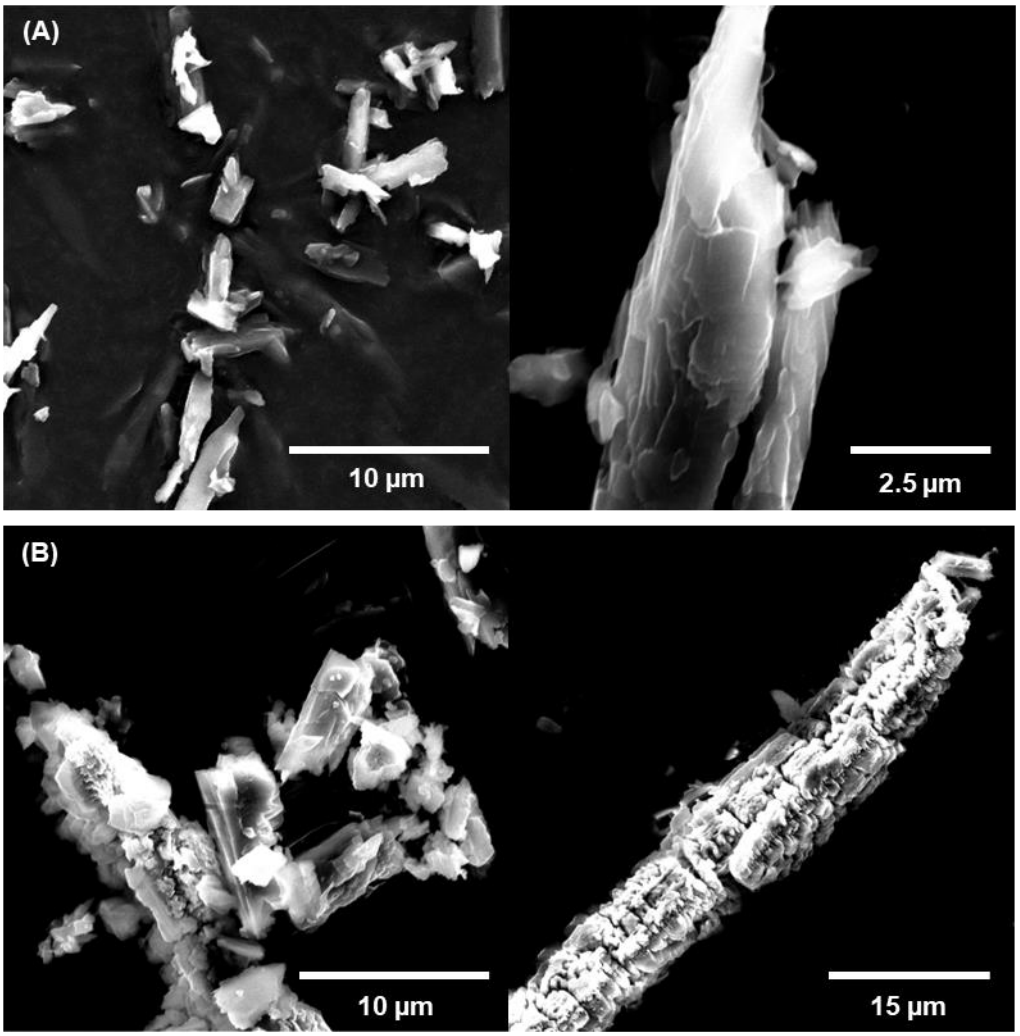

Figure 3.24: SEM images of BioHOF-1 synthesized in the presence of 1 mg/mL ferritin and 0.25 mg/mL guanylated polymer, with (A) tetra-amidinium added first and (B) tetra-carboxylate added first. Samples were washed water (x 2), ethanol, 10% SDS, water (x 2) and ethanol, and were dried under vacuum prior to analysis. Both samples exhibit significant deformation compared to crystals of ferritin@BioHOF-1, with this deformation being more prevalent when the tetra-carboxylate is added first in the HOF synthesis.

3.5.4 Summary

Inspired by molecular glues, guanidinium-modified poly(ethyleneimine) was used to increase the loading of ferritin in BioHOF-1. DLS and zeta potential studies indicated that G-PEI interacted with the surface of ferritin, causing ferritin aggregation at low concentrations but maintaining free ferritin at high concentrations. Encapsulation of

ferritin/G-PEI resulted in a potential increase in loading in BioHOF-1, from 2% to 3 or 4% depending on the order of linker addition, however contribution of G-PEI to the assay means these values should be regarded as an upper estimate of loading. The resulting crystals had a markedly different appearance to FER@BioHOF-1, with larger, intergrown crystals forming, particularly for samples prepared by addition of the tetra-carboxylate linker prior to the tetra-amidinium linker. These deformed crystals could possess additional interesting properties, however with the effect on loading minimal, we did not pursue further experiments using G-PEI to increase loading in BioHOF-1.

3.6 Layer-by-Layer Encapsulation of BioHOF-1 for Enhanced Protein Protection

3.6.1 Background

With broadly applicable approaches to increasing protein loading in BioHOF-1 proving ineffective, our attention was shifted towards developing other methods to increase the utility of this HOF. Our studies on increasing loading revealed that proteins have an overwhelming preference to bind to the surface of the HOF rather than be encapsulated. For example, FER@BioHOF-1 has a wt.% loading of 15.4%, which decreases to 2.0% after removal of surface-bound protein by SDS washing (**Figure 3.5**), indicating that only 13% of the immobilized protein was encapsulated in the framework. Surface adsorption affords less protection than encapsulation,[1, 3] as direct contact is maintained between the protein and the outside environment. Protein is also more susceptible to leaching, which is undesirable for composite reuse in biocatalysis. If additional protection could be provided to protein@BioHOF-1 composites such that surface-bound protein is as well-protected as encapsulated protein, the preference for protein to bind to the surface of BioHOF-1 would be inconsequential to the eventual use of the framework.

With this in mind, we pursued a means through which additional protection could be imparted to surface-bound protein. This could be achieved by encapsulating BioHOF-1 within a thin layer of a secondary material. Coating of porous frameworks, particularly MOFs, has been widely reported for a variety of coating types and applications. ZIF-8 alone, for example, has been coated with species including functionalized PEGs,[43] other metal organic frameworks (e.g. MOF-74, ZIF-67),[44-46] polydopamine,[47] and polyelectrolytes.[48, 49] However, the approaches available for adding a secondary coating to BioHOF-1 are more limited, as the conditions for the coating must be biocompatible. For this reason, we chose to pursue layer-by-layer (LBL) encapsulation in alternating polyelectrolytes as a method adding a secondary layer to BioHOF-1.

LBL encapsulation has been previously utilized for a variety of biologically relevant applications. For example, whole cell encapsulation has been widely reported,[50-53] commonly using a combination of polyelectrolytes such as poly(styrene sulfonate) (PSS) and poly(allylamine) (PAH).[50] Enzyme-containing polyelectrolyte capsules have

also been synthesized. In this process, bovine liver catalase crystals were suspended in buffer, and incubated with alternating poly(styrene sulfonate) and poly(allylamine), gradually developing a coating of polymer around the crystals. Dissolution of the catalase crystals resulted in the formation of spherical capsules with a high internal catalase concentration, which showed retained activity even after protease digestion,[54] akin to the types of conditions we would like to protect surface-bound protein from in the case of BioHOF-1.

LBL encapsulation of metal-organic frameworks has also been demonstrated, with the methanol-based synthesis of a PSS/PAH shell around ZIF-8 previously reported. The ZIF-8 core of the composites could be decomposed by exposure to acidic conditions, forming a hollow polymer shell which retained shape reminiscent of ZIF-8 for over one month.[49] As such, the LBL encapsulation of both porous frameworks and enzymes has been demonstrated in the past. However, the existing synthesis conditions for each of these methods precludes compatibility with the other. For example, the acidic buffer used for the LBL encapsulation of catalase crystals would not be compatible with ZIF-8, whilst the methanol-based procedure for the LBL encapsulation of ZIF-8 would denature proteins. As we may in the future wish to extend our LBL synthesis to ZIF-based biocomposites, we aimed to carry it out under conditions that were compatible with BioHOF-1, ZIF-8, and protein, thus requiring a trial of several different solvent systems. The proposed synthesis procedure for protein@BioHOF-1@PSS/PAH is summarized in **Scheme 3.2**.

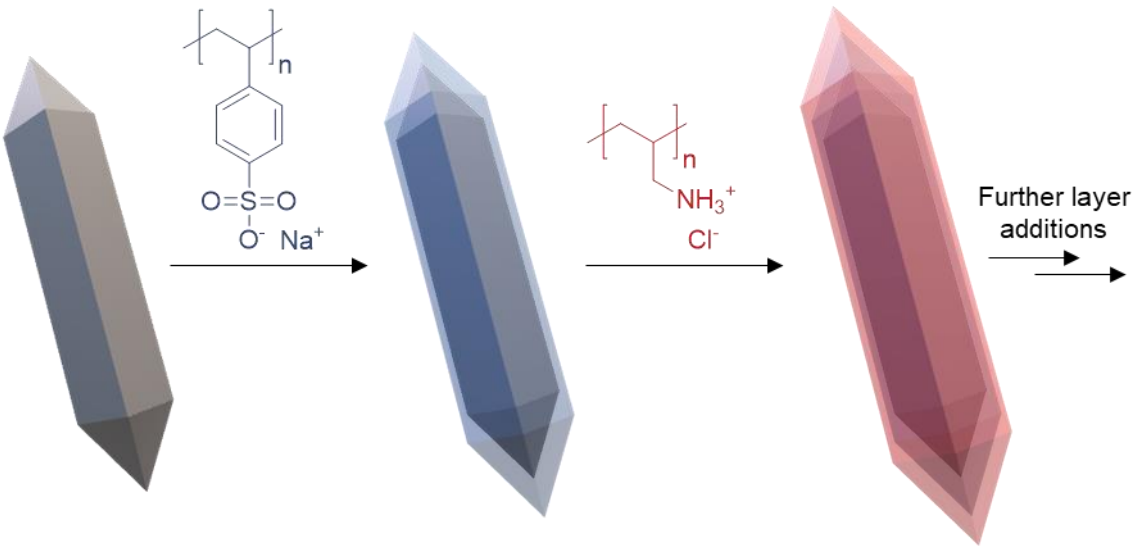

Scheme 3.2: Synthesis of protein@BioHOF-1 coated in alternating layers of poly(styrene sulfonate) and poly(allylamine). The solvent system can be adjusted to maximize biocompatibility. Layer-by-layer coating would form a barrier between surface-bound protein and the outside environment, leading to enhanced protection.

3.6.2 Trialling layer-by-layer encapsulation in water

To assess the layer-by-layer coating of a material, zeta potential can normally be used, as the charge on the surface should fluctuate as each alternate layer is added. Zeta potential has been previously used to verify LBL encapsulation of materials such as ZIF-8,[48, 49] as well as biological entities such as microbes.[52] However, attempts to measure the zeta potential of BioHOF-1 were unsuccessful, with identical samples of HOF producing significantly different zeta potential readings. This is likely because the HOF crystals are needle-like, whilst zeta potential measurements assume a spherical particle shape,[55] leading to misleading zeta potential distributions. Thus, zeta potential was not used as a method of verifying successful LBL encapsulation. Instead, PAH was tagged with FITC, and thus the deposition of every second layer could be visualized using CLSM.

In initial testing, LBL encapsulation of BioHOF-1 was conducted in pure water. This was decided as BioHOF-1 and the protein are both stable to repeated water washes. However, encapsulation of the HOF crystals was unsuccessful under these conditions. CLSM images indicate that although some polymer adheres to the surface of the HOF, the coverage of the framework by the polymer is only partial (**Figure 3.25**), with SEM

of the composite appearing near-identical to as-synthesized BioHOF-1 (**Figure S3.9**). This may be due to the limited solubility of PAH in water, which could cause the polymer to form localized clumps on the surface of the HOF. This is further supported by the large amount of free polymer aggregates present in the sample. With LBL encapsulation in water showing little promise, attention was shifted towards replicating the synthesis conditions for LBL coated ZIF-8.

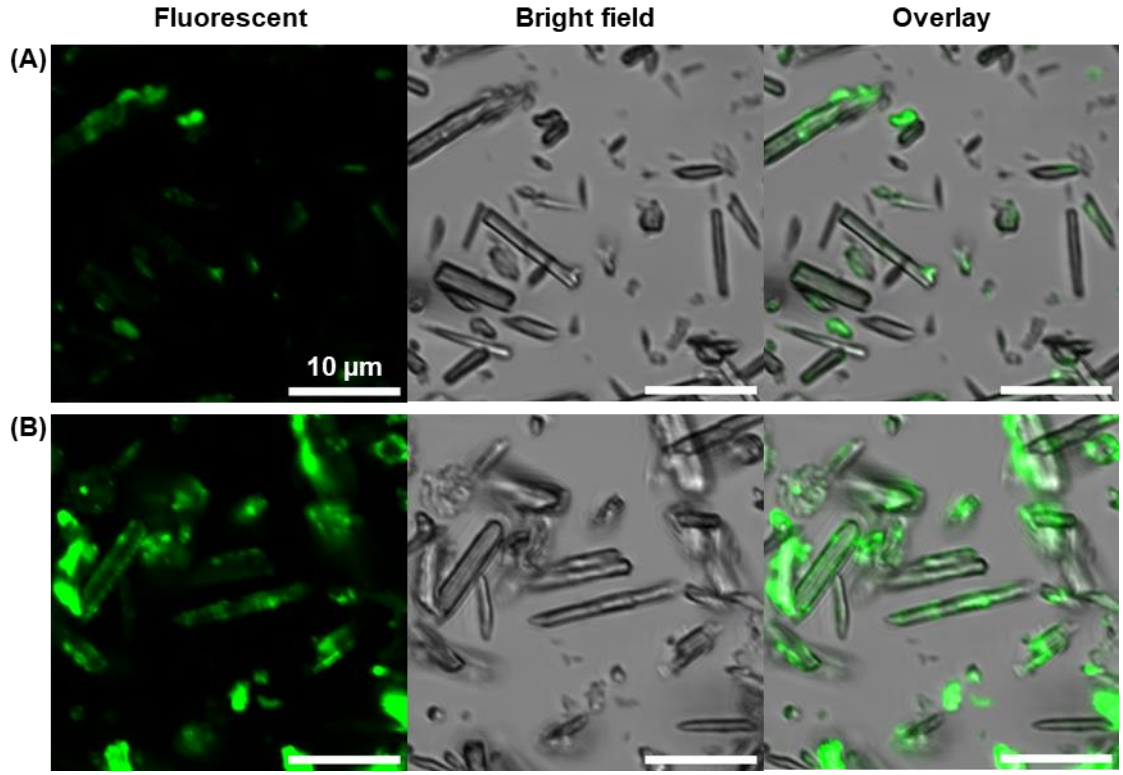

Figure 3.25: CLSM overlay image of BioHOF-1 coated with (**A**) 4 and (**B**) 8 layers of alternating poly(styrene sulfonate) and FITC-tagged poly(allylamine), synthesized in water. Samples were analyzed as a suspension in water. Clusters of fluorescence indicate a non-homogeneous coat of F-PAH on the surface of the material.

3.6.3 Layer-by-layer encapsulation in methanol/water mixtures

The existing literature procedure for the LBL encapsulation of ZIF-8 utilizes methanol as the solvent. Although this solvent system is not biocompatible, it allowed the feasibility of LBL encapsulation of a species that has an elongated shape to be assessed. For the LBL process in methanol, the polymers first had to be converted to their methanol-soluble form. Otherwise, the process was identical to that undertaken for the

LBL encapsulation in water. In this solvent, the process resulted in a more homogeneous coating of polymer on the surface of the HOF, indicated by CLSM (**Figure 3.26**). Moreover, the coating was thick enough to be visualized using SEM, with the coated samples displaying a more rounded, textured surface when compared to pure BioHOF-1 (**Figure 3.27**). Small, regularly spaced cracks can be seen on the surface of the LBL-coated HOF. These cracks are likely a result of the drying process, with the polymer shrinking as the methanol is removed, and thus would not impact the protection afforded to the framework surface in solution. Alongside the coated crystals, a significant amount of aggregated polymer is visible. Despite the polyelectrolyte encapsulation, the crystallinity of the underlying HOF was retained, as indicated by PXRD (**Figure 3.28**). Thus, although imperfect, the LBL encapsulation of BioHOF-1 was successful, demonstrating that the shape of the crystals does not impact the applicability of LBL encapsulation. Knowing this information, LBL encapsulation of BioHOF-1 using biocompatible conditions was further pursued.

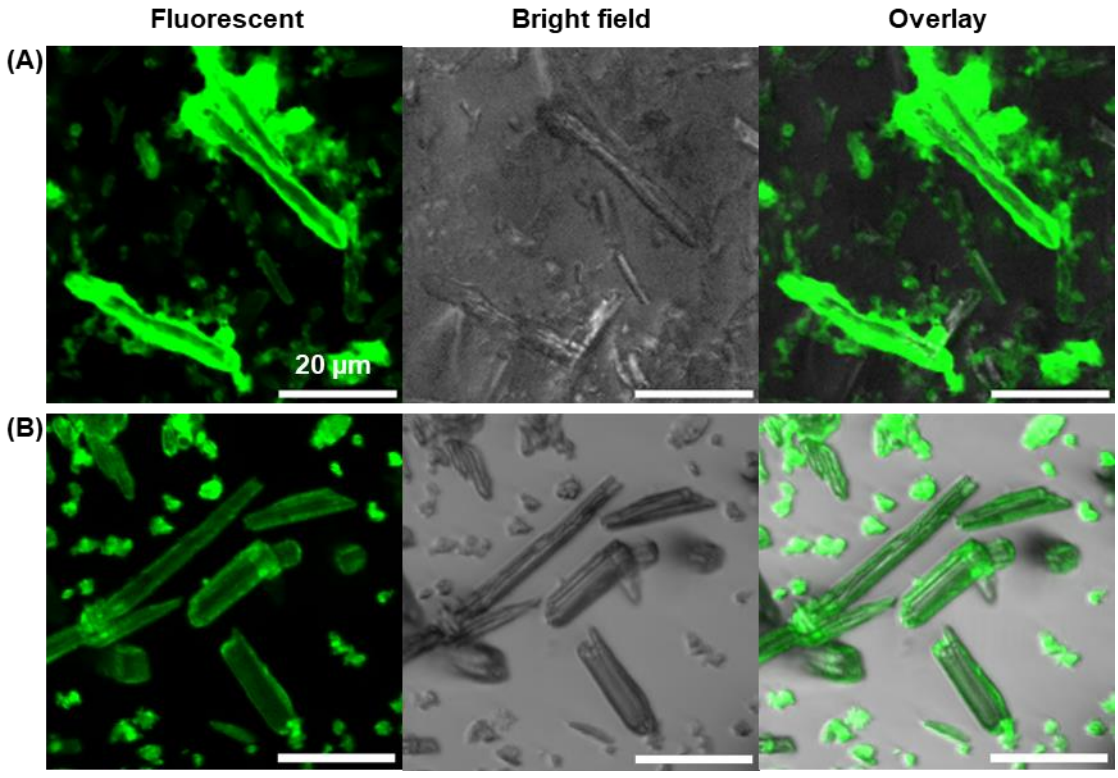

Figure 3.26: CLSM overlay image of BioHOF-1 coated with (**A**) 4 and (**B**) 8 layers of alternating poly(styrene sulfonate) and FITC-tagged poly(allylamine), synthesized in pure methanol. Samples were analyzed as a suspension in water. Uniform fluorescence around the outside of the material indicates a homogenous coating of F-PAH on the surface of the material.

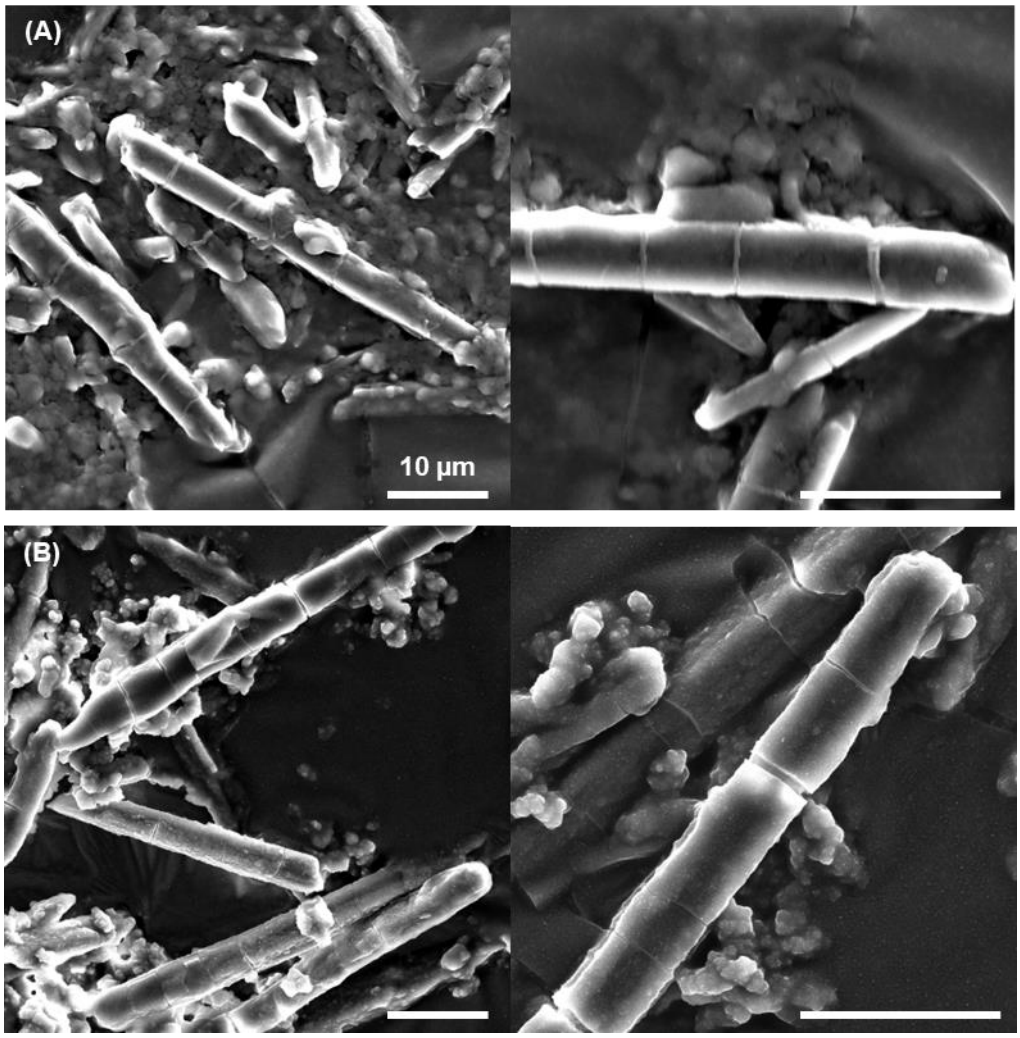

Figure 3.27: SEM image of BioHOF-1 coated with (**A**) 4 and (**B**) 8 layers of alternating poly(styrene sulfonate) and FITC-tagged poly(allylamine), synthesized in methanol. Samples were dried under vacuum prior to analysis. Crystals have a more rounded appearance than pure BioHOF-1. Cracks along the width of the coated crystals are likely a result of the drying process.

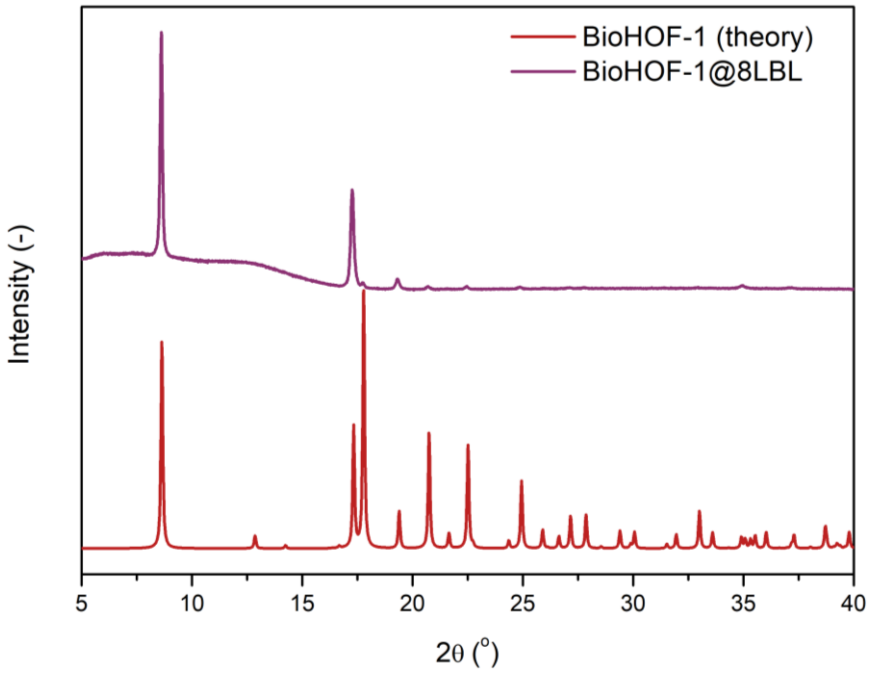

Figure 3.28: PXRD pattern of BioHOF-1 coated with 8 layers of alternating poly(styrene sulfonate) and FITC-tagged poly(allylamine), synthesized in methanol. Samples were suspended in ethanol and air dried prior to analysis. Low peak height relative to the baseline is likely a result of the limited amount of material available for analysis, in addition to contribution to the baseline by the amorphous polymer.

Given the success of the LBL encapsulation in pure methanol, methanol/water mixtures were explored for the encapsulation of BioHOF-1. These mixtures were more biocompatible than pure methanol yet allowed the polymers to be administered in their uncharged form, with deprotonated PAH and protonated PSS, which may benefit the LBL encapsulation. 10, 25, 50 and 75% MeOH mixtures were trialed as solvents for the LBL procedure. All samples showed a uniform coating of F-PAH, indicating successful encapsulation (**Figure 3.29**). By SEM, the crystals again had a more rounded, textured surface than plain BioHOF-1 (**Figure 3.30**). Although difficult to discern, the roundedness of the LBL coat appeared to increase as the concentration of methanol increased, accompanied with an increase in the size and frequency of cracks in the material. For all samples, free polymer aggregates remained present. This is undesirable as it is a waste of the polyelectrolyte materials and would decrease the wt.% loading of protein in the final composite. Nonetheless, for preliminary testing purposes, free precipitated polymer should not have a significant impact on enzymatic activity and could be rectified in the future if the system proved promising. With confidence that the LBL

procedure was working effectively, LBL coating of a catalase-on-BioHOF-1 sample was performed.

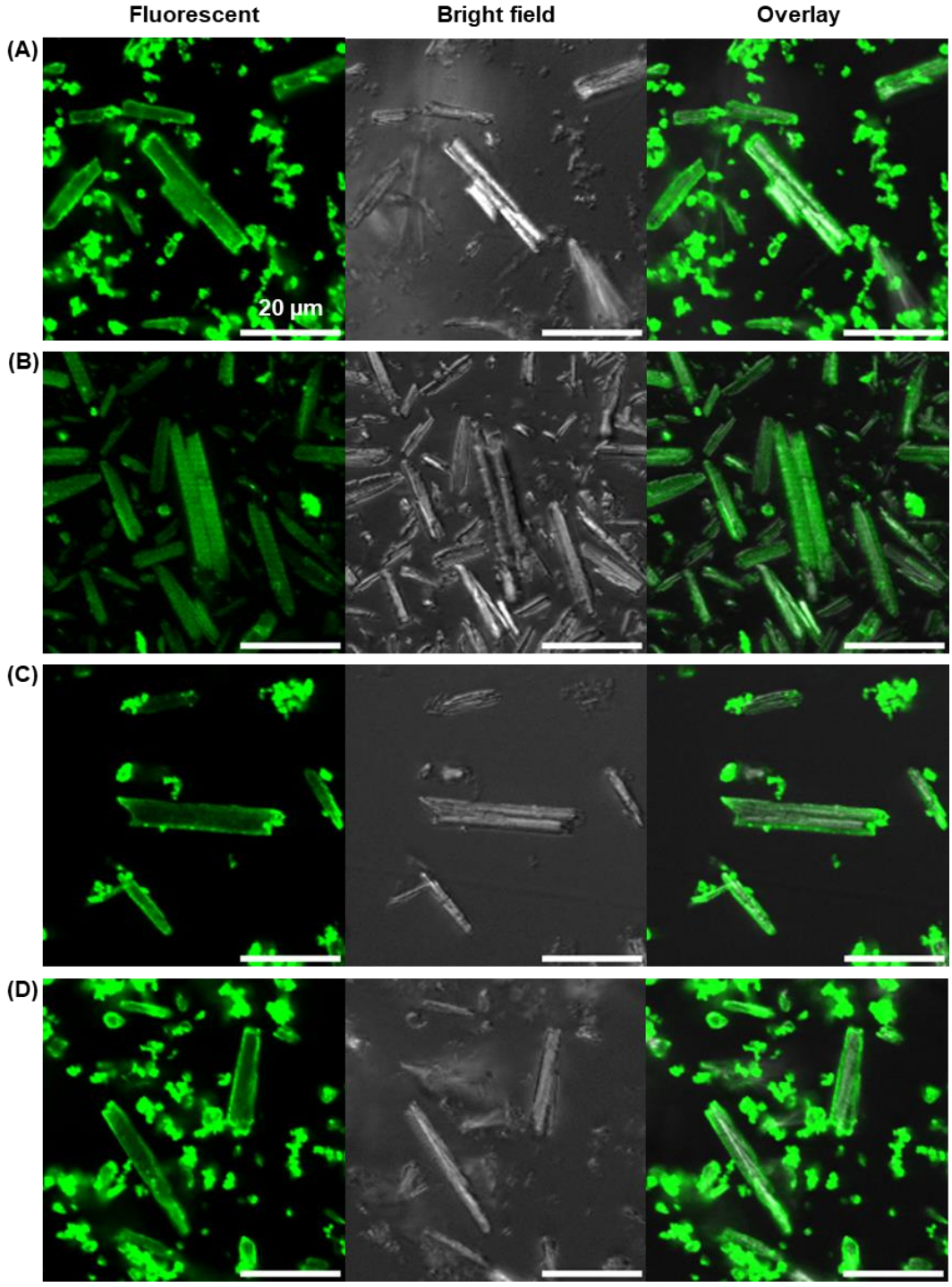

Figure 3.29: CLSM images of BioHOF-1 coated with 4 layers of alternating poly(styrene sulfonate) and FITC-tagged poly(allylamine), synthesized in (**A**) 10%, (**B**) 25%, (**C**) 50%, and (**D**) 75% MeOH. Samples were analyzed as a suspension in water. Uniform fluorescence around the outside of the material indicates a homogenous coating of F-PAH on the surface of the material.

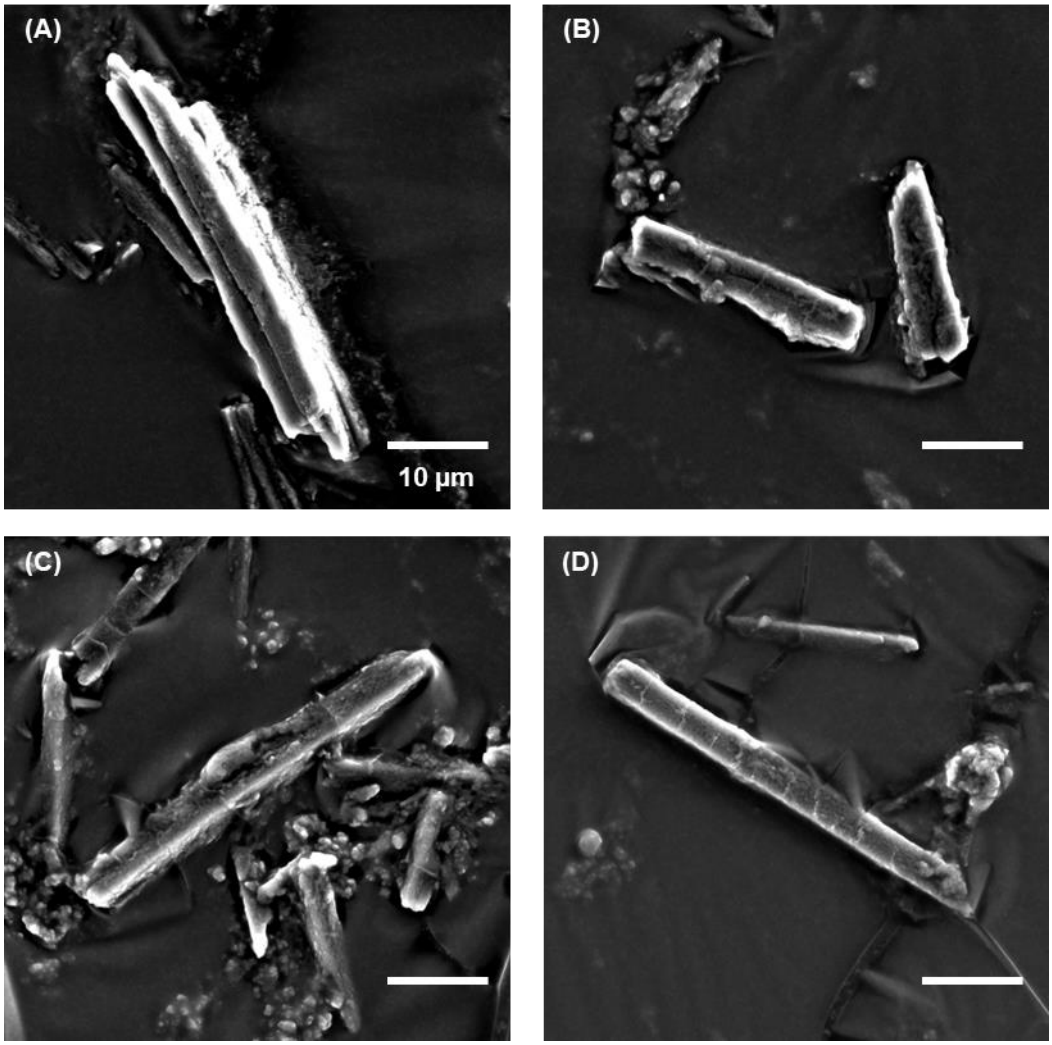

Figure 3.30: SEM image of BioHOF-1 coated with 4 layers of alternating poly(styrene sulfonate) and FITC-tagged poly(allylamine), synthesized in (**A**) 10%, (**B**) 25%, (**C**) 50%, and (**D**) 75% MeOH. Samples were dried under vacuum prior to analysis. Coated crystals exhibit a more rounded appearance as the concentration of methanol is increased.

As previously discussed, proteins are highly sensitive to non-aqueous media, which often has a detrimental impact on enzymatic activity. Thus, for LBL encapsulation of catalase-on-BioHOF-1, 10% MeOH was used as the solvent system, the lowest MeOH% system previously tested. The surface bound catalase appeared to have little effect on the LBL coating, with a uniform coat of F-PAH visible by CLSM (**Figure 3.31**). Further, PXRD indicated that the HOF did not lose crystallinity during the LBL process (**Figure 3.32**).

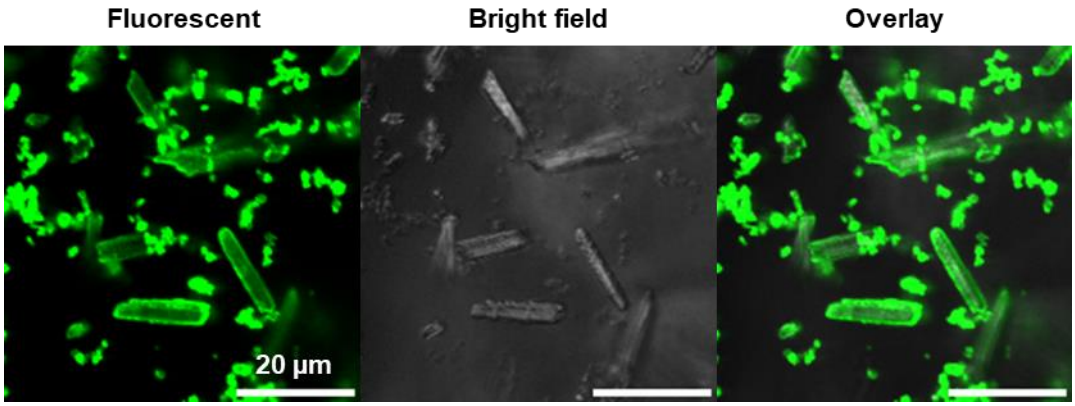

Figure 3.31: CLSM images of catalase-on-BioHOF-1 coated with 4 layers of alternating poly(styrene sulfonate) and FITC-tagged poly(allylamine), synthesized in 10% methanol. Samples were analyzed as a suspension in water. Uniform fluorescence around the outside of the material indicates a homogenous coating of F-PAH on the surface of the material.

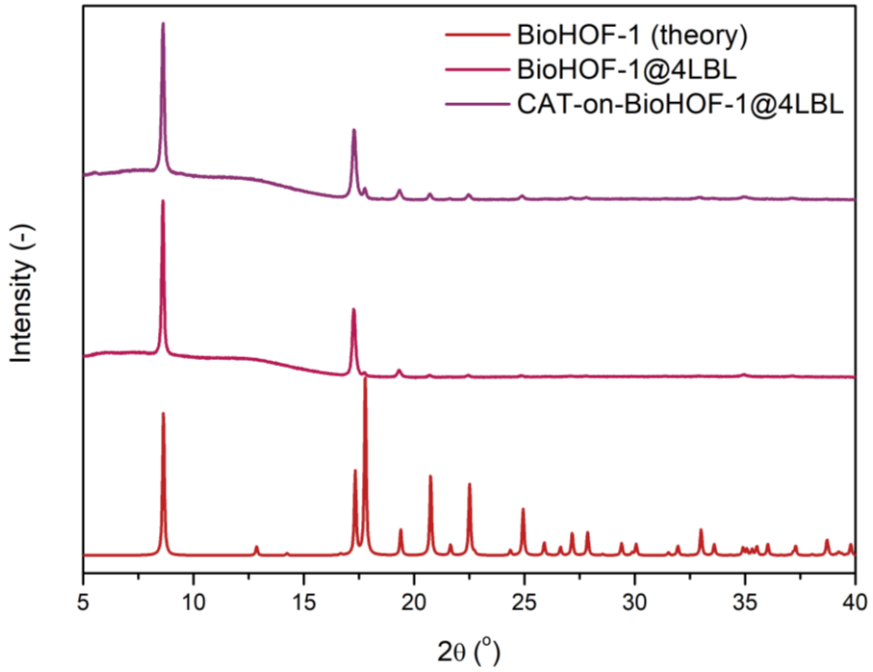

Figure 3.32: PXRD of BioHOF-1 and catalase-on-BioHOF-1 coated with 4 layers of alternating poly(styrene sulfonate) and FITC-tagged poly(allylamine), synthesized in 10% MeOH. Samples were suspended in ethanol and air dried prior to analysis. Low peak height relative to the baseline is likely a result of the limited amount of material available for analysis, in addition to contribution to the baseline by the amorphous polymer.

With catalase-on-BioHOF-1 successfully encapsulated in a LBL coating, activity testing was performed, which revealed that catalase activity was lost in the LBL process (**Figure 3.33**). Prior control studies indicated that 10% MeOH decreased catalase activity by ~60% but did not result in complete activity loss (**Figure S3.10**). On review of the system, it was found that the pH of the PSS in 10% MeOH solution was 3, below the range which a protein would be expected to tolerate. In the LBL coating, the 1-layer sample was prepared from F-PAH alone, and thus some activity was retained for the first layer addition as no PSS was present. However, when the PSS layer was added, the protein would have denatured upon immersion in the highly acidic solution, leading to the dramatic decrease in activity observed upon addition of the second layer. With this solvent system, we could not envisage a pathway that would allow us to encapsulate the HOF with polymer without exposing it to the acidic PSS solution. Thus, a new solvent system was pursued, using a buffer to ensure that the protein was not denatured by the acidity or basicity of the polymers.

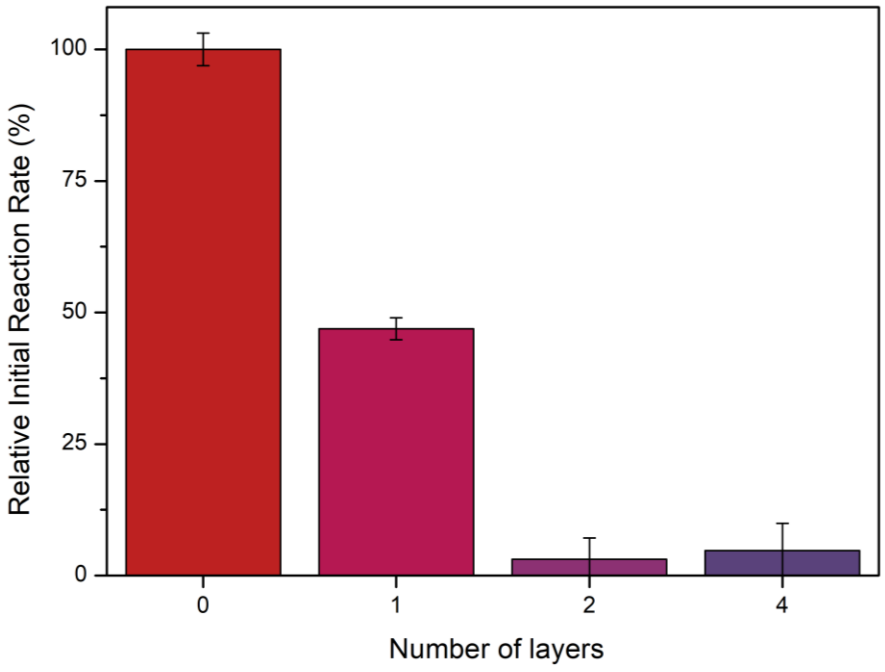

Figure 3.33: Relative initial rate of H_2O_2 decomposition by catalase-on-HOF samples coated with alternating layers of F-PAH and PSS, synthesized in 10% MeOH. The enzyme concentration in the reaction was 500 nM. Samples are normalized relative to uncoated catalase-on-BioHOF-1. Error bars represent the standard error in the slope of the linear regression from which the relative initial reaction rate was derived. Samples

lose 50% activity after the addition of the first F-PAH layer, with near-complete activity loss resulting upon addition of the following PSS layer,

3.6.4 Layer-by-layer encapsulation in tris buffer

Based on the reasoning that the initial LBL encapsulation attempts in water were unsuccessful due to the limited solubility of the polyelectrolytes, the solubility of PSS and F-PAH in different concentrations of tris buffer was assessed. Tris buffer was chosen as it does not degrade the HOF and provides the opportunity to extend the LBL process to ZIFs in the future, which are unstable to other common buffers such as PBS.[56-63] It was found that at low concentrations of tris buffer, F-PAH solubility was limited, with extensive heating and ultrasonication required to dissolve the polymer, albeit incompletely. Only high concentrations of tris buffer (1 M and above) resulted in adequate dissolution of both polymers without additional energy input. This is likely a result of the higher ionic strength of the solution, which is known to increase the solubility of a secondary electrolyte.[64, 65] Studies have also shown that the ionic strength of the solution can have an impact on the ability of polymers to adsorb to a surface in LBL encapsulation.[66] For example, it has been demonstrated that sodium chloride increases the amount of chitosan, a polysaccharide, adsorbed onto the surface of a film in a chitosan/PSS LBL synthesis.[66] Furthermore, layer permeability is impacted by the ionic strength of the solution, with layer permeability decreasing as ionic strength is increased.[67] Thus, the use of tris buffer may be beneficial for the LBL encapsulation beyond the increased solubility of the polyelectrolytes.

Typically, it is undesirable to expose enzymes to high tris buffer concentrations as it can be detrimental to enzymatic activity, with 1 M tris buffer known to decrease the activity of certain enzymes by up to 90%.[68, 69] However, control studies indicated that catalase was not significantly impacted by 5-hour exposure to 1 M tris buffer (**Figure S3.10**), and so this buffer was able to be used for the LBL encapsulation of catalase-on-HOF composites.

The 1 M tris buffered system provided the most promising results for the LBL encapsulation of all solvent systems tested. CLSM showed a uniform coat F-PAH on the surface of catalase-on-HOF samples (**Figure 3.34**), whilst the polyelectrolyte coating can also be seen by SEM (**Figure 3.35**). Linking of individual catalase-on-BioHOF-1 crystals by the polymer is evident, with the extent of clustering increasing as the number of layers

is increased. This may be because the HOF does not disperse as readily in water when compared to the MeOH/water mixtures, and thus tends to cluster during the LBL process. This was not as prevalent in the samples analyzed by CLSM, and so some of this clustering may also be a result of the drying process. Compared to the LBL process in other solvent systems, less free polymer aggregates are present. This may stem from the improved solubility of the polyelectrolytes in tris buffer, or increased adsorption to the surface of the HOF in a mixture with higher ionic strength. Importantly, PXRD indicated that the product remained crystalline and thus the buffer and encapsulation procedure did not break down the HOF (**Figure 3.36**). Due to material availability constraints, a small amount of sample was loaded for PXRD, hence the peaks in the PXRD have relatively low intensity.

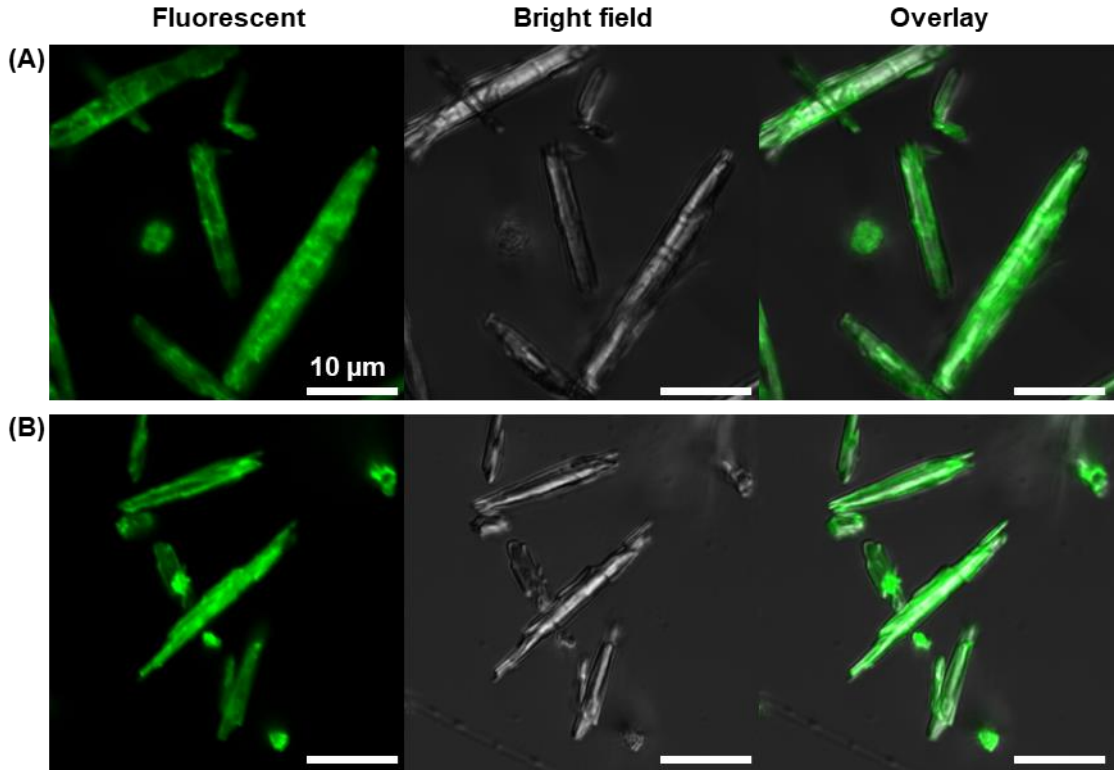

Figure 3.34: CLSM overlay image of catalase-on-BioHOF-1 coated with (a) 4 and (b) 8 layers of alternating poly(styrene sulfonate) and FITC-tagged poly(allylamine), synthesized in 1 M tris buffer. Samples were analyzed as a suspension in water. Uniform fluorescence around the outside of the material indicates a homogenous coating of F-PAA on the surface of the material.

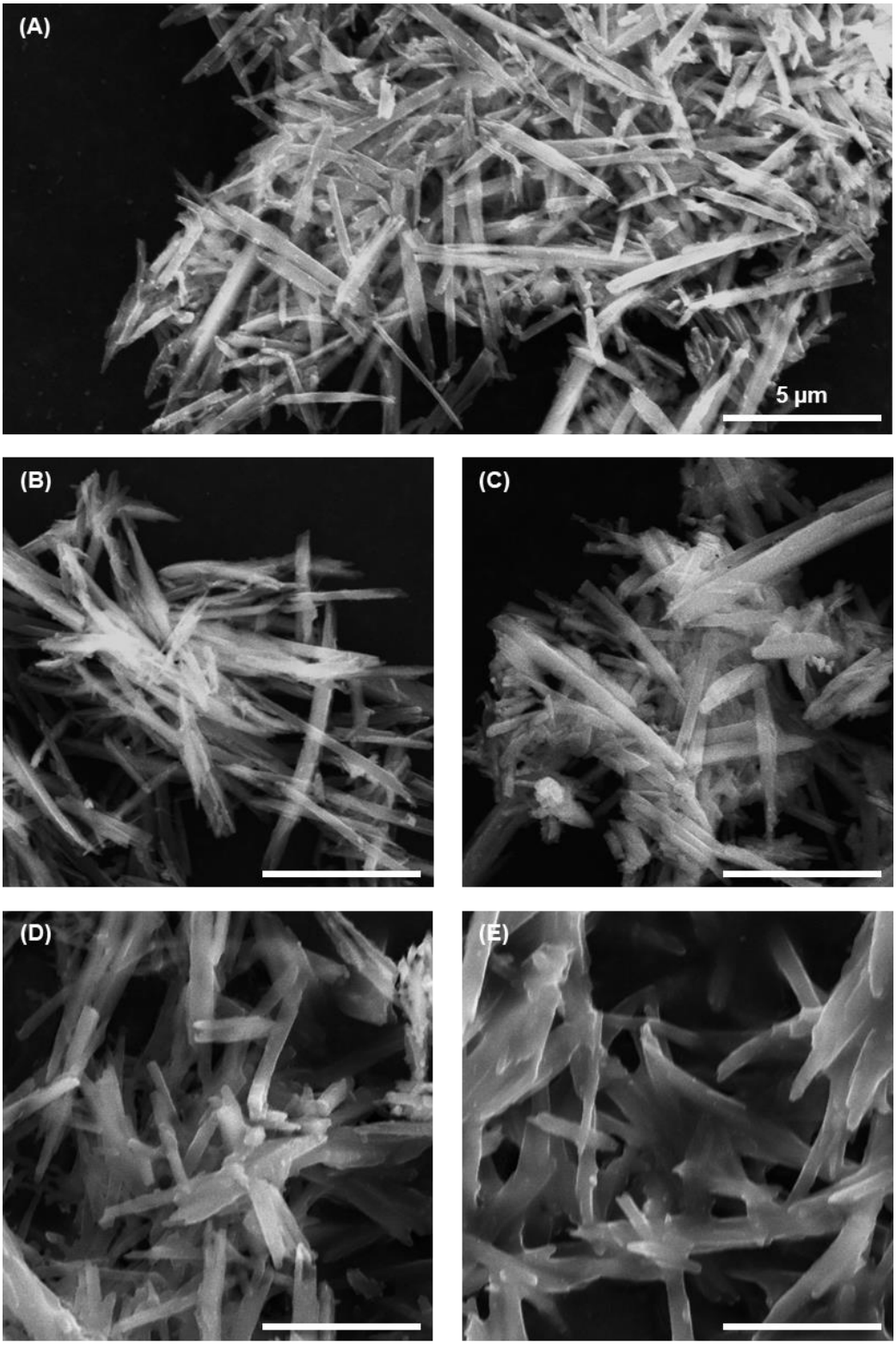

Figure 3.35: SEM images of BioHOF-1 coated with (**A**) 0, (**B**) 2, (**C**) 4, (**D**) 6, and (**E**) 8 layers of alternating poly(styrene sulfonate) and FITC-tagged poly(allylamine), synthesized in 1 M tris buffer. Samples were dried under vacuum prior to analysis. As more layers are added, the crystals adopt a more softened appearance and cluster together with a shared polymer coat.

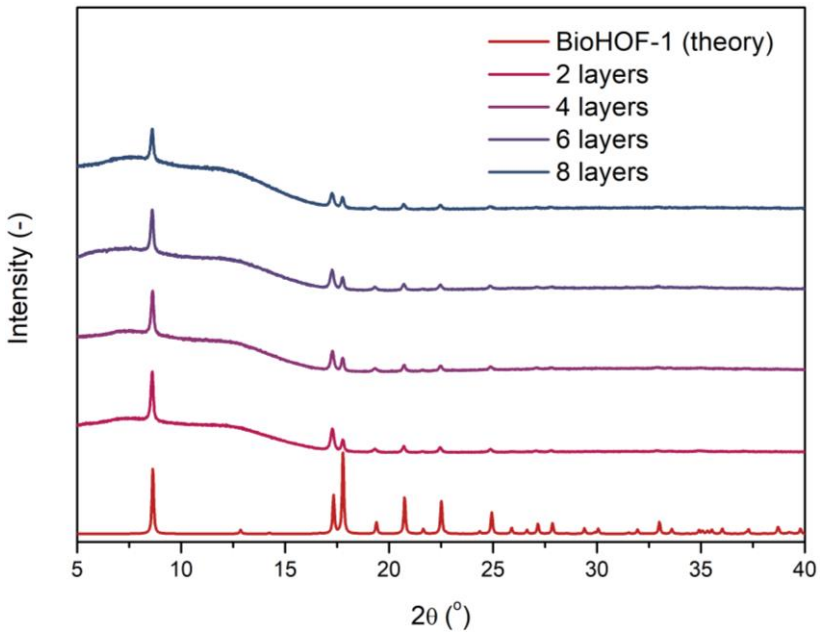

Figure 3.36: PXRD of catalase-on-BioHOF-1 after layer-by-layer encapsulation in alternating layers of PSS and F-PAH, synthesized in 1 M tris buffer. Samples were suspended in ethanol and air dried prior to analysis. Low peak height relative to the baseline is likely a result of the limited amount of material available for analysis, in addition to contribution to the baseline by the amorphous polymer.

To ensure that the LBL coating was not having a detrimental effect on the protein, the catalytic activity of the surface-bound catalase was assessed under ambient conditions. For a pure catalase-on-HOF sample, the activity was significantly lower than would be expected compared to free catalase. Lower activity on the surface of the HOF could be a result of several factors, including partial unfolding of catalase upon adsorption on the HOF surface, exposure to free acidic/basic HOF linkers in solution, and gradual loss of catalase from the surface of the framework. As such, all LBL samples were compared to as-synthesized catalase-on-BioHOF-1 instead of free catalase.

Samples with a 2-layer coating of polymer appeared to have a higher activity than the pure catalase@BioHOF-1 from which they were prepared (**Figure 3.37**). Initially, it was thought that this could result from a loss of catalase from the surface of the HOF, which is instead retained with a thin LBL coat. However, BCA data of the supernatant and pellet of catalase-on-BioHOF-1 after 7 days storage indicated that only approximately 9-13% of the originally adsorbed protein returned to the supernatant, which does not account for the 41% decrease in activity between the 2- and 0-layer samples. The discrepancy in activity of the samples was thus reasoned to be due to slight

variation in the storage conditions for the composites, as the LBL samples were stored in 50 mM tris buffer whilst the pure catalase-on-BioHOF-1 samples were stored in ultrapure water. This indicates that the slight acidity/basicity of the HOF linkers could be detrimental to enzymes encapsulated in BioHOF-1, and that in the future storage and/or synthesis in tris buffer may be desirable.

Besides the discrepancy between the activities of the 0- and 2-layer samples, for all other samples the activity decreased as the number of polyelectrolyte layers was increased. This decreasing activity could be due to a combination of increasing diffusion limitations, removal of loosely bound enzyme, and loss of material in washing steps as each layer is added. Loss of material is likely the most significant factor contributing to the activity loss, as even with extensive centrifugation a small portion of the HOF does not settle and so is removed in subsequent washing steps. Refinement of the washing procedure could thus be used to obtain composites with higher activity in the future.

With the LBL polyelectrolyte encapsulation and activity testing successful, the effectiveness of the LBL coat at providing increased protection from harsh conditions was assessed. Samples were digested with trypsin, a proteolytic enzyme, and the activity retention determined for each sample (**Figure 3.37**, **Figure 3.38**). For the 0- and 2-layer samples, activity retention was minimal, indicating that the surface-bound catalase was accessible to trypsin. However, as the number of layers was further increased, activity retention increased, with the 6- and 8-layer samples reporting 94 and 100% retention, respectively. Notably, the activity of these samples was significantly higher than both catalase and catalase-on-BioHOF-1 after trypsin digestion. A 6-layer coat provided the optimal combination of properties for enzyme protection applications. This sample retained most of its activity following trypsin digestion, suggesting that only a small proportion of catalase was accessible by proteases, whilst addition of further layers resulted in marginal gains in protection for the activity lost. Additionally, the clustering and co-encapsulation of multiple HOF crystals is less prevalent for the 6-layer sample compared to an 8-layer sample, ensuring that maximum surface area is maintained for optimal catalytic performance. Though overall the activity of this sample was far below what would ultimately be desired, optimization of the system had not been performed, and thus enhanced activity could be achieved with further studies.

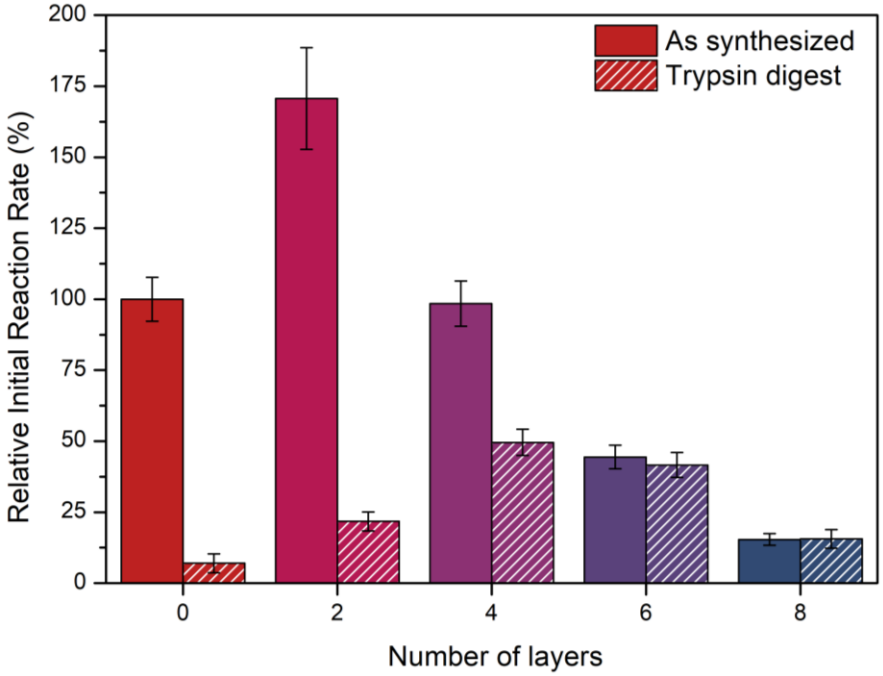

Figure 3.37: Relative initial reaction rates of catalase-on-HOF samples coated with varying amounts of alternating PSS and F-PAH in 1 M tris buffer, before and after trypsin digestion. The enzyme concentration in the reaction was 500 nM. Samples are normalized relative to uncoated catalase-on-BioHOF-1. Error bars represent the standard error in the slope of the linear regression of **Figure S3.11** from which the relative initial reaction rate was derived. As more layers are added, the activity of the composite decreases, however the activity after Trypsin digestion is enhanced.

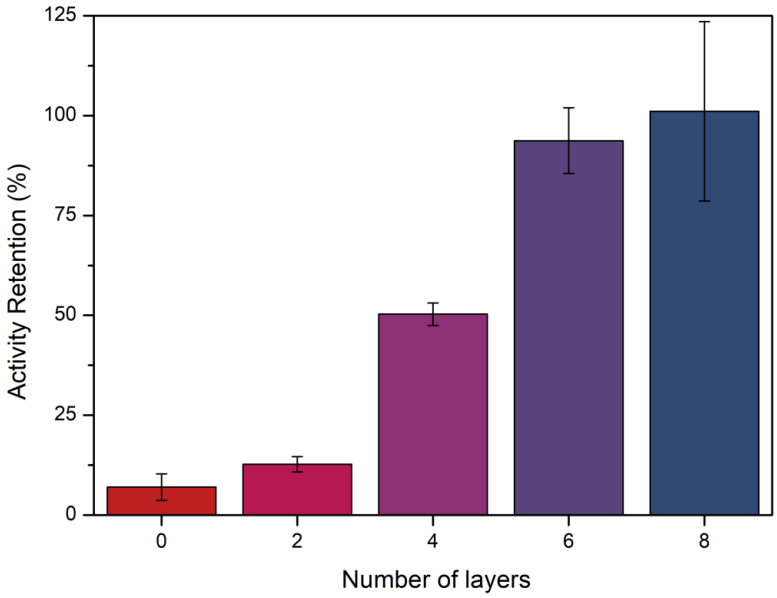

Figure 3.38: Retention of activity of catalase-on-HOF samples coated with varying amounts of alternating PSS and F-PAH in 1 M tris buffer, after digestion with trypsin.

The enzyme concentration in the reaction was 500 nM. Error bars represent the standard error in the activity retention of the sample. As more layers are added, greater protection is provided from Trypsin digestion.

Due to time constraints, further studies on the LBL encapsulation of catalase-on-BioHOF-1 samples could not be performed. However, the results thus far were promising and could yield highly active enzyme-on-BioHOF-1@PSS/PAH composites with further optimization and testing. There is a clear path forward regarding additional variables that could be investigated to improve the activity of these composites, in particular the storage and washing conditions, which had a detrimental impact on enzymatic activity. These variables, along with other future directions for this work, are discussed in the following chapter.

3.6.5 Summary

In this section of the project, the layer-by-layer encapsulation of BioHOF-1 in a polyelectrolyte multilayer was achieved, which we believe to be the first example of LBL encapsulation of a hydrogen-bonded organic framework. Thick polyelectrolyte coatings were initially formed by sequential deposition of poly(styrene sulfonate) and FITC-tagged poly(allylamine) in various water/methanol mixtures, however these conditions were detrimental to surface-bound protein. 1 M tris buffer was then trialled for the LBL encapsulation. Coating of the sample with 6 or more layers of alternating PSS/F-PAH was sufficient to protect >90% of the surface-bound catalase from protease digestion, indicating that LBL encapsulation is effective at imparting protection to proteins immobilized on porous supports. Further testing and optimization of this system could yield high-activity layer-by-layer coated enzyme@HOF biocomposites with enhanced protection from harsh conditions.

3.7 Conclusions

Various methods were trialed to increase the loading of protein in BioHOF-1. Modifying the protein surface chemistry showed minor impact on protein loading, suggesting a different mechanism of encapsulation compared to ZIF-8 and single-component HOFs. Sodium sulfate showed an inconsistent impact on loading depending on the identity of the protein, as it did not slow the framework growth as intended, and instead impacted loading by preventing the aggregation of certain proteins with the BioHOF-1 precursors. Meanwhile, pre-incubation of the protein with guanidinium-modified poly(ethyleneimine) had some impact on protein loading, however the loading values were far below what has been reported for single-component HOFs. In all cases, a significant amount of protein was adsorbed to the surface of BioHOF-1 prior to SDS washing. To provide additional protection to this surface-bound protein, layer-by-layer polyelectrolyte encapsulation was investigated, however significant activity loss was observed as the number of layers was increased. Further optimization of this layer-by-layer system could provide more promising results.

3.8 Experimental

3.8.1 Materials & characterization

Materials

All materials were purchased from Merck unless otherwise stated. Catalase from bovine liver (C9322) was purchased from Sigma Aldrich as a Lyophilized powder and the concentration of solutions of catalase assessed by measuring the UV/vis absorbance at 280 nm. Bovine serum albumen (BSA, A6003) was used as received and 100% purity was assumed. 4,4',4",4"'-methanetetrayltetrabenzoic acid (A1083829) was purchased from AmBeed and converted to its sodium salt prior to usage. 4,4',4",4"'-methanetetrayltetrabenzimidamide hydrochloride (A1193206) was purchased from AmBeed and used as received. Ultrapure Milli-Q water with resistivity of >18 MΩ cm-1 (Merck Millipore purification system) was used for all syntheses, wash protocols and buffer preparations.

Powder x-ray diffraction (PXRD)

PXRD data of dry samples were collected on a Bruker D4 Endeavor x-ray diffractometer. A Co anode was used to produce K_α radiation (λ = 1.78897 Å). Flat plate diffraction data was collected over the range $2\theta = 5-40°$. THE PXRD data were converted by PowDLL converter (version 2.97.0.0) and presented as the Cu-source irradiated patterns (λ = 1.54056 Å).

Transmission electron microscopy (TEM)

TEM images were collected on a Philips CM200 Transmission Electron Microscope. Samples were dispersed in ethanol and drop-cast onto 3 mm TEM grids prior to analysis.

Scanning electron microscopy (SEM)

SEM images were collected on a FEI Quanta 450 FEG Environmental Scanning Electron Microscope (ESEM), operating at 10.0 kV with a spot size of 3.0, and under ultrahigh vacuum (10 7 – 10-12 hPa) conditions. Samples were dried and loaded onto 12 mm carbon tabs on aluminium stages and sputter-coated with carbon prior to analysis.

Confocal laser scanning microscopy (CLSM)

CLSM images were collected on an Olympus FV3000 Confocal Microscope. The samples were suspended in water on a multi-well plate. Samples were excited at 488 nm and the fluorescence signal was collected in a window from 495 to 545 nm.

Dynamic light scattering (DLS) & zeta potential measurements

DLS and zeta potential measurements were taken on a Malvern Zetasizer Nano ZSP dynamic light scattering instrument. Data were analyzed using Malvern Zetasizer software (version 8.01.4906).

Dynamic light scattering of proteins was performed using 12 mm polystyrene cuvettes. Proteins were dissolved to a concentration of ~1 mg/mL in 1 x PBS and passed through a 0.2 µm syringe filter prior to analysis. Measurements were performed in triplicate, with each measurement consisting of 15 runs of 10 s each, with a 120 s prior incubation period. The following measurement parameters were used: Temperature = 25.0 ^{o}C, material RI = 1.450, dispersant RI = 1.332, dispersant viscosity = 0.9082 cP.

Zeta potentials of proteins were obtained using folded capillary zeta cells (DTS1070). Proteins were dissolved to a concentration of ~1 mg/mL in 10 mM KCl and passed through a 0.2 µm syringe filter prior to analysis. Measurements were performed in triplicate, with each measurement consisting of 30 runs with a 120 s prior incubation period. The following measurement parameters were used: Temperature = 25.0 ^{o}C, material RI = 1.450, dispersant RI = 1.330, dispersant viscosity = 0.8854 cP, dispersant dielectric constant = 78.5, f(Ka) = 1.5 (Smoluchowski approximation).

UV/visible spectroscopy

UV/vis spectroscopy data were collected on a Shimadzu UV-3600 Plus spectrophotometer. UV/vis absorption measurements for the purposes of assays or transmittance studies were performed in polystyrene cuvettes, whilst UV/vis absorption measurements of pure proteins were performed in quartz cuvettes. The wavelength of the incident light varied by experiment and is specified in the text.

3.8.2 Protein encapsulation and loading quantification

Pure BioHOF-1 preparation

For synthesis of the pure BioHOF-1 framework, sodium 4,4',4",4"'-methanetetrayltetrabenzoate (3 mg, 0.005 mmol) in water (1 mL) was added to 4,4',4",4"'-methanetetrayltetrabenzimidamide hydrochloride (4 mg, 0.006 mmol) in water (1 mL). The mixture was left undisturbed overnight then washed as described further below.

Protein@BioHOF-1 composite preparation

For encapsulation of protein in BioHOF-1, sodium 4,4',4",4"'-methanetetrayltetrabenzoate (3 mg, 0.005 mmol) in water (1 mL) was added to 4,4',4",4"'-methanetetrayltetrabenzimidamide hydrochloride (4 mg, 0.006 mmol) with protein (2 mg) in water (1 mL). The mixture was left undisturbed overnight then washed as described further below.

Protein-on-HOF preparation

Protein-on-HOF samples were prepared by stirring a 2.5 mg/mL HOF suspension (2 mL) with 1 mg/mL protein for 2 hours. The samples were washed as described further below.

Washing procedures

The washing procedure used for HOF samples varied by experiment. In a typical washing step, the solid was suspended in the wash solution and then isolated by centrifugation at 16000 g for 5 minutes, and the supernatant removed. The sequence of washes depending on the future use of the sample was as follows:

Activity studies – The solid was washed with water (3 x 1 mL) and stored at 4 °C as an aqueous suspension.

Loading – The solid was washed with water (2 x 1 mL) and ethanol (1 mL), and dried under vacuum overnight.

SDS washed loading – The solid was washed with water (2 x 1 mL) and ethanol (1 mL). The sample was then washed with 10% aqueous SDS (1 mL) by gentle shaking for 5 minutes. Following the SDS wash, the sample was washed further with water (2 x 1 mL) and ethanol (1 mL), and dried under vacuum overnight.

Protein loading quantification

A BCA assay was used to quantify the loading of protein in/on the HOF. The HOF was suspended to 2.4 mg/mL in DMSO and subject to ultrasonication for 5 minutes. 75 µL of this suspension was added to 0.1 M NaOH (75 µL) and dissolved by ultrasonication. Water (600 µL) was used to make the sample up to a final volume of 750 uL. BCA reagent (750 uL, prepared as per standard Sigma-Aldrich protocol[15]) was then added to the sample, and the sample briefly shaken. After incubation at room temperature overnight, the absorbance at 562 nm was compared to a calibration curve of identically prepared protein samples of known concentration. For each assay, a sample of pure HOF was also analyzed, and used to account for absorbance caused by the HOF in protein@HOF samples. All samples, including the calibration curve and pure digested HOF, were prepared on the same day to minimize the impact of minor variations in the incubation conditions.

3.8.3 Surface modification of ferritin

Amination reaction

An aqueous EDA solution (2 M, 2 mL, 4.01 mmol) was prepared and adjusted to pH 4.5 using 6 M HCl. Ferritin (20 mg) was then added followed by EDC.HCl (7.2 mg, 0.038 mmol), and the solution stirred on ice for 120 minutes. The aminated protein was then washed with phosphate buffered saline (1x, pH 7.4) and twice with water by centrifugation through a 10 kDa filter. The concentration of protein was determined by BCA assay, with incubation at 37 °C for 2 hours. The aminated protein was stored as an aqueous solution at 4 °C.

Succinylation reaction

Ferritin (20 mg) was dissolved in phosphate buffered saline (1x, pH 8, 4 mL) with stirring. A 50-fold molar excess of succinic anhydride, relative to the number of lysine residues on the protein, was added in small increments over 1 hour. The pH was regularly adjusted back to 8 using 2 M NaOH. After the succinic anhydride was added, the solution was stirred for a further hour. The succinylated protein was then washed with phosphate buffered saline (1x, pH 7.4) and twice with water by centrifugation through a 10 kDa filter. The concentration of protein was determined by BCA assay, with incubation at 37 °C for 2 hours. The succinylated protein was stored as an aqueous solution at 4 °C.

3.8.4 Modulator studies

Time-course UV/vis transmittance studies of BioHOF-1 formation

4,4',4",4"'-methanetetrayltetrabenzimidamide hydrochloride (4 mg, 0.006 mmol) was dissolved in water (1 mL), and the spectrophotometer blanked using this solution. Using a syringe and needle, sodium 4,4',4",4"'-methanetetrayltetrabenzoate (3 mg, 0.005 mmol) in water (1 mL) was added, and the absorbance at 700 nm monitored for 5 minutes, with 0.1 second data collection intervals.

Protein@BioHOF-1 synthesis in the presence of sodium sulfate

Sodium 4,4',4",4"'-methanetetrayltetrabenzoate (3 mg, 0.005 mmol) and sodium sulfate (varying equivalents, relative to amount of tetra-amidinium) were dissolved in water (1 mL). This solution was then added to 4,4',4",4"'-methanetetrayltetrabenzimidamide hydrochloride (4 mg, 0.006 mmol) with protein (2 mg) in water (1 mL). The mixture was left undisturbed overnight then washed as previously described for loading studies.

Aggregation studies with tetra-amidinium, protein, and sodium sulfate

4,4',4",4"'-methanetetrayltetrabenzimidamide hydrochloride (4 mg, 0.006 mmol) was dissolved in water (1 mL), and analyzed by DLS. Ferritin or F-BSA (1 mg) was then added, and the DLS size distribution remeasured. This was repeated for a sample containing sodium sulfate (17 mg, 0.12 mmol) together with the tetra-amidinium.

3.8.5 Functionalized polymer synthesis and interaction studies

Polymer guanylation (synthesized and reported by Dr. Adrian Markwell-Heys)

1H-Pyrazole-1-carboxamidine hydrochloride (5 g, 68.22 mmol) was taken up in MeOH (25 mL) and Et_3N (10 mL) was added in one portion and stirred for 5 mins. PEI (Mw ≈ 600-800 Da, 4 mL) was added in one portion. The resulting mixture was stirred for 24 hours at room temperature, and the solvent was removed under reduced pressure. The resulting crude gum was redissolved in MeOH (10 mL), followed by addition of i-PrOH (30 mL) which led to separation of the organic phase, leading to formation of a

gum at the bottom of the flask. The solvent was decanted, and this solvent washing process was repeated 4 times followed by drying under vacuum overnight. The dried polymer was obtained as a white solid. This solid was dissolved in water to approximately 50-100 mg/mL, and the pH adjusted to 7.

Aggregation studies of G-PEI with ferritin

1.5 mL of various concentrations of guanylated poly(ethyleneimine) were prepared (0.02, 0.1, 0.125, 0.15, 0.2, 0.25, 0.5 mg/mL). To each solution, ferritin (1.5 mg) was added and stirred for 30 minutes. All samples were analyzed by DLS.

Ferritin@BioHOF-1 synthesis in the presence of G-PEI

Ferritin (2 mg) was added to G-PEI (0.5 mg) dissolved in water (1 mL) and stirred for 30 minutes. 4,4',4'',4'''-methanetetrayltetrabenzimidamide hydrochloride (4 mg, 0.006 mmol) was then added, followed by sodium 4,4',4'',4'''-methanetetrayltetrabenzoate (3 mg, 0.005 mmol) in water (1 mL). This was repeated with reversed order of addition of the tetra-amidinium and tetra-carboxylate linkers. Both samples were left undisturbed overnight then washed as previously described for loading studies.

3.8.6 Layer-by-layer HOF encapsulation

FITC tagging of poly(allylamine hydrochloride)

Poly(allylamine hydrochloride) (100 mg, MW 50 kDa) was dissolved in water (48 mL). A small amount of polymer remained as a suspension. Fluorescein isothiocyanate (4 mg, 0.01 mmol) in DMSO (2 mL) was added, and the sample shaken briefly. The sample was left for 24 hours at 4 °C, during which time the remaining suspended polymer dissolved. The sample was purified by dialysis against water for 24 hours, and freeze dried for 16 hours to afford FITC-tagged poly(allylamine hydrochloride) as a lightweight, orange solid.

Dialysis of poly(sodium 4-styrene sulfonate)

All poly(sodium 4-styrene sulfonate) for layer-by-layer encapsulation was dialyzed prior to use. PSS (100 mg) was dissolved in water (50 mL), and then dialyzed against water for 24 hours. The sample was freeze dried for 72 hours to yield poly(sodium 4-styrene sulfonate) as a lightweight, colorless solid.

Layer-by-layer encapsulation in water

Prior to layer-by-layer encapsulation, stock solutions of F-PAH (MW 50 kDa) and PSS (MW 70 kDa) were prepared. Each polymer was finely ground, and then suspended in water to a concentration of 1 mg/mL. The solutions were stirred for several hours with intermittent mild heating and ultrasonication to assist dissolution, and were then passed through a 0.45 μm syringe filter. Stock solutions were stored at 4 °C.

For the layer-by-layer process, a suspension of BioHOF-1 (10 mg/mL, 250 μL) was prepared. Aqueous PSS solution (1 mg/mL, 250 μL) was added, and the sample gently agitated for 15 minutes. The sample was washed with water (3 × 250 μL) by repeated centrifugation (16000 g, 5 minutes) and resuspension, and then redispersed in water (250 μL). Aqueous PAH solution (1 mg/mL, 250 μL) was then added and gently agitated for 15 minutes. The sample was washed with water (3 × 250 μL), and then redispersed in water (250 μL). This process was repeated until the desired number of layers were added. The product was stored as a 2.5 mg/mL suspension in water at 4 °C.

Layer-by-layer encapsulation in methanol

Prior to layer-by-layer encapsulation, stock solutions of F-PAH (MW 50 kDa) and PSS (MW 70 kDa) in methanol were prepared. Each polymer was finely ground, and then suspended in methanol to a concentration of 1 mg/mL. For the FITC-tagged poly(allylamine hydrochloride) suspension, Amberlyst A26 hydroxide form was added. For the poly(sodium 4-styrene sulfonate) suspension, Amberlite IR-120 H-form was added. Each sample was stirred for 2 hours, or until the polymer was completely dissolved. The solutions were then separated from the ion exchange resin and passed through a 0.45 μm syringe filter. Stock solutions were stored at 4 °C.

For the layer-by-layer process, a suspension of BioHOF-1 (10 mg/mL, 250 μL) in methanol was prepared. PSS in methanol (1 mg/mL, 250 μL) was added, and the sample gently agitated for 15 minutes. The sample was washed with methanol (3 × 250 μL) by repeated centrifugation (16000 g, 5 minutes) and resuspension, and then redispersed in methanol (250 μL). PAH in methanol (1 mg/mL, 250 μL) was then added and gently agitated for 15 minutes. The sample was washed with methanol (3 × 250 μL), and then redispersed in methanol (250 μL). This process was repeated until the desired number of layers were added. The product was stored as a 2.5 mg/mL suspension in water at 4 °C.

Layer-by-layer encapsulation in methanol/water mixtures

For the encapsulation in 25, 50, and 75% MeOH, the polymer stock solutions were prepared as follows. Each polymer was finely ground, and then suspended in methanol to a concentration of 1 mg/mL. For the FITC-tagged poly(allylamine hydrochloride) suspension, Amberlyst A26 hydroxide form was added. For the poly(sodium 4-styrene sulfonate) suspension, Amberlite IR-120 H-form was added. Each sample was stirred for 2 hours, or until the polymer was completely dissolved. The solutions were then separated from the ion exchange resin and passed through a 0.45 µm syringe filter. Methanol was then evaporated under blowing nitrogen until the concentration of the solution was 4 mg/mL. Each stock solution was then diluted with water/MeOH to obtain the desired percentage of methanol. Stock solutions were stored at 4 °C.

For the encapsulation in 10% MeOH, the polymer stock solutions were prepared as follows. Each polymer was finely ground, and then suspended in methanol to a concentration of 10 mg/mL. The samples were stirred for an hour, followed by the addition of water for a final polymer concentration of 1 mg/mL, with stirring for a further 30 minutes. For the FITC-tagged poly(allylamine hydrochloride) suspension, Amberlyst A26 hydroxide form was added. For the poly(sodium 4-styrene sulfonate) suspension, Amberlite IR-120 H-form was added. Each sample was stirred for 2 hours, or until the polymer was completely dissolved. The solutions were then separated from the ion exchange resin and passed through a 0.45 µm syringe filter. Stock solutions were stored at 4 °C.

For the layer-by-layer process, a suspension of BioHOF-1 or catalase-on-BioHOF-1 (10 mg/mL, 250 µL) in each water/MeOH mixture was prepared. PSS in water/MeOH (1 mg/mL, 250 µL) was added, and the sample gently agitated for 15 minutes. The sample was washed with water/MeOH (3 × 250 µL) by repeated centrifugation (16000 g, 5 minutes) and resuspension, and then redispersed in methanol (250 µL). PAH in water/MeOH (1 mg/mL, 250 µL) was then added and gently agitated for 15 minutes. The sample was washed with water/MeOH (3 × 250 µL), and then redispersed in water/MeOH (250 µL). This process was repeated until the desired number of layers were added. The product was stored as a 2.5 mg/mL suspension in water at 4 °C. NOTE: For the 1-layer sample synthesized in 10% MeOH, F-PAH was used as the

sole polymer instead of PSS. This was to allow the visualization of this sample by CLSM. All other samples were prepared by addition of PSS first.

Catalytic testing of catalase

The Ferrous Oxidation in Xylenol orange (FOX) assay was used to assess the activity of catalase-containing samples. The FOX reagent is composed of 100 mM sorbitol, 25 mM H_2SO_4, 250 µM ammonium ferrous sulfate, and 100 µM xylenol orange.

In activity testing, catalase, catalase-on-HOF, or LBL catalase-on-HOF were stirred in tris buffer (0.05 M, pH 7.4, 500 µL), followed by the addition of hydrogen peroxide (160 µM, 500 µL). The catalase concentration in the enzymatic reaction varied by experiment and is specified in the text. At defined time intervals, 50 µL samples of the reaction mixture were taken and mixed with 950 µL of FOX reagent. After incubation for at least 30 minutes at room temperature, the UV/vis absorbance at 585 nm was recorded to assess the breakdown of hydrogen peroxide by catalase.

Layer-by-layer encapsulation in 1 M tris buffer

Prior to layer-by-layer encapsulation, stock solutions of F-PAH (MW 50 kDa) and PSS (MW 70 kDa) were prepared. Each polymer was finely ground, and then suspended in tris buffer (1 M, pH 7.4) to a concentration of 1 mg/mL. The solutions were stirred for 2 hours until dissolved, and were then passed through a 0.45 µm syringe filter. Stock solutions were stored at 4 °C.

For the layer-by-layer process, a suspension of BioHOF-1 or catalase-on-BioHOF-1 (10 mg/mL, 250 µL) was prepared. PSS in 1 M tris (1 mg/mL, 250 µL) was added, and the sample gently agitated for 15 minutes. The sample was washed with 1 M tris (3 × 250 µL) by repeated centrifugation (16000 g, 5 minutes) and resuspension, and then redispersed in 1 M tris (250 µL). PAH in 1 M tris (1 mg/mL, 250 µL) was then added and gently agitated for 15 minutes. The sample was washed with 1 M tris (3 × 250 µL), and then redispersed in 1 M tris (250 µL). This process was repeated until the desired number of layers were added. The product was stored as a 2.5 mg/mL suspension in 50 mM tris at 4 °C.

3.9 References

1. Liang, W.; Carraro, F.; Solomon, M. B.; Bell, S. G.; Amenitsch, H.; Sumby, C. J.; White, N. G.; Falcaro, P.; Doonan, C. J. Enzyme encapsulation in a porous hydrogen-bonded organic framework. *Journal of the American Chemical Society* **2019**, *141* (36), 14298-14305. DOI: 10.1021/jacs.9b06589.

2. Liang, K.; Ricco, R.; Doherty, C. M.; Styles, M. J.; Bell, S.; Kirby, N.; Mudie, S.; Haylock, D.; Hill, A. J.; Doonan, C. J.; et al. Biomimetic mineralization of metal-organic frameworks as protective coatings for biomacromolecules. *Nature Communications* **2015**, *6* (1), 7240. DOI: 10.1038/ncomms8240.

3. Liang, W.; Xu, H.; Carraro, F.; Maddigan, N. K.; Li, Q.; Bell, S. G.; Huang, D. M.; Tarzia, A.; Solomon, M. B.; Amenitsch, H.; et al. Enhanced activity of enzymes encapsulated in hydrophilic metal–organic frameworks. *Journal of the American Chemical Society* **2019**, *141* (6), 2348-2355. DOI: 10.1021/jacs.8b10302.

4. Chen, G.; Huang, S.; Shen, Y.; Kou, X.; Ma, X.; Huang, S.; Tong, Q.; Ma, K.; Chen, W.; Wang, P.; et al. Protein-directed, hydrogen-bonded biohybrid framework. *Chem* **2021**. DOI: 10.1016/j.chempr.2021.07.003.

5. Du, Y.; Gao, J.; Liu, H.; Zhou, L.; Ma, L.; He, Y.; Huang, Z.; Jiang, Y. Enzyme@silica nanoflower@metal-organic framework hybrids: A novel type of integrated nanobiocatalysts with improved stability. *Nano Research* **2018**, *11* (8), 4380-4389. DOI: 10.1007/s12274-018-2027-7.

6. Wu, X.; Ge, J.; Yang, C.; Hou, M.; Liu, Z. Facile synthesis of multiple enzyme-containing metal–organic frameworks in a biomolecule-friendly environment. *Chemical Communications* **2015**, *51* (69), 13408-13411. DOI: 10.1039/C5CC05136C.

7. Tang, J.; Liu, J.; Zheng, Q.; Li, W.; Sheng, J.; Mao, L.; Wang, M. In-situ encapsulation of protein into nanoscale hydrogen-bonded organic frameworks for intracellular biocatalysis. *Angewandte Chemie International Edition* **2021**, *60* (41), 22315-22321. DOI: 10.1002/anie.202105634.

8. Chen, G.; Kou, X.; Huang, S.; Tong, L.; Shen, Y.; Zhu, W.; Zhu, F.; Ouyang, G. Modulating the biofunctionality of metal–organic-framework-encapsulated enzymes through controllable embedding patterns. *Angewandte Chemie International Edition* **2020**, *59* (7), 2867-2874. DOI: 10.1002/anie.201913231.

9. Piludu, M.; Medda, L.; Monduzzi, M.; Salis, A. Gold nanoparticles: A powerful tool to visualize proteins on ordered mesoporous silica and for the realization of

theranostic nanobioconjugates. *International Journal of Molecular Sciences* **2018**, *19* (7). DOI: 10.3390/ijms19071991.

10. Xie, J.; Zheng, Y.; Ying, J. Y. Protein-directed synthesis of highly fluorescent gold nanoclusters. *Journal of the American Chemical Society* **2009**, *131* (3), 888-889. DOI: 10.1021/ja806804u.

11. Biter, A. B.; Pollet, J.; Chen, W.-H.; Strych, U.; Hotez, P. J.; Bottazzi, M. E. A method to probe protein structure from UV absorbance spectra. *Analytical Biochemistry* **2019**, *587*, 113450. DOI: 10.1016/j.ab.2019.113450.

12. Bradford, M. M. A rapid and sensitive method for the quantitation of microgram quantities of protein utilizing the principle of protein-dye binding. *Analytical Biochemistry* **1976**, *72* (1), 248-254. DOI: 10.1016/0003-2697(76)90527-3.

13. Sjöback, R.; Nygren, J.; Kubista, M. Absorption and fluorescence properties of fluorescein. *Spectrochimica Acta Part A: Molecular and Biomolecular Spectroscopy* **1995**, *51* (6), L7-L21. DOI: 10.1016/0584-8539(95)01421-P.

14. Klonis, N.; Clayton, A. H.; Voss, E. W., Jr.; Sawyer, W. H. Spectral properties of fluorescein in solvent-water mixtures: applications as a probe of hydrogen bonding environments in biological systems. *Photochemistry and Photobiology* **1998**, *67* (5), 500-510.

15. Sigma Aldrich. *QuantiPro™ BCA Assay Kit*. Sigma Aldrich, 2022. https://www.sigmaaldrich.com/AU/en/product/sigma/qpbca (accessed 2023 January 6).

16. Olson, B. J. S. C.; Markwell, J. Assays for determination of protein concentration. *Current Protocols in Protein Science* **2007**, *48* (1), 3.4.1-3.4.29. DOI: 10.1002/0471140864.ps0304s48.

17. Smith, P. K.; Krohn, R. I.; Hermanson, G. T.; Mallia, A. K.; Gartner, F. H.; Provenzano, M. D.; Fujimoto, E. K.; Goeke, N. M.; Olson, B. J.; Klenk, D. C. Measurement of protein using bicinchoninic acid. *Analytical Biochemistry* **1985**, *150* (1), 76-85. DOI: 10.1016/0003-2697(85)90442-7.

18. Wied, P.; Carraro, F.; Bolivar, J. M.; Doonan, C. J.; Falcaro, P.; Nidetzky, B. Combining a genetically engineered oxidase with hydrogen-bonded organic frameworks (HOFs) for highly efficient biocomposites. *Angewandte Chemie International Edition* **2022**, *61* (16), e202117345. DOI: 10.1002/anie.202117345.

19. Crichton, R. R.; Eason, R.; Barclay, A.; Bryce, C. F. The subunit structure of horse spleen apoferritin; the molecular weight of the oligomer and its stability to

dissociation by dilution. *Biochemical Journal* **1973**, *131* (4), 855-857. DOI: 10.1042/bj1310855.

20. Ford, G. C.; Harrison, P. M.; Rice, D. W.; Smith, J. M. A.; Treffry, A.; White, J. L.; Yariv, J.; Miller, A.; Phillips, D. C.; Williams, R. J. P. Ferritin: design and formation of an iron-storage molecule. *Philosophical Transactions of the Royal Society of London. B, Biological Sciences* **1984**, *304* (1121), 551-565. DOI: doi:10.1098/rstb.1984.0046.

21. Naydenova, K.; Peet, M. J.; Russo, C. J. Multifunctional graphene supports for electron cryomicroscopy. *Proceedings of the National Academy of Sciences* **2019**, *116* (24), 11718-11724. DOI: doi:10.1073/pnas.1904766116.

22. Maddigan, N. K.; Tarzia, A.; Huang, D. M.; Sumby, C. J.; Bell, S. G.; Falcaro, P.; Doonan, C. J. Protein surface functionalisation as a general strategy for facilitating biomimetic mineralisation of ZIF-8. *Chemical Science* **2018**, *9* (18), 4217-4223. DOI: 10.1039/C8SC00825F.

23. Cai, K.; Frant, M.; Bossert, J.; Hildebrand, G.; Liefeith, K.; Jandt, K. D. Surface functionalized titanium thin films: Zeta-potential, protein adsorption and cell proliferation. *Colloids and Surfaces B: Biointerfaces* **2006**, *50* (1), 1-8. DOI: 10.1016/j.colsurfb.2006.03.016.

24. Helmick, H.; Hartanto, C.; Bhunia, A.; Liceaga, A.; Kokini, J. L. Validation of bioinformatic modeling for the zeta potential of vicilin, legumin, and commercial pea protein isolate. *Food Biophysics* **2021**, *16* (4), 474-483. DOI: 10.1007/s11483-021-09686-8.

25. Mazur, A.; Litt, I.; Shorr, E. Chemical properties of ferritin and their relation to its vasodepressor activity. *Journal of Biological Chemistry* **1950**, *187* (2), 473-484. DOI: 10.1016/S0021-9258(18)56191-3.

26. Expasy. *Compute pI/Mw tool*. Swiss Institute of Bioinformatics, 2023. https://web.expasy.org/compute_pi/ (accessed 2023 January 6).

27. Tang, Z.; Li, X.; Tong, L.; Yang, H.; Wu, J.; Zhang, X.; Song, T.; Huang, S.; Zhu, F.; Chen, G.; et al. A biocatalytic cascade in an ultrastable mesoporous hydrogen-bonded organic framework for point-of-care biosensing. *Angewandte Chemie International Edition* **2021**, *60* (44), 23608-23613. DOI: 10.1002/anie.202110351.

28. Chen, G.; Tong, L.; Huang, S.; Huang, S.; Zhu, F.; Ouyang, G. Hydrogen-bonded organic framework biomimetic entrapment allowing non-native biocatalytic activity in enzyme. *Nature Communications* **2022**, *13* (1), 4816. DOI: 10.1038/s41467-022-32454-2.

29. Muang-Non, P.; Toop, H. D.; Doonan, C. J.; White, N. G. Use of modulators and light to control crystallisation of a hydrogen bonded framework. *Chemical Communications* **2022**, *58* (2), 306-309. DOI: 10.1039/D1CC06164J.

30. Dong, G.; Ding, Y.; He, S.; Sheng, C. Molecular glues for targeted protein degradation: From serendipity to rational discovery. *Journal of Medicinal Chemistry* **2021**, *64* (15), 10606-10620. DOI: 10.1021/acs.jmedchem.1c00895.

31. Stanton, B. Z.; Chory, E. J.; Crabtree, G. R. Chemically induced proximity in biology and medicine. *Science* **2018**, *359* (6380), eaao5902. DOI: doi:10.1126/science.aao5902.

32. Mogaki, R.; Hashim, P. K.; Okuro, K.; Aida, T. Guanidinium-based "molecular glues" for modulation of biomolecular functions. *Chemical Society Reviews* **2017**, *46* (21), 6480-6491. DOI: 10.1039/C7CS00647K.

33. Okuro, K.; Kinbara, K.; Tsumoto, K.; Ishii, N.; Aida, T. Molecular glues carrying multiple guanidinium ion pendants via an oligoether spacer: Stabilization of microtubules against depolymerization. *Journal of the American Chemical Society* **2009**, *131* (5), 1626-1627. DOI: 10.1021/ja800491v.

34. Mogaki, R.; Okuro, K.; Ueki, R.; Sando, S.; Aida, T. Molecular glue that spatiotemporally turns on protein–protein interactions. *Journal of the American Chemical Society* **2019**, *141* (20), 8035-8040. DOI: 10.1021/jacs.9b02427.

35. Burgess, R. R. Use of polyethyleneimine in purification of DNA-binding proteins. *Methods in Enzymology* **1991**, *208*, 3-10. DOI: 10.1016/0076-6879(91)08003-z.

36. Marenchino, M.; Armbruster, D. W.; Hennig, M. Rapid and efficient purification of RNA-binding proteins: application to HIV-1 Rev. *Protein Expression and Purification* **2009**, *63* (2), 112-119. DOI: 10.1016/j.pep.2008.09.010.

37. Mazzaferro, L.; Breccia, J. D.; Andersson, M. M.; Hitzmann, B.; Hatti-Kaul, R. Polyethyleneimine–protein interactions and implications on protein stability. *International Journal of Biological Macromolecules* **2010**, *47* (1), 15-20. DOI: 10.1016/j.ijbiomac.2010.04.003.

38. Chen, W.; Walker, S.; John C, B. The mechanism of floc formation in protein precipitation by polyelectrolytes. *Chemical Engineering Science* **1992**, *47* (5), 1039-1045. DOI: 10.1016/0009-2509(92)80230-A.

39. Gregory, J. Flocculation by polymer and polyelectrolytes. *Solid/Liquid Dispersions* **1987**, 163-181.

40. Gupta, V.; Nath, S.; Chand, S. Estimation of proteins in the presence of polyethylenimine. *Biotechnology Letters* **2000**, *22* (11), 927-929. DOI: 10.1023/A:1005676531595.

41. Burgess, R. R. Chapter 20 Protein precipitation techniques. In *Methods in Enzymology*, Burgess, R. R., Deutscher, M. P. Eds.; Vol. 463; Academic Press, 2009; pp 331-342.

42. Yuan, S.; Zou, L.; Qin, J.-S.; Li, J.; Huang, L.; Feng, L.; Wang, X.; Bosch, M.; Alsalme, A.; Cagin, T.; et al. Construction of hierarchically porous metal–organic frameworks through linker labilization. *Nature Communications* **2017**, *8* (1), 15356. DOI: 10.1038/ncomms15356.

43. Chen, X.; Zhuang, Y.; Rampal, N.; Hewitt, R.; Divitini, G.; O'Keefe, C. A.; Liu, X.; Whitaker, D. J.; Wills, J. W.; Jugdaohsingh, R.; et al. Formulation of metal–organic framework-based drug carriers by controlled coordination of methoxy PEG phosphate: Boosting colloidal stability and redispersibility. *Journal of the American Chemical Society* **2021**, *143* (34), 13557-13572. DOI: 10.1021/jacs.1c03943.

44. Guo, C.; Liang, C.; Qin, X.; Gu, Y.; Gao, P.; Shao, M.; Wong, W.-t. Zeolitic imidazolate framework cores decorated with Pd nanoparticles and coated further with metal-organic framework shells (ZIF-8@Pd@MOF-74) as nanocatalysts for chemoselective hydrogenation reactions. *ACS Applied Nano Materials* **2020**, *3* (7), 7242-7251. DOI: 10.1021/acsanm.0c01566.

45. Panchariya, D. K.; Rai, R. K.; Anil Kumar, E.; Singh, S. K. Core-shell zeolitic imidazolate frameworks for enhanced hydrogen storage. *ACS Omega* **2018**, *3* (1), 167-175. DOI: 10.1021/acsomega.7b01693.

46. Pan, Y.; Sun, K.; Liu, S.; Cao, X.; Wu, K.; Cheong, W.-C.; Chen, Z.; Wang, Y.; Li, Y.; Liu, Y.; et al. Core-shell ZIF-8@ZIF-67-derived CoP nanoparticle-embedded N-doped carbon nanotube hollow polyhedron for efficient overall water splitting. *Journal of the American Chemical Society* **2018**, *140* (7), 2610-2618. DOI: 10.1021/jacs.7b12420.

47. Tu, Y.; Lei, C.; Deng, F.; Chen, Y.; Wang, Y.; Zhang, Z. Core-shell ZIF-8@polydopamine nanoparticles obtained by mitigating the polydopamine coating induced self-etching of MOFs: prototypical metal ion reservoirs for sticking to and killing bacteria. *New Journal of Chemistry* **2021**, *45* (19), 8701-8713. DOI: 10.1039/D1NJ00461A.

48. Beyer, S.; Schürmann, R.; Feldmann, I.; Blocki, A.; Bald, I.; Schneider, R. J.; Emmerling, F. Maintaining stable zeolitic imidazolate framework (ZIF) templates during polyelectrolyte multilayer coating. *Colloid and Interface Science Communications* **2018**, *22*, 14-17. DOI: 10.1016/j.colcom.2017.11.004.

49. Ejima, H.; Yanai, N.; Best, J. P.; Sindoro, M.; Granick, S.; Caruso, F. Near-incompressible faceted polymer microcapsules from metal-organic framework templates. *Advanced Materials* **2013**, *25* (40), 5767-5771. DOI: 10.1002/adma.201302442.

50. Liu, T.; Wang, Y.; Zhong, W.; Li, B.; Mequanint, K.; Luo, G.; Xing, M. Biomedical applications of layer-by-layer self-assembly for cell encapsulation: current status and future perspectives. *Advanced Healthcare Materials* **2019**, *8* (1), 1800939. DOI: 10.1002/adhm.201800939.

51. Li, W.; Lei, X.; Feng, H.; Li, B.; Kong, J.; Xing, M. Layer-by-layer cell encapsulation for drug delivery: The history, technique basis, and applications. *Pharmaceutics* **2022**, *14* (2). DOI: 10.3390/pharmaceutics14020297.

52. Franz, B.; Balkundi, S. S.; Dahl, C.; Lvov, Y. M.; Prange, A. Layer-by-layer nano-encapsulation of microbes: controlled cell surface modification and investigation of substrate uptake in bacteria. *Macromolecular Bioscience* **2010**, *10* (2), 164-172. DOI: 10.1002/mabi.200900142.

53. Van der Meeren, L.; Verduijn, J.; Li, J.; Verwee, E.; Krysko, D. V.; Parakhonskiy, B. V.; Skirtach, A. G. Encapsulation of cells in gold nanoparticle functionalized hybrid layer-by-layer (LbL) hybrid shells – remote effect of laser light. *Applied Surface Science Advances* **2021**, *5*, 100111. DOI: 10.1016/j.apsadv.2021.100111.

54. Caruso, F.; Trau, D.; Möhwald, H.; Renneberg, R. Enzyme encapsulation in layer-by-layer engineered polymer multilayer capsules. *Langmuir* **2000**, *16* (4), 1485-1488. DOI: 10.1021/la991161n.

55. Ohshima, H. Zeta potential. In *Encyclopedia of Colloid and Interface Science*, Tadros, T. Ed.; Springer Berlin Heidelberg, 2013; pp 1423-1436.

56. Maddigan, N. K.; Linder-Patton, O. M.; Falcaro, P.; Sumby, C. J.; Bell, S. G.; Doonan, C. J. Influence of the synthesis and storage conditions on the activity of Candida antarctica lipase B ZIF-8 biocomposites. *ACS Applied Materials & Interfaces* **2021**. DOI: 10.1021/acsami.1c04785.

57. Luzuriaga, M. A.; Benjamin, C. E.; Gaertner, M. W.; Lee, H.; Herbert, F. C.; Mallick, S.; Gassensmith, J. J. ZIF-8 degrades in cell media, serum, and some - but not

all - common laboratory buffers. *Supramolecular Chemistry* **2019**, *31* (8), 485-490. DOI: 10.1080/10610278.2019.1616089.

58. Velásquez-Hernández, M. d. J.; Ricco, R.; Carraro, F.; Limpoco, F. T.; Linares-Moreau, M.; Leitner, E.; Wiltsche, H.; Rattenberger, J.; Schröttner, H.; Frühwirt, P.; et al. Degradation of ZIF-8 in phosphate buffered saline media. *CrystEngComm* **2019**, *21* (31), 4538-4544. DOI: 10.1039/C9CE00757A.

59. Spitsyna, A. S.; Poryvaev, A. S.; Sannikova, N. E.; Yazikova, A. A.; Kirilyuk, I. A.; Dobrynin, S. A.; Chinak, O. A.; Fedin, M. V.; Krumkacheva, O. A. Stability of ZIF-8 nanoparticles in most common cell culture media. *Molecules* **2022**, *27* (10). DOI: 10.3390/molecules27103240.

60. Gao, Y.; Doherty, C. M.; Mulet, X. A systematic study of the stability of enzyme/zeolitic imidazolate framework-8 composites in various biologically relevant solutions. *ChemistrySelect* **2020**, *5* (43), 13766-13774. DOI: 10.1002/slct.202003575.

61. Wang, H.; Jian, M.; Qi, Z.; Li, Y.; Liu, R.; Qu, J.; Zhang, X. Specific anion effects on the stability of zeolitic imidazolate framework-8 in aqueous solution. *Microporous and Mesoporous Materials* **2018**, *259*, 171-177. DOI: 10.1016/j.micromeso.2017.10.011.

62. Zhang, H.; Liu, D.; Yao, Y.; Zhang, B.; Lin, Y. S. Stability of ZIF-8 membranes and crystalline powders in water at room temperature. *Journal of Membrane Science* **2015**, *485*, 103-111. DOI: 10.1016/j.memsci.2015.03.023.

63. Sheng, L.; Yang, F.; Wang, C.; Yu, J.; Zhang, L.; Pan, Y. Comparison of the hydrothermal stability of ZIF-8 nanocrystals and polycrystalline membranes derived from zinc salt variations. *Materials Letters* **2017**, *197*, 184-187. DOI: 10.1016/j.matlet.2017.03.077.

64. Willey, J. D. The effect of ionic strength on the solubility of an electrolyte. *Journal of Chemical Education* **2004**, *81* (11), 1644. DOI: 10.1021/ed081p1644.

65. Stumm, W. *Aquatic Chemistry: Chemical Equilibria and Rates in Natural Waters*; John Wiley & Sons, Incorporated, 1995.

66. Lvov, Y.; Onda, M.; Ariga, K.; Kunitake, T. Ultrathin films of charged polysaccharides assembled alternately with linear polyions. *Journal of Biomaterials Science, Polymer Edition* **1998**, *9* (4), 345-355. DOI: 10.1080/09205063.1998.9753060.

67. Sörensen, M. H.; Samoshina, Y.; Claesson, P. M.; Alberius, P. Sustained release of ibuprofen from polyelectrolyte encapsulated mesoporous carriers. *Journal of Dispersion Science and Technology* **2009**, *30* (6), 892-902. DOI: 10.1080/01932690802644095.

68. Schmidt, J.; Wei, R.; Oeser, T.; Belisário-Ferrari, M. R.; Barth, M.; Then, J.; Zimmermann, W. Effect of Tris, MOPS, and phosphate buffers on the hydrolysis of polyethylene terephthalate films by polyester hydrolases. *FEBS Open Bio* **2016**, *6* (9), 919-927. DOI: 10.1002/2211-5463.12097.

69. Williams, E. T.; Ehsani, M. E.; Wang, X.; Wang, H.; Qian, Y.-W.; Wrighton, S. A.; Perkins, E. J. Effect of buffer components and carrier solvents on in vitro activity of recombinant human carboxylesterases. *Journal of Pharmacological and Toxicological Methods* **2008**, *57* (2), 138-144. DOI: 10.1016/j.vascn.2007.11.003.

70. Sigma Aldrich. *Bradford Reagent*. Sigma Aldrich, 2023. https://www.sigmaaldrich.com/AU/en/product/sigma/b6916 (accessed 2023 February 8).

3.10 Supporting Information

3.10.1 Protein encapsulation and loading quantification

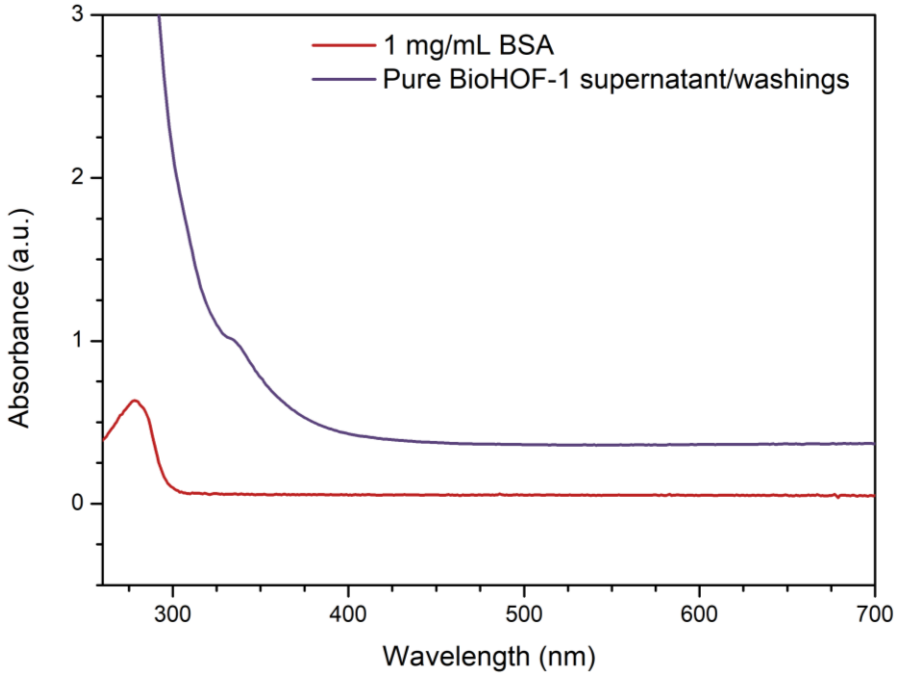

Figure S3.1: Control studies to assess if the 280 nm peak of the supernatant/washings of protein@BioHOF-1 composites can be used to determine loading. The supernatant over BioHOF-1 shows significantly higher absorbance that BSA, and thus this method could not be used to determine loading.

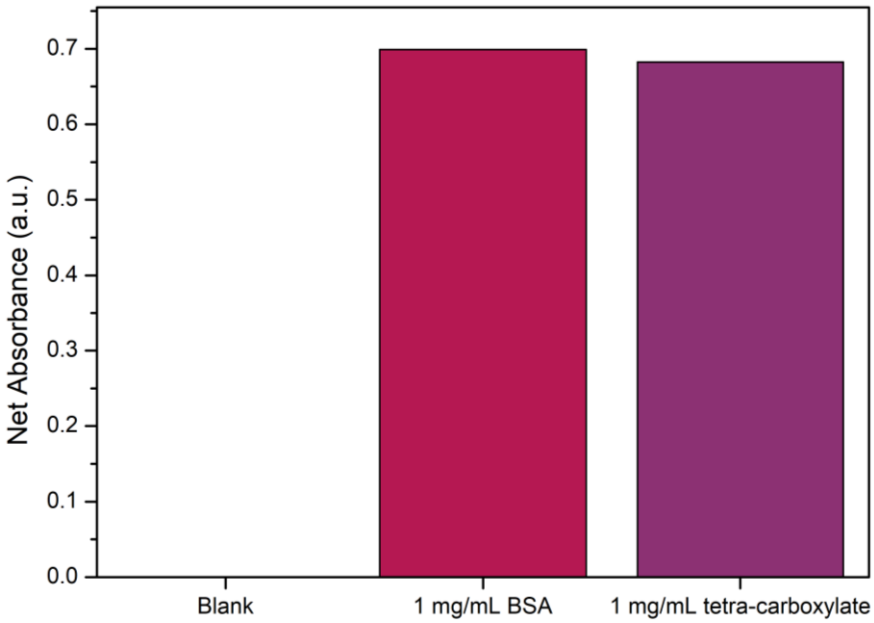

Figure S3.2: Control studies to assess if the Bradford assay can be used to quantify protein loading in BioHOF-1. The tetra-carboxylate linker shows significant interference in the Bradford assay. Samples were prepared as per Sigma Aldrich protocol, with the absorbance measured at 562 nm.[70]

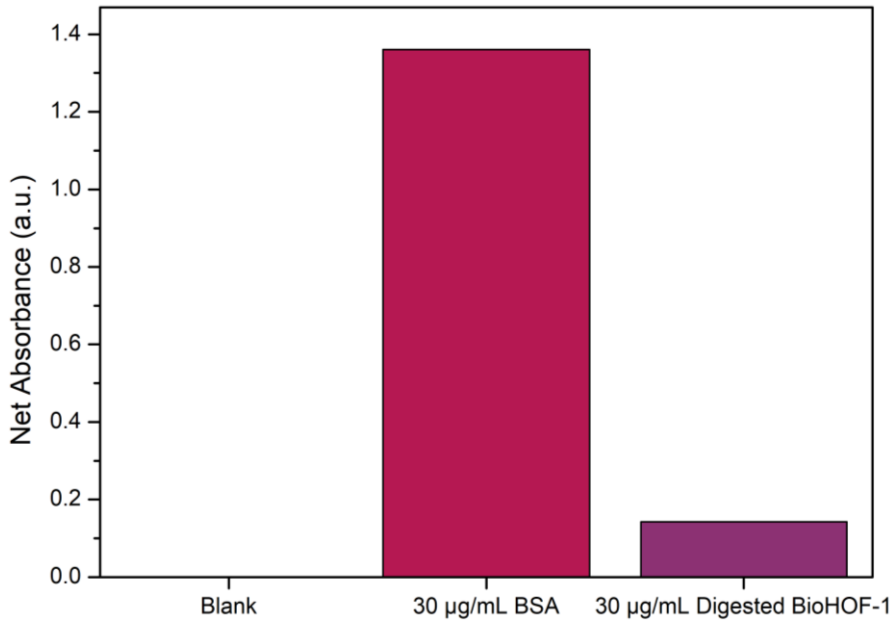

Figure S3.3: Control studies to assess if the BCA assay, with 1 hour incubation at 70 °C, can be used to quantify protein loading in BioHOF-1. A digested sample of BioHOF-1, in 0.01 M NaOH with 10% DMSO, shows some (~0.14) absorbance in the assay. As BioHOF-1 is expected to be in large excess to protein in protein@BioHOF-1 samples, this would interfere with loading calculations. Samples formed a large amount of precipitate, likely due to interaction between Cu(II) of the assay and the HOF linkers. Samples were prepared as per Sigma Aldrich protocol, with the absorbance measured at 562 nm,[15] and all samples subjected to centrifugation before conducting UV/vis analysis.

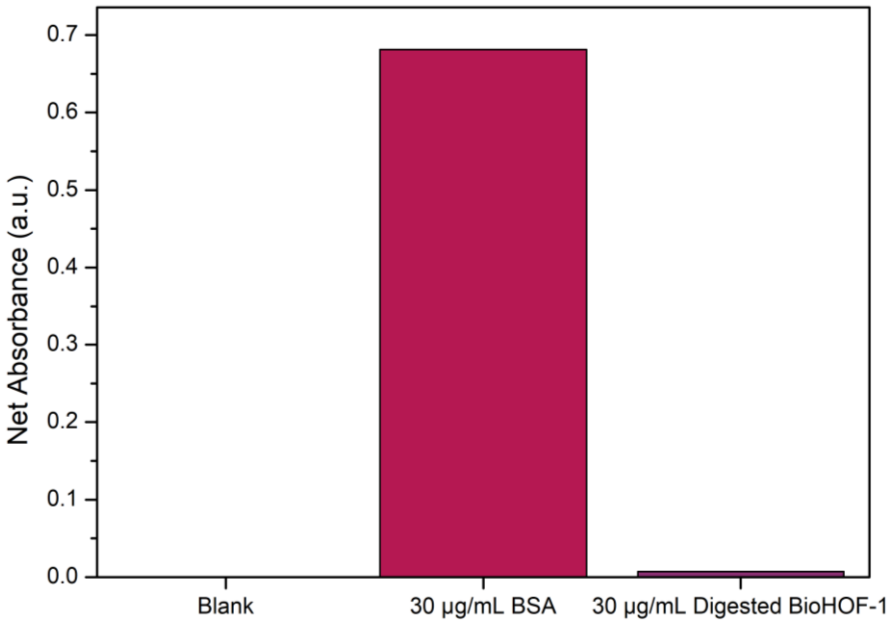

Figure S3.4: Control studies to assess if the BCA assay, with overnight incubation at room temperature, can be used to quantify protein loading in BioHOF-1. A digested sample of BioHOF-1, in 0.01 M NaOH with 10% DMSO, shows minimal (~0.007) absorbance in the assay. Samples were prepared as per Sigma Aldrich protocol, with the absorbance measured at 562 nm.[15]

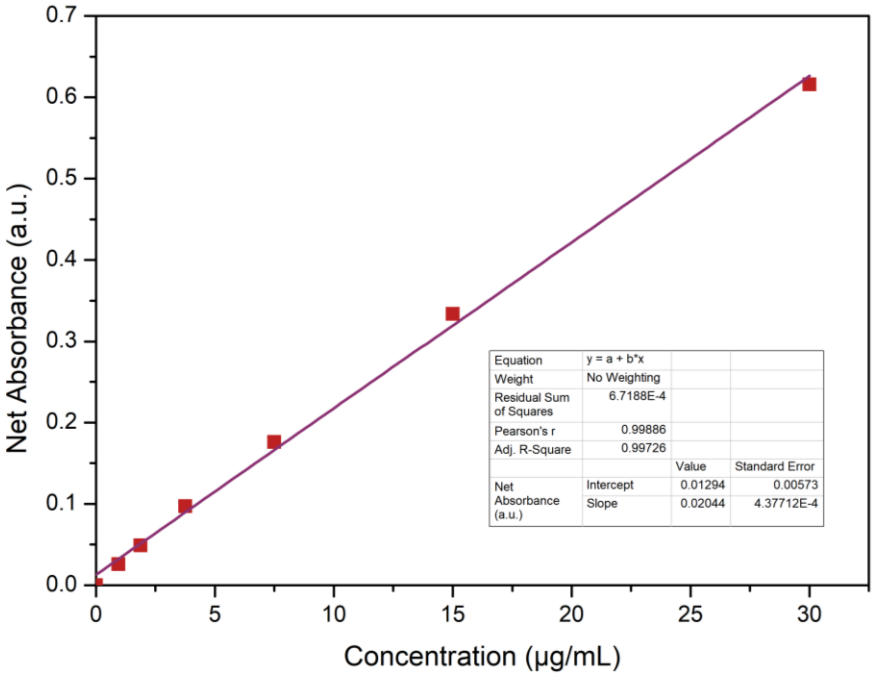

Figure S3.5: Example calibration curve for the determination of protein loading in BioHOF-1. Example curve was prepared using BSA, in 0.01 M NaOH with 10% DMSO.

3.10.2 Surface modification of ferritin

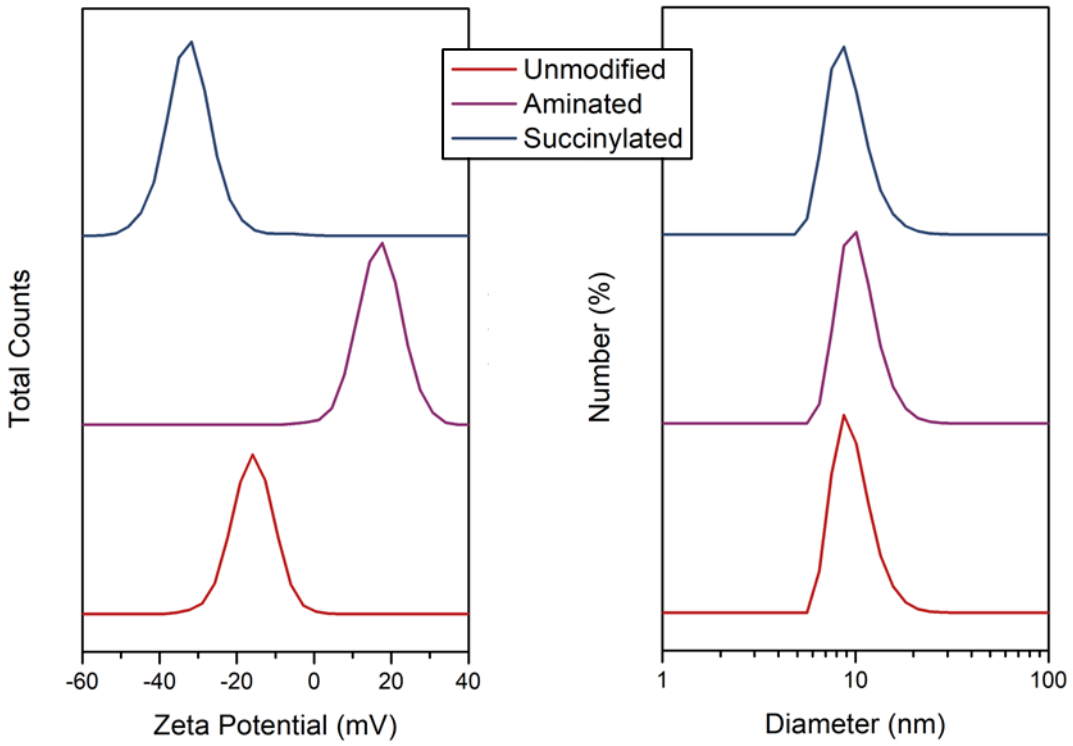

Figure S3.6: (**A**) Zeta potential and (**B**) number size distributions of modified ferritin. Zeta potentials were measured at a protein concentration of 1 mg/mL in 10 mM KCl. Size distributions were measured at a protein concentration of 1 mg/mL in 1 x PBS.

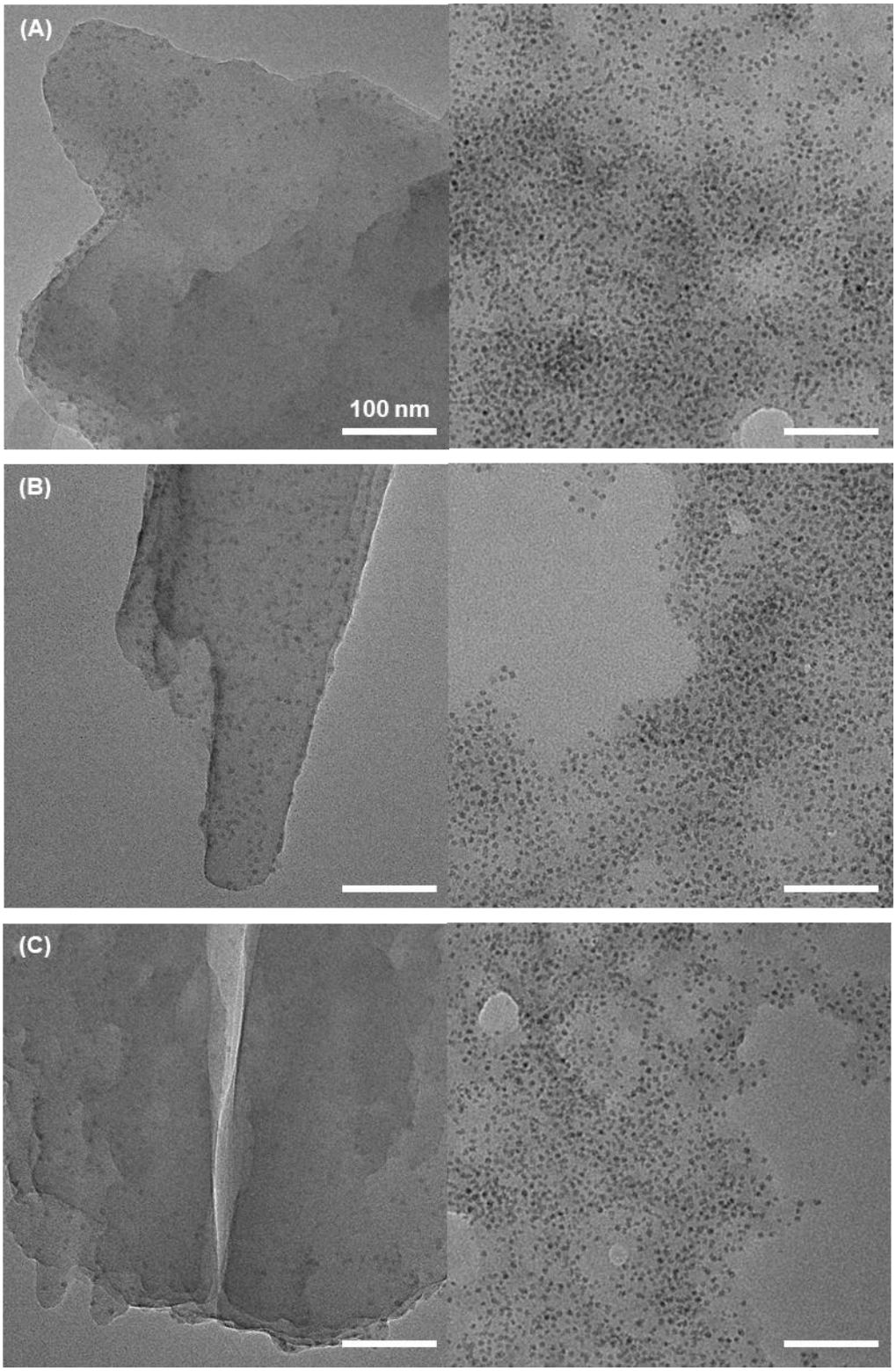

Figure S3.7: TEM images of BioHOF-1 synthesized in the presence of (A) unmodified, (B) aminated, and (C) succinylated ferritin. Samples were washed solely with water (x 2) and ethanol, and thus surface-bound and aggregated protein remains in the sample. Protein is seen in/on the HOF in all samples (left), however a significant amount of ferritin is also present as amorphous aggregates (right).

3.10.3 Modulator studies

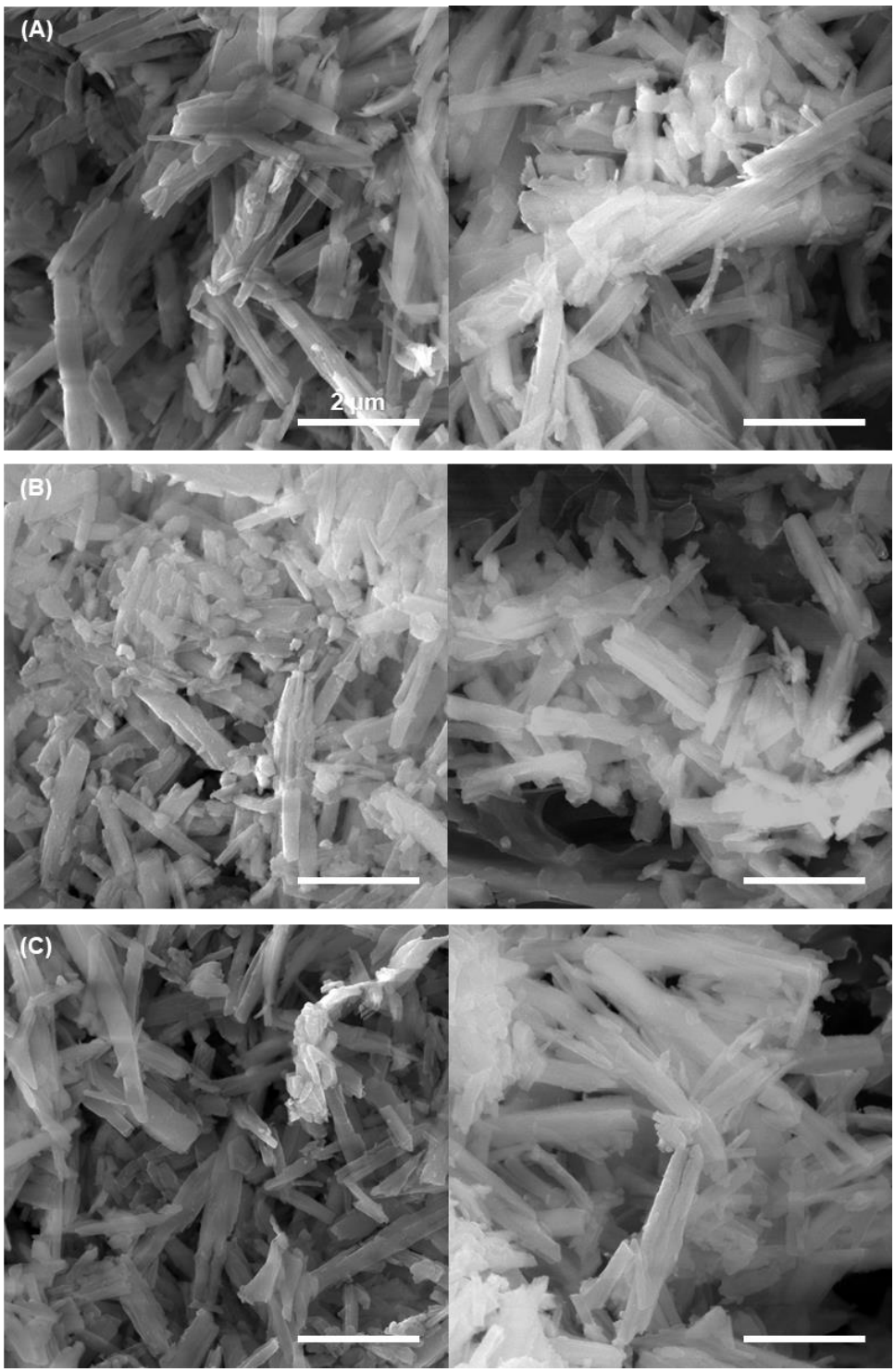

Figure S3.8: SEM images of FER@BioHOF-1 synthesized in the presence of (A) 0, (B) 20, and (C) 100 equivalents of sodium sulfate. Samples were washed with 10% SDS prior to imaging. A large amount of fragmentation of crystals is evident, likely due to extensive washing and partial degradation of the crystals by 10% SDS. It can be seen that sodium sulfate had little impact on the size of the HOF crystals formed.

3.10.4 Layer-by-layer HOF encapsulation

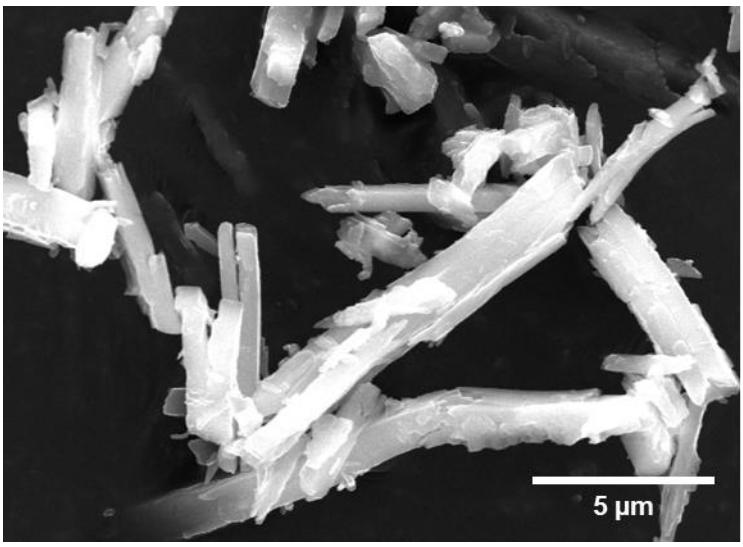

Figure S3.9: SEM image of BioHOF-1 with attempted coating of 8 layers alternating poly(styrene sulfonate) and FITC-tagged poly(allylamine), synthesized in water. No significant difference is seen compared to pure BioHOF-1, outside of additional crystal fragmentation due to extensive sample washing.

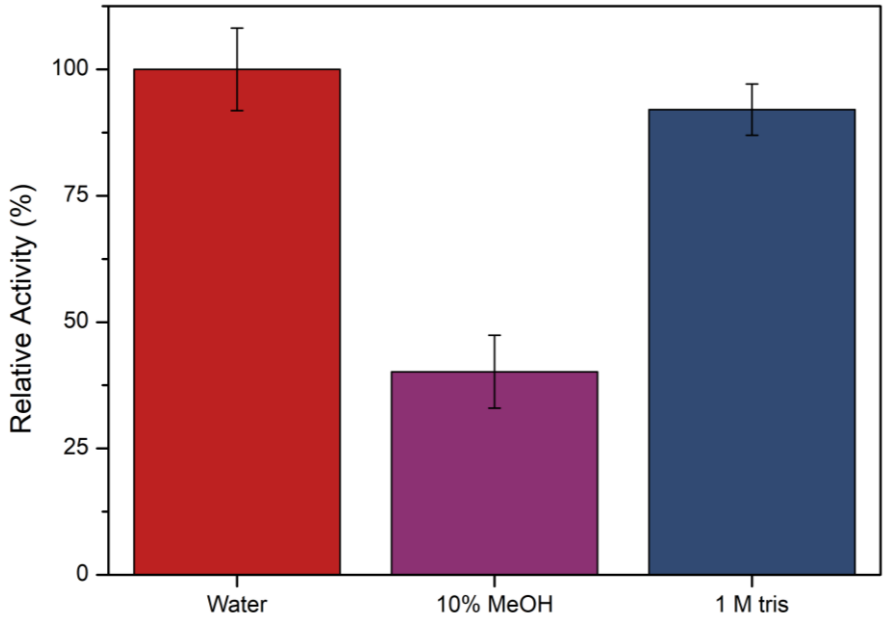

Figure S3.10: Catalytic activity of catalase exposed to 10% MeOH and 1 M tris buffer (pH 7.4) for 5 hours. The enzyme concentration in the reaction was 20 nM. Samples are normalized relative to catalase stored in ultrapure water for 5 hours. Error bars represent the standard error in the relative activity of the sample.

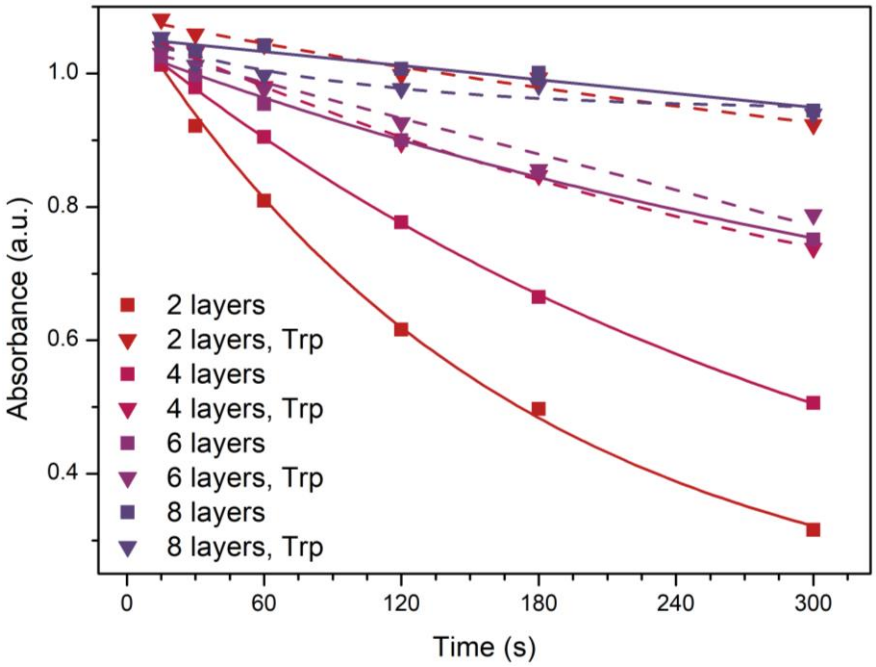

Figure S3.11: Raw data for the catalytic testing of catalase-on-HOF samples coated with varying amounts of alternating PSS and F-PAH in 1 M tris buffer, before and after trypsin digestion. The enzyme concentration in the reaction was 500 nM.

CHAPTER 4

Conclusions and Future Directions

4.1 Outlook

This thesis investigated methods of increasing the utility of biocomposites constructed using porous frameworks. MOFs and HOFs have been researched extensively as supports for biomolecule encapsulation, however each has limitations that currently withhold them from widespread biocatalysis applications.

In **Chapter 2**, enzyme@ZIF-8 biocomposites were investigated, with the objective to create composites that allow the retention of the activity of sensitive enzymes. Previous research has demonstrated that certain enzymes, such as catalase and alcohol oxidase, lose activity upon encapsulation in ZIF-8.[1, 2] For catalase, this is due to disruption of the tertiary protein structure by the hydrophobic ZIF-8 surface.[1] In our work, we used physical barriers as a method of tuning the protein-framework interface, to prevent protein denaturation. However, the two-step encapsulation of catalase in a single enzyme nanogel followed by ZIF-8 proved unsuccessful at retaining enzymatic activity. Attempts to protect catalase by conjugation to poly(acrylic acid) returned similar results. Further investigation revealed that catalase exhibits partial activity loss after overnight storage in 2-methylimidazole. In conjunction, ZIF-8 stored as an aqueous suspension released 2-methylimidazole from the framework, which was estimated to reduce catalase activity by 30-40% per day. It was thus concluded that loss of catalase activity in ZIF-8 is not solely due to contact with the hydrophobic surface, but also due to exposure to 2-methylimidazole, both during the synthesis and afterwards due to framework degradation. Previous studies have investigated the activity of ZIF-8 biocomposites stored in different buffers[3] and the instability of ZIF-8 in various storage conditions.[3-10] However, to our knowledge, a study specifically targeting the impact of the degradation products of ZIF-8 on proteins has not been conducted. Such a study would greatly benefit understanding of these unique cases where ZIF-8 precursors are partially responsible for enzymatic activity loss. Further, it may allow the development of combined systems which limit ZIF-8 degradation whilst also protecting protein from the hydrophobic surface, resulting in composites that allow sensitive enzymes to retain function in ZIF-8.

In **Chapter 3**, protein@BioHOF-1 composites were investigated. These composites provide protection to a broader variety of enzymes than ZIF-8 biocomposites[2], however currently possess relatively low protein loadings and are thus economically impractical. In this work, the spatial location of proteins in BioHOF-1 was

studied. Ferritin was identified as an ideal model protein, as encapsulated ferritin could be visualized by TEM. In combination with quantitative techniques, this was used to assess methods of increasing protein loading in BioHOF-1. Protein surface functionalization was largely ineffective at increasing protein loading, indicating the encapsulation behavior of BioHOF-1 is significantly different to that of ZIF-8 and single-component HOFs.[11, 12] Slowed framework growth also did not increase loading, although sodium sulfate promoted the encapsulation of certain proteins by preventing aggregation with the tetra-amidinium linker. This phenomenon could be further pursued to identify the characteristics of protein, such as surface charge, that promote aggregate formation with the tetra-amidinium, and thus the circumstances under which sodium sulfate is effective at increasing loading in BioHOF-1. Lastly, the pre-incubation of ferritin with a guanidinium-terminated polymer was used as a method of promoting interaction with the tetra-carboxylate linker, which slightly increased protein encapsulation. With all methods showing only slight increases in protein loading, it was reasoned that loadings comparable to that reported in the literature for single-component HOFs are not achievable for BioHOF-1. This could be due to inherent limitations of the BioHOF-1 framework, though the lack of extensive investigation on the localization of proteins in single-component HOFs suggests that loadings reported in the literature may require reevaluation.

To overcome the significant preference for protein to adhere to the surface of BioHOF-1, layer-by-layer polyelectrolyte encapsulation was used to provide additional protection to surface-immobilized protein. Coating catalase-on-BioHOF-1 in 6 layers of alternating poly(styrene sulfonate) and poly(allyl amine) provided near complete protection of surface-bound protein from Trypsin digestion. With further optimization, this could greatly increase the protection afforded in protein@HOF biocomposites. Variables that should be investigated include the washing conditions, storage conditions, polymer concentrations, and incubation times. The layer-by-layer encapsulation process also revealed that storage of the HOF in 50 mM tris afford a higher activity composite than when stored in ultrapure water. Further studies on the storage and synthesis conditions of BioHOF-1 should thus be performed, similar to previous studies conducted on protein@ZIF-8 biocomposites.[3] This could ultimately produce composites that exhibit higher activity and greater protection than has been previously reported for protein@BioHOF-1 composites.

Though HOFs are only a recent development in the field of enzyme immobilization, they present many advantages over other well-established frameworks. This can come in the form of applicability to a broader variety of proteins and enzymatic reactions, as well as enhanced stability over common supports such as ZIF-8. At the time of writing, the number of papers investigating biomolecule encapsulation in HOFs rests in single-digit figures. The development that has been made in such a short space of time highlights the enormous potential for HOFs to reach and exceed the benchmark set by other frameworks. The results obtained in this thesis have broadened our understanding of BioHOF-1 as a support for enzyme immobilization, paving the way for further optimization of this system for eventual biocatalysis applications.

4.2 References

1. Liang, W.; Xu, H.; Carraro, F.; Maddigan, N. K.; Li, Q.; Bell, S. G.; Huang, D. M.; Tarzia, A.; Solomon, M. B.; Amenitsch, H.; et al. Enhanced activity of enzymes encapsulated in hydrophilic metal–organic frameworks. *Journal of the American Chemical Society* **2019**, *141* (6), 2348-2355. DOI: 10.1021/jacs.8b10302.

2. Liang, W.; Carraro, F.; Solomon, M. B.; Bell, S. G.; Amenitsch, H.; Sumby, C. J.; White, N. G.; Falcaro, P.; Doonan, C. J. Enzyme encapsulation in a porous hydrogen-bonded organic framework. *Journal of the American Chemical Society* **2019**, *141* (36), 14298-14305. DOI: 10.1021/jacs.9b06589.

3. Maddigan, N. K.; Linder-Patton, O. M.; Falcaro, P.; Sumby, C. J.; Bell, S. G.; Doonan, C. J. Influence of the synthesis and storage conditions on the activity of Candida antarctica lipase B ZIF-8 biocomposites. *ACS Applied Materials & Interfaces* **2021**. DOI: 10.1021/acsami.1c04785.

4. Luzuriaga, M. A.; Benjamin, C. E.; Gaertner, M. W.; Lee, H.; Herbert, F. C.; Mallick, S.; Gassensmith, J. J. ZIF-8 degrades in cell media, serum, and some - but not all - common laboratory buffers. *Supramolecular Chemistry* **2019**, *31* (8), 485-490. DOI: 10.1080/10610278.2019.1616089.

5. Velásquez-Hernández, M. d. J.; Ricco, R.; Carraro, F.; Limpoco, F. T.; Linares-Moreau, M.; Leitner, E.; Wiltsche, H.; Rattenberger, J.; Schröttner, H.; Frühwirt, P.; et al. Degradation of ZIF-8 in phosphate buffered saline media. *CrystEngComm* **2019**, *21* (31), 4538-4544. DOI: 10.1039/C9CE00757A.

6. Spitsyna, A. S.; Poryvaev, A. S.; Sannikova, N. E.; Yazikova, A. A.; Kirilyuk, I. A.; Dobrynin, S. A.; Chinak, O. A.; Fedin, M. V.; Krumkacheva, O. A. Stability of ZIF-8 nanoparticles in most common cell culture media. *Molecules* **2022**, *27* (10). DOI: 10.3390/molecules27103240.

7. Gao, Y.; Doherty, C. M.; Mulet, X. A systematic study of the stability of enzyme/zeolitic imidazolate framework-8 composites in various biologically relevant solutions. *ChemistrySelect* **2020**, *5* (43), 13766-13774. DOI: 10.1002/slct.202003575.

8. Wang, H.; Jian, M.; Qi, Z.; Li, Y.; Liu, R.; Qu, J.; Zhang, X. Specific anion effects on the stability of zeolitic imidazolate framework-8 in aqueous solution. *Microporous and Mesoporous Materials* **2018**, *259*, 171-177. DOI: 10.1016/j.micromeso.2017.10.011.

9. Zhang, H.; Liu, D.; Yao, Y.; Zhang, B.; Lin, Y. S. Stability of ZIF-8 membranes and crystalline powders in water at room temperature. *Journal of Membrane Science* **2015**, *485*, 103-111. DOI: 10.1016/j.memsci.2015.03.023.

10. Sheng, L.; Yang, F.; Wang, C.; Yu, J.; Zhang, L.; Pan, Y. Comparison of the hydrothermal stability of ZIF-8 nanocrystals and polycrystalline membranes derived from zinc salt variations. *Materials Letters* **2017**, *197*, 184-187. DOI: 10.1016/j.matlet.2017.03.077.

11. Chen, G.; Huang, S.; Shen, Y.; Kou, X.; Ma, X.; Huang, S.; Tong, Q.; Ma, K.; Chen, W.; Wang, P.; et al. Protein-directed, hydrogen-bonded biohybrid framework. *Chem* **2021**. DOI: 10.1016/j.chempr.2021.07.003.

12. Maddigan, N. K.; Tarzia, A.; Huang, D. M.; Sumby, C. J.; Bell, S. G.; Falcaro, P.; Doonan, C. J. Protein surface functionalisation as a general strategy for facilitating biomimetic mineralisation of ZIF-8. *Chemical Science* **2018**, *9* (18), 4217-4223. DOI: 10.1039/C8SC00825F.